INFORMATION TO USERS

This manuscript has been reproduced from the microfilm master. UMI films the text directly from the original or copy submitted. Thus, some thesis and dissertation copies are in typewriter face, while others may be from any type of computer printer.

The quality of this reproduction is dependent upon the quality of the copy submitted. Broken or indistinct print, colored or poor quality illustrations and photographs, print bleedthrough, substandard margins, and improper alignment can adversely affect reproduction.

In the unlikely event that the author did not send UMI a complete manuscript and there are missing pages, these will be noted. Also, if unauthorized copyright material had to be removed, a note will indicate the deletion.

Oversize materials (e.g., maps, drawings, charts) are reproduced by sectioning the original, beginning at the upper left-hand corner and continuing from left to right in equal sections with small overlaps. Each original is also photographed in one exposure and is included in reduced form at the back of the book.

Photographs included in the original manuscript have been reproduced xerographically in this copy. Higher quality 6" x 9" black and white photographic prints are available for any photographs or illustrations appearing in this copy for an additional charge. Contact UMI directly to order.

NOTE TO USERS

The original manuscript received by UMI contains pages with slanted print. Pages were microfilmed as received.

This reproduction is the best copy available

UMI

University of Alberta

The Modified Creeping Cone Mining Method

by

Steffen Mothibedi Nareetsile   ©

A thesis submitted to the Faculty of Graduate Studies and Research in partial fulfillment

of the requirements for the degree of **Master of Science**

in

Mining Engineering

Department of Civil and Environmental Engineering

Edmonton, Alberta

Spring 1998

University of Alberta

Faculty of Graduate Studies and Research

The undersigned certify that they have read, and recommend to the Faculkty of Graduate Studies and Research for acceptance, a thesis entitled **The Modified Creeping Cone Mining Method** submitted by **Steffen Mothibedi Nareetsile, B. Eng. (Hons), (CSM)** in partial fulfillment of the requirements for the degree of **Master of Science** in Mining Engineering.

Dr. Josef Szymanski
(Supervisor)

Dr. Samuel Frimpong
(Co-Supervisor)

Dr. Stefan Planeta
(External Examiner)

Prof. Ian Murhead

Dr. Peter Schiavone

Date thesis approved by committee:

DEDICATION

TO MUM AND DAD WITH ALL MY HEART AND SOUL

ABSTRACT

The Creeping Cone (CC) mining method was introduced at BCL Selebi North mine in Botswana to control high dilution and side wall failures, which threatened the economic viability of the mine. A 50% reduction in dilution was achieved but further reductions were necessary for economic viability. Analytical, numerical and empirical methods of open stope design and dimensioning, coupled with geotechnical mapping were used to design the Modified Creeping Cone (MCC) mining method to achieve further reductions in dilution.

The design results showed that 50 metres high open stopes, supported with 2 by 2 metres cable bolt pattern on the hanging wall side and staggered stub stub pillars left inside the stopes, could be mined with spans ranging from 70 to 255 metres depending on their location. The results further showed that dilution could be reduced from the current level of 33.2% to 18.6% with projected financial gains of 41%.

.

ACKNOWLEDGEMENTS

TABLE OF CONTENTS

LIST OF TABLES

.

LIST OF FIGURES

LIST OF SYMBOLS AND ABBREVIATIONS

W — distributed load

Fy — vertical forces

M — resisting moments

V — shear resistance

T — tensile force

σ_m - maximum extreme fibre stress

c — distance from the extreme fibre to the neutral axis

Fn — normal forces

$\bar{y}$ - distance to the centroid

y — distance to the outside fibre

Ma — moment about neutral axis

I — moment of inertia

E — rock mass stiffness

σ_c — uniaxial compressive strength

α — inclination angle

Z — arch thrust moment

Fm — maximum stress

Fav — average arch stress

ΔL - arch shortening

N — ratio of arch thickness to beam thickness

Tcr — minimum stable slab width

H — width of orebody

σ_1 — major principal stress

σ_2 - intermediate principal stress

σ_3 - minor principal stress

p — field stress

k — stress concentration factor

q — aspect ratio

b_k — buckling factor

H1 — vertical dimension of an ellipse

W1 — horizontal dimension of an ellipse

σ_v — vertical stress

σ_h - horizontal stress

z — depth below surface

σ_h — boundary stress on the crown

σ_u — boundary stress on the side

σ_p - pillar stress

w_0 — stope width

w_p — pillar width

σ_s - pillar strength

r — rock mass strength

f — pillar shape

u_n — principal compressive strength of a cube of rock mass

s — Hoek and Brown constant

RMR — rock mass rating

h — pillar height

F_s — factor of safety

SM — safety margin

σ_n — normal stress

$\varnothing$ — angle of friction

τ — shear stress

R — radius of trap door

P_v — applied pressure

A_r — area

P — perimeter

c_h — cohesion

l — length of rectangle

b — breath of a rectangle

Wp — planned waste tonnage

Tm — mining reserves tonnage

Tg — geological reserves grades

PDF — planned dilution factor

ADF — additional dilution factor

Wa — additional waste tonnage

Tt — run-of-mine ore tonnage

Wt   – total waste tonnage

FDF   – final dilution factor

Q   - rock tunneling quality index

Q'   - modified rock tunneling quality index

N   – stability number

N'   - modified stability number

A   – rock stress factor

B   – joint orientation adjustment factor

C   – gravity adjustment factor

RQD   – rock quality designation

Jn   – joint set number

Jr   – joint roughness number

Ja   – joint alteration number

Jw   – water reduction factor

SRF   – stress reduction factor

N_w – stope wall plane to the north

E_w – stope wall plane to the east

D_w – stope wall plane downwards

N_j – joint plane in the north direction

E_j – joint plane in the east direction

D_j - joint plane in the downwards direction

HR   – hydraulic radius

Θ - angle of rosette relative to coordinate system

P   – pressure in biaxial cell

e   – strain

D   – overcore external radius

d   – internal radius

μ - Poisson's ratio

R_e – extraction ratio

CC   - creeping cone

MCC   - modified creeping cone

HW   - hanging wall

FW   - footwall

UCS   - uniaxial compressive stress

l_o - opening length

l_p - pillar length

CHAPTER 1

INTRODUCTION

1.1 MINE SITE LOCATION

Selebi North Mine is located in the eastern part of Botswana and is one of the mines operated by BCL Limited, a subsidiary of Botswana Roan Selection Trust (BRST) around the Selebi-Phikwe area. The main shareholders are Anglo American Corporation, De Beers Consolidated Mines, The Government of Botswana, who hold 40%, 25% and 30% respectively, with the rest of the shares held by the public. The mining complex consists of three underground mines, a concentrator and a smelter, and the usual allied services. BCL Limited operates a large copper/nickel mining complex located at Selebi Phikwe on the edge of the Kalahari Desert as illustrated in Figure 1.1. The total labour force is approximately 5000. The town is accessible by road, rail and air and is significantly diversified in terms of the industries supporting the mining operation.

1.2 PROBLEM DEFINITION

The Selebi North mine commenced delivery of development ore in January 1990. The mine produces copper/nickel run-of-mine ore using the creeping cone open stoping mining method. The ore is concentrated and smelted on site, with the matte shipped to

ANGOLA
ZAMBIA
ZIMBABWE
NAMIBIA
Chobe R.
Zambezi R.
Okavango Swamps
Maun
Orapa
Bulawayo
Francistown
Phoenix
Selebi-Phikwe
REPUBLIC
OF
BOTSWANA
Limpopo R.
Tropic of Capricorn
Gaborone
Nossob R.
Molopo R.
Lobatse
BOTSWANA
REPUBLIC
OF
SOUTH AFRICA
500 Km.
Johannesburg
N

LOCATION MAP

KEY

———— Tarred road

-+-+-+- Railway

-·-·-·-´ International Boundary

- - - - - Secondary road
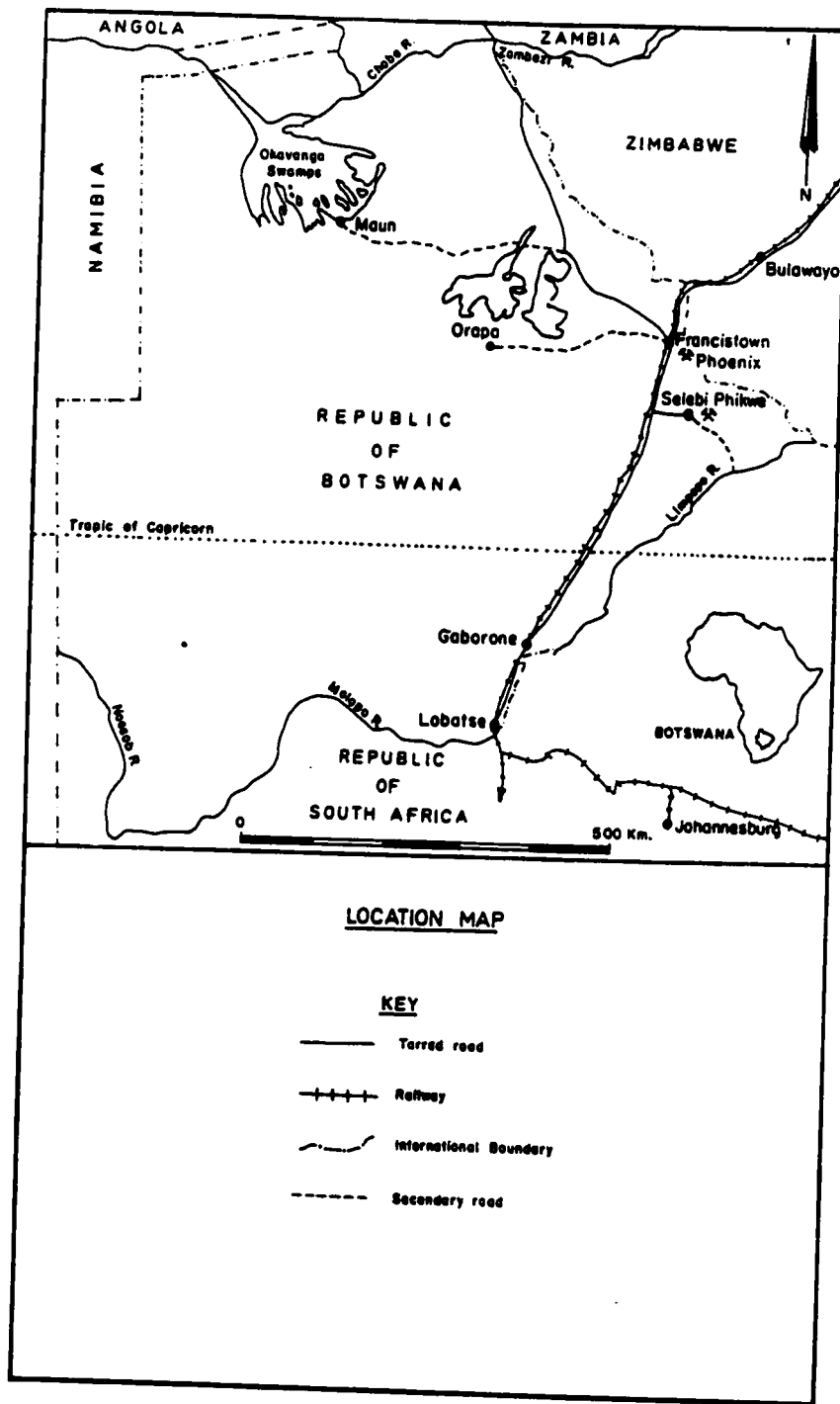
Figure 1.1: Map of Botswana showing the locality of Selebi-Phikwe copper/nickel deposit.

2

Zimbabwe and Norway for further refining. The matte purchasing agreement with Amax Nickel Inc., a subsidiary of Amax Inc of USA, was replaced in July 1995 with a long-term contract with Falconbridge International Ltd. (FIL). BCL supplies matte to FIL's refinery in Kristiansand, Norway, and is committed to supply some 35 000 tonnes annually to 1999. BCL also supplies around 10 000 tonnes per year of matte to Centametall AG for refining in Zimbabwe.

The mining grades realized from the run-of-mine ore are far below the geological grades due to side wall failures of the creeping cone open stopes causing dilution, putting the viability of the Selebi North mine at risk. Due to the remote location of the mine, backfill material is not readily available except for development waste. As a result, the stopes are left unfilled, which cause them to cave in with time, and this problem can progressively lead to subsidence.

As mining progresses deeper, the regional tectonic stresses and the induced stresses due to mining make both the hanging wall and footwall of the stopes fail by either slabbing or gravity falls. The problem is further intensified by blasting induced stresses which in most cases cause both hanging wall and footwall overbreak and reduce the competency of the rockmass. The result is an increase of the run-of-mine ore due to additional dilution which was not planned for or anticipated. The need for a new modified creeping cone mining method to mine out the lower portion of the ore reserves cannot be over emphasized as the mine enters the second phase of its development.

1.3 OBJECTIVE OF THE PROJECT

The primary objective of this research was to modify the creeping cone mining method used at Selebi North mine in order to be able to mine the lower part of the orebody as the mine enters phase two of its development. In particular emphasis was placed on the stope stability and dimensioning using the current technology in open stope design. The elements of this objective include:

- Improving the current mining system at Selebi North mine in terms of productivity, safety and economic viability of the project.
- Modifying the creeping cone mining method with costs within the economic capability of the project.
- Maintaining a balance between implementation of the proposed modified creeping cone mining method and the findings made in reduced dilution.
- Developing a systematic way of dimensioning the stopes based on the understanding of the rock mass behaviour and response to induced stresses.
- Providing an understanding of hangingwall and footwall behaviour, including failure modes such that support pillars can be designed and strategically located within the orebody to provide the necessary support for anticipated failure.
- Developing a more efficient and modified creeping cone mining method.

1.4 LIMITATIONS AND SCOPE

The limitations in this project included:

- Insufficient finance to purchase modeling program PHASES which models the near field stresses.

- Restricted access to information from Selebi North mine as critical data was classified as confidential.

- Lack of sufficient published data regarding the performance of the creeping cone mining method in mines other than Selebi North mine.

- Limited published information in the use of mathematical models or analytical methods in designing maximum spans for open stope mining in hard rock.

The scope of this research comprises the technical aspects of open stope design and dimensioning using present technology. The design focused on the use of the beam theory. voussoir arch and stability graph methods to design a modified creeping cone mining method. With the primary focus on finding ways of reducing dilution at Selebi North mine. The projected economic benefits of the modified creeping cone were analyzed using the anticipated gains in the actual contained metal tonnes in the run-of-mine ore. However, the project did not cover detailed fanancial analysis such as the net present value or the internal rate of return as the details of the operating costs were not available.

1.5 METHODOLOGY

This research was primarily concerned with open stope mining method design and operation in a hard rock environment. It covered all aspects of design and operations currently used in hard rock open stopes, such as analytical, numerical and empirical methods. An extensive literature survey was conducted in order to select the best possible methods of design for use in this project. This was followed by geological data collection at Selebi North mine. Experimental design and experimentation using the results were undertaken using Selebi North mine as a case study.

1.6 STRUCTURE OF STUDY

This thesis is divided into two parts: the first part (Chapters 1 - 6) describes the current state of practice in open stope mining methods used in hard rock mining. The second part (Chapters 7 - 12) focuses on the design of the proposed modified creeping cone mining method. Chapter 1 deals with the introduction of the thesis with particular focus on the project location, its problems and the research , the scope and limitations, the methodology and the report structure. Chapter 2 looks at the regional geology of the area under consideration including the ore reserves and the geomechanics of both the host and ore body rocks. In Chapter 3, the author reviews the current state of practice in sub-level open stoping, with particular focus on the design trends as regard to pillar design, stope dimensioning and computer aided design. The analytical methods of open stope design are reviewed in Chapter 4 and Chapter 5 deals with a review of the empirical methods of

open stope design. These methods are then used for open stope design in the subsequent chapters of the second part of this thesis.

Chapter 6 reviews the Creeping Cone (CC) mining method as it is currently practiced at Selebi North mine. This chapter briefly explains the evolution of the method and the mechanics of its operation. Chapter 7 describes the methods of geological data collection and its analysis, including discontinuities mapping at Selebi North mine, and determination of the Rock Quality Designation (RQD) from surface exploration holes. It also looks at the Rock Mass Rating (RMR) of the Selebi North rocks, as well as, observations made in the existing stopes at the mine. The procedure for determining the magnitude and orientation of induced stresses due to the redistribution of the virgin stress caused by the pressure of mining stresses at the mine and the calculation of the rock mass response elastic constants are outlined in Chapter 8. Analytical methods are used in Chapter 9 for preliminary mine design to establish the maximum span between the rib pillars, the pillar dimensions and the distance between draw points, as well as, the location of the main ramp systems. In Chapter 10, empirical methods (Stability Graph) applied to open stoping stability are used for preliminary mine design. Chapter 11 outlines the proposed Modified Creeping Cone (MCC) mining method layout, operations and projected economic benefits when compared with the actual achievements of the CC, based on the exchange rate of C$1.00 to P2.10 during the second half of 1997. Chapter 12 looks at the concluding remarks, recommendations and further work. There is also a list of references and the details of the mathematical calculations and tables are included in an appendix at the end of this thesis.

CHAPTER 2

GEOLOGY OF THE DEPOSIT

2.1 REGIONAL GEOLOGY

The Selebi North sulphide deposit is part of the economic sulphides confined within a stratiform mafic sill enclosed in highly folded and metamorphosed Precambrian metasediments. The dominant sulphide is pyrrhotite, with pentlandite and chalcopyrite as the main sources of nickel and copper respectively. The subsequent remobilization due to folding and metamorphism resulted in a structurally complex ore body.

The majority of north-eastern Botswana lies within the Limpopo Belt which extends as a broad zone of metamorphic rocks 300 km wide, situated between the Kaapvaal and Rhodesian cratons (Gallon, 1986). This region has been subjected to repeated periods of structural deformation and high-grade metamorphism. This effect of tectonic deformation divided the ore into three groups based on their sulphur content. Wakefield (1974) indicated that dating at Selebi-Phikwe reflected ages of 2660 Ma as the last major metamorphic event to affect rocks in the mine area, though the Limpopo orogenic event is dated at between 3 570 and 2 600 Ma. Both Gallon (1986) and Wakefield (1974) suggested that the nickel-copper deposits of Eastern Botswana are located in complexly folded and metamorphosed Archaean paragneisses of the Central Zone of the Limpopo Belt. Gallon (1986) further suggested that the mineralisation was associated with mafic

8

and ultramafic intrusive rocks, the later injected into a thick succession of quartzo-feldspathic gneisses. As a result the wall rock at Selebi-Phikwe consists of thick interbedded meta-arkoses and meta-greywackes, which are typically geosynclinal in origin with a concordant sill-like amphibolite which represent the ore zone host. In addition, dolerite dykes of Karoo age are generally oriented north-west/south-east, cross cutting the major rock structures.

The current regional interpretation of the stratigraphy is such that the hanging wall biotite gneiss is about 130 m thick, and consists of medium to coarse grained white feldspar biotite gneiss with bands richer in hornblende in some places. It is also a general consensus by the mine geologists that, 10 m above the ore horizon, the grain size decreases and the rock strength increases, probably resulting from high metamorphism due to the proximity of the sill host [Gallon (1986)]. The ore horizon, which could be as wide as 45m in some places, comprises an amphibolite host rock with mineralisation varying from poorly disseminated sulphides to the total replacement of the host by massive sulphides. The immediate footwall gneiss which is in excess of 200m thick is highly disturbed with overturned folding and is mainly hornblende-rich gneisses interbedded with biotite schists.

2.2 STRUCTURAL GEOLOGY

Figure 2.1 shows the locations of the mines in relation to the major geological structures in the region. The interplay of the F2 and F3 fold phases (Figure 2.2) has resulted in the
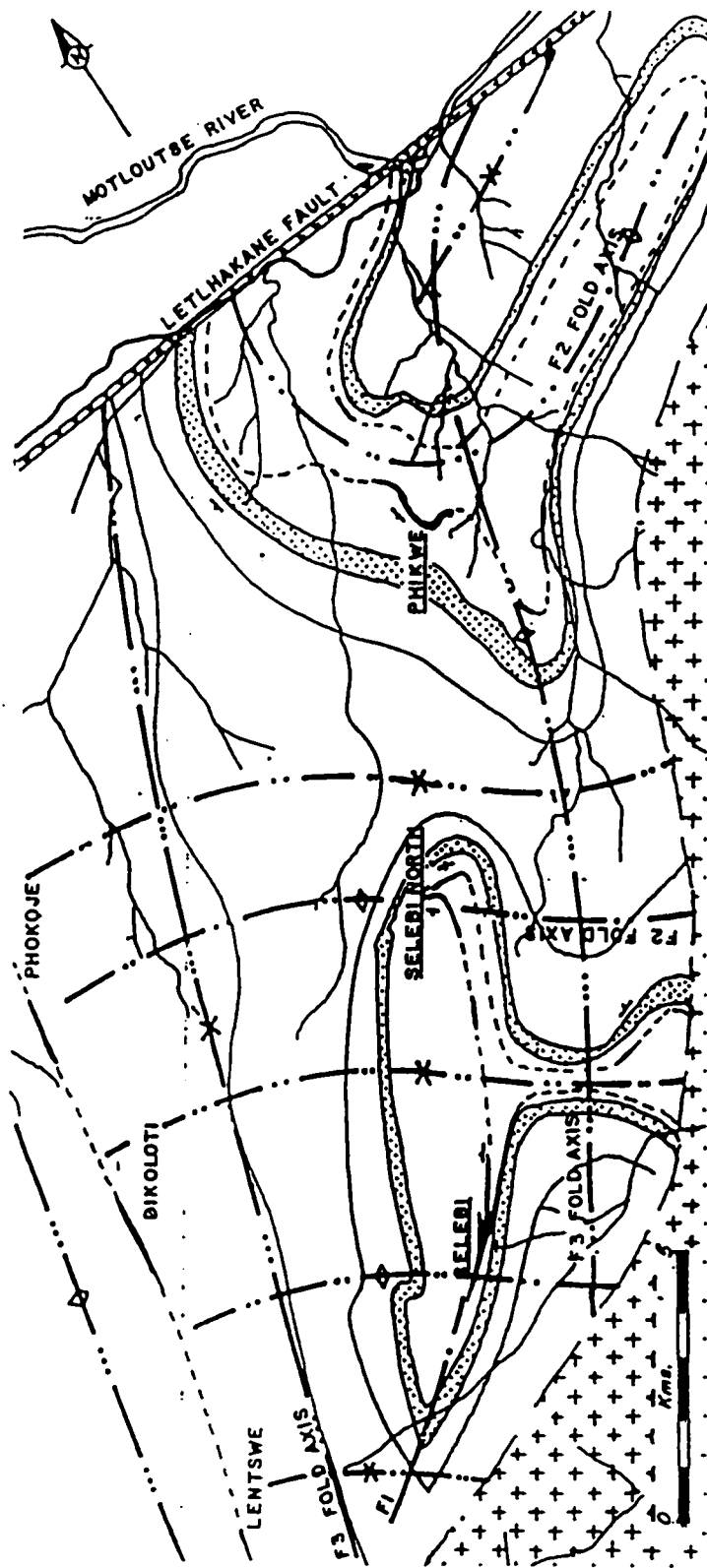
Figure 2.1: Simplified plan showing ore body outcrops and the major fold axes in the Selebi-Phikwe area.
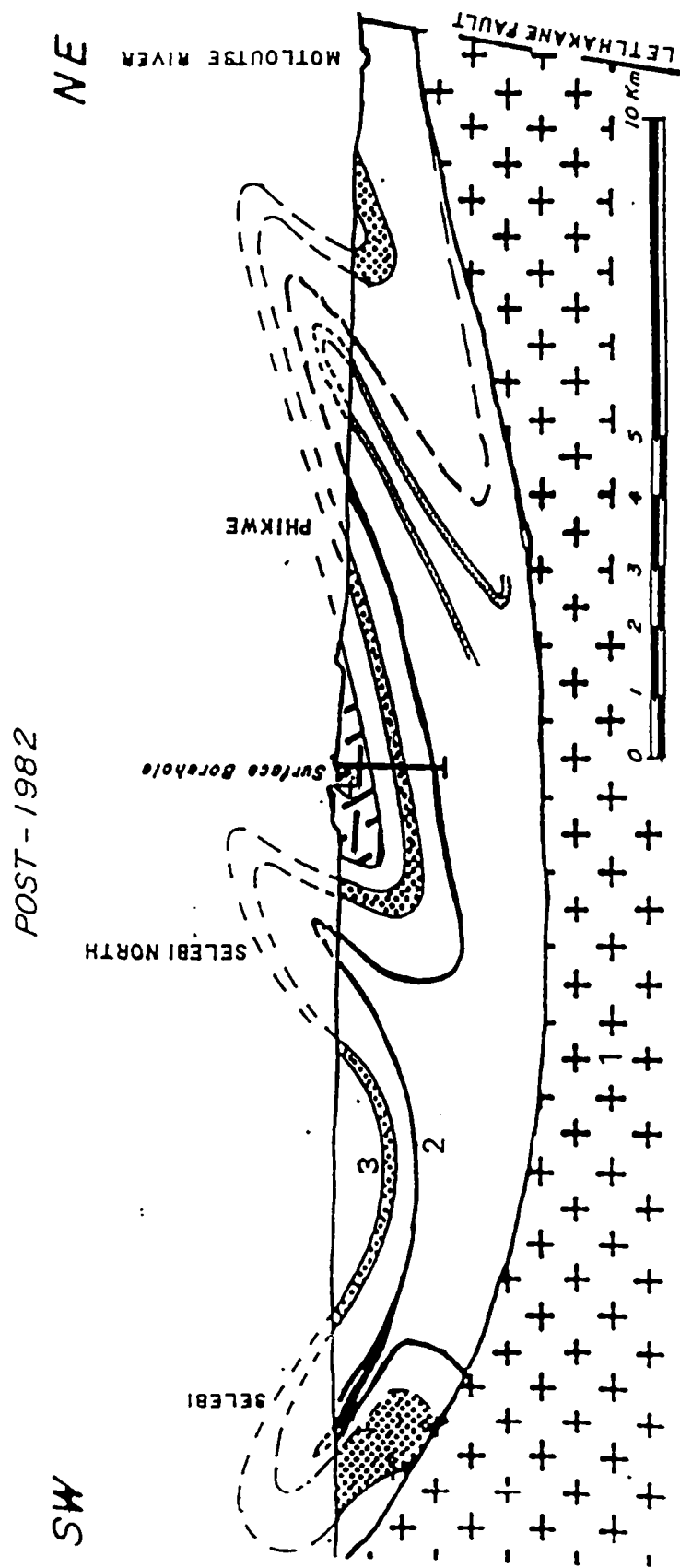
Figure 2.2: Simplified Sections showing the structural relationship between Selebi, Selebi North and Phikwe.

complex pattern of domes and basins as seen in the area and documented by Gallon (1986). Three fold phases F1, F2 and F3 have been identified in the area, with the effects of the earliest phase of folding (F1), being masked by the later phases. The second phase of folding (F2) was accompanied by plastic and cataclastic deformation and is associated with amphibolite-grade metamorphism. F3 folding is characterized by open folds with wave amplitudes twice those of the F2 folds. The folds are interrupted by the Letlhakane tear fault on the north.

A detailed major regional geological mapping undertaken in 1982, revealed that the structure between Selebi North and Phikwe was an anticline with basement granites exposed as shown in Figure 2.2, and according to Gallon (1986), two deep surface diamond drill holes intersected ore at 1 500 m.

The Selebi-Phikwe ores are divided into three main groups based on their sulphide content and the effects of tectonic deformation - massive sulphides, semi-massive sulphides and disseminated sulphides. In the massive sulphides, the host rock is almost entirely replaced by the sulphides; this occurs along the ore body wall rock contact as well as being concentrated in the fold axes. Most of these sulphides comprise pyrrhotite with interstitial pentlandite grains and remnants of the host occur as boulders and fragments of amphibolite, biotite and rounded quartz pebbles. Pentlandite occurs as exsolution lamellae in the pyrrhotite and chalcopyrite is found as irregular masses or around the boulders of amphibolite. Semi-massive sulphides contain 40 - 70 per cent sulphide in a matrix of host amphibolite. Garnets commonly form at the contacts of

sulphide - amphibolite, with the disseminated sulphides uniformly distributed through out the host. More massive sulphides concentrations tend to be erratic. Lastly the disseminated sulphide ore is found in thick horizons but is of low grade.

2.3 HOST ROCK PETROLOGY

The host rock is amphibolite which tends to vary distinctly in three areas of the deposit. In the Phikwe area, the change from north to south appears to be controlled by the F3 fold, with the northern ore characterized by thickness, low-grade and dissemination of sulphides. Further south from Phikwe is the Selebi North area, the amphibolite host is almost totally replaced by massive and semi-massive sulphides. In this region the amphibolites are preserved in the form of large "boulders" as noted by Gallon (1986). The wall rocks are gneisses and are preserved as small pebbles and assimilated grains of quartz. Towards the south-eastern edge of the deposit, the quartz content increases, resulting in a proportional decrease in the sulphide content. In this region the lateral extent of the ore zone remains open to the south. Selebi, still south of Selebi North area, has a thick host amphibolite which shows a high degree of differentiation. The massive and semi-massive sulphides tend to concentrate on the hanging wall contact of the upper units and along the footwall of the lower unit.

2.4 SELEBI NORTH ORE DEPOSIT

The BCL mining operations are centered at Selebi in the south and at Phikwe 14 km to the north. The Selebi North deposit is situated equidistant between Selebi mine in the south and Phikwe mine in the north. The deposits are separated by a distance of 7 km (see Figure 2.3). This deposit is an over-turned anticline plunging at 55 to 60 degrees south-west (see Figure 2.4 and 2.5). The fold starts relatively tight at surface and opens with depth, forming a fold nose of ore thickness ranging from 28 to 30 meters. The limbs thin rapidly to about less than a metre at about 200 metres from the fold axis. The ore potential of the horizon is being trebled by the presence of common congruous drag folding with amplitudes of 20 to 30 metres on both limbs of the fold according to Gallon (1986).

The north limb has been detached from the main fold due to shearing. and it contains 1 to 2 metres of almost exclusive massive sulphides mineralisation, and this is referred to as N3 limb (see Figure 2.6). The extent of the N3 limb has been traced for 350 m down dip and for 200 m along strike where it abruptly ends, and efforts are being made to locate the extension of ore using both geochemical and geophysical methods. The general thickness of both the North and South limbs is 6 metres and the dip is estimated at not less than 75 degree. Mapping and underground drilling revealed that at the nose area of the fold axes, the mineralisation is concentrated in the top 10 metres of the amphibolite. and is underlain by barren phlogopite amphibolite which marks the mining cut-off of 0.45% Ni and Cu.
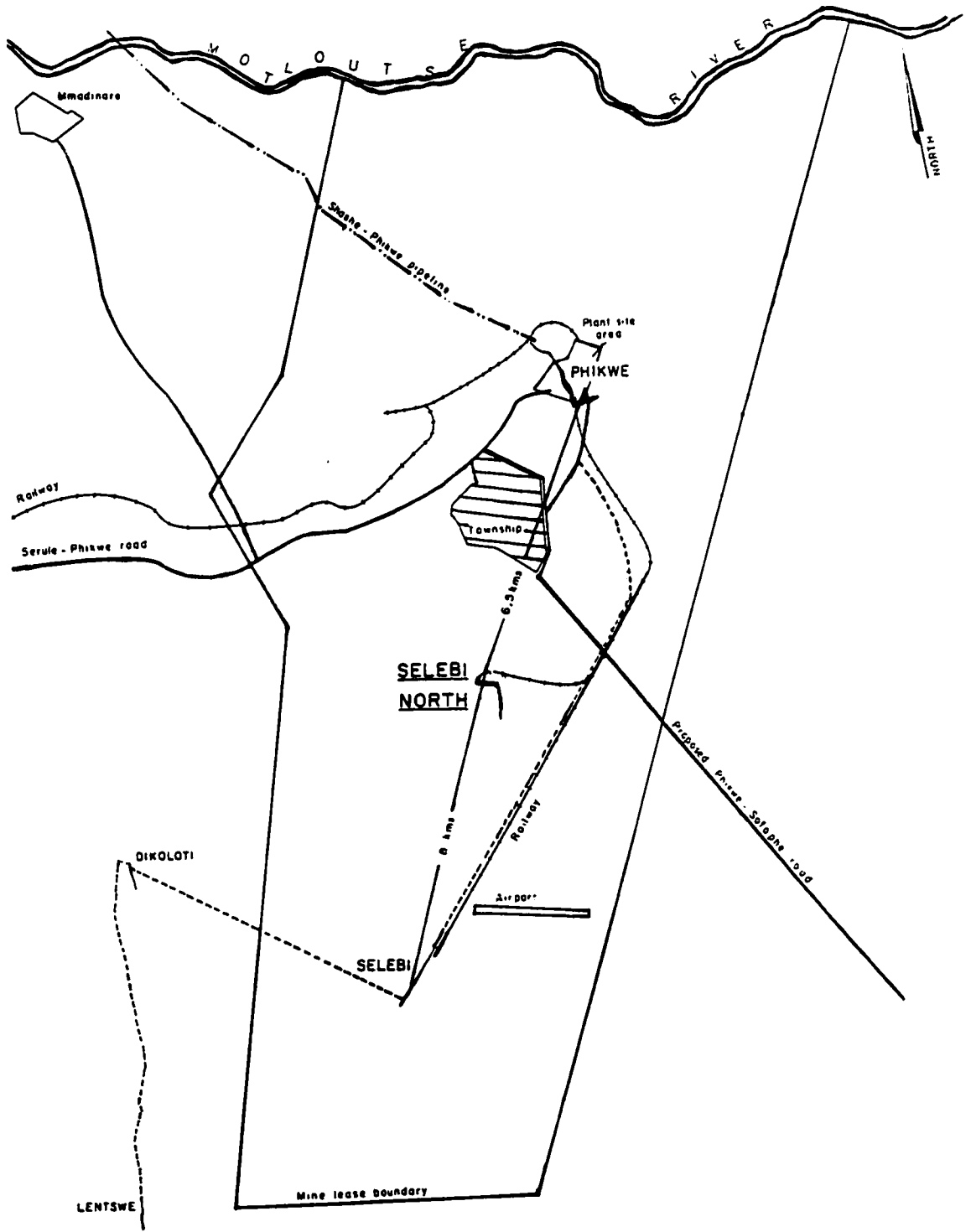
Figure 2.3: Selebi North location map
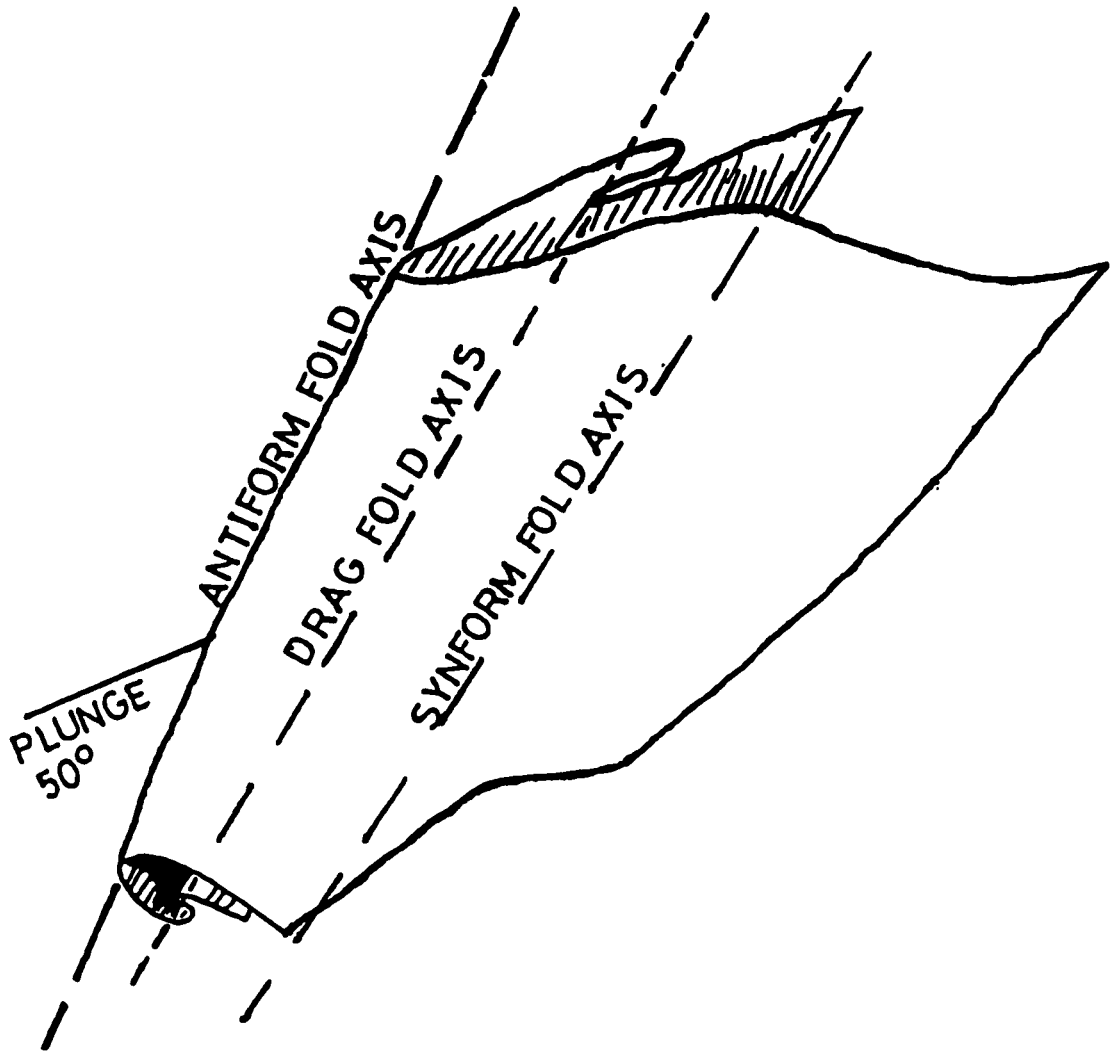
Figure 2.4: General structure of the Selebi North orebody
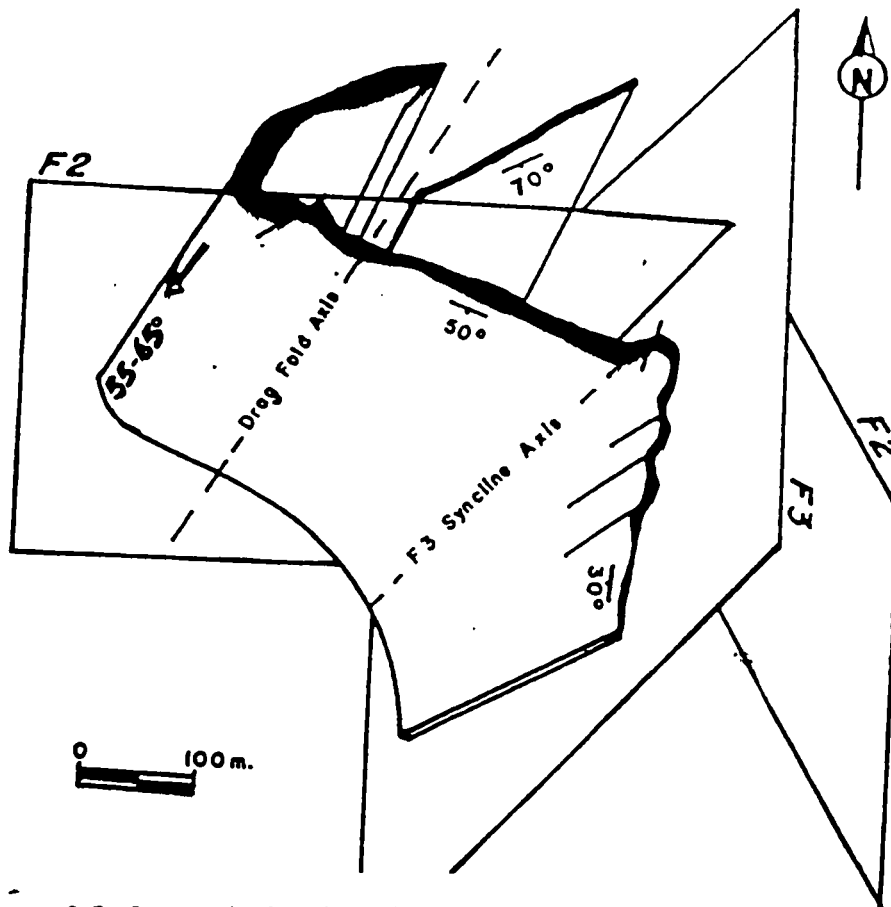
Figure 2.5: Isometric drawing of the Selebi North deposit

deposit the grade is estimated at 0.82 % Nickel and 0.83% Copper (Larkin, 1995). Nickel/Copper ratios vary between 1 : 2 on the limbs to 1 : 1 in the nose area. The hanging wall contact in the nose area is defined by thick massive sulphides which invaded the wall rocks by injection. The mineralized zone have only been proven to 400 metres below surface by detailed diamond drilling program, however further drilling is underway to determine the depth of the ore body.

N3 LIMB

High grade massive sulphides, rare amphibolite.
0.5 - 4m thick
Dip = 70 - 90^0

N2 LIMB

Thin sheared amphibolite with patchy sulphides
0 - 5 m thick, dipping at +/- 45^0

N1 LIMB

Amphibolite +SMS/MS increasing towards hanging wall contact
3 - 6 m thick, dip 70 - 90^0

FOLD NOSE

Amphibolite + locally thick MS concentrated in area of low strain up to 15 m thick (MS = 6m)
Plunges WSW at 50^0

SOUTH LIMB

Mineralized amphibolite, Locally with MS/SMS overlying barren phlogopitic amphibolite on the F/W.
8 - 16 m thick
Dip = 55^0

MS - Massive sulphides
SMS - Semi massive sulphides

Figure 2.6: Schematic plan view of the Selebi North orebody

2.5 GEOMECHANICS

Though the general area has been subjected to massive and complex folding due to tectonic stresses, there are no major discontinuities as yet intersected by diamond drilling. However, randomly oriented joints have been mapped on both the ore body and the host rock at Selebi North mine. And these are to be used in preliminary design and further observations would be done as mining continues.

There are no major faults intersecting the Selebi North orebody except the major folds which are advantageous to mining in the sense that they concentrated the ore. The rock mass is classified as good for both the hanging wall and footwall rocks and there is a distinct cut-off (contact) between the orebody and the host rock. The in-situ stresses in the area have been measured and are fairly average at 0.027 MPa/m vertically and 0.0245 MPa/m along strike with 0.035 MPa/m on the down dip direction. The hydrogeology of the area can be considered dry, with the bulk of anticipated water coming from the drilling equipment used and very little from the surrounding rock mass.

2.6 ORE RESERVES

The Phikwe, Selebi and Selebi North mines were commissioned in 1973, 1980 and 1988 respectively. Other mineral resources have been identified at Lentswe, Dikoloti and Phokoje in the surrounding areas. Current in-situ proven mineral reserves are estimated at 94 million tonnes (Mt.), 55 Mt. at Phikwe, 30 Mt. at Selebi and 9 Mt. at Selebi North

mine. The latter orebody contains the highest ore grades, 0.83 % copper and 0.82 % nickel (Larkin, 1995). The mining complex currently produces 3 657 084 tonnes of run-of-mine ore annually at an average grade of 0.71% nickel and 0.74% copper (BCL report) at a cut-off grade of 0.45% copper/nickel.

It is mandatory by law for BCL limited to issue an annual reserve certificate showing reconciled ore reserves at the end of every year. The information include proven and probable ore reserves conforming with the standards set by the U. S. Bureau of Mines. rate of annual depletion of the said ore reserves including the exploration programme and the mining plan, the alternative sources of ore and the exhaustion date.

The reserves are divided into Class I, Class II and Class III with Class III further divided into proven and probable ore reserves. Class I is the fully developed reserves that have been evaluated and developed to within 95% of completion and are available for mining. In the case of Selebi North mine, Class I reserves include developed open stopes that are available for mining and any pillars available for mining. Class II reserves are partially developed and evaluated but are not available for mining. They include stopes that will become available for mining on the completion of development and evaluation. They also include reclamation pillars that have been evaluated but will not be mined until the end of mine life. Class III reserves are undeveloped but have been evaluated by surface diamond drilling only. These reserves are sub-divided into proven ore and probable ore dependent on the density of drilling. Proven ore reserves are outlined by drill hole spacing sufficiently close (less than approximately 150m) to estimate the reserves to

within 20% confidence of the actual tonnage and grades. Probable ore reserves are outlined by a drill hole spacing (greater than 150m and less than 300m) in which the confidence is lower than that for proven ore.

2.6.1 Ore Evaluation Formulae (OEF)

Ore Evaluation Formulae is an expression of the value of mineable ore at mine bin (hoisted ore), after all costs including corporate taxes and processing costs have been established. For any grade of ore, OEF expresses in Pula/tonne (P/t) the money remaining to support the cost of mining (cost/tonne of mineable ore to mine bin) and producing a profit, based on break-even predictions. The OEF can simply be expressed as follows;

$$P/t \text{ (value of mine bin ore)} = \text{Revenue from refined metals - Processing costs} \qquad (2.1)$$

In equation (2.1), the revenues from refined metals are equivalent to a constant multiplied by nickel and copper grades to reflect mill and smelter recoveries. This include credits for focused metal prices less corporate expenses. The processing costs are costs of milling, smelting and refining the ore.

CHAPTER 3

SUB-LEVEL OPEN STOPING METHOD REVIEW

3.1 INTRODUCTION

Over the past 20 years, a lot of development has taken place in the optimization of underground mining methods. These developments have mainly focused on equipment improvement or change in order to handle high tonnages for profit maximization. However, little change have taken place in the design of hardrock mining methods as regard to open stope dimensioning and design.

Today's mining is focused on improved production with the lowest costs but highest safety record. As a result, more companies are adopting massive (bulk) mining methods which are operated on a non-entry basis and which are easily mechanized and automated. As a result, sublevel open stoping has become a mining method to take the mining industry into the next millennium. This bulk mining method lends itself to high technological developments in stope design, with heavy mechanization and improved production rate, safety and economic gains [Mukhopadhyay and Bharathan. 1993]. The method is also open for complete automation with a central controlling system.

3.2 BACKGROUND

Sublevel open stoping is a non-entry mining method which uses long and large diameter blasting holes as illustrated by Figure 3.1. Developments are usually concentrated on the footwall side of a steeply dipping orebody, with production drifts going through the orebody along the strike. These drill drives are called sublevels and are joined together by long big blast holes. The stope spans along the strike and the vertical distance between the draw points are usually determined by the geomechanical characteristics of the orebody and host rock. The full width of the orebody forms the stoping width. The drill equipment is selected based on appropriate design. The ore is then blasted into a slot raise joining the production drifts. The blasted ore is then accessed by means of draw points which are crosscuts from the footwall drives towards the orebody. Crown pillars are usually used to separate the stopes and are left below the draw points.

3.3 PAST PRACTICES IN SUB-LEVEL OPEN STOPING

3.3.1 Design Approaches

Literature survey has revealed that very little research results were published on the subject of sub-level open stoping prior to the eighties [Stewart, 1981]. By then the need for massive mining methods had become apparent and the mining industry had led the way by a series of in-house trials on massive mining methods.
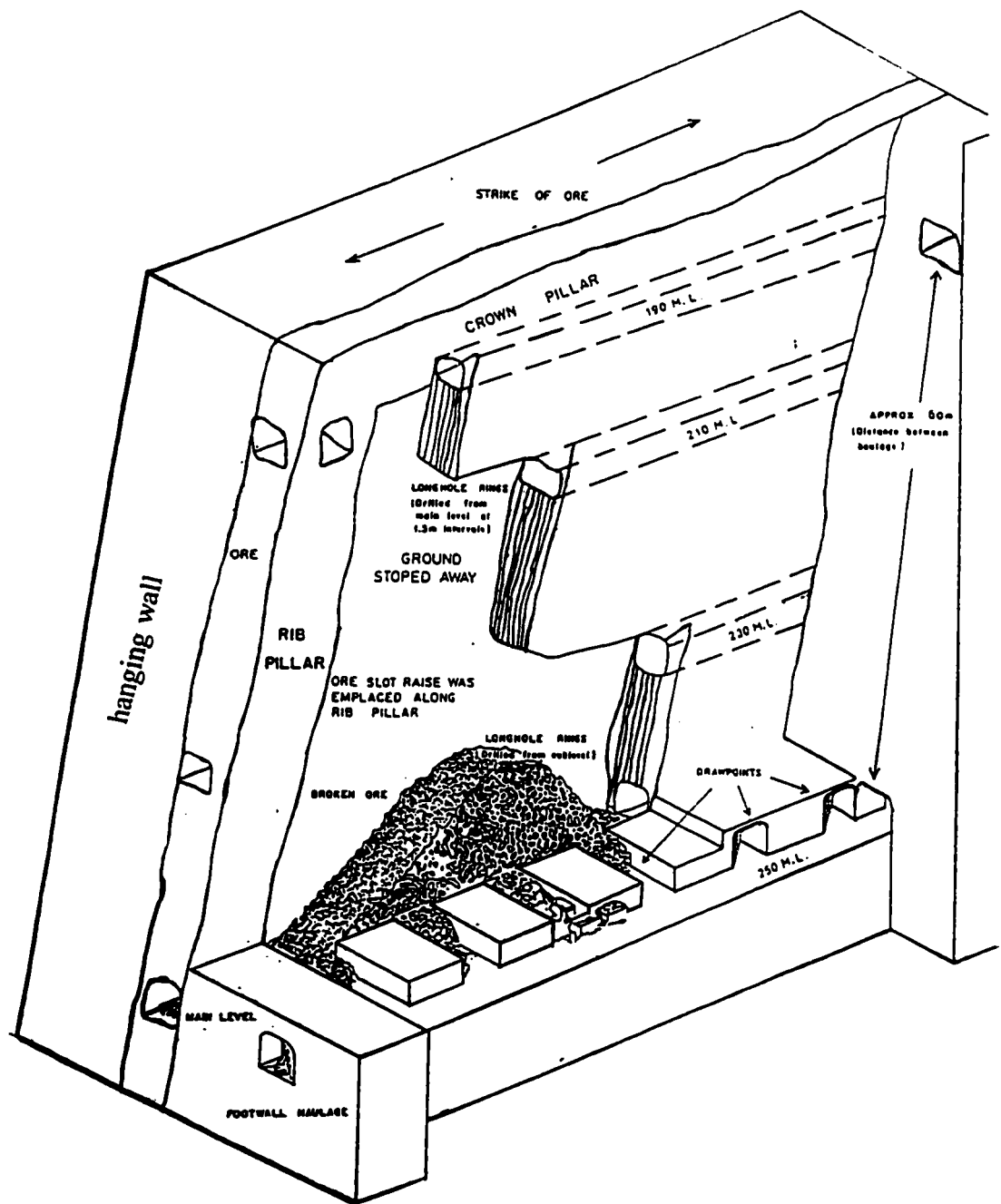
Figure 3.1: Sublevel longhole open stoping method as used at Selebi North mine.

The revelation was that sublevel caving, induced block caving, shrinkage stoping. vertical crater retreat and sublevel open stoping mining methods, work using similar concepts to achieve massive production with minimum costs.

In the past, mining started with an open pit and subsequently evolved into underground mining, due to both economic and safety reasons as the pit got deeper. In that case the mining personnel had a great opportunity of collecting data during the open pit operations. This data was correlated to the local conditions and subsequently used to form the basis of design parameters for underground mining. During the transition from surface to underground mining, advantage was taken of the high pressure exerted by the loose rock that had accumulated at the base of the open excavation. Due to the collapse of the sidewalls and underground tunnels were used to draw the fractured ore. This draw of fractured ground from big blocks was first introduced in the 1890s and have revolutionalised the mining production with little change until about the seventies [Bucky, 1945; Stewart, 1981]. During this period, unexploited orebodies were increasingly becoming elusive hence the introduction of sublevel open stoping mining method which offered more flexibility and multiple access to the ore through the use of draw points.

With today's high investment capital and the need for high returns, emphasis has been placed on the selection of the mining method with a high probability of attaining the expected tonnage. Though empirical experience from similar orebodies is still important. emphasis is more on the geometry and grade distribution of the deposit. as well as, the

rock mass strength for the ore zone, the hanging wall, and the footwall. Therefore, numerical methods were then developed and used in conjunction with the empirical methods to select either single or multiple drilling sublevel designs.

The problems experienced with sublevel open stoping varied from massive loss of draw points to high dilution rates due to stress distribution around the stope walls. As a result, rock mechanics became an important component in the design of the mine layout. These problems were further intensified by the introduction of large long hole blasts as emulsified explosives were introduced in bulk mining. As mining progressed deeper, heavy support was required in drill drives and the stress problems drew the attention of both operators and planners, as pillars continued to fail violently with massive losses in both property and human life.

With less scientific knowledge available, rib or crown pillar design was done on experimental basis by either increasing the size of the pillar or reducing the span in order to stabilize the stopes. These pillars and stopes were then monitored and data gathered was then used to form empirical design formulae in the late seventies. These developments were then followed by computer applications in the form of finite element method for the assessment of field stresses and boundary element method for the assessment of the near-field stresses around the stoping areas. Such determinations were used to predict the behaviour of the stope structural elements due to the redistribution of stresses as a result of mining operations.

3.3.2 Production

In the early eighties it was then clear that sublevel open stoping was best suited to steeply inclined orebodies with simple structures and strong footwall and hangingwall. Considerable variations of the method were then introduced in Zambia as reported by Madson and Russel (1981) to suit complexly folded ore bodies as they were encountered. Grizzly and stope chute extraction methods were used in steep ore bodies with high extraction rate from a particular draw point. With the introduction of rubber-tyred LHD equipment, trackless draw point loading was then possible. Similar to trackless draw point loading, tracked draw point loading method was then introduced, where track mounted loaders were used to load direct into ore trains. Matikainen (1981) reported that more than ten mines in Finland had adopted sublevel open stoping as their main mining method and that contributed to more than 80% of the total underground tonnage. In Japan sublevel open stoping method was considered to be one of the best methods for achieving high productivity, low cost, easy grade control and safety [Takata et al., 1981]. Approximately 51% of all ore production by underground metal mines in Canada is derived directly from open stoping operations [Pakalnis et al., 1993].

3.4 CURRENT PRACTICES IN SUB-LEVEL OPEN STOPING

The nineties have seen considerable applications of computers to mining and this has resulted in great improvements in the areas of rock mechanics, grade control, mine design and planning with a better scientific background. However, the empirical methods of design still dominate open stope dimensioning. A design philosophy was adopted which

uses the systematic observations of mining events to calibrate the results of geotechnical analysis. The outcome of such calibration is to predict mining events, such as dilution, stability or blasthole closure rather than geotechnical events such as stress or strain. However, mining has become an increasingly competitive business and the remaining orebodies are more complex both geometrically and geologically, requiring a state of the art technology for exploitation. There has been a lot of changes in the laws governing mining which further aggravated the situation. Sublevel open stoping has proved its superiority as a massive mining method to meet today's demand for high quality production with lower costs and improved safety.

3.4.1 Current Design Approaches

The nineties have seen the implementation of refined techniques learned in the eighties as practical mining tools, as a result of the increased collaboration between mine operators and researchers. The mining industry is now willing more than ever before to budget for improved technical skills and to develop research areas aimed at improving the industry in general. The academic institutions have also stepped up their efforts in improving the quality of their programs in order to meet the challenges of the industry.

Pine et al. (1992) used the elastic model in conjunction with an empirical model to predict the extent of low-stress zones in the hanging-wall, and related stability to rock mass rating (RMR) and hydraulic radius. With this method, known values of RMR were plotted in an empirical graph of adjusted RMR values against the hydraulic radius (area divided by perimeter) from which the stope span was calculated for a known stope

height. The result was an allowable hanging wall span as a function of rock mass quality. The hydraulic radius was defined as the total area of exposed hanging wall in the sub level open stope divided by the total perimeter of immediately adjacent support (abutment and/or ribs). The method assumed the stope width to be equal to the orebody thickness.

In trying to define the concept of maximum span required for either a drill drive or a stope, Franklin et al. (1993) suggested that the solution may lie in the concept of stand-up time, as proposed by earlier researchers. He proposed a method combining existing rock mass classification systems. Such concept was based on the fact that unique factors for use in the design of mine structures in jointed rocks cannot be obtained from determined strength and stress values obtained from laboratory and numerical analysis. because in a mining situation problems are unique to individual stopes. However. researchers realize the fact that design methods are analytically based on the analyses of stresses and deformation around mine structures, observing the ground movement to detect measurable instability and empirically assessing the stability of mines by the use of statistical analysis.

Considering the fact that most of the stoping operations of ore are carried out in what is conventionally termed 'jointed' ground, the new design strategy monitors the mining events to predict stope behavior [Pakalnis et al., 1993]. As a result a method using dilution approach for estimating open stope stability has been proposed, for stopes previously designed by the classical beam theory approach. The method uses a concept

similar to that first suggested by Pine et al. (1992) which has been modified to include the rate of extraction and the stope configuration, as well as, the previously suggested hydraulic radius and rock mass rating of the hanging wall. The dilution method assumes three stope configurations of isolated, rib or echelon depending on their location in relation to each other on the mine plan.

In this method the design factors are known, and the acceptable level of dilution governs the choice of the stope dimensions. The main disadvantage of this method is the fact that it ignores blasting-induced dilution which is significant and it assumes that dilution is due to the hanging wall failure but not to the footwall or roof.

Although substantial progress has been achieved in static design of underground excavation in jointed rock, comparable progress has not been maintained in dynamic design. An underground excavation is produced in stages (or elements), each of which constitutes a small fraction of the complete excavation. As production blasting continues towards the final stope geometry (shape and size), the excavation becomes more unstable. During stope production, one of the most critical issues is the determination of the 'critical' blast vibration levels that will induce excavation damage to the surrounding rock mass. Blast damage can be defined simply as the weakening of the rock mass through fracturing or extension of existing fractures caused by near-field blast vibration and entry of explosion gases. It can also be defined as the dislodging of wedges and key blocks caused by resonant effect of cyclic loading of these structures in the mid to far

field regions. In the near-field region, blast amplitudes are relatively high and the corresponding frequencies are also high (generally in the order of kilohertz).

The damage mechanism in the near-field involves the creation of new fractures, extension of existing fractures, weakening of joint bonding and dislodging of blocks due to high accelerations. In the mid to far field regions, the dominant mechanism of wall damage or failure is the shaking of wedges, key blocks or pre-conditioned volumes of rock due to cyclic loading of the walls from subsequent mid and far-field blasts. Repetitive blasting of benchs along the ore bodies has been known to severely weaken the stope surfaces by decreasing the joints shear strength and accumulation of shear displacements at joints.

The most popular approaches to determine the critical peak particle velocities likely to induce damage take the form of the empirical relationships. These approaches generally use a number of rock constants or parameters which infer the characteristics of rock mass, the geometry between the explosive charge at the point of interest and the amount of explosive. The main limitations of these approaches are that they do not explicitly take into account actual characteristics of the rock mass, i.e., whether the rock is massive or heavily jointed, the degree of fracturing, joint characteristics or the presence of key blocks. These parameters relate damage to critical level of the peak vibration velocity alone and do not consider the total energy contained in the vibration, the duration of the vibration and the frequency of the disturbance. While the approaches described are applicable to what is designated as pre-conditioning of the rock mass, they are certainly invalid for mid to far-field damage.

To date, no existing blast damage model combines the contributions of shock and gas energy. In order to fully understand the blast process, it is equally important to study both mechanisms. Dr. Szymanski commenced work on the development of a computer model using Jozef's Distinct Element method (JDE), aimed at predicting rock fragmentation and blast-induced damage in the surrounding rock mass. The charge surrounding rock mass is simulated as a random assembly of rigid elements bonded together in a dense packing. Deformability of the rock is simulated via normal and shear stiffness at contacts while the strength of material is simulated by bond stiffness and the element-element friction coefficient and the damage by progressive bond breaking. Contact-surface springs are used for fully connected surfaces of continuum. and contact-point springs for partially connected rock blocks. Blast loading is considered by radial contact force surrounding the charge. Conservative equations and the ideal gas formulate the behaviour of an internal point of charge. The first order reaction rate and the thermal explosion initiation are applied.

The methods analyzed above put emphasis on the empirical design method of open stope span approximation. According to the authors, these methods have shown superiority by winning confidence of the mining industry personnel. This increased level of confidence might be due to the fact that database used for the design is based on individual mine, hence the experience gained during mine operation can also be used for design. The main disadvantage is that the methods are site-specific, hence a new mine is designed on assumptions. The methods also put emphasis on the use of the rock mass rating and the use of the hydraulic radius, which could be assumed to be inversely proportional to the

stand-up time. The inclusion of dilution as a design parameter by Pakalnis et al. (1993) and the combination of the existing rock mass classification by Franklin et al. (1992) are important steps towards the credibility of design methods in open stope design.

3.4.2 Sublevel Open Stope Pillar Design.

Due to the massive collapse of open stopes and violent failure of stope pillars resulting in the loss of both equipment and life, the need to increase the safety of the working areas cannot be over-emphasized. As a result, several proposals have been made in relation to pillar design with regard to their loading and the subsequent induced stresses against the pillar strength. When calculating the pillar strength, Pine et al. (1992) proposed an average pillar strength which was calculated using the compressive strength of intact rock, the rock mass strength factor, and pillar shape factor. In calculating the induced stresses in pillars, the main input values were taken from the stope, pillar and abutment geometry normal to the plane of the stope and the in-situ stress data.

With the increased pressure from the governing professional bodies, engineers are now required to include risk assessment as an integral part of their systematic design. The probability approach to risk analysis has been an obvious choice to most engineers. Pine and Thin (1993) applied risk analysis to a rib pillar designed at South Crofty Mine, Cornwall, England. In their application, the safety factor was used to measure safety and was defined as the ratio of capacity to demand, where capacity and demand refer to pillar mean strength and mean imposed stress respectively.

Note that in sublevel open stoping the rib pillar is vertical with width and length measured along the plane of the orebody. New methods are needed for determination of a peak and post-peak behaviour of pillars using the back analysis procedure within time dependent visco-elastic rock mass. In order to implement current technology to reduce rock related accidents and improve productivity, new ideas and research are necessary to overcome changing conditions in depth, environment, geology and rock mass. Recent experience shows that current pillar systems no longer provide adequate regional support in deep mines. Therefore, an understanding of and obtaining post-excavation constitutive rock mass model are needed to develop effective non-linear techniques of solid mechanics to allow the exploitation of computer-aided modelling and design in the evaluation of mining strategies.

The engineering approach to the geomechanical mine design problem requires prior definition of stress-strain behaviour of the rock mass. Important aspects of this behaviour are constants relating stress and strain in the elastic range, the stress level at which yield, fracturing or slip occurs within the rock mass, and the post peak stress-strain behaviour of the fractured or 'failed' rock. Most of the rock mass does not deform immediately after loading, but rather deformation develops progressively with time. The term 'creep' is used to denote slow progressive deformation that solid bodies undergo under long term loading. In the theoretical analysis of peak and post-peak deformation of a rock mass, an equivalent time dependent physical model could be considered. This could involve a series connection of Hooke's and Kelvin-Voit models which are well fitted for use as a simulation of stress-strain relation of rock mass surrounding mine pillars under rapidly

imposed load, and a Kelvin model for a simulation of a non-linear irreversible post failure deformation progress of a pillar. To date, no analytical procedure has been developed to assess the initial displacement and parameters of the time dependent rock mass behaviour, such that the resultant stress-strain curves obtained from field measurements, are in good agreement with the post-excavation constitutive rock pillar model.

If stope pillars are left inside a sublevel open stope, the pillars would be loaded horizontally as opposed to the traditional loading assumed by the tributary area method of analysis. In this case the overburden stress due to the rock weight on the hanging wall side of the orebody is not vertically loaded on top of the pillar, but rather its horizontal component is added to the mining-induced stress and both act on the pillar horizontally. This fact makes it difficult for researchers to develop a formula to define the situation as it has been defined for near horizontal orebodies and more notably for coal.

The stability graph method was first proposed by Mathews (1983), and was followed up by Potvin (1988), Potvin and Milne (1992) and Nickson (1992). The modified stability graph method is adapted in this research and used to dimension and assess the stability of the open stopes. The stability graph method of cable bolt design is the most influential key factor in sublevel open stope design. The recent version of the method is based on the analysis of more than 350 case histories collected from Canadian underground mines [Hoek et al., 1995]. This method assesses the stability of the stope to determine whether the stope will be stable without support, stable with support, or unstable even if

35

supported. The input parameters are the strength and structure of the rock mass, the stresses around the opening and the size, shape and orientation of the opening. The design method is based on the calculation of the modified stability number, N', and the shape factor or hydraulic radius, HR.

3.4.3 Cable bolt Design in Open Stopes

For a stope requiring support, the cable bolt density design chart is used as a preliminary design guide for the cable bolt intensity [Nickson, 1992]. The chart relates, the cable bolt density to the frequency of jointing through the block size (parameters RQD/J_n) and the hydraulic radius of the opening. The guide lines for design have been proposed such that the length of the cable should be approximately the same size as the excavation span, and the design method has been modified to include the mode of failure, such that the kinematics of failure are considered during design.

As with all empirical methods, the main disadvantage of the stability graph method, which is used to dimension open stopes, is that it is site specific. Hence when the method is being applied to a different mine other than the one where the case histories data came from, the method should only be limited to similar conditions to those where it was developed. Hoek et al (1993) further cautions that there might be uncertainties in the value of the modified Tunneling Quality Index, Q', due to the fact that the number of joints and other discontinuities in a rock mass is highly variable. The quality of cable installation, grouting and tensioning could have adverse results on the performance of the cable bolts. This design method does not include the modifying elements like plates or

birdcage cable bolts since the use of these items was limited when the graphs were developed.

Bawden et al. (1992) investigated the variation in cable bolt capacity due to rock mass and mining induced effects, in order to optimize cable bolt performance at any operation. Once the design has been implemented and mining commences, the performance of the cable-bolt is monitored as mining of the stope progresses. If failure occurs, it could be due to breaking cables, stripping of rock and grout off of the cables or pulling of cables out of the holes. If the cables break, the pattern could be tightened or the cable could be changed to a twin stranded cable which has more load capacity. In the case where the rock strips off of the cables or the cables pull out, the cable bolt performance is unsatisfactory and the engineer must re-evaluate the design.

It should be noted that the use of cable bolts is now seen as a solution to curb dilution in sublevel open stopes. The stopes are cable-bolted from the adjoining drill drives so that during mining the stope hanging wall does not cave in causing dilution. The reduction in dilution is supposed to balance the cost of cable bolt installation. There has also been the introduction of cemented backfill in sublevel mining. This is mainly notable in the mining of the thick orebodies where echelon stope configuration is unavoidable.

3.5 NUMERICAL METHODS IN OPEN STOPE DESIGN

Though numerical models are not the solution to all problems, the last decade has seen a dramatic increase in their use to solve geotechnical problems. Large-strain continuum codes (FLAC and FLAC^{3D}) and large relative displacement discontinuum code (UDEC and 3DEC) have been applied to problems in civil, mining and petroleum engineering. Research areas have included numerical experiments on rough joints in shear, studies of tunnel break-out and notch formation, and dynamic analysis of explosion-induced rock failure (including fragmentation and gas interaction) [Lorig, 1997].

Models have been used in geotechnical engineering in an attempt to identify and understand failure mechanisms, and geologic factors of importance in controlling response. They have also been used to guide field investigations, conduct parametric evaluations for optimizing design and assess hazard or risk. The methodology for modelling involves the rock mass which has unknown structure, stress state, properties and large unknown variables. Hence the modelling methodology must be different from that of a fabricated structure (in which these things are known). Therefore the computer model is used as a laboratory to perform experiments leading to understanding of mechanisms, knowledge of parameter dependence and means to check theories or hypotheses. The new knowledge may lead to new theories or simple conceptual models that can be used in design.

Starfield and Cundall (1988) have attributed the reason for upsurge in numerical modelling to the availability of versatile and powerful computer packages. It may also be due to dramatic increase in the ability to include geological detail in the construction of a model and the manifest success of modelling in other branches of mechanics. The reasons to use numerical methods to solve geomechanics problems are that other methods (e.g. analytic, limit equilibrium) are not available, or tend to oversimplify the problem, leading to overly conservative solutions. Empirical methods are also limited because they cannot be extrapolated to solve other field problems. Numerical methods allow for the explanation of observed physical behaviour (e.g. collapse) and multiple possibilities (e.g. hypothesis, design options) can be evaluated.

A review of the modelling methods has revealed four numerical methods comprising the discrete continuum, boundary element, discontinuum and hybrid methods. The choice of numerical methods for geomechanical problems is between continuous and discontinuum methods. The continuous methods comprise the boundary element (integral) and the finite element/finite difference (differential) methods. While the discontinuum methods comprise the discrete element and limit equilibrium. Each method has advantages and disadvantages which need to be matched to a particular problem [Lorig, 1997].

Typically, boundary element methods are applied where elastic material behaviour is expected for limited number of material types in a quasi-static analysis. The finite element/finite difference is used for a non-linear material behavior for multiple material types in a dynamic or quasi-static analysis. The discrete element is used in jointed media

with multiple integrating bodies where the failure mode is unknown, and finally the limit equilibrium is used for a specified failure mode with few densely packed bodies.

The role of modeling in rock engineering is generally in back-analysis to understand mechanisms, design conceptualization, detailed design and research. The key areas of uncertainty in application are rock mass geology, rock mass properties, constitutive model and in-situ stress. Some modelling difficulties include extreme dependence of behavior on initial conditions (chaos) and the release of kinetic energy when a local collapse occurs (physical instability).

3.6 THE TOTAL OPEN STOPE DESIGN APPROACH

Szymanski et al. (1997) proposed the total open stope design approach to provide engineers with simple design guidelines and practical methods. These methods account for the impact of blasting including geomechanics during excavation design stage by modelling and systematically addressing blast related problems. The method is built on the practical and theoretical achievements to date and was aimed at developing a classification scheme to describe rock mass blastability. A classification scheme to describe the potential of the rock mass to suffer damage from blast vibrations of known characteristics. A model of fragmentation, which is sensitive to blasthole timing; and a method to extend the application of conventional stability charts, used in excavation design to incorporate the effects of blasting and blast damage. The method also emphasized an integrated design system which utilises these engineering tools to enable a

site engineer to continually assess the likely impact of blasting operations on excavation performance, damage, dilution and general stability. And the development of a comprehensive data base for data storage, designs and field performance so as to encourage a systematic approach to the engineering of blasts guided by actual site performance and experience. The optimization of fragmentation, minimization of dilution and maintenance of stability are critical to the economics of many mines. These factors are particularly important to operations extracting low grade deposits, narrow irregular ore bodies or operations that use small stoping methods such as benching where fragmentation, dilution and stability requirements are critical to the drilling, blasting, support and mucking cycle.

However, there is a continuing gap between published research and its effective application to the routine problems facing mining operations. A number of mine operators continue to use trial and error methods to determine stable stope spans or the size of hanging wall exposures that can be achieved under different mining and geological conditions. This is particularly true in sublevel and bench stopes with steeply dipping or weak hanging walls. Blast effects can prevent the achievement of the spans or exposures designed and deemed stable using static analyses. The blasting effects are not well understood and therefore are not incorporated into existing design methods.

In narrow orebodies, situations often arise where parallel stopes separated by a narrow pillar need to be extracted simultaneously. A conservative approach is often adopted where a stope is fully mined and filled before mining is begun in the adjacent stope.

There are usually significant economies of scale if the second stope can be worked while the adjacent stope is still open. This is not routinely practised because of the impact of blasting on exposed hanging walls. Also, narrow pillars may not be well understood to allow the design of simultaneous operations with sufficient confidence and safety. In addition, fragmentation requirements should be specified in order to maximise productivity in downstream processes such as transport, crushing and grinding.

CHAPTER 4

ANALYTICAL METHODS OF OPEN STOPE DESIGN

4.1 INTRODUCTION

This section describes the mathematical models used to assess the stability of open stopes' surface dimensions. The classical flexure equation, originally derived for a simple beam with a distributed load, has been used to simulate either a crown pillar or mine hanging wall. It was used to determine the maximum allowable span without failure by rupture or by shearing at the ends of the beam. Another attempt has been made to represent a mine roof with a voussoir beam, a concept derived from civil engineering practice. This method has been adapted to derive the maximum allowable span for a mine roof or crown pillar in a steeply dipping orebody.

The stresses around the stope boundaries are difficult to model mathematically. However, preliminary analysis could be verified using boundary element software in the form of PHASES. The mechanics of drawing ore from the draw points have been modeled mathematically using equations originally derived for ore-bin drawing [Coates. 1965]. An attempt has also been made to look at the mechanics of planned and unplanned dilution.

4.2 SIMPLE BEAM THEORY

Coates (1965) assumed that beams are structural elements that support loads applied transversely to their length and, as such, are similar to the cases of roof rock over extensive workings or at shallow depths. Beams are subjected to bending stresses and shear stresses as a consequence of supporting loads in this manner. If the roof of a mine or the crown pillar in a steeply dipping orebody was assumed to behave like a transversely loaded simply supported beam, the resultant stresses can be determined by creating free body diagrams and using the equations of equilibrium, as shown in Figures 4.1 (a) and (b).

Figure 4.1 a) A loaded simply supported beam, b) Section cut through the beam

If a section dX was cut out of the crown pillar or roof rock and was supporting a distributed load W as shown in Figure 4.1(b), the equations of equilibrium and compatibility can be applied to the section. By analysis, the equilibrium of the section can be established from the sum of vertical forces and the sum of the moments about any corner as follows;

$$\sum Fy = W + \frac{dV}{dX} = 0 \qquad \text{i.e.} \qquad W = -\frac{dV}{dX} \tag{4.1}$$

$$\sum M = VdX = dM = 0 \qquad \text{i.e.} \qquad V = \frac{dM}{dX} \tag{4.2}$$

The equilibrium equations relate loading W, shear resistance V and the resisting moment M. If a point in the crown pillar was known where the shear force V was zero, (i.e. $\frac{dM}{dX} = 0$), the resisting moment M will be a maximum.
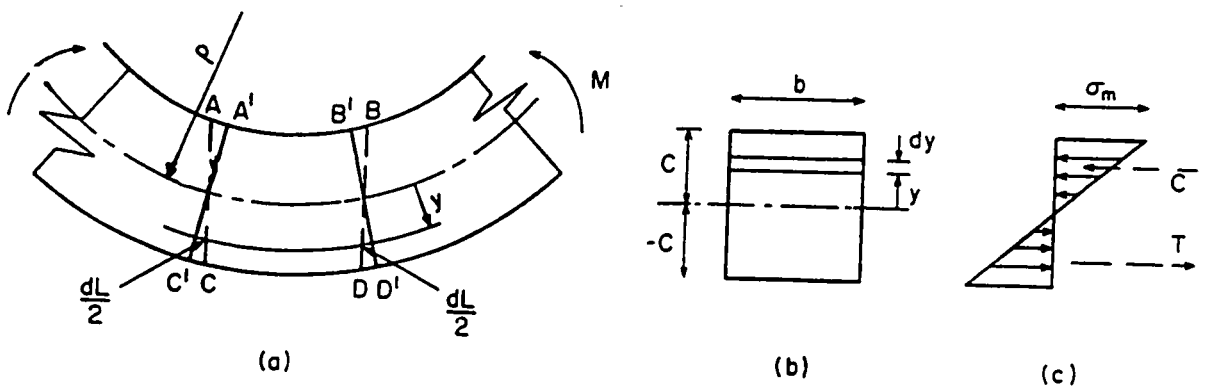
Figure 4.2 Pure bending of a beam

These assumptions satisfy the state of the crown pillar or roof rock in equilibrium. However, the internal effects of the external loading has to satisfy the requirements of compatibility as shown by Figures 4.2 (a) and (b). If the equilibrium equations could be applied by taking the horizontal forces acting externally on the face BD, there would be a compressive force, C, and a tensile force, T, acting as shown in Figure 4.2 (c) to give equation (4.3), where σ_m is the extreme fiber stress.

$$\sum Fn = \int_{+c}^{-c} \sigma_m \left(\frac{y}{c} \right) dA_r = \sigma_m \int_{+c}^{-c} \left(\frac{y}{c} \right) dA_r \tag{4.3}$$

dA_r is the elemental area shown in Figure 4.2 (b) (i.e. $dA_r = bdy$); c is the distance of the neutral axis from the extreme fiber; and σ_m is the extreme fiber stress. Equation (4.3) can also be re-written as;

$$\sum Fn = \left(\frac{\sigma_m}{c}\right)\int_{+c}^{+c} ydA_r = \frac{\sigma_m}{c}.\overline{y}.A_r = 0 \qquad (4.4)$$

$\overline{y}$ is the distance to the centroid of area A_r. The centroid of the crown pillar or roof rock is defined by;

$$\int_{-c}^{+c} ydA_r = \overline{y}A_r \qquad (4.5)$$

The neutral axis of the crown pillar or the roof rock coincides with the centroidal axis of the cross-sectional area. This only occurs when straight, non-curved crown pillars or roof rocks are considered. Equating the external moment to the section BD in Figure 4.2 (a) with the couple resulting from the tension and compression acting normal to the section BD, results in equation (4.6). In equations (4.6) and (4.7), Ma is the moment about the neutral axis and M is the sum of moments of the external forces respectively.

$$Ma = \int_{+c}^{-c} y.\left\{\sigma_m\left(\frac{y}{c}\right)\right\}dA_r - M = 0 \qquad (4.6)$$

$$M = \frac{\sigma_m}{c}\int_{+c}^{-c} y^2 \, dA_r \qquad (4.7)$$

Then,

$$I = \int_{+c}^{-c} y^2 dA_r \qquad (4.8)$$

and

46

$$\sigma_m = \frac{Mc}{I} \qquad (4.9)$$

M is applied to one side of the section and taken about the neutral axis of the section. I is the moment of inertia of the cross-sectional area as given by equations (4.8) and (4.9). This analysis could be used to determine the span and thickness of the crown pillar and to assess its stability with respect to rupture or shear failure at the ends. The maximum span allowable for the roof could also be assessed for stability flexure and shear failure.

4.3 VOUSSOIR BEAM AS LINEAR ARCH

Excavations of large span openings parallel to laminated or bedded structures are characteristic to open stope mining. Standard beam analysis can be used to evaluate the stability of the roof or hanging wall, provided the discontinuity forming the lamination is the sole structural feature to be considered. The beam analysis would require the excavation technique, which minimises damage to the surrounding rock including overbreaking into the hanging wall. However, in most cases, structures crosscut the main laminations reducing or eliminating the ability of the rock to carry tensile loads parallel to the lamination, making standard elastic beam analysis inapplicable. In this case, an alternative technique called the voussoir arch is used (Figure 4.3).

According to Hutchinson et al. (1996), Evans first applied the Voussoir analysis in rock mechanics in 1941. However, it has since been modified over the years [Beer and Meek, 1982; Brady and Brown, 1985], correcting some earlier assumptions and improving the solution technique.

σ_{MAX}

CRUSHING

DILATATION

ORIGINAL OPENING

σ_{MAX}
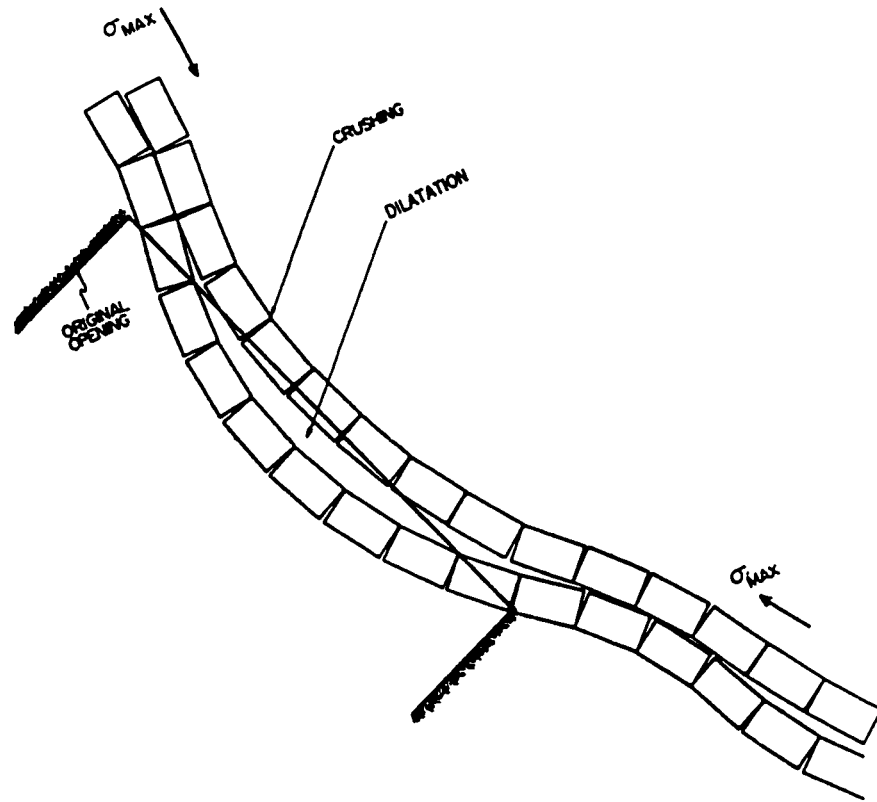
Figure 4.3: Stope hanging wall showing general voussoir-arch deformation

Though a lot of work is still going on in this method, Hutchinson et al. (1996) tried to correctly incorporate arch deflections and to incorporate more acceptable design confidence limits into the solution by making the following assumptions:

- The authors assumed that the out-of-plane depth of the beam is very large compared to the in-plane. Only a unit depth is considered with all deformations occurring in a plane.

- Cross-cutting structure is angled from the wall normal at significantly less than the minimum angle of friction assumed for the jointed surfaces.

- The beam is not capable of sustaining tension, as it deflects, a parabolic compression arch develops.

- Initial lateral stress resulting from in-situ stress and excavation geometry is not considered in this analysis. The beam is assumed to be initially stress free.

- The abutments are stiff - they do not deform under the arching stress. For large span to lamination thickness ratios, the deformation of the abutments can normally be assumed to be negligible compared to the shortening of the roof beam.

There is no explicit solution to this problem and the iteratively obtained solution is approximate, rendering the problem statistically indeterminate. The problem is highly sensitive to rockmass modulus, hence, the lowest expected value should be used and a safety factor of 1.5 to 3 is advisable. For a horizontal beam, the problem geometry is represented by Figure 4.4.
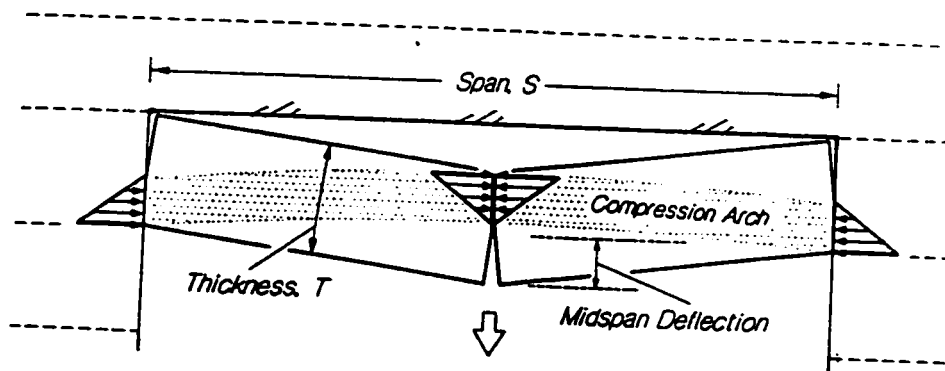
Figure 4.4: Problem geometry for Voussoir stability analysis.

When using the voussoir arch method, certain input parameters must be specified. The rockmass stiffness (E), measured in Mpa, parallel to the excavation surface, uniaxial compressive strength of the rock σ_c, also measured in MPa should be specified. The specific gravity (dimensionless) or the specific weight of the rock (γ) must also be specified. The thickness of the continuous laminations (T) parallel to the excavation surface should be specified in metres. The span of the excavation (S) should also be specified in metres. If the excavation to be analysed is long, S should be taken as the short dimension. The inclination or dip of the excavation surface (α) should be measured in degrees from horizontal.

Mine spans can be longer than the spans determined by a continuous beam analysis, because of the arching similar to the voussoir arch. The fractured roof would be entirely supported by compression and shear resistance in a voussoir arch unlike a continuous beam which depends on the tensile or flexural strength of the rock. In a voussoir arch, two failure modes are analyzed. The beam can fail by crushing at the top and bottom resulting in beam failure when the compressive strength of the rockmass is exceeded. The other failure mode could be by snap-thru at the middle of the beam resulting in immediate collapse. This is controlled mainly by geometry. Both failure modes are dependent on inclination and density and are most sensitive to rockmass modulus as shown in Figure 4.5.

The calculation flow chart for the iterative voussoir solution is shown in Figure 4.6. The auxiliary variables include the arch thrust moment arm between the centre and the abutments (Z), the maximum and average arch stresses, Fm, and, Fav, respectively. The arch shortening is represented by ΔL, while the ratio of arch thickness to beam thickness is represented by N. It should be noted that the buckling limit is directly proportional to the unsolvable cases of N.

Brady and Brown (1981) estimated N of 0.75 to minimize the number of iterations required for the solution. Their iterative process assumed a beam initially free of lateral thrust and subject only to gravity loading, and it was aimed at finding the final state of lateral thrust. Hutchinson et al. (1996) iteration procedure is the one shown in Figure 4.6.
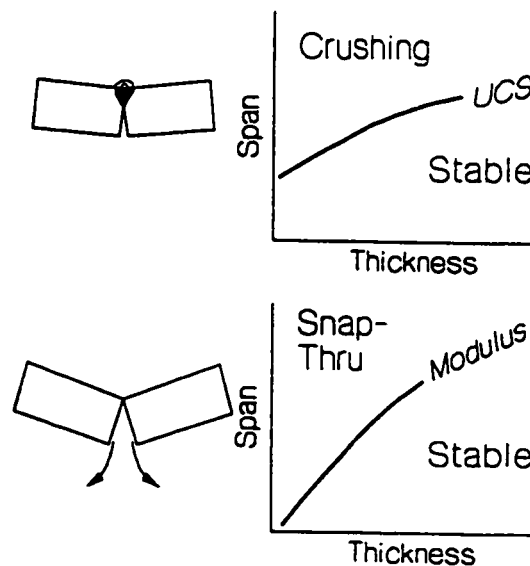
Figure 4.5: Voussoir arch failure modes.

START

Input:
S
T
E
γ
α
σ_c

1) $\gamma_e = \gamma \cos \alpha$

PRIMARY LOOP: N
$N = 0.01$ to 1.00 (increment by 0.01)

2) $Z_0 = T(1 - \frac{2}{3}N)$

3) $L = S + \frac{8}{3S}Z_0^2$

SECONDARY LOOP: ΔL
INITIAL $\Delta L = 0$ (calculate new ΔL)

ABORT current N - GOTO next N

4) $Z_{chk} = (\frac{8Z_0^2}{3S} - \Delta L)$

$Z_{chk} < 0$??

YES
(unsolvable)

NO (solvable)

Record Min. & Max. solvable values of N
N_{min} N_{max}

5) $Z = \sqrt{\frac{3S}{8}} Z_{chk}$

6) $F_m = \frac{\gamma_e S^2}{4NZ}$

7) $F_{av} = \frac{F_m}{2}(\frac{2}{3} + \frac{N}{2})$

8) $\Delta L_{prev} = \Delta L$

9) $\Delta L = (\frac{F_{av}}{E}) L$

END LOOP when $|\Delta L - \Delta L_{prev}| \approx 0$

Record Min. value of $F_m \Rightarrow F_m'$
and corresponding N', Z' and Z_0'

END LOOP when $N > = 1$

Output:

10) Buckling Potential
$= 1 - (N_{max} - N_{min})$

11) F.S. for Crushing
$= \frac{\sigma_c}{F_m'}$

12) Midspan Deflection
$= Z_0' - Z'$

END

Figure 4.6: Calculation flow chart for the iterative voussoir solution

4.3.1 Deflection and Stability

According to the mathematical formulation, previously documented presentations of this solution have used an absolute snap-thru limit which is defined as the limit of stable deflection. It is difficult to reliably estimate lamination thickness, a parameter which may change as deflection and layer separation occurs, making the snap-thru limit (Buckling Limit = 1) extremely sensitive. As a result, large safety factors have been recommended [Beer and Meek. 1982; Brady and Brown, 1985]. Hutchinson et al.(1996) published some stability charts which utilized a design limit for snap-thru which is based on sensitivity or design confidence limit equivalent to a buckling limit of 0.35. The authors also realized that beyond this limit, small differences in thickness have an unacceptably large influence on stability, hence they adjusted their graphs for greater confidence in design. Figures 4.7 and 4.8 show a useful component of the analysis which can be utilized in excavation monitoring and design verification. Also for any span. inclination or rock modulus, the design snap-thru limit is reached when midspan displacements reach 10% of the lamination thickness. beyond which stability is unlikely as in point A of Figure 4.7.

Low compressive strength of the rock, as crushing failure becomes dominant, may further reduce the critical displacement of the laminations (deflection at failure). For a stable excavation surface, the actual midspan displacement at equilibrium is dependent on all of the input parameters as shown by point B in Figure 4.7.
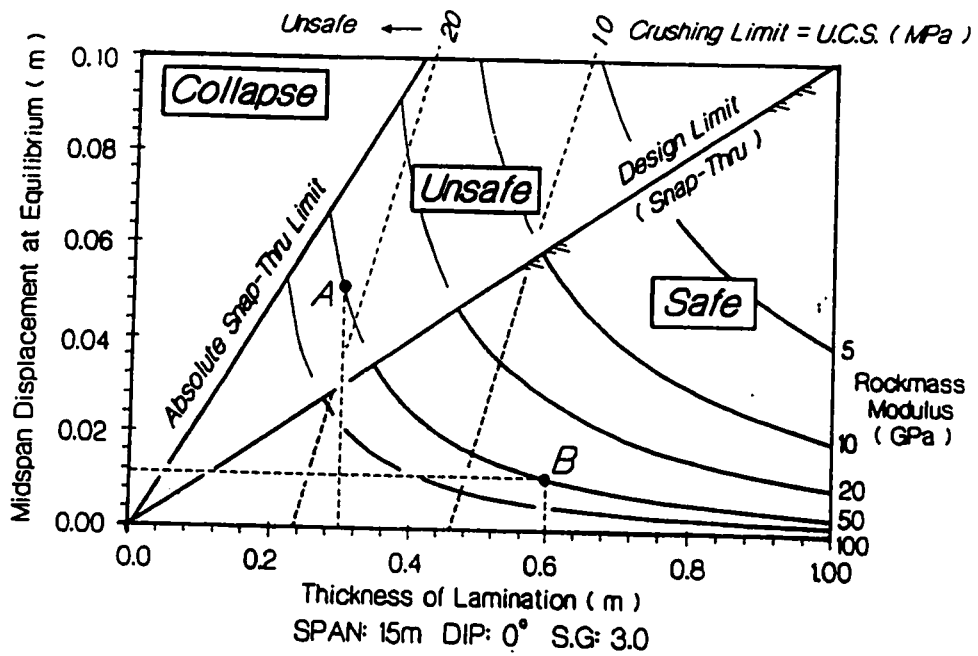
Figure 4.7: Limiting beam deflection for buckling and crushing failure modes
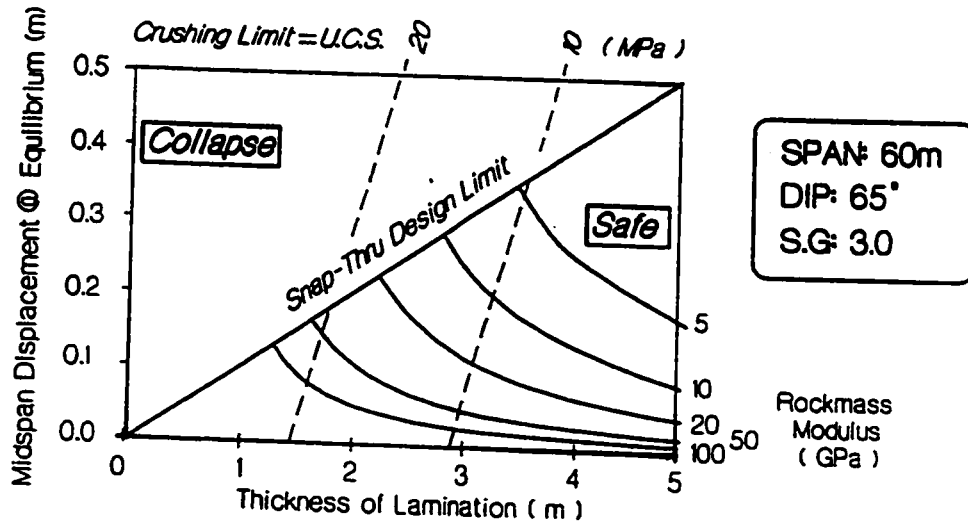
Figure 4.8: Limiting deflection for a beam

4.3.2 Span versus Thickness for Inclined Surfaces

When applying voussoir analysis to inclined surfaces, certain simplifying assumptions must be made which do not consider the distribution of pressures due to self-weight acting parallel to the beam. However, Hutchinson et al. (1996) derived Figures 4.9 and 4.10 for laminated hanging walls inclined at 65° (a case similar to Selebi North mine) and argued that a reasonable solution may be obtained and applied with appropriate factor of safety (>2).

4.3.3 Support Rationale for the Voussoir Beam

If the assumptions made in the voussoir beam analysis could be validated, a support pattern could be developed to create a laminated beam or plate which will then prevent further destabilization of the hanging wall.

In such a beam, the cables near the abutments could reinforce the joint surfaces, increasing resistance to internal shear which could lead to delamination and destabilization (smaller thicknesses have smaller critical spans). These could be cables installed at the top and bottom sublevels of the open stope.

The second role of the cables would be to prevent delamination through the central portion of the beam. The cables could be installed normal to the laminations and covering the span area. These cables should be designed as stiff reinforcement within the zone of rock equivalent in thickness to a self-supporting beam as calculated by the voussoir analysis. Beyond this limit, an optimum cable array would have a more ductile

BEAM (b ≫ a)   *Snap-Thru Rockmass Modulus (GPa)*
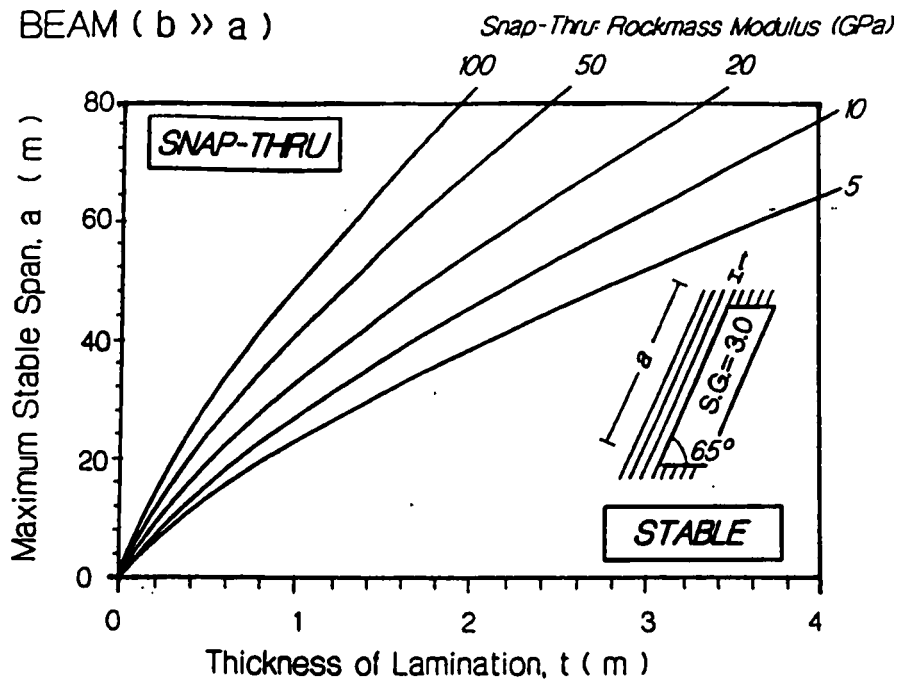
Figure 4.9: Snap-thru failure for laminated inclined hangingwalls
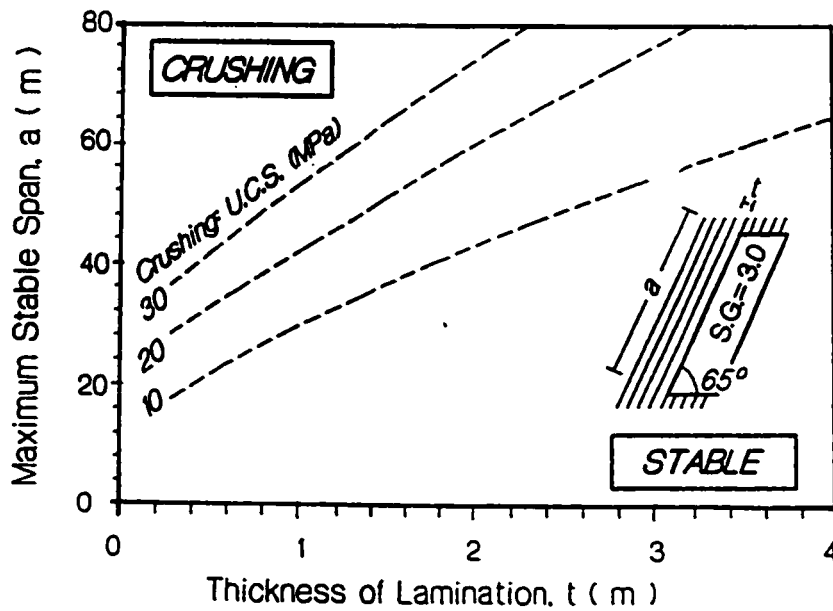
Figure 4.10: Crushing failure for laminated hangingwalls

response to allow the beam to deflect a small amount to generate the required compression for stability.

A suitable anchor length would be required along the open stope periphery. The calculations for the cable spacing (Figure 4.11) are based on the deadload of the beam. Therefore, if the cables can hold the weight of this beam, stability along the hanging wall should be assured. According to Hutchinson et al. (1996), this result is usually much more efficient than a pure deadload estimate on a relaxing hanging wall (no beam formation).
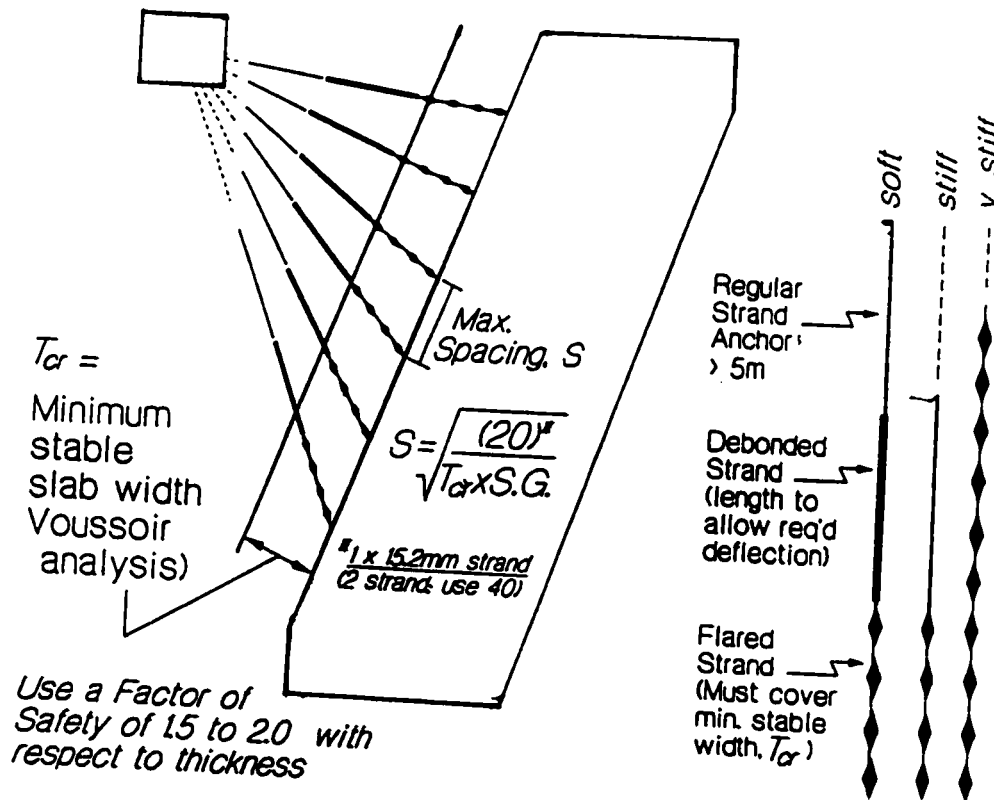
Figure 4.11: Cable spacing and length guide lines using voussoir approach

4.4 ZONE OF INFLUENCE

Brady and Brown (1981) define the zone of influence as that domain in which

$$|\sigma 1 - P\max| \geq 0.05 P\max \tag{4.10}$$

or

$$|\sigma 3 - P\min| \geq 0.05 P\max \tag{4.11}$$

Pmax and Pmin represent the larger and smaller field stresses p and kp, respectively. The ellipse representing the opening has an aspect ratio of $q = \dfrac{a}{b}$. If Wl and Hl are the dimensions of the elliptical zone of influence as shown by Figure 4.12. Brady and Brown (1982), showed that equations (4.10) and (4.11) were satisfied when either

$$W1 = H\left\{10\alpha|q(q+2) - k(3+2q)| \right\}^{\frac{1}{2}} \tag{4.12}$$

or

$$W1 = H\left\{\alpha\left[10(k+q^2) + kq^2\right]\right\}^{\frac{1}{2}} \tag{4.13}$$

The width of the area of influence would be the larger of equations (4.12) or (4.13), and the height of the area of influence would be given by the larger of equations (4.14) or (4.15).

$$H1 = H\left\{10\alpha|k(1+2q) - q(3q+2)|\right\}^{\frac{1}{2}} \tag{4.14}$$

or

$$H1 = H\left\{\alpha\left[10(k+q^2) + 1\right]\right\}^{\frac{1}{2}} \tag{4.15}$$

$\alpha = 1$ if $k < 1$ and $\alpha = \dfrac{1}{k}$ if $k > 1$. For cases involving extreme values of q and k. some

modification of these formulae were needed as follows; (i) if $k > 5$, and $q > 5$. W1 is

increased by 15%; (ii) if $k < 0.2$, and $q < 0.2$, H1 is increased by 15%. This concept can

be used to find out whether or not the main ramps would be developed within the zone of

influence of the stopes, a fact which is necessary to assess their stability.

4.5 STRESSES AROUND UNDERGROUND OPENINGS

Hoek and Brown (1994) used the boundary element method to produce stress contour

plots for various underground excavations, which provide a useful guideline for design.

However, if Figure 4.12 represents a mine opening with p as the vertical stress. k is the

stress concentration factor. and W and H are the stope dimensions.
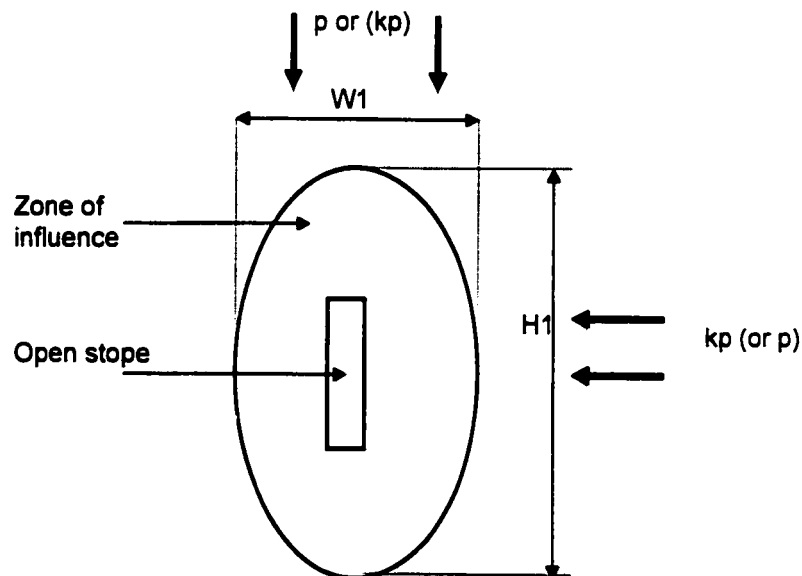
Figure 4.12: Nomenclature for defining the zone of influence of an open stope.

Hoek and Bray (1985) derived a manual solution for analyzing stresses around openings using various geometric parameters. The scope of such analysis is beyond this thesis. However, if the critical stress concentration was less than the uniaxial strength (compressive or tensile) failure will not occur around the excavation. Hence in designing a single opening, the critical stress should not exceed the uniaxial strength, as safety factor is defined as tolerable stress (i.e. strength) divided by critical stress and if it is less than 1, failure would occur. In order to estimate the in-situ stresses acting on an element of rock at depth, Hoek et al. (1995) assumed the following relationships:

$$\sigma_v = \gamma z \qquad\qquad (4.16)$$

$$\sigma_h = k\sigma_v = k\gamma z \qquad\qquad (4.17)$$

σ_v is the vertical stress; γ is the unit weight of the overlying rock; z is the depth below surface and σ_h is the horizontal stress, and k is the ratio of the average horizontal stress to the vertical stress. For a case shown by Figure 4.13, equations (4.18) and (4.19) define the state of the stresses at the sides and crown respectively.
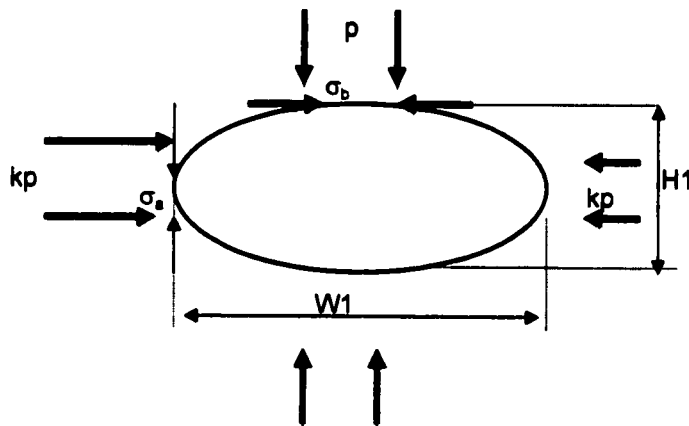
Figure 4.13: Underground excavation with axis parallel to the field stresses

$$\sigma_a = p(1-k+2q) \tag{4.18}$$

$$\sigma_b = p\left(k-1+\frac{2k}{q}\right) \tag{4.19}$$

σ_a and σ_b are the respective boundary circumferential stresses in the side wall and crown of the excavation.

4.6 STRESS DISTRIBUTION ON PILLARS

Coates (1965) suggested that for practical purposes, when the orebody dips between 60 degrees and 90 degrees, the dip angle could be assumed to be 90 degrees for average pillar shear stress calculations.
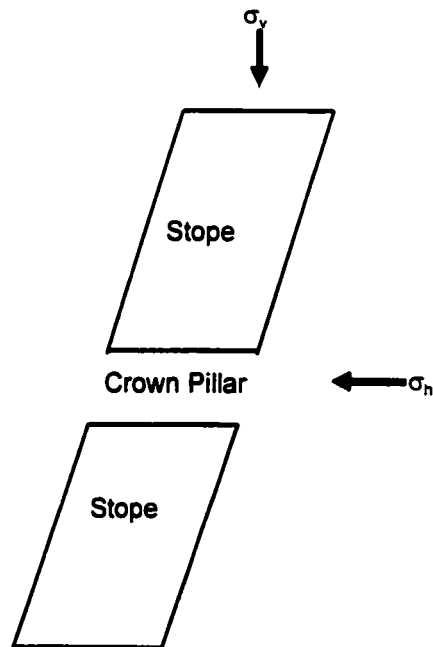
Figure 4.14: Typical Crown Pillar

If Figure 4.14 represents a typical crown pillar between steep open stopes, where the vertical stress, σ_v, and the horizontal stress, σ_h, are acting as shown, the average pillar stress, σ_p, could be calculated by equation (4.20).

$$\sigma_p = \gamma z (1 + \frac{w_o}{w_p})$$ (4.20)

w_o and w_p are the widths of stope and pillar respectively. Substituting equation (4.17) into equation (4.20), the pillar stress is then calculated by equation (4.21).

$$\sigma_p = k \gamma z (1 + \frac{w_o}{w_p})$$ (4.21)

The average pillar strength, σ_s, is calculated using the compressive strength of the intact rock, σ_c, the rock mass strength factor, r, and pillar shape factor f. Therefore, the pillar strength is given by equation (4.22).

$$\sigma_s = \sigma_c.r.f$$ (4.22)

The product of a and b gives the strength of a cube of rock mass size and the principal compressive strength, σ_u, is related to the uniaxial compressive strength of the intact rock by the Hoek and Brown constant, s.

$$\sigma_u = \sqrt{s}.\sigma_c$$ (4.23)

where

$$s = \exp\left(\frac{RMR - 9}{9}\right)$$ (4.24)

RMR is the unadjusted rock mass rating; the factor f is defined as follows:

$$f = 0.778 + 0.222 \frac{w_p}{h}$$ (4.25)

h is the pillar height. The factor of safety, F_s, is calculated as follows:

$$F_s = \frac{\sigma_s}{\sigma_p}$$

(4.26)

The safety margin (SM) is given by Pine (1991) as:

$$SM = \sigma_s - \sigma_p$$

(4.27)

Failure would occur when F_s and SM are 1 and 0 respectively.

4.7 ORE DRAWING

A theory originally derived for the determination of pressure in ore bins was used by Coates (1965) to analyze the stresses that exist in blasted ore in the stope immediately before drawing occurs. Figure 4.15 represents an idealized case of ground above a circular trap-door of radius R. To support the ground above the trap-door, a pressure P_v is applied. The major and minor principal stresses are assumed to be vertical and horizontal respectively. An angle of $45 + \frac{\phi}{2}$ is assumed for any incipient failure plane.

A horizontal slice of thickness, dz, is taken from the ground, with a vertical stress σ_v acting on the top surface and $\sigma_v + d\sigma_v$ acting upwards at the bottom surface; dW is the gravitational body force acting downwards on the element. The shear stress, τ, is acting upwards on the side of the element while σ_h is a horizontal normal stress (see Figure 4.15). The equilibrium of the element is analyzed when there is no motion.
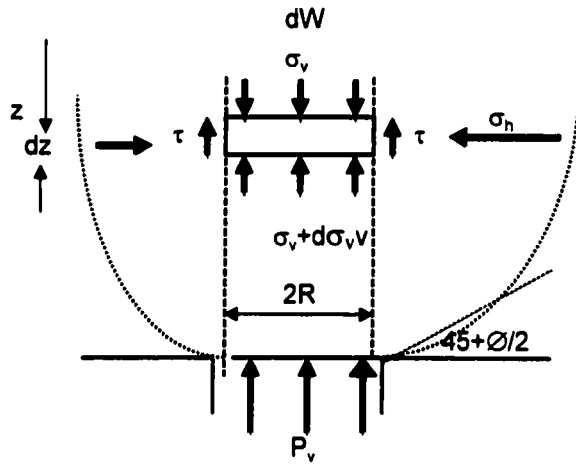
Figure 4.15: Mechanics of Ore Drawing

If equation (4.17) is used, the sum of the vertical forces is given by equation (4.28) for equilibrium.

$$\sum Fy = dW + \sigma_v.A_r - (\sigma_v + d\sigma_v)A_r - \tau.P_v.dz = 0 \tag{4.28}$$

A is the horizontal area of the slice; P_v is the perimeter; $dW = \gamma.A_r.dz$ and γ is the unit rock weight. Therefore,

$$\frac{d\sigma_v}{dz} = \gamma - \tau.\frac{P_v}{A_r} \tag{4.29}$$

With the flow along the plane on which τ is acting, the maximum value of τ is:

$$\tau = c_h + \sigma_h \tan\phi \tag{4.30}$$

$$= c_h + k\sigma_v \tan\phi$$

Thus,

$$\frac{d\sigma_r}{dz} = \gamma - c_h \cdot \frac{P_v}{A_r} - k\sigma_v \tan\phi \cdot \frac{P_v}{A_r}$$

(4.31)

The solution for the differential equation results in

$$\sigma_v = \frac{\frac{A_r}{P_v}\left(\gamma - c_h \cdot \frac{P_v}{A_r}\right)\left(1 - e^{-kz\tan\phi} \cdot \frac{P_v}{A_r}\right)}{k \tan\phi}$$

(4.32)

and

$$\sigma_h = \frac{\frac{A_r}{P_v}\left(\gamma - c_h \cdot \frac{P_v}{A_r}\right)\left(1 - e^{-kz\tan\phi} \cdot \frac{P_v}{A_r}\right)}{\tan\phi}$$

(4.33)

Thus, on the trap-door, $\sigma_v = P_v$, and if $c_h = 0$

$$P_v = \frac{\frac{A_r}{P_v} \cdot \gamma \left(1 - e^{-kz\tan\phi} \cdot \frac{P_v}{A_r}\right)}{k \cdot \tan\phi}$$

(4.34)

And if $z = \infty$ and $c_h = 0$,

$$P_v = \frac{\frac{A_r}{P_v} \cdot \gamma}{k \cdot \tan\phi}$$

(4.35)

If A_r is an area of a circle of radius R, for $z = \infty$ and $c_h = 0$, then

$$P_v = \frac{R \cdot \gamma}{2 \cdot k \cdot \tan\phi}$$

(4.36)

If A_r is a rectangle bxl, for $z = \infty$ and $c_h = 0$, then

$$P_v = \frac{\gamma \cdot b}{2 \cdot \left(\frac{b}{l} + 1\right) k \cdot \tan\phi}$$

(4.37)

and if $l \gg b$:

$$P_v = \frac{b.\gamma}{2.k.\tan.\phi} \qquad (4.38)$$

and

$$P_v = \frac{b.\gamma}{2.\tan.\phi} \qquad (4.39)$$

If the boundaries of flow above the trap-door were assumed vertical and flow was assumed to follow Mohr's diagram of stresses, then for a cohesionless material;

$$k = \frac{\sigma_h}{\sigma_v} = \frac{1}{1+2\tan^2\phi} \qquad (4.40)$$

The ratio of horizontal to vertical stress for a material with cohesion is given by;

$$k = \frac{\sigma_v - 2.c_h.\tan\phi}{\sigma_v\left(1+2.\tan^2\phi\right)} \qquad (4.41)$$

The above analysis could be used to determine the minimum size of box hole (draw point) required to draw a cohesive ore by solving for b while $P_v = 0$ in equation (4.32).

4.8 ORE DILUTION

In the case of non-entry mining systems, cables are one of the only options for support of inaccessible rock faces for stability and dilution control. The cost of mining a stope. could be directly affected by dilution control. The cost of dilution is many-fold: waste rock with little or no economic value is blasted, mucked, trammed. crushed, skipped. milled and impounded in a tailings dam, all at great costs which most companies cannot afford. In addition, the mill works at effectively only partial ore capacity, despite producing at the maximum possible milling rate. Additional costs are also incurred from

the unscheduled delays required to deal with oversize rocks, mucking waste rock and with consequent changes to the mining schedule.

According to Anderson and Grebenc (1995), Hemlo Gold mines employ modern technology to monitor individual stope performance. They use laser survey to collect the required information of each stope after mining is complete. Then the following factors are considered in assessing the performance of a stope.

$$\% Dilution = \frac{Waste\ dilution(t) + Backfill\ dilution(t)}{Planned\ tonnes(t)} x100$$

$$\% Recovery = \frac{Planned\ tonnes(t) - Ore\ lost\ in\ stope(t)}{Planned\ tonnes(t)} x100$$

$$\% Overbreak = \frac{Ore\ sloughing(t)}{Planned\ tonnes(t)} x100$$

Understanding the cause of failure in one stope, and the effective support design for the adjacent stope, dilution control could be achieved as illustrated by Figure 4.16. Due to some mining constraints which may require smoothing of stope outlines to facilitate blasting or due to other sources of planned dilution, all modern mining will have some minimal dilution limit. In cases where the orebody and the host rock are distinctly different (ore/waste contact), unplanned dilution due to sloughing waste rock can quickly render the stope uneconomic. It is this unplanned dilution component which can be tackled through improved stope design and through the use of cable bolt support. Cable bolts have proved to be effective in reducing sloughing and thereby reducing dilution. On the other hand cablebolts can facilitate the safe extraction of larger stopes. Pakalnis et

al. (1995) plotted some theoretical dilution values as a function of span and sloughing

depth for an unsupported stope of simplified geometry (Figure 4.17).
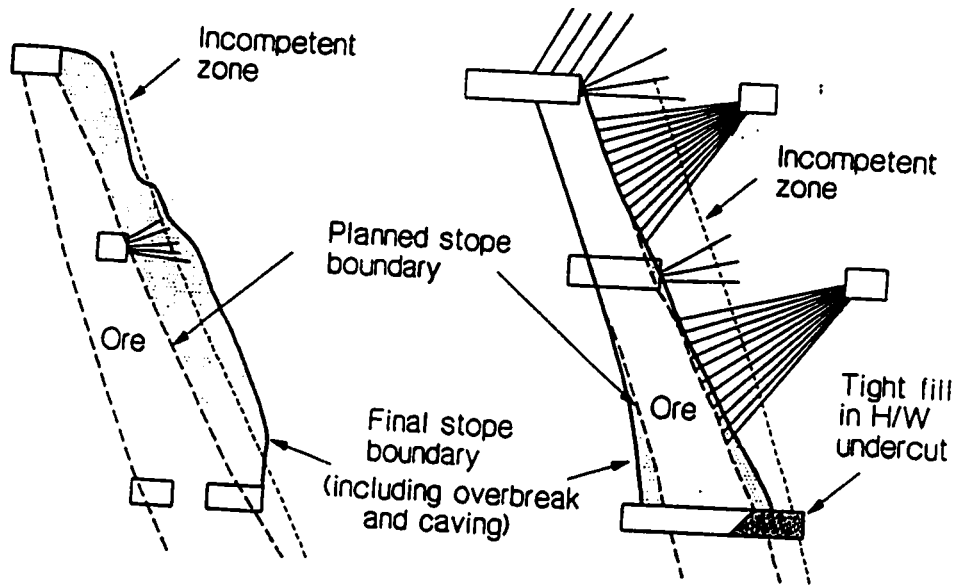
Figure 4.16: Cablebolting pattern and dilution surveyed in adjacent stopes at Hemlo

Gold (After Aderson and Grebenc, (1995))
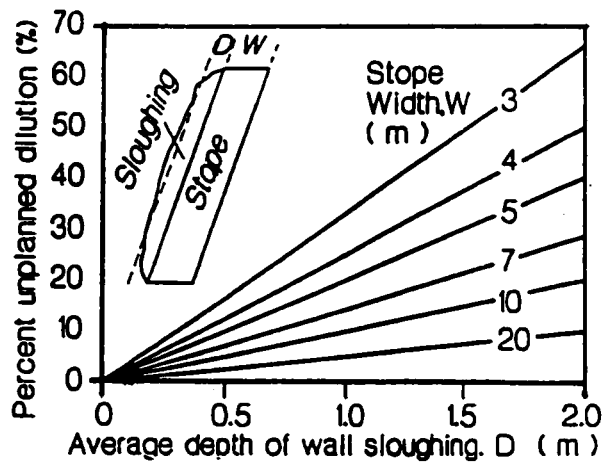
Figure 4.17: Dilution vs sloughing and span

Bawden et al. (1989) illustrated the extreme economic consequences of dilution (Figure 4.18), by showing how dilution moves through the system incurring additional mucking. haulage and hoisting costs as well as (and most importantly) displacing profitable ore (grade reduction) in the mill. Due to unplanned downtime required to handle oversized waste rocks, additional costs and losses are incurred. In the mines where cablebolting is effective in reducing dilution, the cost of cablebolting is often minuscule by comparison.

The economic importance of rock dilution is given throughout the mining literature and was analyzed by Planeta and Szymanski (1996). The authors evaluated 10 analytical
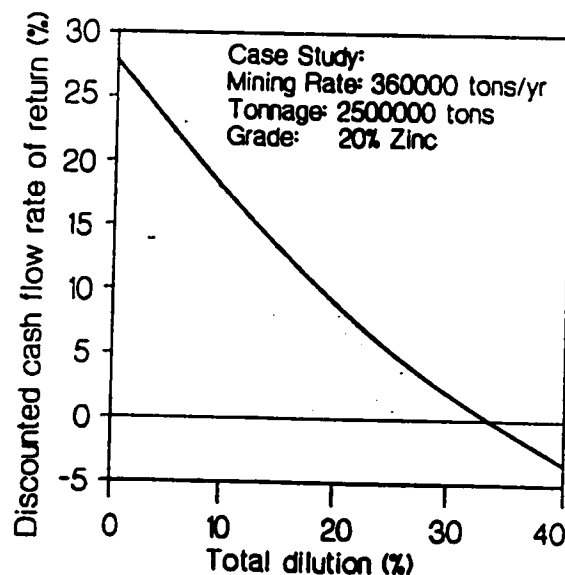
Figure 4.18: Economic impact of dilution (after Bawden (1993))

expressions which were used to express dilution as a percentage and showed that the results varied considerably depending on the method used. The authors then proposed a method to assess dilution using only two factors: (i) planned dilution factor related to

the stoping method and (ii)   the additional dilution factor related to the ability to mine within the design specifications. And they defined dilution as the action of increasing the mined tonnage and reducing its grade.

i) The Planned Dilution Factor (PDF).

This allowed for the consideration of the ratio of the mining reserves, Tm, to the geological reserves, Tg, at the mine planning stage in order to assess the mining method stoping efficiency. Once the PDF has been established, the mining reserve tonnage and the planned waste tonnage, Wp, were calculated using equations (4.42) and (4.43) respectively.

$$Tm = Tg \times PDF \tag{4.42}$$

$$Wp = Tg(PDF - 1) \tag{4.43}$$

ii) The Additional Dilution Factor (ADF).

This allows for the evaluation of the ratio between run-of-mine ore tonnage, Tt, and the mining reserve tonnage, Tm, during the actual stope operation and allows for quality control on the stoping method. The method also allows for the estimation of the run-of-mine ore tonnage and the additional waste tonnage (Wa) based on the mining reserve tonnage by using equations (4.44) and (4.45).

$$Tt = Tm \times ADF \tag{4.44}$$

$$Wa = Tm(ADF - 1) \tag{4.45}$$

iii) Final Dilution Factor (FDF)

This is the product of the Planned Dilution Factor and the Additional Dilution Factor. If the PDF is known, the run-of-mine ore tonnage and the total waste tonnage (Wt) is calculated based on the geological reserve tonnage using equations (4.46) and (4.47) respectively.

$$Tt = Tg \times FDF \tag{4.46}$$

$$Wt = Tg(FDF - 1) \tag{4.47}$$

Using the PDF, ADF and FDF it is easy to perform dilution analysis for a particular mining operation, and this method will be applied to the Selebi North mine project.

CHAPTER 5

EMPIRICAL METHODS OF OPEN STOPE DESIGN

5.1 INTRODUCTION

Most classical empirical variables such as Rock Mass Rating (RMR) and Rock Tunneling Quality Index (Q) were developed from database collected primarily from civil engineering structures at low to moderate depth. These systems resulted in conservative designs for large temporary or non-entry mining excavations as regards dimensioning and support requirements.

Though these systems are appropriate for high traffic mining roadways such as main ramps and haulages, waiting places and underground garages where stability must be paramount, they have proved difficult to apply to the problems of dimensioning and support design for large open stopes. Where access is limited, structures could be designed as temporary and in the case of non-entry stopes minor failures could be tolerated provided dilution is under control and stability is maintained. Hence permitting a more economical design suited to mining operations.

Design modifications are possible in mining with the use of RMR based on reduced stand-up times [Bieniawski, 1989; 1993], while the Q system attempts to include mining applications through the use of Equivalent Support Ratio (ESR) [Barton et al., 1974].

However, Laubscher and Taylor (1976) introduced a classification system for caving operations and for stability of mining excavations, and they also modified the RMR.

In large scale open stoping methods, such as Creeping Cone, longhole and blasthole stoping, rely on the selection of a limiting stope dimension. It is every mining engineer's wish to design these stopes as self-supporting, which is not always possible. Because of miners' greed, which results in larger stopes mandating support, cable bolts are normally used in such cases. However, an empirical method of dimensioning open stope span was proposed by Mathews et al. (1981) based on modified Q (Q') and on three factors accounting for stress, structural orientation and gravity effects. Using a combination of these three factors and the hydraulic radius of individual stope faces, each face can be dimensioned. Note that the hydraulic radius accounts for shape, as well as, size of the stope face.

Potvin (1988) modified this original method and calibrated it using 175 case histories. Nickson (1992) increased the number of case histories and modified Potvin's support design guidelines. Hoek et al. (1995) reported that the number of case histories have increased to 350. These case histories include hanging walls, footwalls, stope ends and backs from a wide variety of mining environments.

73

5.2 THE STABILITY GRAPH METHOD

The design of open stopes in Canada and many parts of the world is now focused on the formalized empirical design for open stope dimensioning. The most popular technique in use is the Modified Stability Graph method (empirical method of dimensioning open stopes), pioneered by Mathews et al. (1981) and calibrated by Potvin (1988) and modified by Potvin and Milne (1992). Nickson (1992) applied the required cable-bolt support to the method. The method has been developed mainly from data collected from Canadian underground mines and accounts for the key factors influencing open stope design.

According to Hoek et al. (1995), information about the rock mass strength and structure, the stresses around the opening and the size, shape and orientation of the opening are used to determine the stability of the stope. That is, whether the stope will be stable without support, stable with support, or unstable even if supported. When the design is in the realm of 'stable with support', the method also suggests ranges of cable-bolt density. The method depends on the calculation of N', the modified stability number. N' represents the ability of the rock mass to stand up under a given stress condition.. and HR, the shape factor or hydraulic radius accounts for the stope size and shape.

5.2.1 The Modified Stability Number, N'

Potvin (1988), Potvin and Milne (1992) and Bawden (1993) specified that the classification of the rock mass and of the excavation problem itself is accomplished in the

74

Modified Stability Graph Method through the use of the Modified Stability Number, N'. Though N' is similar to the value N proposed by Mathews et al. (1981), it is somehow weighted differently. Hutchinson and Diederichs (1996), reported that Canadian mines use Potvin's N' while the Australian mines use Mathews' analysis and N. Several names have been synonymous with this method, mainly Potvin method, the Mathews/Potvin method, the Modified Stability Graph method and the Stability Graph method. In this thesis the later name will be used for the rest of this discussion for clarity and brevity.

The modified stability number N' is defined as follows;

$$N' = Q' \times A \times B \times C$$

(5.1)

Where;

Q' is the modified Tunneling Quality Index, and is discussed in the next section.

A is the rock stress factor, which is a measure of the ratio of intact rock strength to induced stress. Factor A degrades to reflect the related instability due to rock yield as the maximum compressive stress acting parallel to a free stope face approaches the uniaxial strength of the rock.

B is the joint orientation adjustment factor, which is a measure of the relative orientation of dominant jointing with respect to the excavation surface. Joints, which are subject to failure (i.e. to slip or separate), form a shallow oblique angle (10 - 30 degrees) with the free face. While those perpendicular to the face are assumed to have the least influence on stability.

C is the gravity adjustment factor, which is a measure of the influence of gravity on the stability of the face being considered. Maximum detrimental influence on stability is due to overhanging stope faces (backs) or structural weaknesses, which are oriented unfavorably with respect to gravity sliding.

5.2.2 The Modified Rock Tunneling Quality Index, Q'.

$$Q' = \frac{RQD}{J_n} \times \frac{J_r}{J_a} \qquad (5.2)$$

The variables defining Q' are the Rock Quality Designation (RQD), joint set number (Jn), joint roughness number (Jr) and joint alteration number (Ja). The absence of the stress reduction factor (SRF) and the water reduction factor (Jw) which were normally found in Q is due to the fact that the conditions assumed here are for a dry rock mass subjected to medium stress and hence both parameters are put to 1. When the SRF is set to 1, the assumed conditions are equivalent to a moderately clamped but not overstressed rock mass. In addition, in most underground hard rock mining environments, the excavations are relatively dry, including at Selebi North mine (not considering transient mine water flow from drilling). Therefore Jw can justifiably be set to 1 in this case.

These parameters are defined as follows;

$\frac{RQD}{Jn}$ is a measure of block size for a jointed rock mass. Though this is a crude representation of average block size, the ratio does however, provide a means of comparison and can be used to empirically estimate support spacing and surface retention requirements. The extreme calculated values range from 0.5 to 200.

76

Jr/Ja is a measure of joint surface strength and stiffness. This parameter represents the integrity and strength of a joint surface favoring rough, unaltered, discontinuous joints. Rocks are considered detrimental to stability when they are smooth or slickensided (polished by shear) and/or if they contain low friction coatings or filling. In stability analyses the critical value of Jr/Ja should be used. This is the value of the joint set most likely to cause problems based on the values of Jr and Ja and on the joint geometry. Critical joints are those making a shallow angle (<35°) with respect to a surface and are seconded by joints parallel to the surface. Joints perpendicular to the excavation surface are considered to be the least critical. Inclined joints (>35° with respect to the horizontal) are likely to be critical in the case where gravity sliding is the dominant failure mode.

RQD indicates the percentage of rock which can be expected to posses strength and stiffness properties comparable to a 10 cm laboratory sample of intact rock and it ranges from 10 to 100 when being used in the calculation of Q'. Jn accounts for the number of repetitive joint sets and the relative dominance of random fracturing and jointing and it ranges from a value of 0.5 when there are no joints to a value of 20 when the rock is completely crushed. Jr describes the large and small scale surface texture of the critical joint set. Jr ranges from 0.5 (unfavorable) to 4.0 (favorable). Ja describes the surface alteration and frictional resistance of the critical joint set and ranges from 0.75 (unfavorable) to 20 (favorable). Jw is the Water Reduction Number and it accounts for the destabilizing effect of high water pressures and of joint washout by water influx. Jw ranges in value from 1.0 for dry excavation to 0.05 for excavations with excessive inflow and pressure.

Moreover, Hoek et al. (1995) stated that this system has not been applied in conditions with significant groundwater. The influence of both water pressure and stress are included in the analysis of stresses acting on the rock mass for which failure is defined by the Hoek-Brown failure criterion. The parameter Q' should reflect the inherent character of the rock mass, independent of the excavation size and shape which are considered separately in subsequent analyses. Therefore Q' would be used to estimate rock mass modulus and strength together with several other factors (accounting for jointing, stope geometry and overstress). These will determine the Modified Stability Number, N', which is used in the Modified Stability Graph method [Mathews et al.,1981: Potvin, 1988; Bawden, 1993; Hoek et al., 1995]. The analysis will be used for dimensioning of open stopes in mining and for the design of cable bolt support in these environments, typical values are shown in Table 5.1.

Table 5.1: Range of values (*for hard rock mining)

Range	RQD/Jn	Jr/Ja	A	B	C	N'
Lower	0.5	0.025	0.1	0.2	2	0.0005
Upper	200	5	1	1	8	8000
Typical*	2.4	0.1	0.1	0.2	2	0.1
	25	5	1	1	8	1000

(after Hutchinson et al. (1996))

5.3 STABILITY GRAPH METHOD - INPUT PARAMETERS

In a normal mine operation, due to the complexity of the contracts governing the overall organization, there will normally be some pre-determined tonnage to be fed to both the concentrator and smelter. This is mostly due to some smelter contracts entered between the mining organization and the refineries. As a result stopes are designed to produce enough tonnage to meet these contractual agreements. Hence stopes are dimensioned after tonnage has already been determined. Therefore, when using the Stability Graph method, the value of the hydraulic radius, HR is determined by dividing the area of the stope by the perimeter and design follows as illustrated in Figure 5.1.

5.3.1 Determination of Stress Factor A

The parameter A represents the stresses acting on the surface of the open stope and is determined from the unconfined compressive strength of the intact rock and the stresses acting parallel to the exposed surfaces of the open stope under consideration.

According to Hoek et al (1995), the stress factor, A, is then determined from σ_c/σ_1. the ratio of the intact rock strength to the induced compressive stress on the stope boundary: for

$$\frac{\sigma_c}{\sigma_1} < 2: A = 0.1$$

(5.3)

for

$$2 < \frac{\sigma_c}{\sigma_1} < 10: A = 0.1125\frac{\sigma_c}{\sigma_1} - 0.125$$

and for

$$\frac{\sigma_c}{\sigma_1} > 10: A = 1.0$$

```
        ┌─────────────────────┐
   ┌───▶│ Compute value for HR│
   │    └─────────────────────┘
   │              │
   │              ▼
   │    ┌─────────────────────┐
   │    │ Measure/calculate   │
   │    │ RQD, Jn, Jr and Ja  │
   │    └─────────────────────┘
   │              │
   │              ▼
   │    ┌─────────────────────┐
   │    │ Compute Q'          │
   │    └─────────────────────┘
   │              │
   │              ▼
   │    ┌─────────────────────┐
   │    │ Evaluate A, B and C │
   │    └─────────────────────┘
   │              │
   │              ▼
   │    ┌─────────────────────┐
   │    │ Calculate N'        │
   │    └─────────────────────┘
   │              │
   │              ▼
   │    ┌───────────────────────────────┐
   │    │ Plot N' against HR and determine│
   │    │ stability and design zone for   │
   │    │ the stope                       │
   │    └───────────────────────────────┘
   │              │
   │ no           ▼
   └────◁ Stability and design zone okay? ▷
                  │
                 yes
                  │
                  ▼
            ┌──────────┐
            │ Design   │
            └──────────┘
```
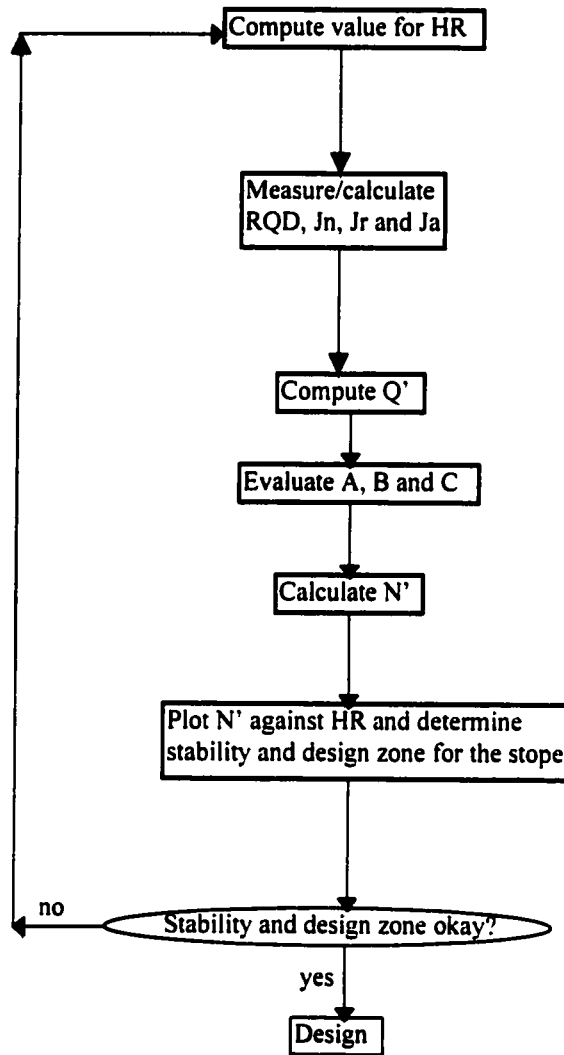
Figure 5.1: Flowchart for Stability Graph design

A plot of the rock stress factor A, for different values σ_c/σ_1 is given on Figure 5.2.

80

Determine maximum induced tangential stress (compressive) acting at the centre centre of the stope face being considered. Obtain uniaxial compressive strength strength for the intact rock. Evaluate Stress Factor. A, using the graph below:

Ratio: $\dfrac{\text{Uniaxial Comp. Strength . U.C.S.}}{\text{Max. Induced Comp. Stress . } \sigma_{max}}$

Obtain σ_{max} from 2D or (preferably) 3D numerical stress modelling.
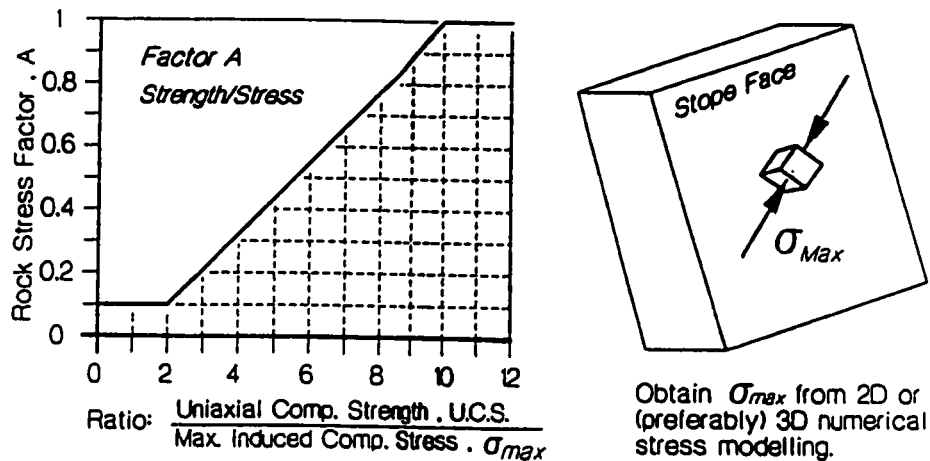
Figure 5.2: Rock Stress Factor A for Stability Graph analysis [Potvin, 1988]

5.3.2 Determination of Factor B

The joint orientation factor, B, accounts for the influence of the joints on the stability of the stope faces, and is high when the joint orientation is unfavorable and low for favorable joint orientation. Structurally, controlled failure occurs along the critical joints which form a shallow angle with the free surface. If the angle between the discontinuity and the stope face is shallow, the rock between the discontinuity and the stope face can be broken by blasting, stress or by another joint set, however if the angle approaches zero the jointed rock block would act as a beam of increased strength. Hoek et al. (1995) noted that the influence of the critical joint on the stability of the excavation surface is highest when the strike is parallel to the free surface of the open stope face, and smallest

when the planes are at right angles to one another. The chart to determine the factor B is shown on Figure 5.3.

Joint Orientation Factor, B: Dips Determination.

Hutchinson et al. (1996) noted that the relative dips and strikes of the planes do not immediately give the true angle between two planes. Therefore, it must be calculated as shown by Figure 5.4 or estimated from a stereonet. As shown in Figure 5.4. (a) the hanging wall face is associated with the joint sets. Hence, the determination of B involves only the pole to face and the mean poles for each joint set 1, 2 and 3. The angle (cone angle) from this pole to each of the joint set poles can be estimated using a series of small circles (cones) centered on the face pole as in Figure 5.4.(b). These small circles (cones) were automatically generated by a computer program DIPS. Cones drawn at 10. 30, 45, 60, and 90 degrees to determine factor B provide sufficient resolution.

The smallest angle between the poles to the plane gives the true angle between planes. Using Figure 5.4.(b) it can be shown that the angle from the face to set 1 = 20 degrees. to set 2 = 53 degrees, and to set 3 = 71 degrees. The corresponding Joint Orientation Factor (B) replaces the angle contours in Figure 5.4.(c), showing clearly that the joint set 1 is critical, and that the factor, B, should be set to 0.2 for the Stability Graph analysis.

Horizontal Back	Inclined Wall	Vertical Wall	True Angle between Face & Joint	Potvin Factor B
			$\alpha = 90°$	1.0
			$\alpha = 60°$	0.8
			$\alpha = 45°$	0.5
			$\alpha = 30°$	0.2
			$\alpha = 0°$	0.3

Factor B

Joint Orientation Factor, B

True Angle Between Face and Joint
(Angle α Between Poles)
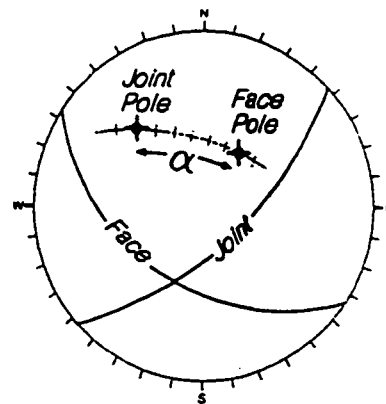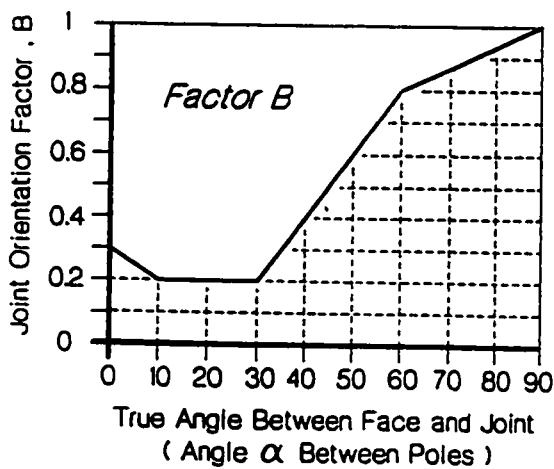
Determination of the minimum or true angle between two planes = Angle α between poles

Figure 5.3: Determination of Joint Orientation Factor, B, for Stability Graph analysis
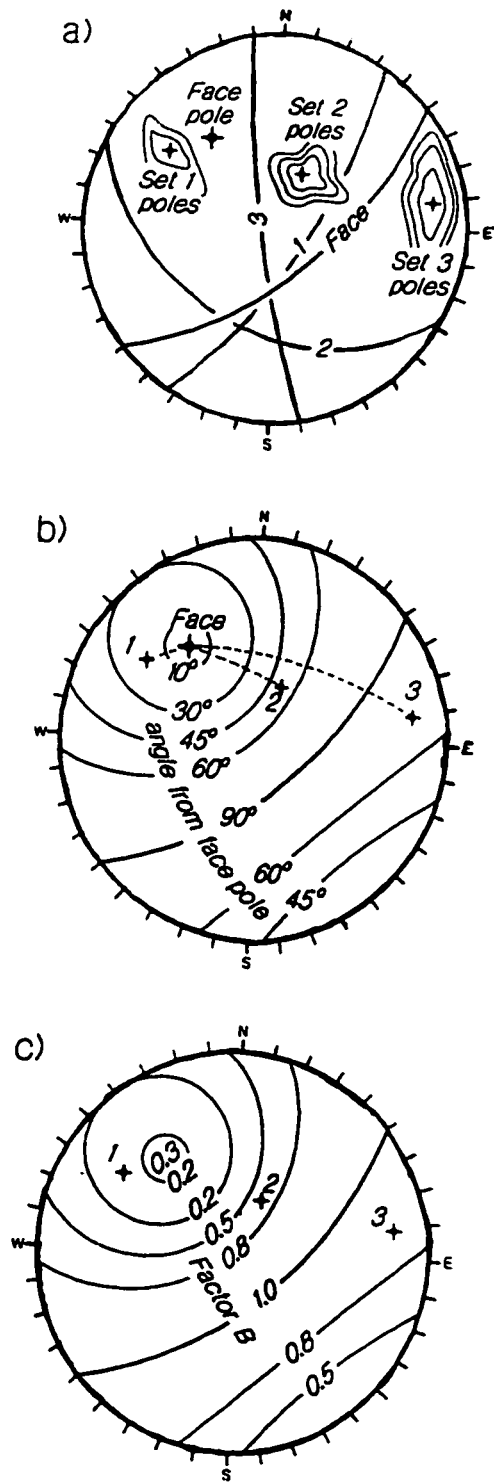
Figure 5.4: Estimation of true interplane angle and joint Factor B.

Joint Orientation Factor, B: Direct Calculation of Interplane angle

The procedure outlined here could be used to determine directly the true interplane angle between the stope face (wall plane) and the joint plane. If the dip and dip direction of a plane are known, the trend and plunge of the corresponding pole (normal vector) can be calculated assuming equations (5.4) and (5.5).

$$T = \text{Trend} = \text{dip direction} + 180° \tag{5.4}$$

$$P = \text{Plunge} = 90° - \text{dip} \tag{5.5}$$

If it is further assumed that a stope wall plane, w, and a joint plane, j, and the direction cosines with respect to the global coordinate grid (North, East, Down) are denoted by N, E and D respectively and are calculated in the following equations.

For the stope wall:

$$N_w = \cos(T_w) * \cos(P_w) \tag{5.6}$$

$$E_w = \sin(T_w) * \cos(P_w) \tag{5.7}$$

$$D_w = \sin(P_w) \tag{5.8}$$

For the joint plane:

$$N_j = \cos(T_j) * \cos(P_j) \tag{5.9}$$

$$E_j = \sin(T_j) * \cos(P_j) \tag{5.10}$$

$$D_j = \sin(P_j) \tag{5.11}$$

The dot product, **w.j**, between the wall face and the joint plane is calculated by equation (5.12).

$$\mathbf{w.j} = N_w N_j + E_w E_j + D_w D_j \tag{5.12}$$

Therefore, the true interplane angle, α, is given by:

$$\alpha = \cos^{-1}(\mathbf{w.j}) = a\cos(\mathbf{w.j}) \tag{5.13}$$

With the true interplane angle calculated, it is possible to assign a Joint Orientation Factor, B.

It is of paramount importance to realize that measurements such as dip and dip direction or strike are made relative to a global coordinate system. Hence, they cannot be used directly to calculate the true angle between two planes since the applicable coordinate system must be changed to be relative to one of the faces, implying that the above procedure must be implemented. However, the calculation of the interplane angle could be simplified if one of the planes is approximately horizontal or near vertical (dip = 0° or 90°). If the true angle is being calculated to determine factor B, the condition must apply to either the stope face or the joint plane (or both). For a horizontal joint or horizontal stope face (back), only the difference in dip between the stope face and the joint plane is considered and factor B is determined using Figure 5.3. However, for a vertical joint or near vertical stope face, the difference in strike (or in dip direction) must also be considered. Therefore, Potvin (1988) noted that Figure 5.5 below should only be used only if one of the planes is near vertical.
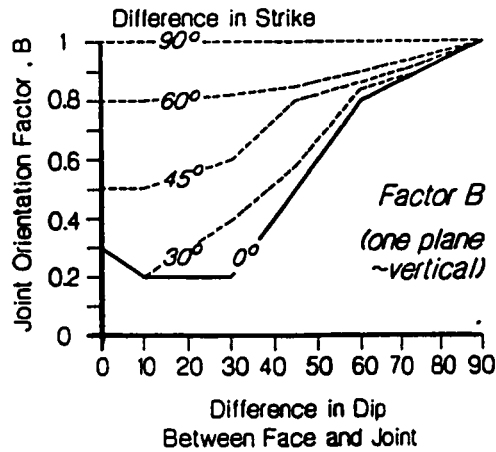
Figure 5.5: Simplified special cases for determining factor B

5.3.3 Determination of Factor C

If failure is induced by gravity or by slabbing, depending on the inclination of the stope surface, α, the factor C can be calculated from the following relationship, after Potvin (1988).

$$C = 8 - 6\cos\alpha \tag{5.14}$$

From equation (5.14), the factor has a maximum value of 8 for vertical stope faces and a minimum of 2 for horizontal stope backs. The graphical derivation of factor C is shown in Figure 5.6. It is also recognized that failure inside the open stope can also occur by sliding depending on the inclination angle of the critical joint.

1) Determine the most likely mode of structural failure in case study using the figures below:

Gravity Fall   Slabbing   Sliding
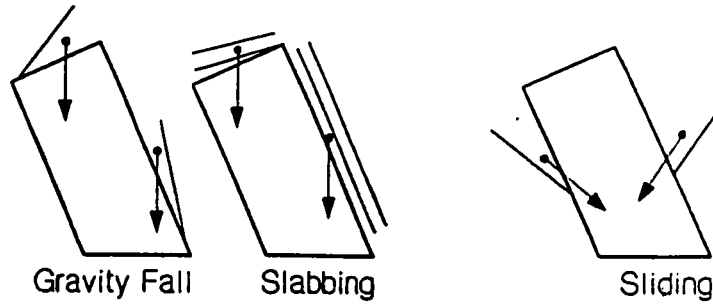
2) Next determine the gravity adjustment factor, *C*, based on the failure mode using the appropriate chart below.
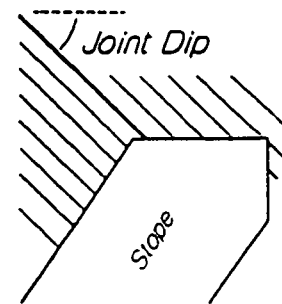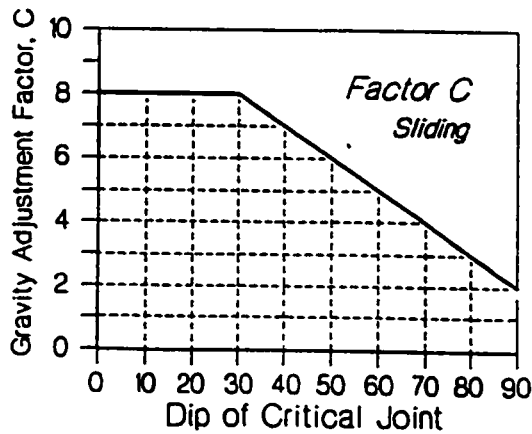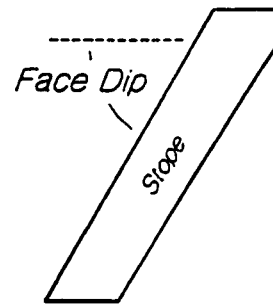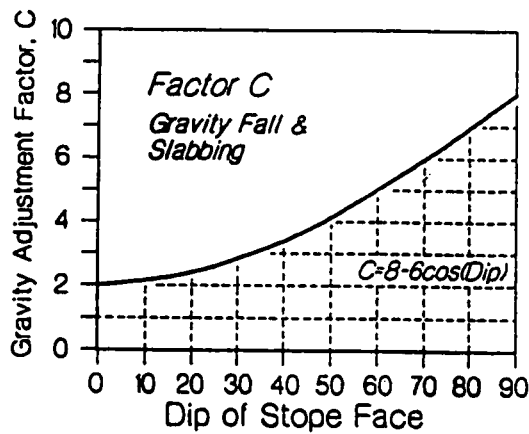
Figure 5.6: Determination of Gravity Adjustment Factor, C, for Stability Graph analysis

88

The hydraulic radius, HR, should also be understood as one of the important input parameters for the Stability Graph method. HR is calculated by dividing the area of a stope face by the perimeter of that face as shown on Figure 5.7 below.

$$HR = \frac{w \times h}{2w + 2h}$$
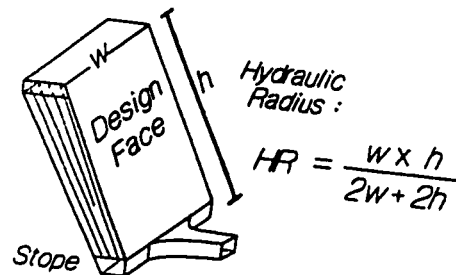
Figure 5.7: Calculation of the hydraulic radius, HR

According to Hutchinson et al. (1996), most classification systems (e.g. RMR and Q) define stability and support zones with respect to a single value of span. In tunnelling, where these methods were derived, the long span can be assumed to be infinite making the short span the critical dimension. If the long span can be reduced while the short span is kept constant, the stability will reduce as a result of the increased confinement and rigidity provided by the extra two abutments. However, Hutchinson et al. (1996) assumed that a face with a dimension ratio greater than 10:1 can be treated as a (tunnel) span equivalent to the shorter dimension.

The hydraulic radius more accurately accounts for the combined influence of size and shape on excavation stability. Familiarity with the range of "spans" for a given hydraulic radius will provide a means of comparison with other design methods, which do not use
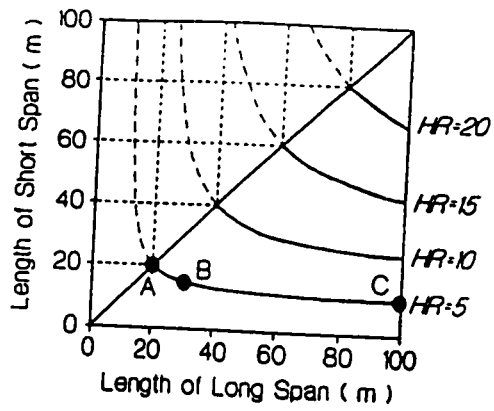
eg:

Square Span (Maximum Short Span)

A
20m 20m   HR = 5

B
30m
15m   HR = 5

C
10m   HR = 5

Figure 5.8: Effect of the hydraulic radius
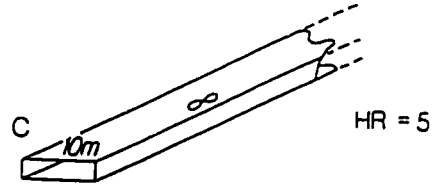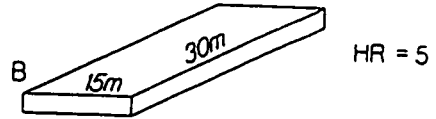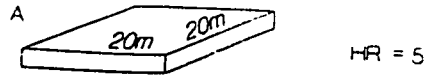
Tunnel Span (Minimum Short Span)

Figure for hydraulic radius showing Length of Short Span (m) versus Length of Long Span (m), with curves HR=20, HR=15, HR=10, HR=5 and points A, B, C.

Ground stability curves plotting Stability number N' against Hydraulic radius S - metres, showing STABLE ZONE, UNSUPPORTED TRANSITION ZONE, STABLE WITH SUPPORT, SUPPORTED TRANSITION ZONE, and CAVED ZONE.
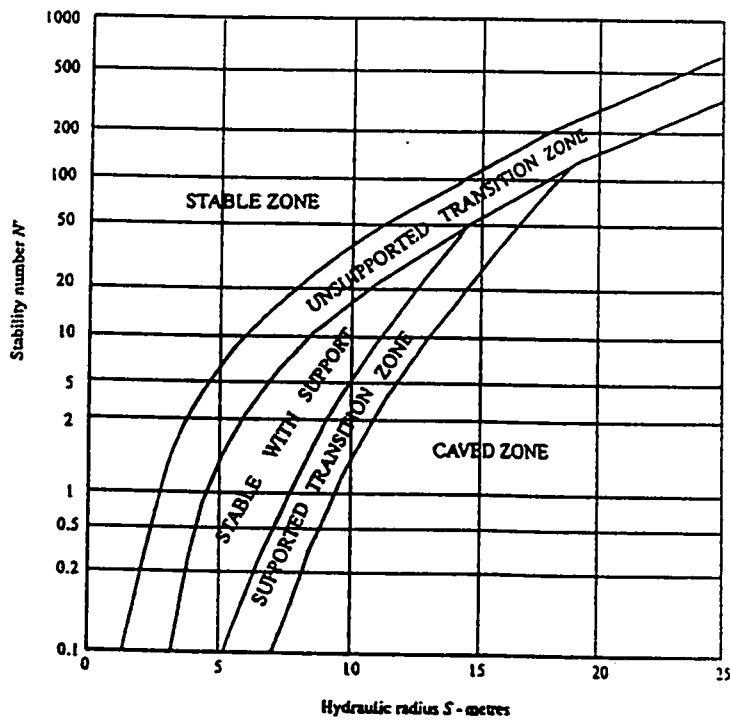
Figure 5.9: Ground Stability Curves (after Potvin (1988), modified by Nickson (1992).

90

HR. Figure 5.8 illustrates the limits for a fixed HR of 5 m. Though these methods could be applied to mining tunnels, they have been specifically designed for open stopes with finite dimensions and lower priority for safety such as in non-entry systems.

Having determined the value of N' as defined previously, the hydraulic radius or the shape factor, HR, for the open stope under consideration is also calculated. The values of N' and HR are used to assess the stability of the stope from the stability graph in Figure 5.9.

5.4 CABLE-BOLT DESIGN

The empirical design of support for sub-level open stoping is effectively in use at Noranda mine, based on the modified Mathews empirical method. A lot of data has been collected in Canadian underground mines by Potvin and Milne (1992) and by Nickson (1992) and has been used in case histories. The method involves detailed data gathering to determine the ground conditions in the stope to be supported.

When the stability graph indicates that the stope could be stable with support, the chart given in Figure 5.10 can be used as a preliminary guide for the cable bolt density. Figure 5.10 relates the cable bolt density to the frequency of jointing through the block size (parameters RQD/Jn) and the hydraulic radius of the opening. However, Potvin and Milne (1992) cautioned that many factors describing rock mass strength are not represented on this graph, such as joint strength properties. These properties did not have
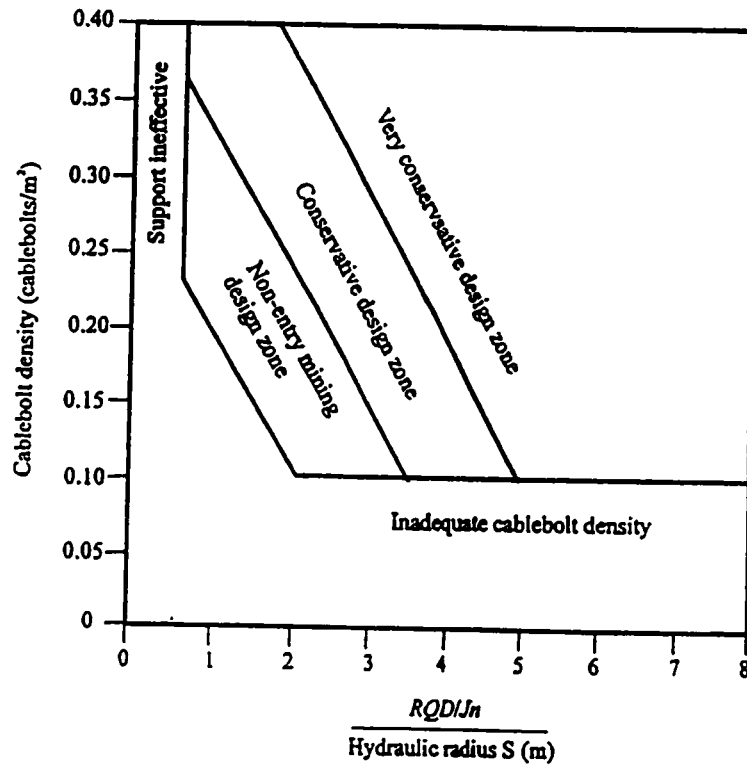
Figure 5.10: Cablebolt density design chart. (after Potvin and Milne (1992))

significant influence on cable bolt support requirements for the database analyzed. They also indicated that the design technique cannot account for discrete geologic features such as faults, shear zones, dykes or waste inclusions which may act to cause instability.

CHAPTER 6

OVERVIEW OF THE CREEPING CONE METHOD

6.1 INTRODUCTION

Most mining operators continue to use trial and error methods to determine stable stope spans or the size of hangingwall exposures that can be achieved under different mining and geological conditions. This phenomena is apparent in sub-level open stopes in complexly folded orebody with steeply dipping or weak hangingwall. It was through trial and error coupled with observations that made Aplin (1997) conceptualize the creeping cone mining method. The author realized that once the Selebi North open stopes had advanced 25 - 30 metres, hanging wall and footwall sloughing started to occur. This contaminated the draw points with big waste rocks which accounted for 15% of the ore transported to surface.

6.2 CREEPING CONE AND EMPIRICAL DESIGN

The sublevel open stoping method accounts for approximately 51% of the tonnage mined in Canadian underground metal mines according to a study by Pakalnis et al. (1993). However, a survey of underground mines in 1988 showed that a major factor in their closure was uncontrolled dilution due to improper stope dimensioning. It was further revealed that 40% of open stope operations were experiencing dilution in

excess of 20%. The economic constraints imposed by this level of dilution cannot be ignored especially when one realizes that a rate of return on a positive project is generally 10% to 20%. It is for this reason that the introduction of the creeping cone mining method was viewed as a turning point in the mining industry, not only at Selebi North mine. The use of this method at Selebi North mine has resulted in improved accuracy of longhole drilling, fragmentation, reduced secondary blasting and more consistent production levels.

Over the past 20 years, a lot of development has taken place in the optimization of underground mining methods. These developments have mainly focused on equipment improvement or change in order to handle high tonnage for profit maximization. Emphasis has been on productivity (tonnes/hour), percentage availability and utilization of equipment. However, little change have taken place in the design of mining methods until the creeping cone method, which is a variation of shrinkage stoping was introduced in 1997 at Selebi North mine. The design of sublevel open stoping in Canada and many parts of the world is now focused on the formalized empirical design for open stope dimensioning. The most popular technique in use is the modified Stability Graph method, pioneered by Mathews et al. (1981) and calibrated by Potvin (1988) and modified by Potvin and Milne (1992). Nickson (1992) applied the required cable-bolt support to the method. The method has been developed mainly from data collected from Canadian underground mines and accounts for the key factors influencing open stope design.

It is the purpose of this research therefore, to derive some design guidelines for the

94

creeping cone method developed in Botswana and compare with the guidelines already developed in Canada. The combination of these methods should result in a powerful tool for the mine engineer working in narrow steep orebodies and substantial savings for mining companies exploiting such deposits not necessarily in base metals.

6.3 THE CREEPING CONE MINING METHOD

This mining method was wholly developed and designed by BCL Limited engineers and was introduced at Selebi North mine in August 1995. The method was used in combination with sublevel open stoping methodology until it completely took over in February 1996. The creeping cone mining method was designed to overcome the adverse effects of inefficiency, which rendered Selebi North mine uneconomic as long as the sublevel open stoping mining method was in operation.

The creeping cone mining method combines long hole open stoping with shrinkage stoping. It was specifically designed to control ore dilution within the open stopes, where the hanging wall and footwall rocks were weak and subject to failure causing dilution. Moreover, the creeping cone mining method eliminated the need for footwall tramming haulage and associated draw points which were predominant during the use of sublevel open stopes. In this method, ore extraction is wholly confined to within the orebody. Aplin (1997) confirmed that, in the case of Selebi North mine, the creeping cone mining method eliminated the need for some 1. 900 m of waste development on each extraction level. According to the 1997 operations development

costs per metre, this meant some savings of about 1.86 million pula (0.543 million dollars) on each extraction level.

While still employing the sublevel open stoping method, Selebi North mine used longhole drilling methods between sublevels placed at 20 metres interval. The drilling was very inaccurate especially in the steeply dipping narrower parts of the orebody. This inaccuracy in longhole drilling, has been reduced by narrowing the sublevel intervals within the orebody from 20 metres to 15 metres. The distance between the primary and secondary extraction levels has also been reduced to 12 metres. The effect of these changes were improved drilling accuracy with shorter holes, hence a reduction in the cost per metre drilled.

Ore extraction is undertaken using hydraulic drill rigs (4.3 tonnes/metre), front end loaders, Load-Haul-Dump (LHD) units (bucket capacity 3.8 m^3) and 20 tonnes dump trucks. Drilling is by 64mm diameter holes (up and down) drilled from the drilling drives, at a 1.5metre burden and spacing. The ore is blasted into a pre-developed slot raise and gravitates to the loading level at the primary and secondary extraction levels. The development round drilled is 1.8metres though, with the drill rigs 3metres round are common. A five- or nine-hole burn cut is used depending on ground conditions. In general, all holes are blasted using pneumatically loaded ammonium nitrate/fuel oil mixture, bottom primed with a 22 mm x 100 mm stick of 60% gelignite. Detonation is via safety fuse with a 6D detonator, ignited using slow burning ignitor cord and electric

starters. For wet ends, 32 mm x 200 mm dynagel sticks are used with 6D detonator. Blasting is done by a centralized electric blasting system.

The ventilation air is downcasted through the main surface twin ramp system. Air distribution to the stoping areas is via sublevel drill drives and up through the stopes, along the 50 and 130metre levels to the exploration winze, which serves as an upcast shaft. The exploration winze is equipped with an axial flow, single-stage fan rated at 120 cubic metres per second at 1.23 Kpa, with adjustable blade settings and a motor rated at 187 KW.

The creeping cone method involves the formation of a cone compacted with blasted ore in the open stope. The cone formed then supports both the hanging wall and the footwall of the open stope, allowing for ore extraction from the stope before dilation of the bedding planes occur. Therefore, ore can be drawn from the open stope before sidewall failure by sloughing, thereby reducing extraneous dilution inside the stope.
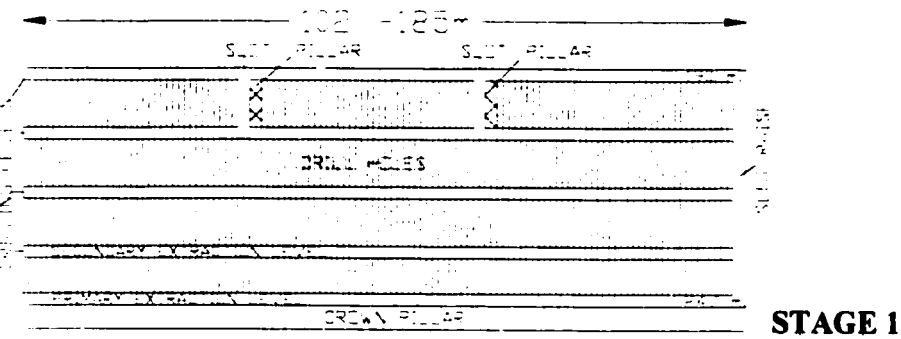
Figure 6.1: Pre- production development of the stope

The creeping cone method allows for the stope to be developed to its extremities (far ends), including production drilling with long upholes within the orebody as shown in Figure 6.1. Once production drilling is completed, a slot raise joining all the sublevels is mined at the extremities of the developed stope. This is then followed by other slot raises established approximately every 30 metres along the strike of the orebody. This second set of slot raises is only established between the top two sublevels. Each slot raise has a 4 metres thick barricade pillar, which supports the upper part of the stope and act as a blasting barricade to ensure that the blasted ore is directed in front of the cone to be established during production blasting.

STAGE 2
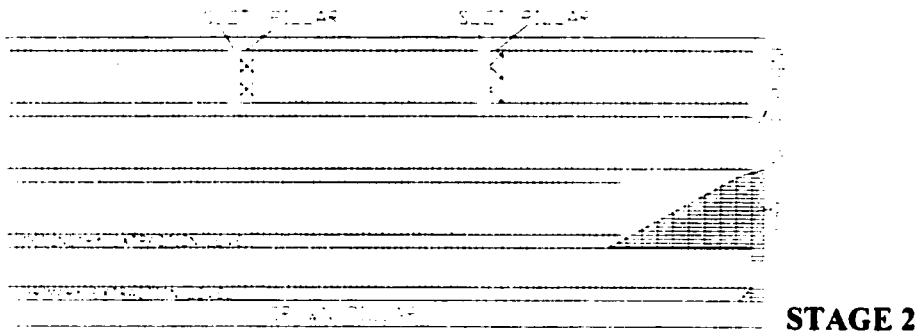
Figure 6.2: Initial production blasting on the secondary extraction level

The primary extraction level of the ore is located just above the crown pillar at the bottom of the stope. However, the first production blasting takes place on the secondary extraction level as illustrated by Figure 6.2. The secondary extraction level is blasted along the orebody strike (the ore is lashed from the same level). Drawing of the swell at this level continues until the blasted ore reaches the next sublevel. At this stage, a cone

has started to form at an angle of repose of the broken ore. Moreover, no extraction of the ore takes place from the primary extraction level.
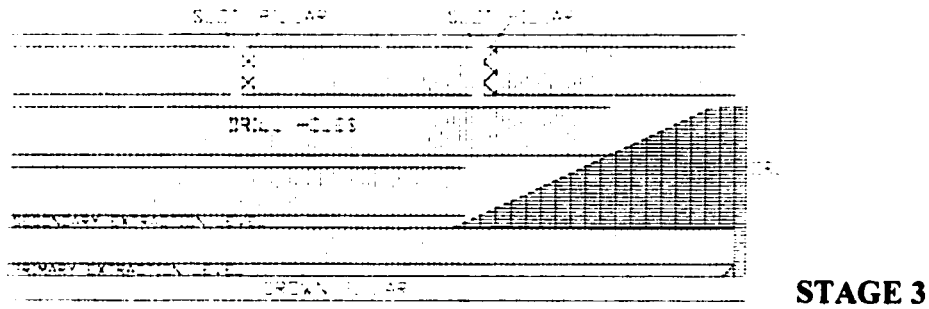
STAGE 3

Figure 6.3: Sublevel blasting

Blasting of the orebody is progressed to the next sublevel above and is simultaneously continued on the lower level as in Figure 6.3. At this stage, blasting the ore on the front face of the cone has the effect of compacting the ore against the hangingwall and footwall sides of the orebody providing the required temporary support. This procedure is continued until the cone has been built up to the elevation of the next level above. However, at this stage, it is very important that the drawing off the cone swell be restricted to the secondary extraction level only.

STAGE 4
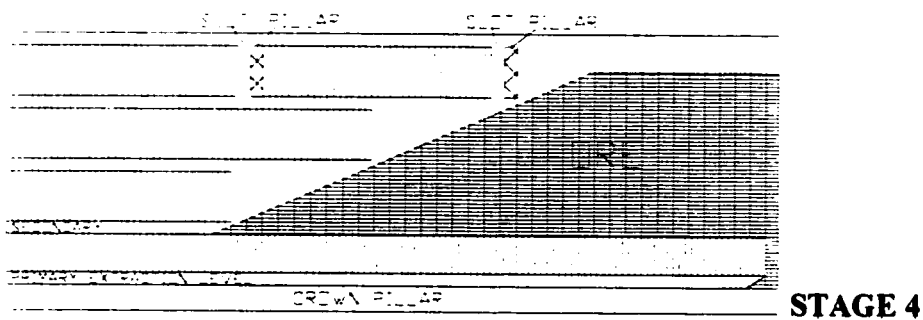
Figure 6.4: Front of the cone established

When the front of the cone has been established to the elevation of the third sublevel. as in Figure 6.4, blasting of the orebody is continued on all sublevels on the front of the ore cone. The swell of the broken ore is pulled on the secondary extraction level to allow all the levels to be blasted as required in order to create the front of the cone relative to the angle of repose of the broken ore. At this stage, the hanging wall and footwall of the stope are now supported by broken compacted ore which prevents sidewall failure by dilation of the bedding planes. It is worthy to note that the void between the sublevel faces and the front of the cone does not exceed the critical distance of 25 - 30 metres which is necessary for failure by dilation of the bedding planes to take place. At this stage the final height of the cone has now been established. However, a large amount of ore is stored in the stope to provide sidewall support, this result in delayed recovery of the costs incurred in developing and blasting the stope which has a negative impact on the economy of the mine..
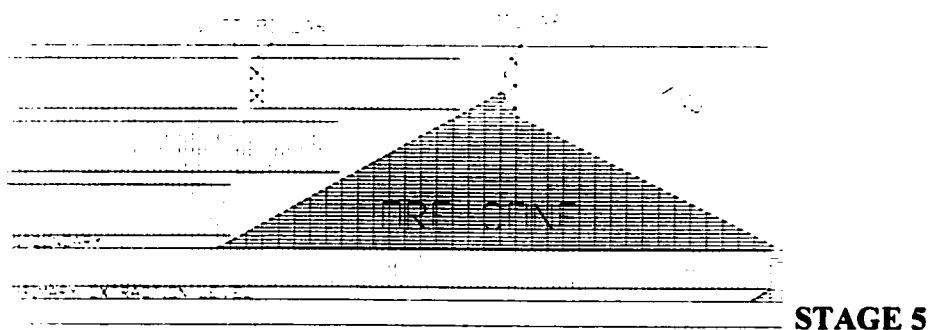
STAGE 5

Figure 6.5: Cone formed at angle of repose of broken ore.

Figure 6.5 shows the front of the cone having retreated far along the strike to allow the angle of repose of broken ore at the back of the cone. At this stage, ore can now be extracted from the primary extraction level. Aplin (1997) noted that the combination of

100

producing from the swell of blasted ore on the front of the cone and the initial production from creating the angle of repose on the back of the cone, represented approximately 54% of the total tonnage in the stope, and this has been extracted with minimal extraneous dilution. The barricade pillar left between the upper sublevels acts as a support for the stope sides and as a blasting barricade diverting the blasted ore to the front of the cone and hence ensuring that the final height of the cone is being maintained.

STAGE 6
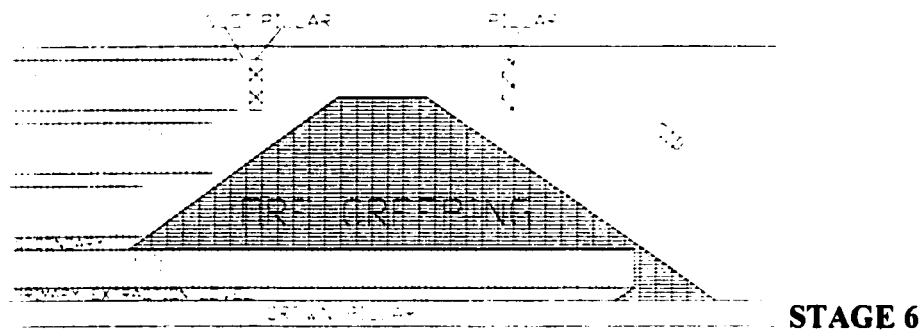
Figure 6.6: The creeping cone

The interval between the secondary and primary extraction levels is maintained at 12 metres, which has proved to be an ultimate height maximizing the ore recovery on the primary extraction level. Blasting is continued at the front of the cone while, at the back of the cone, only one ring of upholes is being blasted with low-heave explosives. Blasting on the primary level allows for the broken ore to slide down the cone into the primary extraction drive. As blasting is continued on both sides of the cone, the cone creeps along the strike of the orebody. Sloughing from the hanging wall and footwall falls behind the cone in the mined out area of the stope and is contained by the crown pillar of the lower stope.

The benefits of operating the creeping cone mining method at Selebi North mine has resulted in improved profitability of the shaft. Other benefits have included significant reduction in waste development, more accurate long hole drilling, improved fragmentation, reduction in secondary blasting and more consistent production output.

However, the limitations of this method are that the blasted ore is left in the stope for a very long time, tempting premature draw from the primary level, hence offsetting the formation of the cone. Also the cost benefit of reduced dilution due to broken ore providing side wall support, is off-set by the cost incurred due to delayed ore withdrawal. Other limitations include the loss of ore in the stopes due to burial by the sloughing sidewalls showing the inefficiency of the method in providing the necessary support and reduced dilution.

CHAPTER 7

DATA COLLECTION AND ROCK MASS CHARACTERIZATION IN THE MINING AREA

7.1 GENERAL

Planning and design of openings in rock benefit from a number of empirical and semi-empirical rules. These serve to enable the designer to make an estimate of the expected stope dimensions and/or support conditions on the basis of a detailed description of the rock mass. The complete design procedure involves two steps. First, the quality of the rock mass is determined on the basis of a pre-defined classification system, and then the expected performance of the underground opening is predicted using empirically derived correlation with the rock quality factor.

The mining industry generally uses two schemes for classifying rock masses, Rock Quality Designation (RQD) and Rock Mass Rating (RMR). Although the systems differ, they rely on similar data to be collected. Once the data is collected, both systems are used to define the quality of the rock mass.

From June to August, 1997, the author collected geological data and other necessary data from Selebi North mine for this research.

According to Hoek et al. (1995), a complete engineering geological rock mass description contains details of the rock material and the natural discontinuities. Such a description comprises weathering/alteration, structure, colour, grain size, intact rock material compressive strength and rock type. It also includes details of the discontinuities, such as, orientation, persistence, spacing, aperture/thickness, infilling, waviness and unevenness for each set of joints. The rock mass can then be described by block shape, block size and discontinuity condition. The description is then completed by an evaluation of the potential influence of groundwater and the number of joint sets, which will affect the stability of the excavation.

The importance of mapping geological structures as an essential component of underground excavation design can never be overemphasized. Structural planes running through a rock mass may divide it, forming discrete blocks which may slide or fall from the excavation boundary, due to inadequate support and stress conditions favorable for structural failure. Such failures may not be acceptable due to threatened safety or increased dilution.

7.2 DETERMINATION OF JOINT ORIENTATION (STRUCTURAL MAPPING)

The equipment used during this mapping exercise were Clar campass (Figure 7.1), clinorule, a 30metre long tape and some empirical tables taken from Hoek et al. (1995). An extensive literature survey and interviews with the mine operating personnel were

conducted before the mapping process. Mine plans from both Survey and Geology departments were studied to establish the areas for mapping and the homogeneous sections within this target areas. The orebody was divided into four distinct areas comprising the South limb, North limb, Nose area and the Detached limb. In the main orebody comprising the South and North
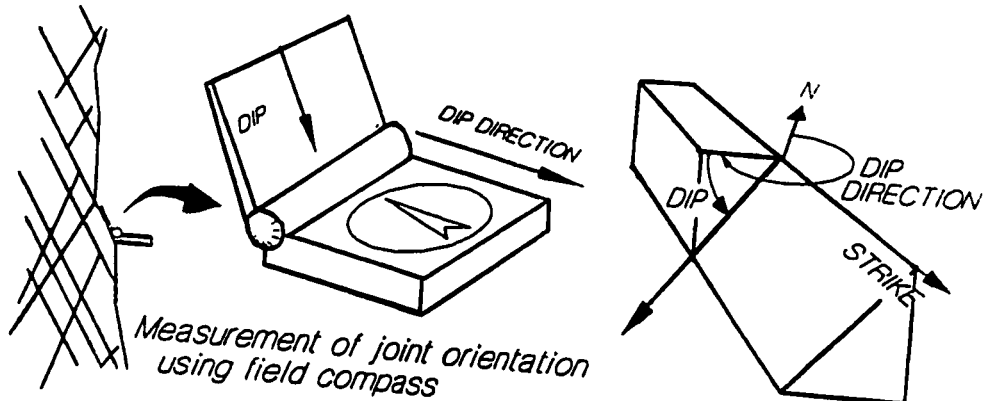
Figure 7.1: Illustration of Clar compass

limb, as well as. the Nose area, a 54metre high block was identified for mapping. The mapping was done at 295, 307, 319, 334 and 349metre level drill drives following the orebody strike from 300 to 1700 sections. In the Detached limb, mapping was done at 259, 274 and 289metre level drill drives defining a mining block of 30 metres in height extending from 1100 to 1400 section lines. Scanlines were established along the drill drives following the survey pegs. All significant features which crossed the scanlines were recorded. Significant features were assumed to be those features that were clearly visible to the naked eye and were more than a metre long. Whenever possible. the

scanlines were orientated along the strike, across the orebody and vertically in order to establish a three-dimensional picture of the orebody, thereby providing maximum coverage of the joint sets. In all about 1, 500 structural features were recorded. Hoek et al. (1995) recommends that, at least 100 measurements of dip and dip direction (or dip and strike) should be made in each structural domain, which is a block of ground considered to have uniform properties.

A geological data always contain some bias. This could be due to the fact that features oriented perpendicular to the traverse will be closest to the true spacing. Features oriented sub-parallel to the surface being mapped will appear to be more widely spaced than they actually are, and fewer measurements will be made. However, a correction for this sampling bias is incorporated into the microcomputer program DIPS which was used to analyse the data. Appendix A shows the input datafiles to the program while Figures 7.2 and 7.3 are the output of the program showing the major planes and rosette respectively for the North limb. Other outputs for various other analyzed areas are included in Appendix A.

This information would be used in the structural stability analyses and support design procedures described later in this thesis.

ORIENTATIONS

#	DIP/DIR.
1	44/174
2	64/157
3	80/183
4	75/238

EQUAL ANGLE
LWR. HEMISPHERE
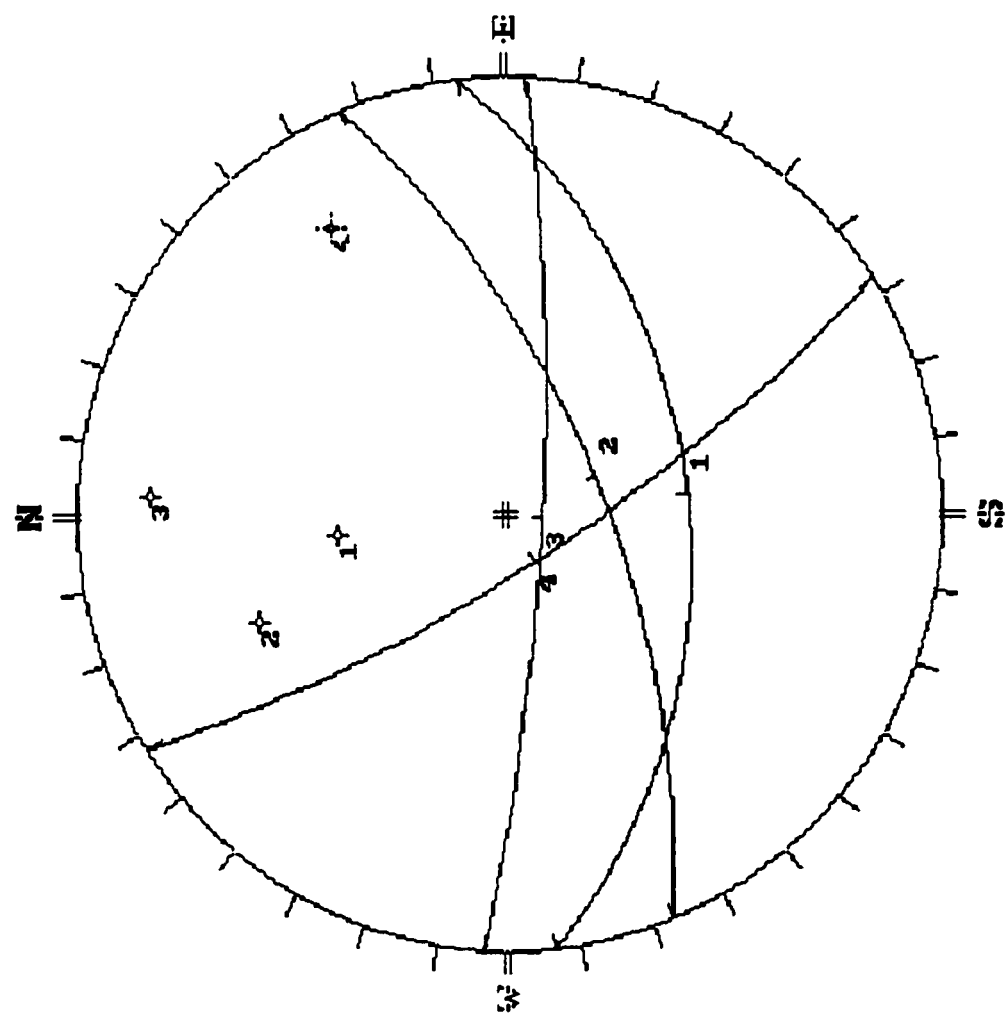
Figure 7.2: Major planes with their poles for the North limb.
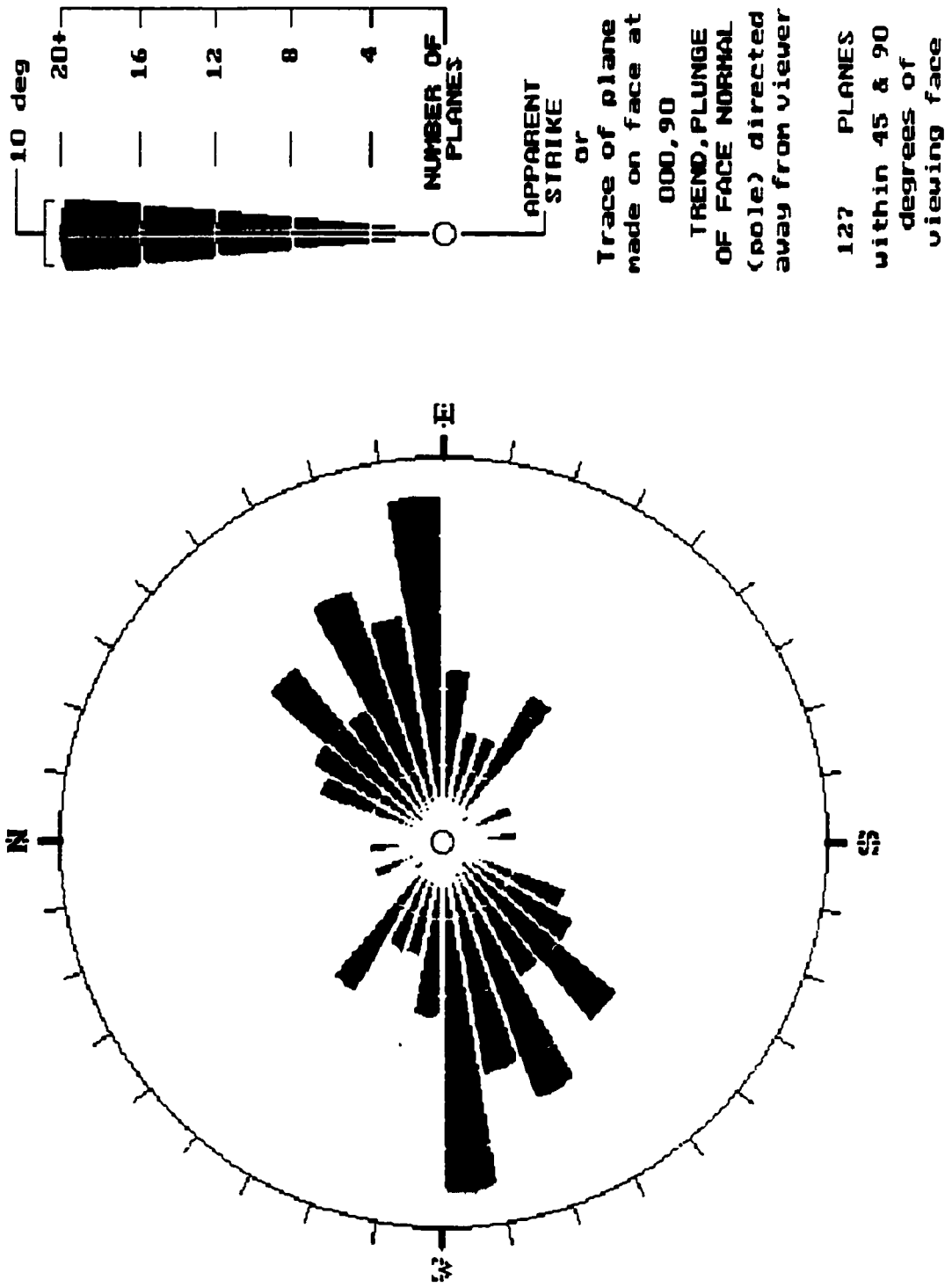
Figure 7.3: Rosette showing apparent strike of planes for the North limb.

7.3 DETERMINATION OF ROCK QUALITY DESIGNATION, RQD.

Deere developed the Rock Quality Designation Index (RQD) in 1967. This index was developed in response to the need for a quick and objective technique for estimating rock mass quality from diamond drill core logs during the initial exploratory phase of construction [Hoek et al., 1995; Hutchinson et al., 1996]. RQD is defined as the percentage of intact core pieces longer than 100 mm to the total length of core. The core for RQD examined in this research study was provided by the Geology department of Selebi North mine. The core was drilled from surface with a double-tube core barrel of NX size (54.7 mm in diameter). These were strategically located surface exploration holes, which intersected the ore at various points.

A total of 9 surface exploration holes were selected for RQD determination with 3 holes intersecting each limb. The core analyzed was 10 metres into both the hanging wall and footwall on either side of the orebody. RQD was then determined for the hanging wall, orebody and footwall and the results are shown in Table 7.1. Non of the surface holes actually intersected the Nose area, and as a result, the average RQD for the South and North limbs was assumed representative of the Nose area. The Selebi North rock mass has an RQD value of fair to good rock according to categories proposed by Deere.

A great deal of work has been done to correlate RQD with joint frequency, rock mass stiffness, and other properties. According to Hutchinson et al. (1996), RQD provides a crude estimate of the percentage of the rock mass, which can be expected to behave in a

fashion similar to a laboratory sample (typically 100 mm long). Therefore a low RQD (<50%) rock mass has few intact blocks larger than 100 mm. In such a case, joints and fractures dominate the rock's response to stress and gravity. The strength and stiffness of the rock, as determined in a laboratory sample, have little relevance here.

$$RQD = \frac{\Sigma \, Length \; of \; core \; pieces > 10 \; cm}{Total \; Length \; of \; Core \; Run} \times 100 \quad (\%)$$

$$eg: \quad \frac{29 + 15 + 13 + 32 + 24 + 33}{200} \times 100 = 73\%$$
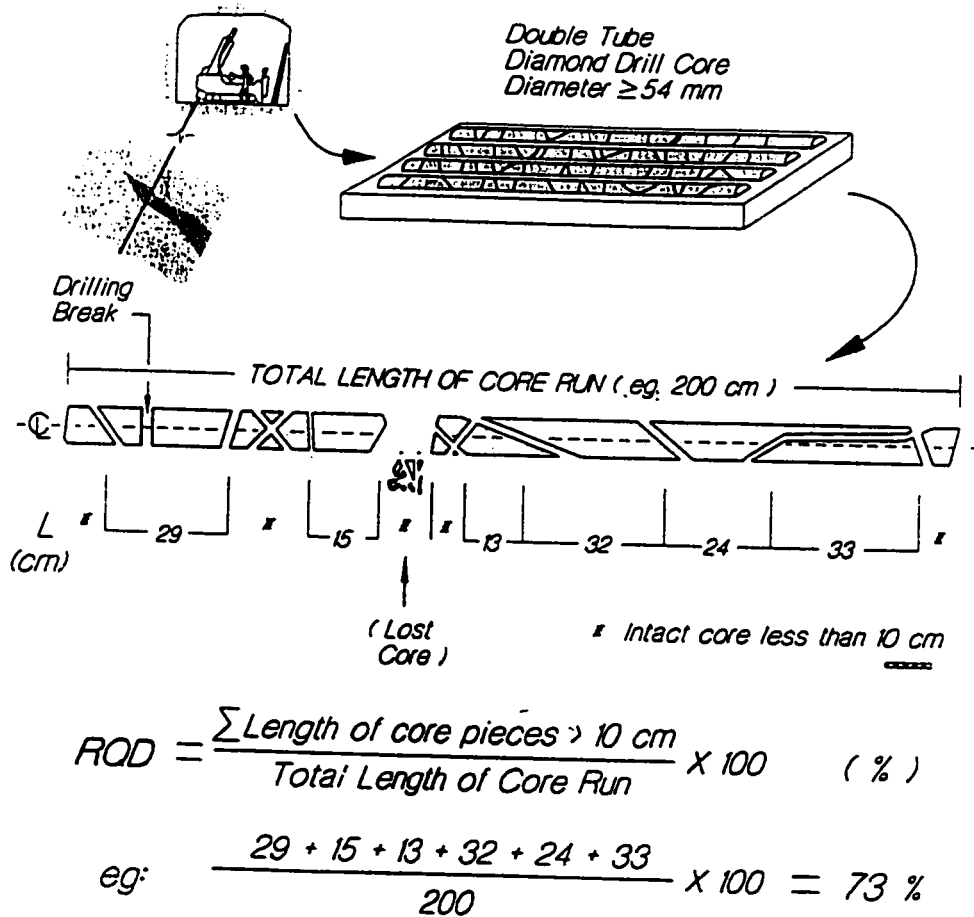
Figure 7.4: Conventional method for evaluation RQD from drill core

Table 7.1: RQD for Selebi North mine

HOLE	LOCATION	RQD(%)		
		Hanging wall	Orebody	Foot wall
SDN 44	South limb	73	72	60
SDN 45	South limb	77	48	61
SDN 46	South limb	49	70	69
Average	South limb	66	63	63
SDN 83	Detached limb	72	72	45
SDN 3	Detached limb	68	64	62
SDN 61	Detached limb	67	93	72
Average	Detached limb	69	76	60
SDN 41	North limb	97	77	80
SDN 43	North limb	81	70	82
SDN 38	North limb	63	70	84
Average	North limb	80	72	82
Average	Nose Area	73	68	73

Similarly, rock masses with RQD > 95% possess strength and stiffness much closer to the values obtained in the laboratory. However, joints may still dominate the rock's behavior

in low stress environments but may have little or no influence at depth provided they are clean and tight.

The measure of RQD is intended to determine the in situ and undisturbed rock mass conditions. As a result, all core broken during drilling, handling and discing, as well as, minor cracks in the core which are not related to established joints were ignored in the calculation of RQD. In hard rock mining applications, such as Selebi North mine. RQD typically measures between 50% and 100%. Values less than this would represent special conditions or an unusually poor rock mass. The case where RQD is measured perpendicular to schistosity or foliation is exempted, since such measurement may be much lower than the RQD of the surrounding rock.

7.4 DETERMINATION OF ROCKMASS RATING, RMR

The RMR classification system was developed by Bieniawski (1976) to predict the behavior of the openings, spans and pillars of tunnels in hard and soft rock. And he continuously redefined the system making changes and adjustments as necessary [Bieniawski, 1989;1993]. The six parameters used to classify the Selebi North rock mass using the RMR system and the adjusted RMR (RMRa) are shown in Table 7.2. Based on the results in Table 7.2, the Selebi North rock mass falls in the region of good rock to very good rock. It should be noted that the RMR values calculated are for the hanging wall rocks only, however the RMR values for both the orebody and footwall could be

calculated if required. A detailed description of the parameters used in RMR can be found in Hutchinson et al. (1996) and Hoek et al. (1995).

Table 7.2: Rock Mass Rating for Selebi North mine

PARAMETER	RATING FACTOR			
	South limb	North limb	Detached limb	Nose area
Uniaxial Compressive strength	12	12	12	12
Rock Quality Designation	13	17	13	13
Spacing of discontinuities	20	20	15	20
Condition of discontinuities	25	30	30	25
Groundwater conditions	15	15	15	15
Orientation of discontinuities	-10	-5	-5	-10
Adjusted RMR (RMRa)	75	89	80	75

Note: Bieniawski (1989) suggests that poor blasting can reduce RMR by up to 20%

A number of modifications which could lead to improved applicability of the RMR classification system, to mining could be found in Bieniawski (1989). Further work by Laubscher (1977; 1984), Laubscher and Taylor (1976), and Page and Laubscher (1990) and Stacey and Page (1986) describe a classification system based on RMR called Modified Rock Mass Rating which account for blasting, stress change, mining influences and reduced design stand-up times encountered in mining.

7.5 STOPE FAILURE ANALYSIS BY FIELD INSPECTION

Following the structural mapping along the drill drives in various areas of the mine as outlined in earlier sections, a visit was made to all the stoped out areas and to operating stopes. Since the stopes are operated on non-entry basis, observations were made from a remore location. The focus was on the behavior of both the hanging wall and footwall during and after mining. Failure modes and block sizes falling from the side walls were recorded. The original drill drive widths were recorded and the after-stoping widths were approximated. Some time was also spent at the primary crusher area determining the amount and size of sloughed side wall rocks, which were transported to surface.

The results of these observations showed that most stopes failed on both the hanging wall and footwall. The hanging walls failed by gravity falls while the footwalls failed by sliding along the weak planes. A typical structure of Selebi North is shown on Figure 7.5.
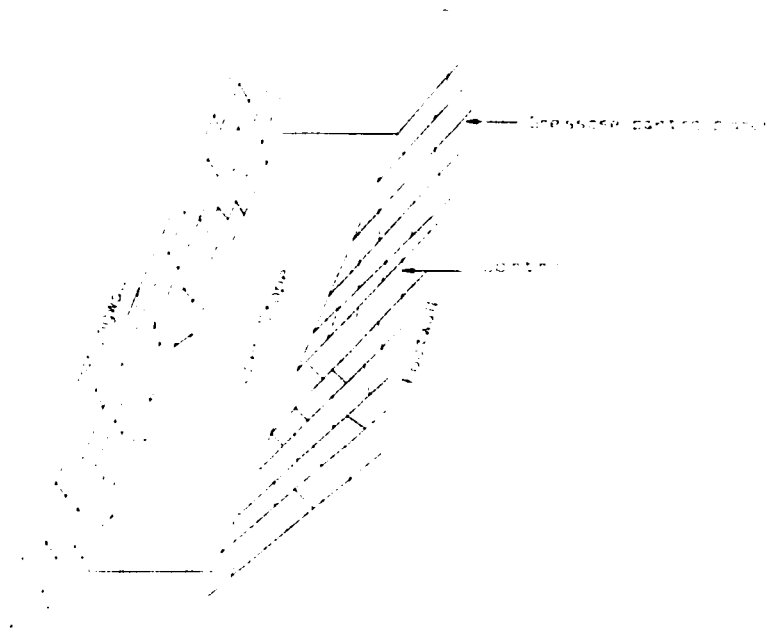
Figure 7.5: Geological discontinuities that affect stability at Selebi North mine.

In some cases, a big proportion of the hanging wall would fall into the stope and possibly burying some ore which might be hard to quantify, but from the field estimates the amount of ore lost is quite substantial. The hanging wall failure is induced by hanging wall overbreak during development, forcing the laminated rock to fall under gravity while rotating at the base. In the North limb, the rock structure is more competent and most stopes observed along the 1700 section had their hanging walls standing well, simply because of proper drilling and blasting techniques during the development of the drill drives. However, in this region, failure came from the footwall due to sliding increasing the stoped out area from the original drill drive of 4.2 m to about 6 - 8 m as shown in Figure 7.6.
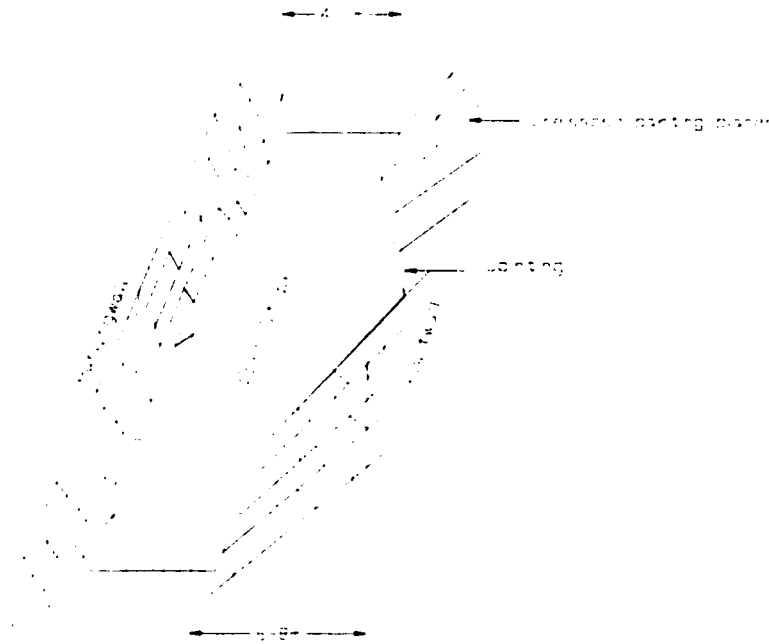
Figure 7.6: Sliding failure mode observed on the North limb stopes.

The stopes on the South limb are dominated by failure of the hanging wall under gravity, sliding of the footwall and wedge failure of the roof. In the region from the 300 to about 600 sections, all the failure modes occur at the same time. From observations, the 500 section on the South limb is the most unstable part of the mine. Stopes in this region of the mine have always been abandoned due to rock falls at a great cost to the mine in terms of uncontrolled ore losses. One of those stopes abandoned is the 280 metre level 500 section stope shown in Figure 7.7. In this stope, sliding failure from the footwall blocked the draw area with big waste rocks while those rocks falling from the hanging wall due to gravity sat on top of the blasted ore. These rocks could easily slide and bury the loader and the driver, and as a result the stope had to be abandoned for safety reasons.
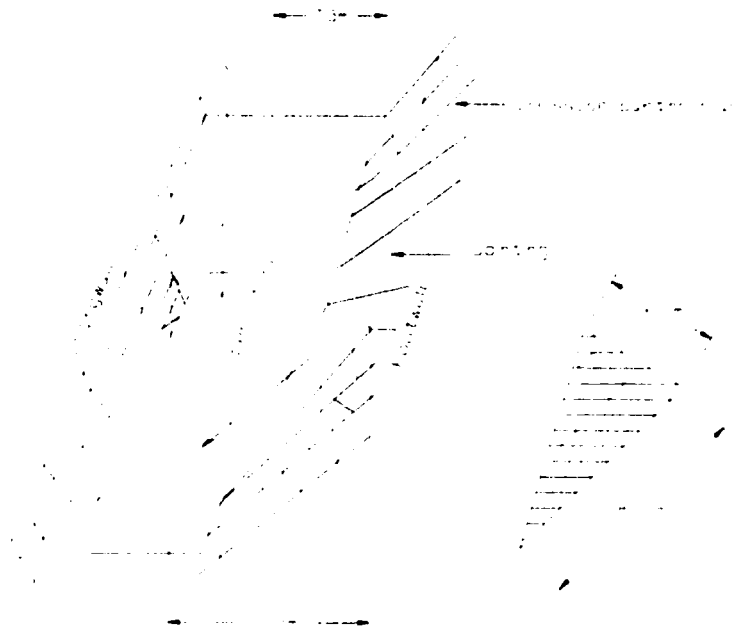
Figure 7.7: Typical cross section of the South limb stope (280/500) showing block sizes.
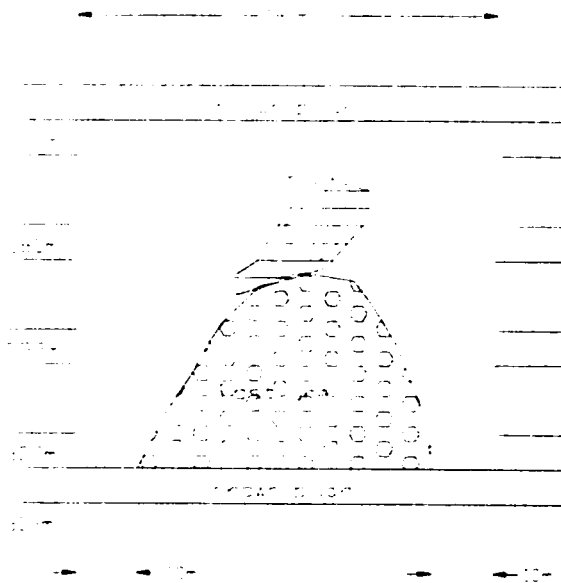
Figure 7.8: Longitudinal section of the South limb stope (280/500).

One of the major problems faced when the ore is frozen inside the stope is that it oxidizes and does not flow at the angle of repose as expected from method design. Figure 7.8 shows the amount of ore lost in the 500 section stope due to side wall failure. The lost ore is estimated to be more than 75 000 tonnes in this stope only. However, Figure 7.9 shows a typical wedge failure as observed along the 280 ml 300 section drill drive which was already being stoped. In this area the failure planes are dominated by shear zones which ran parallel to the orebody, hence this mode of failure was observed from 300 section line to about 600 section line covering a block from 190 ml to 349 ml.
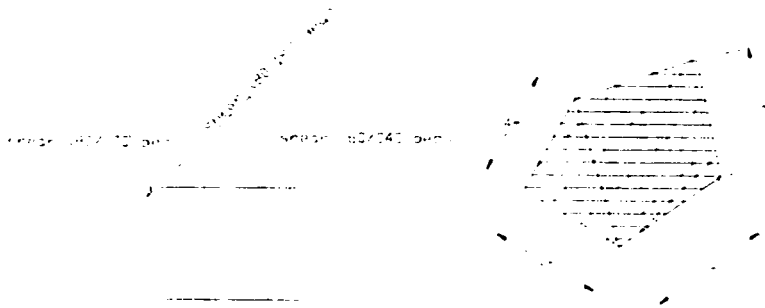
Figure 7.9: Showing the details of wedge failure on the South limb (280/300).

The mine plans show that a block of ground was abandoned between 300 and 400 section lines due to a fall of ground at 190 ml. The other case is the 280 ml 500 section stope shown in Figure 7.8 and several other stopes along the 300 section line. In general, the stopes double in width by the time they are mined out due to side wall failure.

7.6: OBSERVED DILUTION

According to Aplin (1997), serious dilution has been experienced at Selebi North mine during the early stages of the mine. It was observed that once the sublevel stopes exceeded a span of 30 metres along strike, sloughing from the hanging wall and footwall occurred contaminating the draw points. Dilution was said to be caused by geological structures and poor long hole drilling.

Three types of discontinuities have since been identified at Selebi North mine. The stability of the stopes is affected by joints, gneissose parting planes and shears. The hanging wall rock is also intensely jointed with a fracture frequency greater than 4 per metre to a depth of 3 metres. In most cases, the joints are almost parallel to the hanging wall and can be traced over the entire length of the orebody on strike. They tend to form thin (0.2 to 0.5m) plates that buckle readily. The footwall amphibolite is the host of gneissose parting planes, which have little tensile strength. Once the orebody has been mined out and the amphibolite is de-stressed, dilation of the bedding planes occur. The major planes of weakness are the shears, which are mostly found in the South limb and are mostly confined in or around the orebody. In the South limb, where shears occur in sets or with lubricated bedding planes, block and wedge failures are common. Long hole drilling accuracy has been fairly achieved at Selebi North mine with the drilling levels placed at 15 metres apart.

At BCL, dilution (tonnes waste divided by tonnes ore plus tonnes waste) is monitored by geology department on daily basis and dilution figures are released monthly. The monthly dilution figures observed from the Detached limb stopes of 247 ml 1200 and 1300 sections, from May 1996 to April 1997 are shown in Figure 7.10. The figures for the South limb stopes of 307 ml 400 and 500 sections in the same period, are shown in Figure 7.11. The results show that, within this period, average dilution has been more than 100 % in the Detached limb stopes while in the South limb stopes dilution has been above 20 %. It should be noted that the Detached limb ore pinches and swells and could be as thin as 0.5 m in some places and this could be the reason for exceptionally high dilution figures. It might be of interest to note that the creeping cone mining method has been in full operation since February 1996, and as a result the dilution values shown in Figures 7.10 and 7.11 are fully credited to the creeping cone and not to sublevel open stoping.
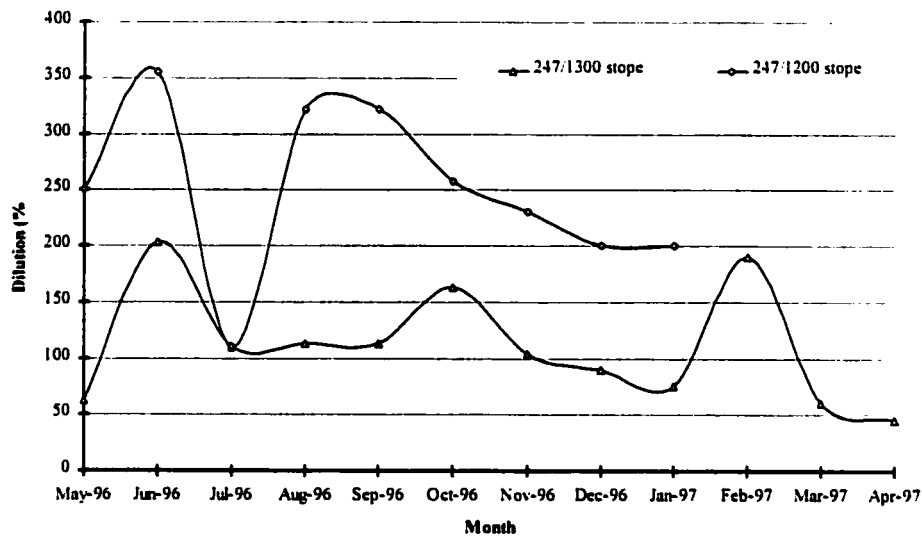
Figure 7.10: Dilution of the Detached limb of Selebi North mine.

The span of the 307 ml 500 section stope along the strike is 191 m with a stoping height of 47 m. At the same stoping height, the 400 stope has a span ranging from 120 to 147m. On the Detached limb, the 1300 section stope has a span ranging from 102 to 185 m and the 1200 section stope has a span ranging from 120 to 133 m. The nominal height of these stopes is 57 m. One objective of this research is to provide appropriate dimensions that minimize dilution and to develop a correlation between stope dimensioning and dilution if any.
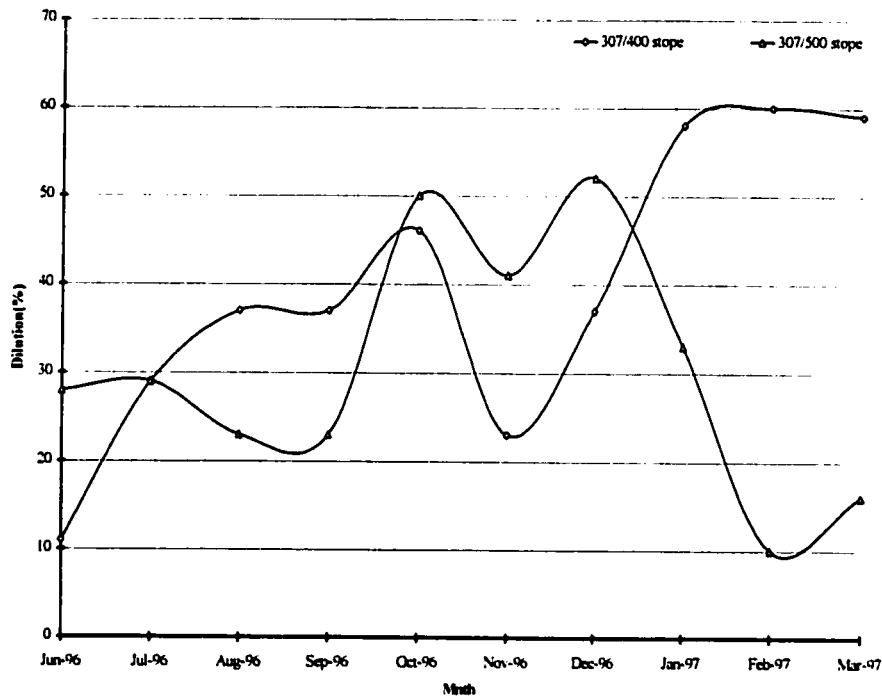
Figure 7.11: Dilution of the South limb of Selebi North mine.

7.7 CONCLUSION

In this chapter, geological data have been analyzed to determine RQD from surface exploration holes drilled into the South, North and Detached limbs. RQD values have been determined for the hanging wall, ore body and footwall rocks. Selebi North mine has RQD values of fair to good rock. The RMR values determined also showed that the rock mass is in the region of good rock to very good rock. The observations made in existing stopes have shown that the hanging wall and stope back fail due to gravity falls while the footwall fail by sliding. These are the main sources of dilution at the mine.

CHAPTER 8

IN-SITU STRESS MEASUREMENT

8.1 INTRODUCTION

The Council for Scientific and Industrial Research (CSIR) triaxial strain cell was used at BCL mine to determine the directions and magnitude of the in-situ stresses at three different locations in the mine. This was followed by biaxial laboratory tests on the overcored sections to determine the elastic properties of the rock. Two sets of measurements were carried out at number Three Shaft, while a third set of measurements was performed at Selebi shaft.

Figures 8.1 and 8.2 illustrate the CSIR triaxial stress cell used to determine the in situ stress field. The deformational characteristics are required to evaluate the tests. These were determined by radial loading tests on the hollow overcored pieces which contained the strain cells. The test was carried out in two boreholes at number Three Shaft, at 810 and 750 metre levels, boreholes RM1 and RM2 respectively. Another borehole RM3 at 650 metre level was used for testing at the Selebi Shaft. The boreholes were pre-drilled to 12 metres in depth and measurements were made in the footwall of the orebody. The bearings were measured clockwise from north while the dip was considered positive from horizontal downwards.
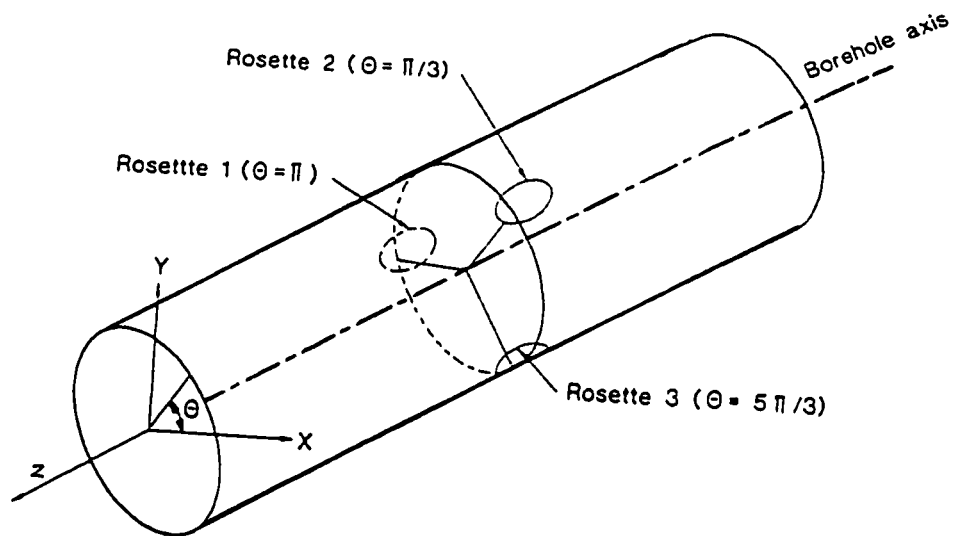
Figure 8.1: Position of three rosette gauges used with the strain cell
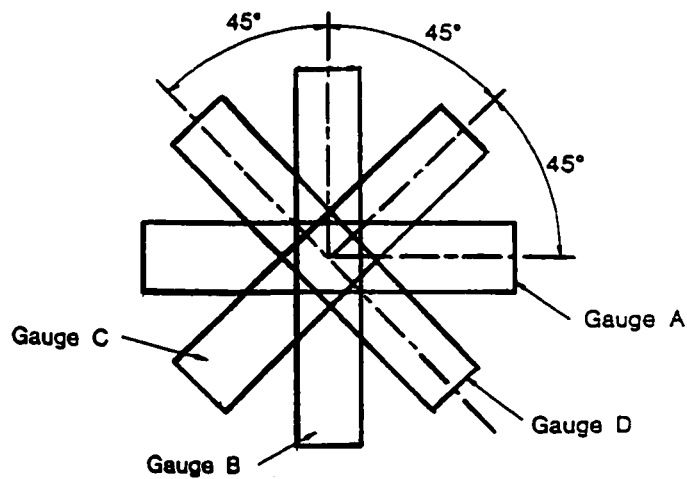
Figure 8.2: Strain gauge configuration for each rosette viewed from borehole axis

The theoretical overburden stress was calculated by the product of density, gravitational constant (9.81 m/s^2) and the depth below surface, the results are shown in Table 8.1.

Table 8.1: Details of the test site.

Borehole number	Location	Bearing (°)	Dip (°)	Depth Below Surface (m)	Density (kg/m^3)	Theoretical Overburden Stress (MPa)
RM1	3 Shaft	272	-6	810	2910	23
RM2	3 Shaft	267	-5	750	2980	22
RM3	Selebi	135	-6	650	2750	18

8.2 TEST PROCEDURE

8.2.1 Field measurement

The CSIR triaxial strain cell was used to carry out measurements in the boreholes. The first measurement in each of the boreholes was made at a distance of at least two and a half times the width of the excavation to insure that it was outside the zone of stress alterations induced by the excavations.

For details on how to operate the CSIR strain cell the reader is referred to Leeman (1969). However, the CSIR strain cell consists of a cylindrical plastic body into which three rosettes are incorporated in such a way that they can be expanded against and glued to the sidewalls of an EX borehole. The position of the strain gauge rosettes, relative to a system of coordinates (x, y, and z) are shown in Figure 8.1. The z-direction coincides with the direction of the longitudinal axis of the borehole. The orientation of the

125

Step

(a) NXCU Borehole drilled to the depth at which the stress is to be determined

(b) EX Borehole drilled into the end of the NXCU borehole

(c) Strain cell installed in the EX portion of borehole and strain readings taken

(d) EX Portion of borehole overcored

(e) Cylindrical core removed and final readings taken
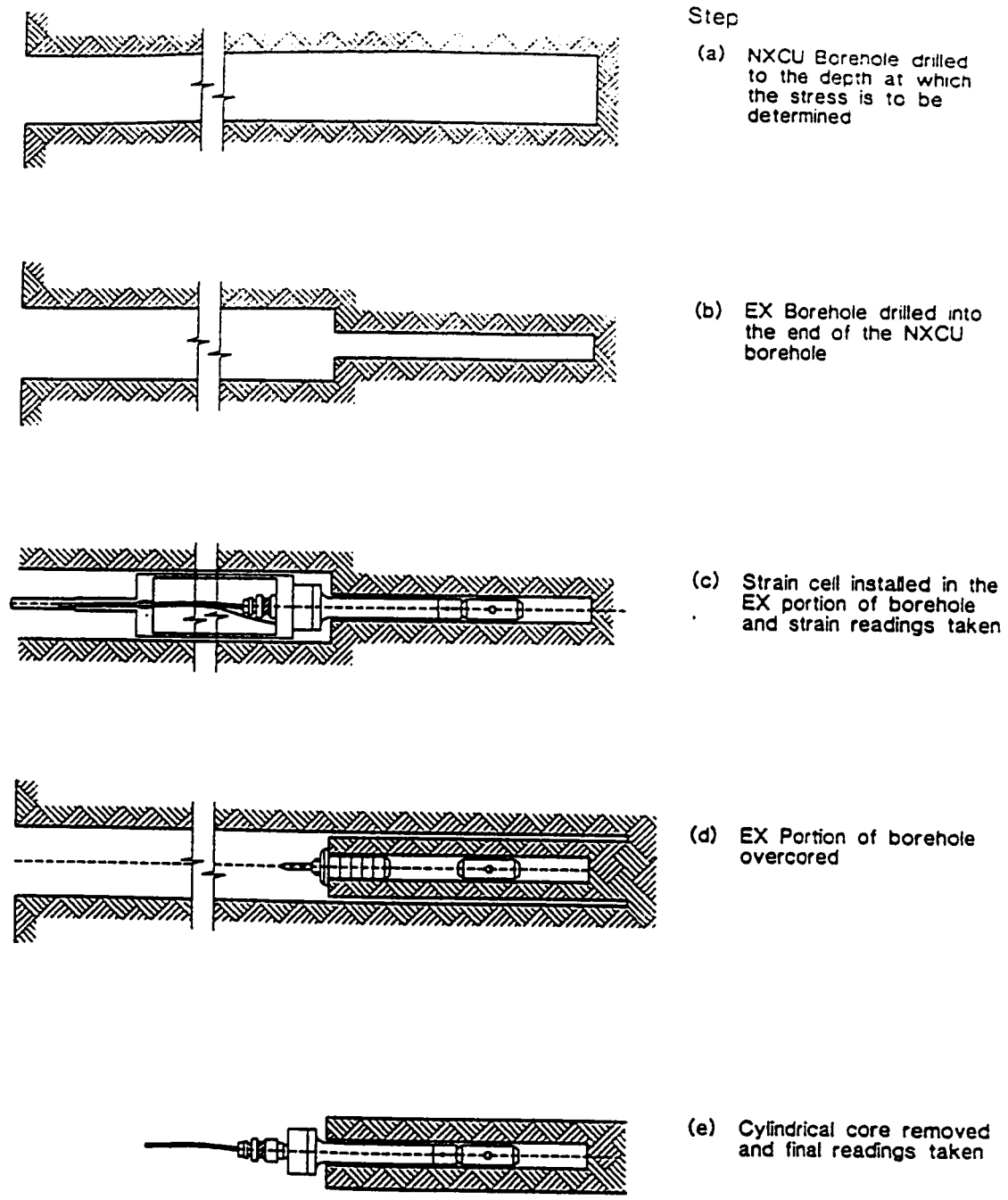
Figure 8.3: Overcoring technique

individual strain gauges in each of the three strain gauge rosettes are shown in Figure 8.2. Figure 8.3 shows the various stages of drilling and testing process.

The process involved grinding flat the existing NXCU borehole, which had been drilled to a depth of 12 metres. Then an EX borehole was drilled concentrically into the end of the NXCU borehole for a distance of 450 mm. To ensure that the glue would adhere to a moist surface, the EX portion of the borehole was sprayed with a suitable primer. After preparing the strain cells, a thin layer of glue was applied to each of the rosette gauges. The cell was installed in the EX portion of the borehole using a suitable installing tool containing orientating device and extension rods.

The glue was then left overnight to harden and initial readings were taken from each of the twelve gauges in the strain cell. The installing tool was removed and the borehole was overcored by extending the NXCU borehole past the end of the EX borehole. The cylindrical core was removed from the borehole and the installation tool was reconnected to the strain cell. A final set of twelve strain readings was then taken.

The stress tensor components were computed from the twelve measurements for strain which are the differences between the final and initial readings, as well as the modulus of elasticity and Poisson's ratio of the rock. These twelve values are referred to as e_i ($i = 1$ to 12).
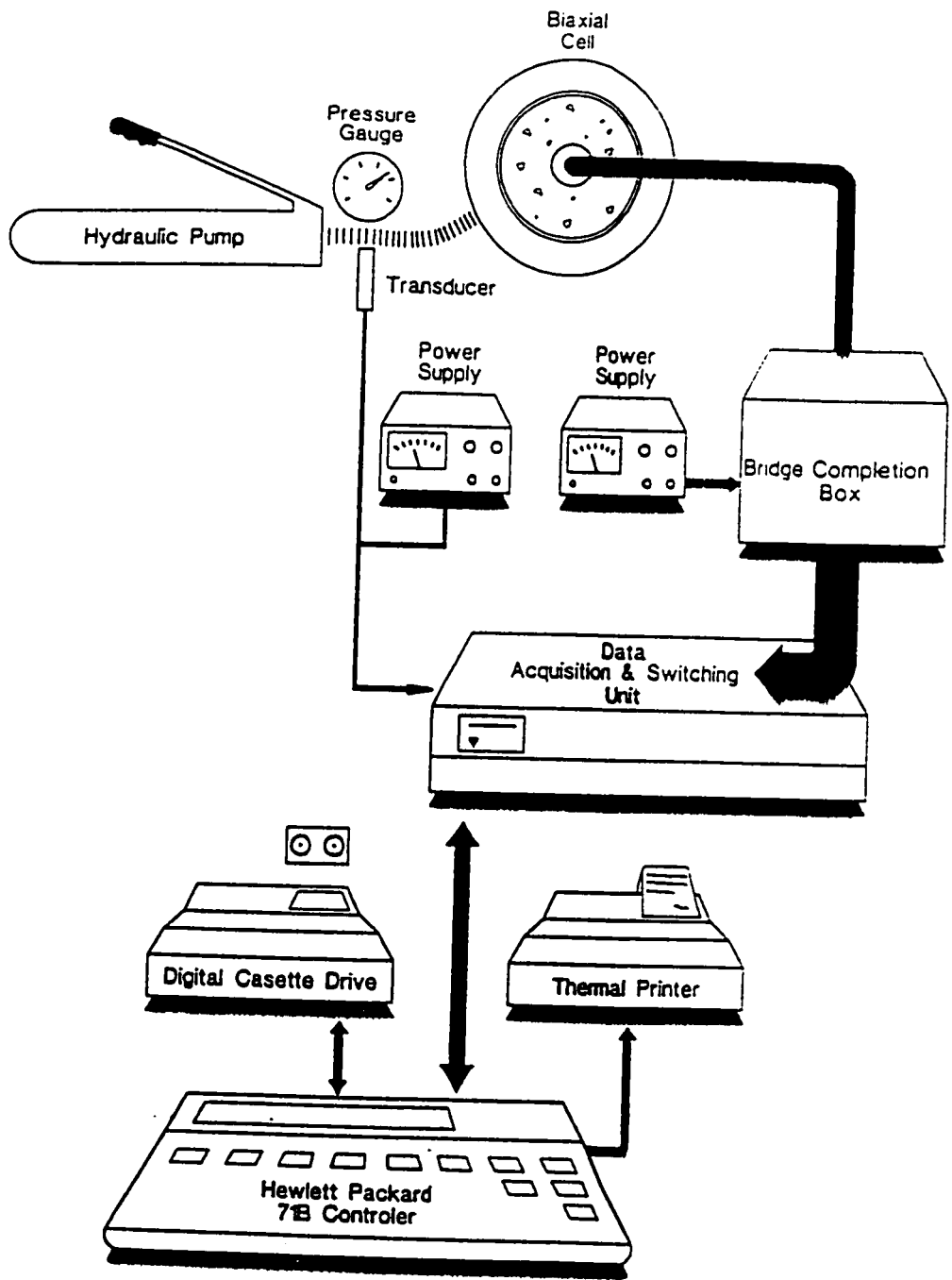
Figure 8.4: Biaxial test instrumentation layout

8.2.2 Laboratory measurements

Each of the overcored specimens was taken into the laboratory and a biaxial loading test was carried out to determine the modulus of elasticity and Poisson's ratio. The overcored specimen was subjected to a radial pressure in a cylindrical pressure cell while measuring the applied stress and the resulting strain measured by the imbedded strain cell. A stepwise loading procedure was followed, taking readings at approximately 2 MPa intervals up to a maximum of 18 MPa. Readings were also taken during unloading at approximately 5 MPa intervals. A computerised data acquisition system was used to accumulate all pressure and strain readings. The biaxial test arrangement is illustrated in Figure 8.4.

8.3 CALCULATION OF RESULTS

The thick-walled cylinder equations were used to calculate the material properties from the biaxial tests using equations (8.1) and (8.2). For the purpose of this research, concentric installations were assumed for the validity of the thick wall cylinder equations.

$$E = \frac{P}{e} \times K \qquad (8.1)$$

$$K = \frac{2D^2}{D^2 - d^2} \qquad (8.2)$$

E = Rock mass stiffness (GPa)

P = Pressure in Biaxial Cell

e = Circumferential strain (gauges 1, 5 & 9)

e = Axial Strain (gauges 2, 6 & 10)

D = Overcore external radius

d = Overcore internal radius

The Poisson's ratio was calculated using equation 8.3 where:

$$\mu = \frac{Axial\ Strain}{Circumferential\ Strain}$$

i.e.

$$\frac{e2}{e1},\ \frac{e6}{e5},\ \frac{e10}{e9} \tag{8.3}$$

The tangent method was used to calculate the elastic constants during the unloading cycle. The graphical output are shown in appendix B together with the detailed calculations of stresses. However, the average stress results are shown in Table 8.2 and 8.3. The values are assumed applicable to Selebi North mine since it is located equidistant between Selebi-Phikwe (3 shaft) and Selebi Shaft and the rock formation is similar.

The in-situ stress calculations were done using measured strains and elastic constants by a computer program which incorporates the method of least squares. The program is such that the z-axis of the coordinate system to which the stresses are referred coincided with the direction of the borehole axis.

Table 8.2: Normal and Shear stresses for Selebi-Phikwe Rocks.

STRESS LOCATION	Normal Stress			Shear Stress		
	Z (vert.) (MPa/m)	X (strike) (MPa/m)	Y (dip) (MPa/m)	YZ (MPa/m)	ZX (MPa/m)	XY (MPa/m)
Selebi-Phikwe	0.030	0.038	0.044	0.0026	-0.0026	-0.006
Selebi	0.023	0.011	0.026	0.012	-0.0021	0.0023
Average (Selebi North)	0.027	0.0245	0.035	0.0073	-0.0024	-0.00185

Table 8.3: Principal Stresses for Selebi Phikwe rocks

Location	σ_1			σ_2			σ_3		
	Stress (MPa)	Bear. (°)	Dip (°)	Stress (MPa)	Bear. (°)	Dip (°)	Stress (MPa)	Bear. (°)	Dip (°)
Selebi-Phikwe	42.69	139	27	18.24	199	2	18.49	149	-13
Selebi	26.37	179	47	10.00	135	-22	2.07	240	-30
Average (Selebi North)	34.53	159	37	13.62	167	-10	10.28	195	-22

The stress transformation laws were used to calculate the stresses with respect to the coordinate system such that the x-axis was along the east- west, y-axis along the vertical and the z-axis along the north-south direction.

Table 8.4 shows other important parameters for the Selebi-Phikwe rocks that are used by BCL Rock Mechanics department for mine design and computer modelling.

Table 8.4: Rock Parameters for Selebi-Phikwe Rocks

PARAMETER	HW	Sulphides	FW	Amphibolite	Dyke
RMR	80	70	82	75	95
UCS (MPa)	122	95	189	125	273
Tensile (MPa)	13	8	15	13	25
Y.Modulus (MPa)	78	80	90	65	98
Poisson's Ratio	0.25	0.24	0.26	0.24	0.27
Hoek&Brown, m	-	4.06	-	1.54	-
s	-	0.016	-	0.013	-
Density (t/m³)	2.88	3.5	2.9	2.95	2.95
Friction Angle °	40	50	40	30	-
Cohesion (MPa)	30	22	21	24	-
Dilation Angle °	12	15	12	12	-
Bulk Mod. (GPa)	52	51	62	42	-
Shear Mod. (GPa)	31	32	37	26	-

(source BCL Ltd. Rock Mechanics Dept., 1991)

8.4 DISCUSSION OF THE RESULTS

Strain measurements can be accurate to about 5 microstrain under controlled laboratory conditions. However, given the less than ideal field conditions where the 'remote control' procedure was used to install and monitor the strain cells underground, the strain measurements are assumed to be accurate to about 50 microstrain. For this investigation, the modulus values varied between 72 and 93 GPa, therefore stresses were assumed to be

measured to an accuracy of 3 to 4 MPa. Stresses can also vary significantly from location to location in the rockmass.

If the strain measurements are correct and the rock is assumed to be homogenous, the relationship $e2 = e6 = e10$ should be true for gauges aligned in the same direction (axial) in the borehole. For the fact that the rock is seldomly perfectly homogenous and elastically isotropic none of the measurements were discarded on the basis of the above relationship. The method of least squares was used to provide the best fit solution since it compensates, to some extend, for the differences in stresses in cases where the above relationship is not exactly satisfied by the field measurements.

Experience has shown that modulus values calculated from biaxial tests are slightly higher than values derived from a direct compression test due to the high sensitivity of the correction applied by the thick wall cylinder equation. To compensate for this bias the average lowest modulus value was used to determine the stresses.

8.5 CONCLUSION

The normal stresses for Selebi North mine have been determined as 0.027 MPa/m in the vertical direction, 0.0245 MPa/m along the ore body strike and 0.035 MPa/m in the dip direction. The respective shear stresses are 0.0073 MPa/m in the XY direction, -0.0024 MPa/m in the ZX direction and -0.00185 MPa/m in the XY direction.

The major principal stress at Selebi North mine was determined as 34.53 MPa at a bearing of 159 degrees and dipping at 37 degrees. The intermediate principal stress was determined as 13.62 MPa acting at a bearing of 167 degrees and dipping at -10 degrees. The minor principal stress was determined as 10.28 MPa with a bearing of 195 degrees and dipping at -22 degrees.

.

CHAPTER 9

THE CREEPING CONE MINING METHOD DESIGN USING ANALYTICAL METHODS

9.1 INTRODUCTION

This chapter looks at the use of analytical methods in designing the stable dimensions for the proposed modified creeping cone mining method. The voussoir arch and the simple beam theory methods are used to calculate the allowable span between rib pillars. An initial safety factor of 4.0 is also assumed as a starting point for methods. Both methods assume that if failure occurs it will be due to buckling of the hanging wall or shearing at the abutments. Two methods are used here in order to build confidence in the calculations in view of the assumptions made during the determination of the input parameters.

9.2 VOUSSOIR ARCH METHOD

This method is used to determine the span between the rib pillars. The span is the strike length of the open stope before failure can occur either on the stope hanging wall or on the crown pillar forming the roof of the stope. The method has been used in the design of minimum span for caving in longwall coal mining [Brady and Brown, 1982]. The minimum span in longwall mining is adapted here as the maximum span allowed between rib pillars before the crown pillar or the stope hangingwall starts to arch in a

hardrock mining environment. This will be similar to a span between a longwall working face and the gob. The unit weight of the hanging wall gneiss is 2.88 tonnes per cubic metre while that of the sulphide orebody is 3.5 tonnes per cubic metre at Selebi North mine. The uniaxial compressive strength of the hanging wall and orebody rocks are 122 MPa and 95 MPa respectively. Young's modulus for both the hanging wall and orebody rocks are 78 GPa and 80 GPa, respectively, and the modulus of rupture is 52 GPa with a buckling factor for general rock products as 1.33.

Detailed calculations of the required span and safety factor are provided in Appendix C. and the results are summarized in this chapter. The initial analysis indicated that the hanging wall was capable of reaching 342 metres and the crown pillar 275 metres before failure can occur due to crushing at the abutments. However, further analysis indicate that buckling failure would occur before shear failure. The design has been limited to a safety factor of 4 which has been assumed in order to shorten the iterative process. The assumed safety factor is a little bit more conservative compared to the recommendations made by Hoek and Brown (1994) for a safety factor of 2 in most mining projects. This is mainly to account for the various assumptions made during the selection of the input parameters used for the design. An iteration process was setup to assess the limiting span for buckling failure. Table 9.1 shows the results of the iterative procedure used to calculate the load/depth factor, N. Small increments in the span of the excavation, have adverse effect in the change of magnitude for both the maximum stress and the arch thrust moment. Table 9.1 show that before the hanging wall can fail by buckling, a span of 120 metres at a safety factor of 4.2 can be achieved, this happens when $Z1 </= 0$.

However, it is worthy to note that the safety factor calculated here is a measure of the uniaxial compressive strength of the hanging wall rock against maximum stress at the ends and center of the outer fiber of the hanging wall rock. The plot of the safety factor against the allowable span is shown in Figure 9.1. It is clear that the safety factor is inversely proportional to the allowable span and it changes rapidly in response to an incremental change in the span.

Table 9.1: Simulation of a mine roof as a voussoir beam.

N	Zo	Fm	S	Fav	d1	d2	d1+d2	Z1	N1	Fs
1.3	2.4	186.0923	120.13	122.51	188.48	272	460.6	249.4	-19.3	0.66
1.315	2.22	170.1719	120.11	112.67	173.34	252	425.1	227.7	-17.5	0.72
1.33	2.04	154.6105	120.09	102.94	158.38	231	389.7	205.9	-15.7	0.79
1.345	1.86	139.3963	120.08	93.337	143.6	211	354.5	184	-13.8	0.88
1.36	1.68	124.5176	120.06	83.842	128.99	191	319.5	162.1	-12	0.98
1.375	1.5	109.9636	120.05	74.455	114.55	170	284.6	140	-10.2	1.11
1.39	1.32	95.72374	120.04	65.172	100.26	150	250	117.7	-8.3	1.27
1.405	1.14	81.7879	120.03	55.991	86.139	129	215.4	94.98	-6.41	1.49
1.42	0.96	68.14648	120.02	46.907	72.165	109	181	71.59	-4.47	1.79
1.435	0.78	54.79024	120.01	37.919	58.338	88.5	146.8	46.43	-2.37	2.23
1.45	0.6	41.71034	120.01	29.023	44.651	68	112.7	10.62	0.61	2.92
1.465	0.42	28.89829	120	20.217	31.103	47.6	78.73	0	0.7	4.22
1.48	0.24	16.34595	120	11.497	17.687	27.2	44.9	8.62	0.78	7.46
1.495	0.06	4.045485	120	2.8605	4.4008	6.8	11.2	10.62	-0.1	30.2
1.51	-0.12	-8.010596	120	-5.694	-8.76	-13.6	-22.4	34.84	-1.4	-15.2
1.525	-0.3	-19.82951	120	-14.17	-21.8	-34	-55.8	61.71	-3.64	-6.15
1.54	-0.48	-31.41818	120.01	-22.57	-34.72	-54.4	-89.2	85.61	-5.63	-3.88
1.555	-0.66	-42.78328	120.01	-30.89	-47.53	-74.8	-122	108.5	-7.54	-2.85
1.57	-0.84	-53.93121	120.02	-39.15	-60.22	-95.3	-155	131	-9.42	-2.26
1.585	-1.02	-64.86814	120.02	-47.33	-72.81	-116	-188	153.2	-11.3	-1.88
1.685	-2.22	-132.8047	120.11	-100.2	-154.2	-252	-406	298.7	-23.4	-0.92
1.785	-3.42	-193.1294	120.26	-150.6	-231.6	-388	-619	443.1	-35.4	-0.63
1.885	-4.62	-247.0536	120.47	-198.8	-305.8	-524	-830	587.1	-47.4	-0.49
1.985	-5.82	-295.5446	120.75	-245.2	-377.2	-660	-1037	731.1	-59.4	-0.41
2.085	-7.02	-339.3842	121.1	-290	-446.2	-796	-1242	875	-71.4	-0.36
2.185	-8.22	-379.211	121.5	-333.5	-513.2	-932	-1445	1019	-83.4	-0.32
2.285	-9.42	-415.5519	121.97	-375.9	-578.3	-1068	-1647	1163	-95.4	-0.29

(d1 + d2 = ΔL in Table 9.1)

Therefore, with the assumptions made to arrive at this solution, a higher value of the safety factor would be used to cater for the uncertainties and the sensitivity of the safety factor to the change in span. The preliminary design will use a maximum allowable span of 120 metres at a safety factor of 4.2 as determined in Table 9.1. These preliminary results will be compared with the results obtained using the simple beam theory method. which follows, in the next section of this chapter. The results will further be compared to those obtained by using empirical methods in the later chapters before choosing the final design parameters.
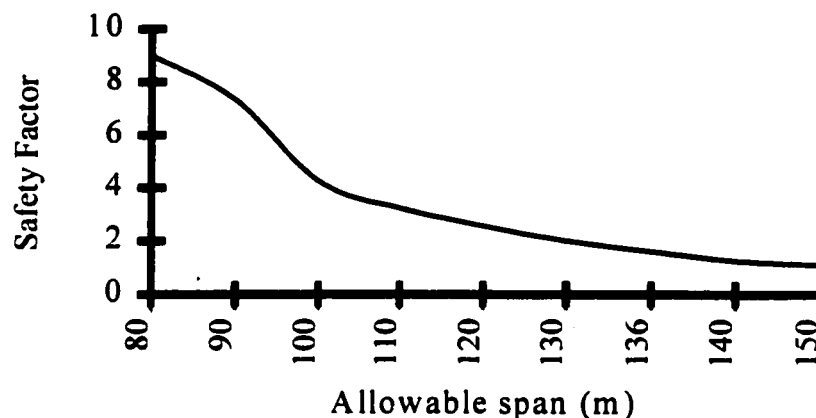
Figure 9.1: Safety factor against allowable span

9.3 BEAM THEORY

Since the overlying rock strata is massive and competent, the beam theory can be used to re-calculate the maximum allowable span between the rib pillars, following the voussoir arch method. The results are then compared to those obtained by the voussoir arch method and are summarized below with detailed calculations done in Appendix C. In

order to calculate the span, a factor of safety of 4 is assumed. The modulus of rapture of the hanging wall rock is 55 GPa. The shear force and the extent of the hanging wall failure were both calculated by the voussoir arch method as 86.87 MN/m and 18 metres respectively from Appendix C.

Therefore, the hanging wall span was calculated as 96 metres at a safety factor of 4 before failure can occur by rupture. Further investigations revealed that, for a safety factor of 4, the hanging wall span could reach 257 metres before shear failure occurs. From the beam theory, for failure to occur by shearing at the hanging wall abutments, the span of the hanging wall between the rib pillars has to exceed 257 metres. Therefore, failure would not occur through shearing of the abutment but would occur by rupture once the hanging wall span exceeds 96 metres.

The two methods provide similar maximum allowable span for the hanging wall rock. The voussoir arch method gave a span of 120 metres with a safety factor of 4.2 and the beam theory method gave the maximum allowable span of 96 metres with a safety factor of 4. Based on these results the preliminary design value for the maximum allowable span is taken as 96 metres.

9.4 RIB PILLAR DESIGN

9.4.1 Pillar Stress

The tributary area theory Coates of (1965), Brady and Brown (1985) and Hoek and Brown (1994), remains the most widely used method in pillar analysis for both metalliferous and non-metal mines. The method assumes that pillars support areas tributary to their locations and that each pillar would be loaded with the normal stress σ_p acting over the area of the wall tributary to it. However, Hoek and Brown (1994) caution that when mining an inclined orebody, the stress field acting upon the stopes and the pillars between the stopes is no longer aligned normal to and parallel to the stope boundaries. Therefore, the inclination of the stress field to the stope boundaries results in a considerable change in the stress distributions induced in the rock surrounding the stopes.

For a rib pillar loaded with normal stress, σ_p, between stopes of width, w_o, and the pillar width being, w_p, the normal stress is given by equation (4.20). Using this equation, the only unknown is w_p. The other variables are assumed in order to determine the pillar width. Mining is assumed to be at 300 metres below surface, the weight of the rock is 28253 N/m^2, and the stoping span is 96 metres from sections 9.2 and 9.3 of this report. Therefore, w_p can be estimated from equation (4.21) as:

$$\sigma_p = 0.028253 \times 300 \times k \times \left(1 + \frac{96}{w_p}\right) \qquad (9.1)$$

k is the stress concentration factor, introduced to compensate for the fact that the pillar loading is somehow horizontal due to the orebody steepness. From the in-situ stress results k is taken as 0.544.

9.4.2 Pillar Strength

Hoek and Brown (1994) expressed the principal stress in terms of material constants. m and s. For defining the relationship between principal stresses and the Mohr's failure envelope for the intact rock specimen and for heavily jointed rock masses. The constants depend on the properties of the rock and the extent to which it has been fractured before being subjected to the principal stresses. However, Pine (1991) calculated the pillar strength as follows;

$$\sigma_{,} = \sqrt{e^{\sqrt{\frac{RMR-100}{9}}}} \times \sigma_{c} \times \left(0.778 + 0.222 \frac{w_{p}}{H} \right) \tag{9.2}$$

Assuming RMR of 80%, σc = 95 MPa for the orebody. A full stoping width of 6 metres will yield a rib pillar of height H = 6 metres. allowing the strength of the rib pillar to be calculated using equation (9.3).

$$\sigma_{,} = \sqrt{e^{\sqrt{\frac{80-100}{9}}}} \times 95 \times \left(0.778 + 0.222 \frac{w_{p}}{6} \right) \tag{9.3}$$

In order to make an estimate of the rib pillar width, a safety factor of 4 is assumed. and expressed in terms of the pillar strength and stress using equations (9.3) and (9.1). respectively.

$$4 = \frac{24.33 + 1.6 w_{p}}{4.61 + \frac{415}{w_{p}}} \tag{9.4}$$

Therefore, from equation (9.4) w_p = 30 metres. Extraction ratio, R_e is given by equation (9.5).

$$R_e = 1 - \left(\frac{30}{30+96}\right) = 76\% \tag{9.5}$$

If the safety factor is reduced to 2, w_p becomes 18 metres at an extraction ratio of 84.21%. Therefore, for preliminary design, the stope length along strike is 96 metres, with an 18metre wide rib pillar and the factor of safety of 2 at an extraction ratio of 84.21%. For pillar design, Hoek and Brown (1994) recommended a factor of safety of 1.6. Due to confidence in the integrity of the input parameters used in equation (9.4), the factor of safety was lowered to 2 without sacrificing safety for the sake of improving production, while maintaining the safety factor of the span as 4.

9.4.3 Crown Pillar

Most of the work done on pillar strength to date assumes that the orebody being mined is horizontal and that the stress distributions in the pillar are symmetrical about a vertical line through the center of the pillar. However, Hoek and Brown (1994) made it clear that these assumptions are no longer valid in an inclined orebody and that the shear stresses parallel to the dip of the orebody gives rise to asymmetrical stress distributions. Therefore, when the orebody is inclined, it can no longer be assumed that the pillar failure follows the same sequence as it does in a horizontal orebody, mainly by a crack forming from the pillar edges and propagating uniformly towards the core of the pillar. The two authors further stated that the pattern of failure propagation in a pillar in an inclined orebody is unknown at the present time and that the tributary area theory is only applicable to orebodies dipping at less than 20 degrees.

The current state-of-the-art technology in rock mechanics does not provide satisfactory solution in the case of inclined orebodies. As a result introducing the stress concentration factor in the pillar strength formula in equation (9.6) has modified the tributary area theory. Effectively, when the orebody is steeply inclined, the horizontal in-situ stress and the horizontal component of the vertical stress are used in place of the vertical stress due to overburden. The distance between crown pillars was estimated as 60 metres using Nilsson (1982) hypothetical method.

$$\sigma_p = 0.028253 \times 300 \times k \times \left(1 + \frac{60}{h_b}\right) \tag{9.6}$$

Hoek and Brown (1994) assumed, in simple terms, a parallel-sided block of height, h_b, and weight, W, acted upon by the average normal stress, σ_n. For limit equilibrium of the block, the following can be written:

$$\sigma_n = \frac{W \times Sin\phi}{2 \times h_b \times Tan\phi} \tag{9.7}$$

ϕ is the angle of friction of the orebody in contact with the host rock and σ is the angle of dip of the orebody. When the average pillar stress, σ_p, is less than σ_n, the crown pillar would be unstable and support would be required to restore stability. Therefore, the following relationship can be assumed:

$$\sigma_p \leq \sigma_n \tag{9.8}$$

and thus using equations (9.6) and (9.7)

$$0.028253 \times 300 \times k \times \left(1 + \frac{60}{h_b}\right) \leq \frac{W \times Sin\phi}{2 \times h_b \times Tan\phi} \tag{9.9}$$

From the above expression, the thickness or width of the crown pillar can be established by solving equation (9.9) for h_b. The width of the crown pillar was calculated as 27 metres (minimum) without support using equation (9.9). However, most mines would rather use support to reduce both the crown and rib pillar sizes. At Selebi North mine, both the crown and rib pillars are designed at 7 metres thickness with support in order to increase the extraction ratio. Again this shows how conservative the mathematical methods are in design of rock mass systems. Hence, in order to take into consideration the effect of support in pillar design, the input parameters would have to be multiplied by a constant proportional to the effectiveness of support on block sizes, and that is beyond the scope of this thesis.

9.5 DESIGN OF DRAW POINTS

The cohesion of the broken sulphide ore is assumed to be 0.022 MPa and the density is 3.5 t/m^3 (0.0345 MN/m^3), in order to calculate the minimum radius of draw point to obtain flow conditions. It is also assumed that the pressure, $P_v = 0$, and that the ore is free to flow from the draw point. Hence, using equation (4.32), with $P_v = 0$, the radius required for free flow of broken ore was calculated as 1.275 meters.

The minimum size of draw point required to permit free flow of broken ore is 2.6 metres, and this would be increased to 4 metres in order to accommodate equipment developing and lashing the draw points. Since in the creeping cone mining method draw points are not used but ore is drawn from the drill drives, the minimum width of the drill drives

would have to be 4 m. However, if the draw points are to be used, they will be developed at a minimum of 8 metres away from each other. This is required to prevent the placing of draw points in the zone of influence of other draw points. This will result in a minimum of 7 draw points per stope, using the solution of the analytical methods.

9.6 ZONE OF INFLUENCE OF THE STOPE

This is a zone defining the volume of material in which the pre-mining stress (field stress) is significantly disturbed by mining. In order to determine the zone of influence, the solutions determined previously were used, mainly the height of the stope of 60 metres and the width of the stope of 6 metres. The width, $W1$, of the zone of influence of the open stope was calculated from using equations 4.12 and 4.13 which gave 235.75 and 141.29 metres respectively. Therefore, the larger of the two answers is taken as the width of the zone of influence, and in this case $W1 = 234.75$ metres. Similarly the height of the zone of influence, $H1$, was calculated from equations 4.14 and 4.15 and the results were 123.37 and 153.44 metres respectively. Therefore, $H1 = 153.44$ metres which is the larger of the two answers.

Hence, for a stope of 6 metres width and 60 metres high, the elliptical zone of influence has a width of 234.75 metres and a height of 153.44 metres. These results mean that all major developments should be placed outside the area influenced by the stope. i.e. the ramp systems should be at least 117 metres away from the center of the open stopes.

9.7 CONCLUSION

The preliminary design with the voussoir arch shows that the stopes could be designed at a maximum span of 120 metres with a safety factor of 4.2. From the beam theory, the hanging wall span was calculated as 96 metres with a safety factor of 4. The rib pillar width was calculated at 18 metres with a safety factor of 2, while that of the crown pillar was calculated at 27 metres. The position of the main ramp system from the centre of the stope was determined as 117 metres.

CHAPTER 10

THE CREEPING CONE MINING METHOD DESIGN USING EMPIRICAL METHODS

10.1 INTRODUCTION

It should be noted that with any empirical data base, the use of the derived design charts should be limited to the conditions similar to those encountered in the mines used as case histories in developing such data. Hoek et al. (1995) cautions that anomalous geological conditions such as faults, shear zones, dykes or waste inclusions, the creation of a slot or a brow within the stope and poor cable bolt installation can all lead to inaccurate results.

Practical observations suggest that the main area of uncertainty in using the Stability Graph method lies in the density of jointing in the rock mass. As a result, the value of Q' will be open to question in areas where the number of joints and other discontinuities per unit volume of rock is highly variable. If these conditions prevail, the results of this method should be regarded as a first step in the design process and local adjustments to the design will have to be made, depending upon the stope conditions as observed.

10.2 SELEBI NORTH MINE STRUCTURAL GEOLOGY

The empirical methods discussed in Chapter 5 are now applied to Selebi North mine to design stope dimensions. Extensive bore hole core logging and underground mapping have been carried out and a total of close to 1 500 features have been recorded covering the South limb, North limb, Detached limb and the Nose area of the orebody. Analysis of the structural geological information by means of the program DIPS was done for the rock mass in each limb and the results are tabulated below.

Table 10.1: Joint sets of the South Limb.

Joint Set	Dip(°)	Dip Direction (°)	Description
A	61	335	Joints are parallel to the orebody.
B	49	025	The area is blocky/seamy with folds
C	57	061	and shears intersecting the joint sets.
			Planar, smooth to medium roughness.

Table 10.2: Joints sets of the North Limb.

Joint Set	Dip (°)	Dip Direction (°)	Description
A	44	172	Slightly rough to rough with tight
B	64	156	apertures. Joints have little infill and are
C	80	180	perpendicular to the ore body.

Table 10.3: Joints sets of the Nose Area.

Joint Set	Dip (°)	Dip Direction (°)	Description
A	74	198	Joints cross the orebody and cut some
B	73	318	parallel laminations on the hangingwall.
C	44	083	Very blocky and seamy. Slightly rough.

Table 10.4: Joint sets of the Detached Limb

Join Set	Dip (°)	Dip Direction (°)	Description
A	77	156	Poor slickensided and weathered
B	44	045	surfaces with compact coatings. Planar.
C	67	235	smooth to medium roughness.

Table 10.5: Structural data for Selebi North mine.

Location	Joints Description	spacing (m)	Ja	Jn	Jr
South	2 sets + random	2.6	1.5	6	3
North	2 joint sets	2.8	1.3	4	4
Nose	3 joint sets	2.1	1.5	9	4
Detached	2 sets + random	1.6	0.75	6	4

Based upon an inspection of the rock mass in the drill drives, development excavations and cross-cuts as well as visits to old stopes, it was concluded that not all identified joints sets occurred at all locations and that a reasonable description of the jointing is as given in Table 10.5. Though joint spacing was measured in the field, the joint alteration number Ja, the joint set number Jn and the joint roughness number Jr were estimated on site based on observations and conditions at the mine using figures and graphs published by Hoek et al. (1995). Histograms were then generated using the program DIPS to give the results in Table 10.5.

These values are dependent on the location of the stope being designed and the joint set or sets being considered to be the most important at that location. Values of RQD and Q' were calculated as outlined above, however laboratory evaluations of the intact rock strength σ_c, Young's modulus E, and Poisson's ratio μ, were performed and where

Table 10.6: Selebi North mine database

Location	RQD (%)	Q'	σ_c (MPa)	E (MPa)	μ
South Limb					
Hangingwall	66	22	122	78	0.24
Ore zone	63	21	95	80	0.23
Footwall	63	21	189	90	0.25
North Limb					
Hangingwall	80	40	122	85	0.25
Ore zone	72	36	95	80	0.24
Footwall	82	41	189	95	0.26
Detached Limb					
Hangingwall	69	35	122	80	0.24
Ore zone	76	39	95	78	0.25
Footwall	60	31	189	84	0.26
Nose Area					
Hangingwall	73	22	122	76	0.24
Ore zone	68	20	95	74	0.25
Footwall	73	22	189	80	0.26

possible the parameters were also estimated in the field and the compromised results are

shown in Table 10.6.

10.3 PRELIMINARY STOPE DESIGN USING STABILITY GRAPH METHOD

The preliminary stope design will be based upon the fact that the stopes would be 6 metres in width and 60 metres in down dip height as determined earlier. These dimensions are considered average for the Selebi North main orebody comprising the North limb, South limb and the Nose area. However, the orebody thickness (hangingwall to footwall) on the Detached limb would be taken as 3 metres with a down dip distance of the stope as 60 metres. The assessment of the stability and the third stope dimension along the strike would depend on the estimates of the factors A, B and C as discussed in Chapter 5.

Factor A, the influence of the mining induced stresses, is found from the ratio of the intact rock strength to the induced compressive stress, $\dfrac{\sigma_c}{\sigma_1}$. While the intact rock strength is discussed above, the induced compressive stresses are estimated from in-situ stresses and are shown in Table 8.1 and 8.2.

A preliminary estimate of the induced compressive stress on each face of the stope boundary can be obtained from simple elastic numerical modelling. As discussed earlier, the thickness of the stope and the down dip dimensions on the hangingwall side were established from practical mining considerations. Then the stability graph method was used to determine a reasonable value for the stope width along the strike.

Table 10.7: Critical joint sets and Factor B for Selebi North Mine.

LOCATION	Joint Set	Difference Strike (°)	Difference Dip (°)	Factor B
South limb				
Hangingwall	A	0	30	0.2
Stope ends	B	0	0	0.3
Stope back	C	60	30	0.8
North Limb				
Hangingwall	A	0	45	0.5
Stope ends	B	0	0	0.3
Stope back	C	60	0	0.8
Detached Limb				
Hangingwall	A	90	0	1
Stope ends	B	45	45	0.7
Stope back	C	90	0	1
Nose Area				
Hangingwall	A	0	0	0.3
Stope ends	B	0	0	0.3
Stope back	C	0	45	0.5

A two-dimensional hybrid model program called PHASES has been developed to meet
the requirements of modelling the post-failure behaviour of rock masses and their

interaction with support (Hoek et al. (1995)). This program uses finite elements to model the heterogeneous non-linear behaviour of the rock close to the excavation boundaries. However, a boundary element model is used to model far field in situ stress conditions. Due to limited research funds PHASES was not available for use in this project.

However, based on the results determined by Hoek et al. (1995) using a computer program PHASES for a stope of similar dimensions and stresses, the induced compressive stress on the back of the stope was taken as 30 MPa, and on the hangingwall was assumed less than 5 MPa. The respective ratios of $\frac{\sigma_c}{\sigma_1}$ were approximated at 3.2 and 24.4. Using these values the rock stress factor, A, was calculated from equation (5.3), giving A as 0.235 for the stope back and A as 1 for the hanging wall.

The influence of the joint orientation on the stope stability is accounted for by the factor B. In general the joint closest to and parallel to the stope boundary, is the most critical and influential in the stope stability. For Selebi North mine, the critical joint sets for the various components of the stope boundary are listed in Table 10.7, together with the values of B, found from Figure 5.3. The influence of the stope wall orientation is accounted for by the factor C. It is assumed here that failure would be dominated by gravity falls from the stope back and buckling failure from the stope hangingwall and ends. From Figure 5.6 or equation (5.14), the gravity adjustment factor, C was derived and shown in Table 10.8.

Table 10.8: Adjustment Factor C for gravity falls

		$C= 8 - 6Cos \, \alpha$
LOCATION	Stope inclination	Factor C
South limb		
Hangingwall	70	6
Stope ends	90	8
Stope back	0	2
North Limb		
Hangingwall	80	7
Stope ends	90	8
Stope back	0	2
Detached Limb		
Hangingwall	70	6
Stope ends	90	8
Stope back	0	2
Nose Area		
Hangingwall	85	7.5
Stope ends	90	8
Stope back	0	2

Table 10.9: Stability Number, N', for stope back and hangingwall

LOCATION	Q'	A	B	C	N'
South Limb					
Hangingwall	22	1	0.2	6	26
Stope back	21	0.235	0.8	2	8
North Limb					
Hangingwall	40	1	0.5	7	140
Stope back	36	0.235	0.8	2	14
Detached Limb					
Hangingwall	35	1	0.5	6	105
Stope back	39	0.235	0.8	2	15
Nose Area					
Hangingwall	22	1	0.3	7.5	50

The stability numbers, N', for the stope back and hangingwall were calculated from equation (5.1) and the results are shown in Table 10.9. N' is plotted on the stability graph to design the stope dimensions for the South, North and Detached limbs and the Nose area.

The stability graph is now used to find the hydraulic radii of the stope that will be stable with and without support. The values of the hydraulic radii and associated stope widths are shown in Table 10.10 to 10.13 for the various regions of the orebody.
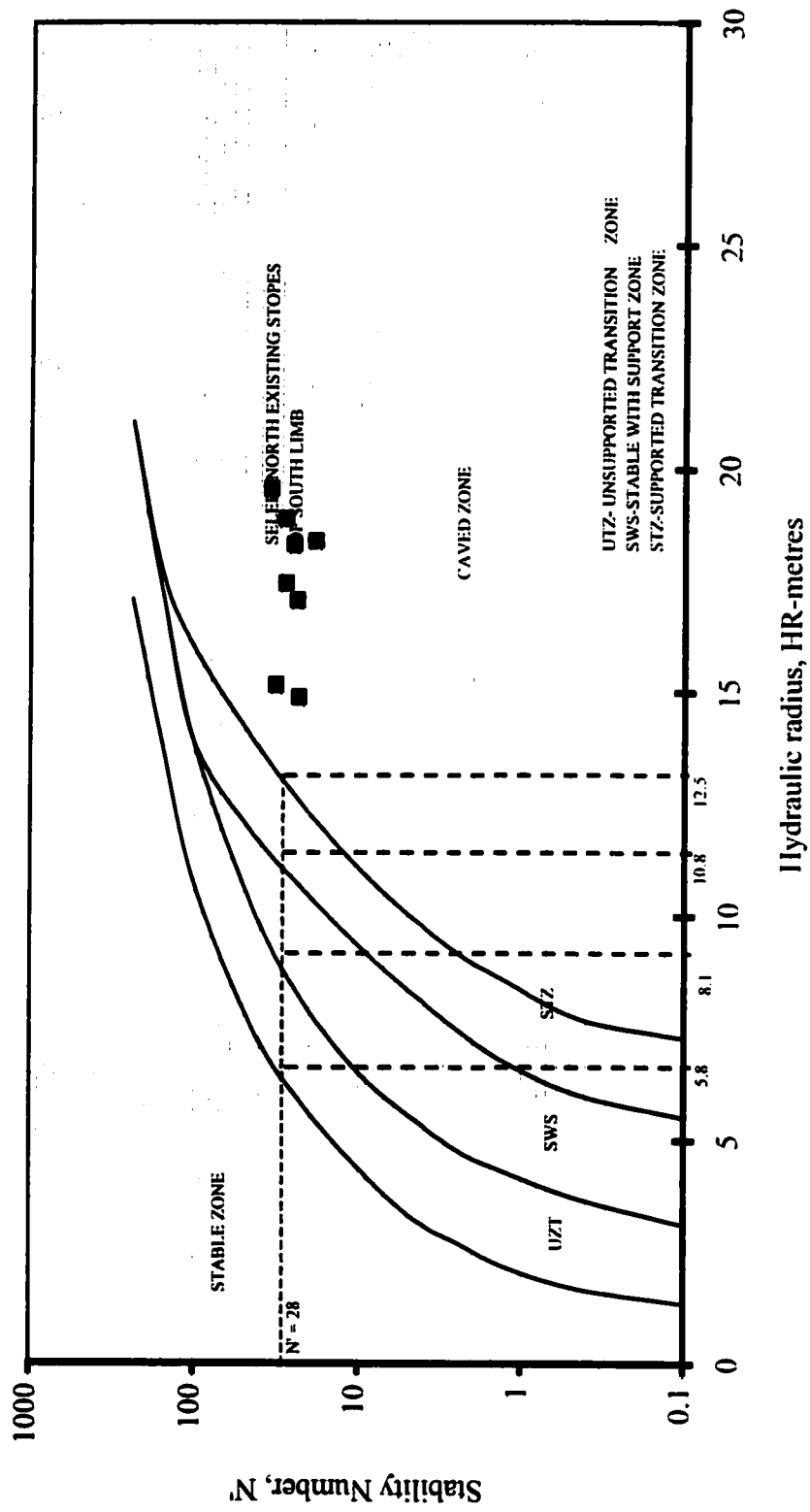
Figure 10.1: Design of the South limb stopes also showing existing stopes

Stability Number, N'

Hydraulic radius, HR-metres

STABLE ZONE

N = 28

UZT

SWS

STZ

SELECTED NORTH EXISTING STOPES

SOUTH LIMB

CAVED ZONE

UTZ- UNSUPPORTED TRANSITION   ZONE
SWS-STABLE WITH SUPPORT ZONE
STZ-SUPPORTED TRANSITION ZONE

157

Table 10.10: South Limb stope widths determined from the Stability Graph.

SOUTH LIMB	Stope Back	H/W	H/W	H/W
Known Dimension	6 m span	50 m Height	60 m Height	70 m Height
Hydraulic radius				
Stable	< 3.9	< 5.8	< 5.8	< 5.8
Unsupported Transition	3.9-6.0	5.8 - 8.1	5.8- 8.1	5.8-8.1
Stable with support	6.0 - 9.0	-10.8	8.1-10.8	8.1-10.8
Supported transition	9.0 -10.8	10.8-12.5	11-13	11-13
Calculated stope width				
Stable		< 15	< 14	< 14
Unsupported transition		15 - 24	14 - 22	14 - 21
Stable with support		24 - 38	22 - 34	21 - 31
Supported transition		38 - 50	34 - 43	31 - 39

Figure 10.1 shows the design of stable stope dimensions for the South limb for N'= 26. The existing stopes in the South limb are also plotted for comparison and they all plot in the caved zone of the graph. Observations at the mine confirmed that the stopes have caved and some of them were abandoned. This is because the stopes were mined at greater spans than the rock mass can accommodate. The plotted results and the design
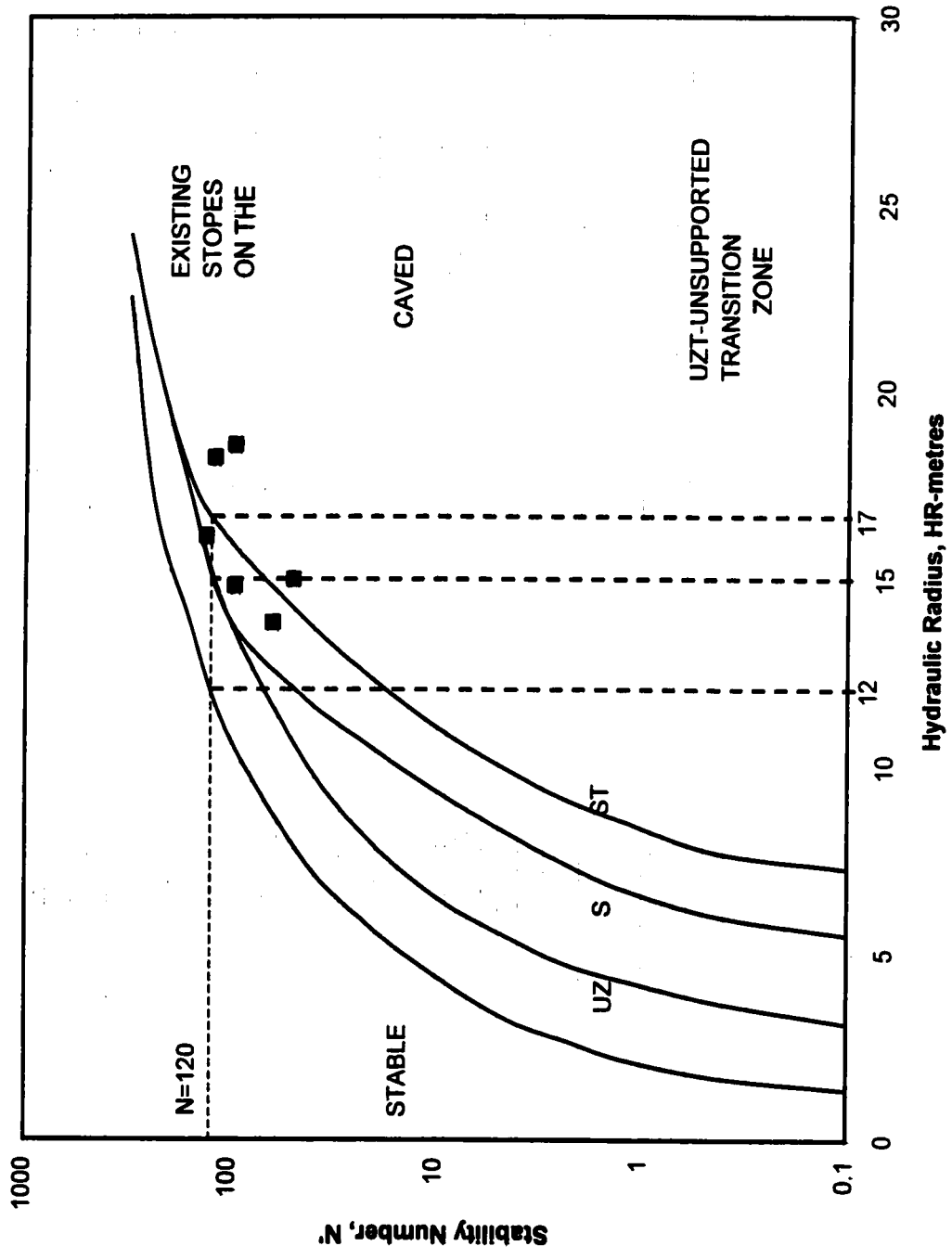
Figure 10.2: Design of the North limb stopes also showing existing stopes

Table 10.11: North Limb stope widths determined from the Stability Graph.

NORTH LIMB	Stope Back	H/W	H/W	H/W
Known Dimension	6 m span	50 m Height	60 m Height	70 m Height
Hydraulic radius				
Stable	< 5	< 12	< 12	< 12
Unsupported Transition	5 - 7	12 - 15	12 - 15	12 - 15
Stable with support	7 - 10			
Supported transition	10 - 12	15 - 17	15 - 17	15 - 17
Calculated stope width				
Stable		< 47	< 41	< 37
Unsupported transition		47 - 78	41 - 62	37 - 54
Stable with support				
Supported transition		78 - 101	62 - 75	54 - 64

are for the hanging wall. The stope dimensions proposed in this design were calculated from the hydraulic radius obtained in Figure 10.1 and the results are shown in Table 10.10. Figure 10.2 shows the design of stable stope dimensions for the North limb for N'= 186 and a plot of the existing stopes in that limb. Three of the existing stopes plot on the supported transition zone of the graph while the other three plot on the caved zone of the graph. Observations at the mine revealed that the North limb side walls were fairly competent compared to the rest of the mine and this was also confirmed during the data
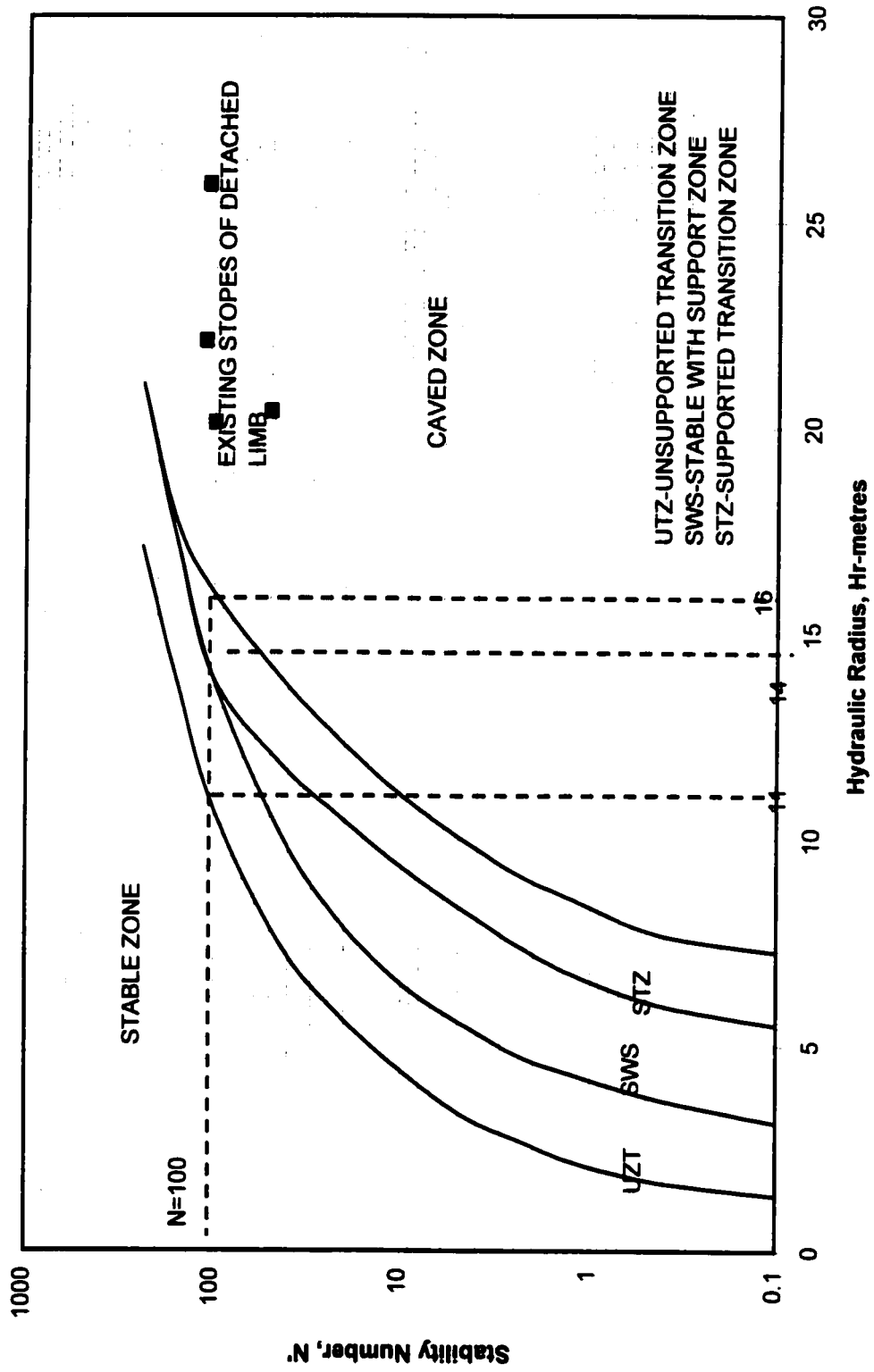
Figure 10.3: Design of the Detached limb stopes also showing existing stopes

Table 10.12: Detached Limb stope widths determined from the Stability Graph.

DETACHED LIMB	Stope Back	H/W	H/W	H/W
Known Dimension	4 m span	50 m Height	60 m Height	70 m Height
Hydraulic radius				
Stable	< 5	< 11	< 11	< 11
Unsupported Transition	5 - 7	11 - 14	11 - 14	11 - 14
Stable with support	7 - 10			
Supported transition	10 - 12	14 - 16	14 - 16	14 - 16
Calculated stope width				
Stable		< 38	< 34	< 31
Unsupported transition		38 - 64	34 - 53	31 - 47
Stable with support				
Supported transition		64 - 89	53 - 69	47 - 59

analysis. However, due to some localized side wall failures, the design proposes a reduction in the hydraulic radius of the stopes and the proposed dimensions are shown in Table 10.11. The results show that the North limb stopes would remain stable between 37 and 47 metres and would transit to failure between 47 and 78 metres. However, if the stopes were supported the transition could occur between 78 and 101 metres for a stope height of 50 metres and 6 metres wide.

Figure 10.3 shows the design for the Detached limb stopes together with a plot of the existing stopes in that limb. Observations at the mine confirmed the failure of the stopes as predicted by the stability graph, indicating that they were over dimensioned. All the stopes plot on the caved zone of the graph. The results of the design in Table 10.12 shows that the Detached limb stopes would remain stable up to a span of 38 metres, and transition would take place when the stope span is between 38 and 64 metres for unsupported stopes of 50 metres high and 4 metres wide. However, if the stopes were supported transition could occur between 64 and 89 metres of span.

Figure 10.4 shows the design of the stope back and hangingwall for the nose area. The results in Table 10.13 shows that the Nose area would allow stopes 22 metres wide to be mined to a span of 24 metres without support, and transition would occur between 24 and 39 metres for unsupported stopes. If the stopes were supported they could be stable between 39 and 50 metres and transist to caved zone between 50 and 68 metres, for a stope height of 50 metres.

The analysis shows that the back is more critical than the stope hangingwall, unless both are supported. For a stope width of 6 metres with a vertical height of 50 to 70 metres, the width of the stope along the strike should be less than 15 metres at most for the stope to be stable without support, for the South limb stopes. Stopes of the same height located on the North Limb would reach a span of 37 to 47 metres without support while those of the Detached Limb would reach spans of 31 to 38 metres without support.
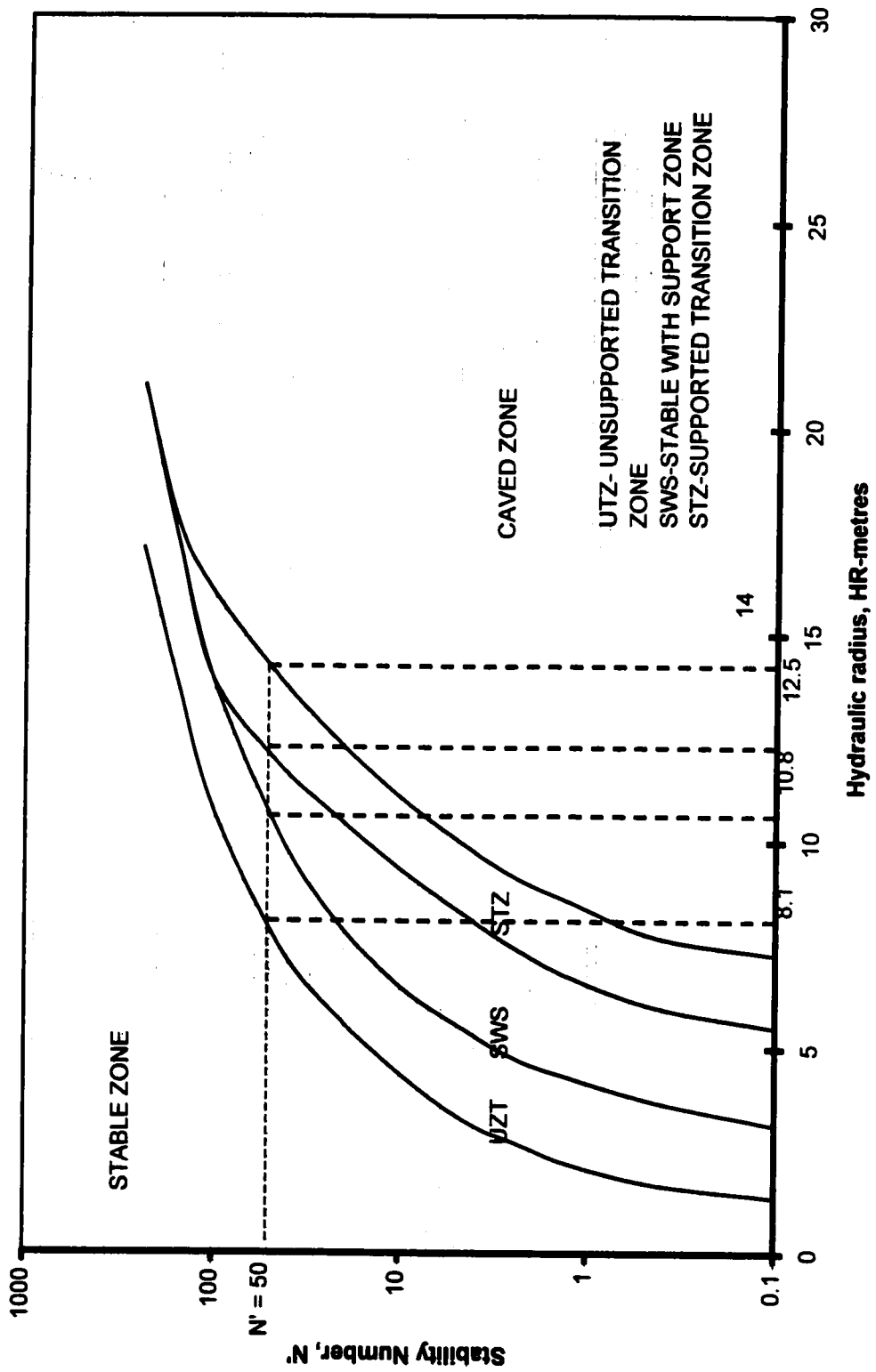
Figure 10.4: Design of the Nose area stopes

STABLE ZONE

CAVED ZONE

UTZ- UNSUPPORTED TRANSITION
ZONE
SWS-STABLE WITH SUPPORT ZONE
STZ-SUPPORTED TRANSITION ZONE

Hydraulic radius, HR-metres

Stability Number, N'

N' = 50

STZ

SWS

UZT

Table 10.13: Nose Area stope widths determined from the Stability Graph.

NOSE AREA	Stope Back	H/W	H/W	H/W
Known Dimension	12 m span	50m Height	60m Height	70m Height
Hydraulic radius				
Stable	< 8	< 8	< 8	< 8
Unsupported Transition	8 - 6	8 - 11	8 - 11	8 - 11
Stable with support	6 - 9	11- 13	11- 13	11- 13
Supported transition	9 - 11	13 - 14	13 - 14	13 - 14
Calculated stope width				
Stable	< 22	< 24	< 24	< 24
Unsupported transition		24 - 39	24 - 35	24 - 32
Stable with support		39 - 50	35 - 43	32 - 39
Supported transition		50 - 68	43 - 55	39 - 49

In all the areas of the ore body investigated, the strike distance is too short to allow for economical and safe extraction of the ore. Therefore, both the back and the hanging wall of the stope would have to be supported for economic extraction.

10.4 CONCLUSION

The maximum safe strike length of a supported stope is controlled by the stability of the

hanging wall and reduces with the increase in the stope down dip distance or stope height. Therefore, for this mine a supported strike distance of 50 metres would be acceptable for a stope height of 50 metres and 6 metres wide located on the South limb. With support the stopes on the North limb could be mined up to 100 metres while those of the Detached limb could reach 90 metres for a 50 metres height. The Nose area could be mined with stopes of 22 metres wide at a span of 68 metres provided support is installed.

It is worth noting that a stope height of 50 metres would produce more tonnage at optimum span when compared with stopes of 60 or 70 metres height since it will give a larger span.

The above analysis shows that the strike length chosen for a particular stope is influenced by the choice made for the stope height. As a result, the decision on a reasonable strike length should be made on the basis of practical mining operations (overall ore body length, stope sequencing, draw point design and drilling equipment which more or less govern the stope height).

CHAPTER 11

MODIFIED CREEPING CONE MINING METHOD (MCC)

11.1 INTRODUCTION

This chapter utilizes the design results obtained so far through out the analysis to design the proposed modified creeping cone mining method. The design of maximum stable spans for the Selebi North ore body has been undertaken using analytical and empirical methods. And the existing stopes in various parts of the mine were also plotted in the design charts in order to compare with the proposed design layout for the modified creeping cone mining method. The analytical methods were applied to the Selebi North mine general rock conditions while the empirical methods specifically dealt with individual limbs at the mine. Existing rock conditions at the mine were also compared to the empirical methods analysis, giving the results of this methodology confidence over those derived by analytical methods.

11.2 MCC MINING METHOD DESIGN

A summary of the design results is shown in Table 11.1 which shows the results derived from the individual methods used through out the research. The results show that the voussoir arch and beam theory methods have suggested stope spans of 120 metres and 96 metres respectively for a stope 60 metres high and 6 metres wide. However, the

Table 11.1: Summary of the design results

Method	Stope width (m)	Stope height (m)	Maximum span Unsupported (m)	Maximum span Supported (m)
Analytical				
Voussoir arch	6	60	120	
Beam theory	6	60	96	
Other				
Crown pillar	18	6	100	
Rib pillar	18	60		
Zone of influence	100	100		
Empirical				
South limb	6	50	24	50
North limb	6	50	78	101
Detached limb	4	50	64	89
Nose area	22	50	39	68
Mine actual				
South limb	6	47	185	
North limb	6	47	140	
Detached limb	6	60	165	
Crown pillar	7 - 8	7 - 8		
Rib pillar	7 - 8	47 - 60		

methods do not specify the location of the said stope in the mine. And in view of the generality of the methods and the assumptions made in their input parameters. less confidence is placed in the results of the analytical methods results.

The results of the empirical methods are site specific in terms of the various areas of the mine considered. The methods predicted respective stope spans of 24 and 50 metres for unsupported and supported stopes in the South limb, 78 and 101 metres in the North limb, 64 and 89 metres in the Detached limb and 39 and 68 in the Nose area. These dimensions are for a 50 metres high and 6 metres wide stopes except for the Detached limb where stopes are designed at 4 metres wide and the Nose area where the stopes are designed at 22 metres width. More confidence is placed in the results of the empirical methods since they consider each case individually and they compare well with the field observations.

The actual stope dimensions used at the mine are also shown in Table 11.1 for comparison. The South limb stopes are mined at a height of 47 metres and an unsupported span of 185 metres, while the North limb stopes are mined at a height of 47 metres and unsupported span of 140 metres span. The stopes in the Detached limb are mined at a height of 60 metres and unsupported span of 165 metres. These results are contrary to the findings of this research which suggest that the longest spans should be in the North limb where the rock is more competent, followed by the Detached limb and lastly the South limb. And this partly explains why nearly all of the stopes plotted in the Stability Graph plotted in the caved side of the graph, except for the three stopes in the

North limb which plotted in the stable with support area. However, a reduction in the stope span and strategic positioning of stub pillars would result in the reduction of the hydraulic radius hence pushing the stopes towards a stable zone in the Stability Graph. It is also clear that even with the reduction in hydraulic radius the stopes would require support, in the form of cable bolts to arrest blocks which cannot be supported by stub pillars.

11.2.1 Pillar Layout for the Modified Creeping Cone (MCC) Mining Method

The proposed stoping layout is based on the results of the maximum allowable spans for supported stopes. The method utilizes staggered stub pillars (5 m wide) with a safety factor of 1.5 (see appendix C) with the load deformation of the hanging wall tributary to them in the near horizontal direction. Single stub pillars (P1 and P4) are placed at the maximum stable span without support (i.e. unsupported transition span) while double stub pillars (P2 and P3) are placed at the maximum span allowable for a stable with support stope (i.e. supported transition span) as shown in Figure 11.1. The maximum span of the entire stope is designed at twice the supported transition span as the double stub pillars divide the stope in two parts and significantly reduce the effective hydraulic radius of the stope. The method allows for higher extraction rate as two stopes are combined and mined as one without sacrificing safety. Therefore, instead of leaving a rib pillar between the stopes, double stub pillars are left between adjacent stopes. This allows for early pillar robbing while mining the stopes and reduces the risk of having to come back for pillar reclamation while the rock conditions have deteriorated. The 'early pillar robbing' method could be applied to the crown pillar, allowing the stopes to be
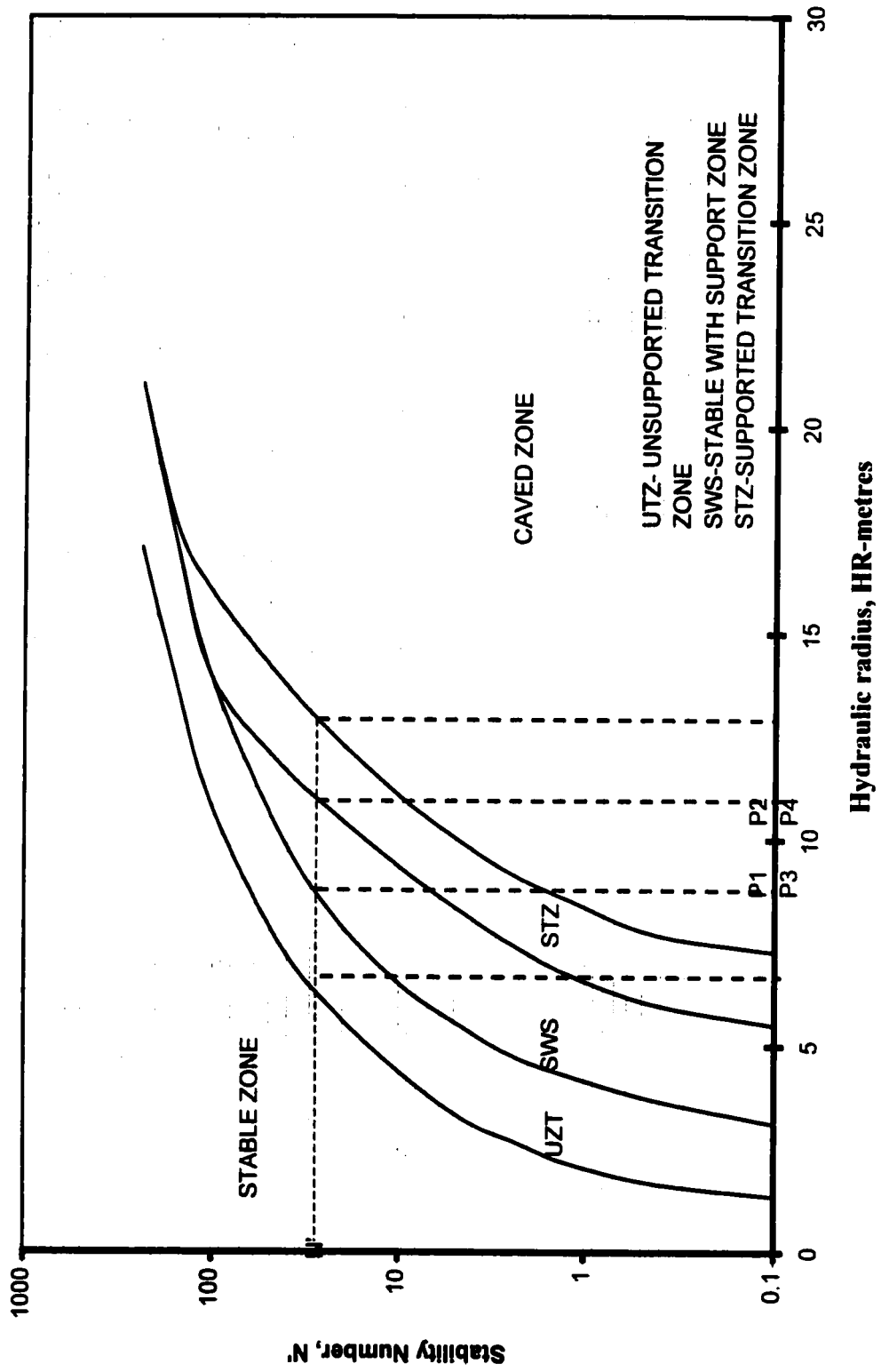
Figure 11.1: Stability Graph showing the stub pillars positions for any N'

CAVED ZONE

UTZ.- UNSUPPORTED TRANSITION ZONE
SWS-STABLE WITH SUPPORT ZONE
STZ-SUPPORTED TRANSITION ZONE

STABLE ZONE

Hydraulic radius, HR-metres

Stability Number, N'

joined both horizontally and vertically, thereby increasing the extraction ratio. The continuous crown and rib pillars are only necessary when there is a risk of flooding or threatened regional instability. However, without the use of back fill the probability of flooding is greatly reduced especially in a dry mining environment, like that of Selebi North mine.

The pillar positions apply to the stope based on it's location in the mine as shown in Table 11.2. The Nose area would be mined with stopes of 50 metres in length and 22 metres wide provided they are supported, there is no need to leave stub pillars in this area

Table 11.2: Proposed pillar positions for Selebi North mine.

STOPES AND PILLARS	Unsupported transition span (m)	Supported transition span (m)	Unsupported transition span (m)	Span (m)
Pillar	**Pillar, P1**	**Pillar, P2&P4**	**Pillar, P3**	
South limb	25	55	85	115
North limb	60	125	185	255
Detached limb	40	85	130	175

in order to maximise recovery of the high grade ore. The bottom (primary) sublevel would be designed to 12 metres in order to have optimum control over ore flow while the secondary sublevels would be 15 metres in height in order to give optimum drilling accuracy. Experience have shown that these dimensions are the

most practical and efficient at Selebi North mine based on the achievement of Simba long hole drill rig.

11.3 MCC STOPE LAYOUT AND SEQUENCE

The mining sequence would require a stope to be developed to its extremities (planned dimensions) within the ore body with slot raises established at the extremities throughout the sublevels. Other slot raises would be established next to the 5 metres wide stub pillars in the direction of mining. The pillars are designed in such a way that they are tributary to the stope and in addition to supporting the stope sides they also help to control the follow of broken ore inside the stope. Figure 11.2 show stage one of the mining sequence.
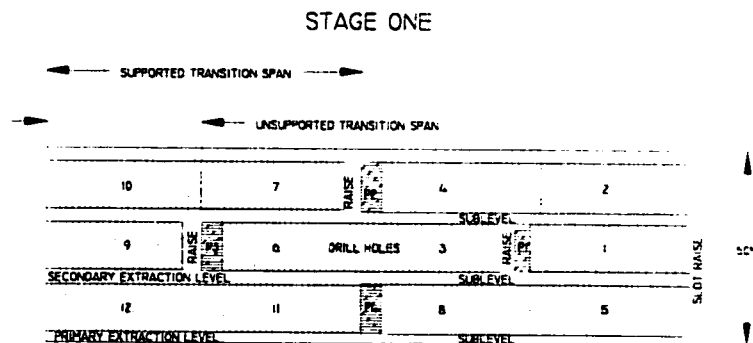
Figure 11.2: A stope is developed to its extremities and longhole drilled with up holes.

STAGE TWO
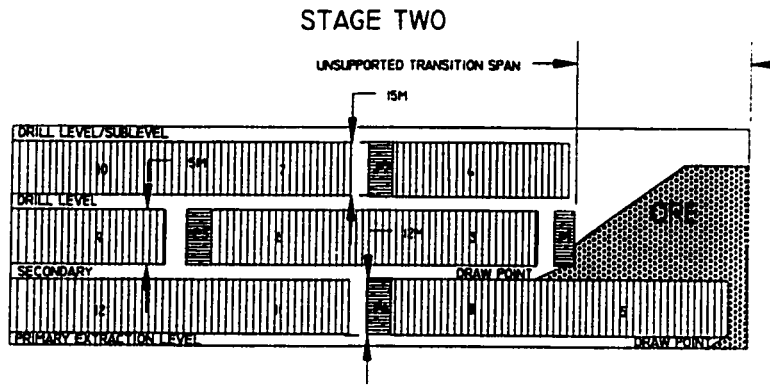
Figure 11.3: Production blasting starting with blocks 1 and 2

STAGE THREE
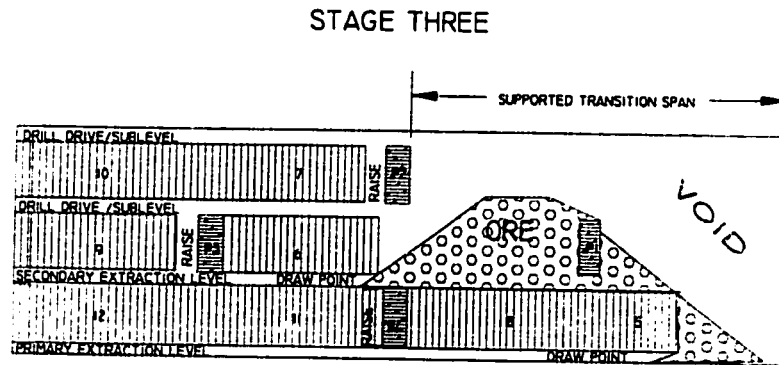
Figure 11.4: Formation of the cone inside the stope at angle of repose of the broken ore

STAGE FOUR
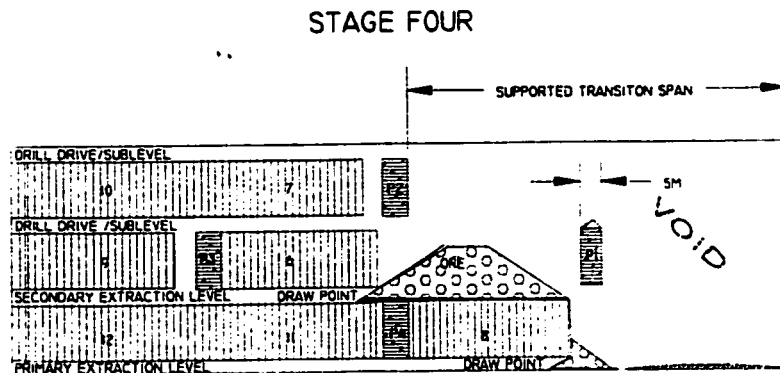
Figure 11.5: The cone moving from unsupported to supported transition zone

174

In Figure 11.2 the pillars are numbered for identification while the mining blocks are numbered to show the sequence of mining. Blasting blocks 1 and 2 as shown in Figure 11.3 starts production mining. At this stage lashing can take place at both secondary and primary extraction levels with ore settling at the angle of repose estimated at 35° for this type of ore body. During stage two of mining, pillar P1 helps to control the flow of ore in addition to supporting the stope sides. Drawing of the ore from the primary extraction level would allow for the formation and creeping of the cone in the direction of mining. Lashing at this level should continue until all the broken ore is resting on top of block 5. At this stage blocks 3, 4 and 5 are blasted as shown in Figure 11.4. Controlled blasting of block 5 should be emphasized such that the blasted ore together with broken ore resting on top of the block does not fly to the back of the stope where it will be difficult to be reached by an LHD. The blast should be controlled to move the ore downwards.

After finishing mining block 5, mining of blocks 6 and 7 should continue while block 8 and P1 are acting as a draw point for the broken ore at the back of the cone. Lashing at the primary extraction level should continue until the broken ore rest on top of block 8 as shown by Figure 11.5. Then similarly controlled blasting is done on block 8. At this stage the cone of broken ore has crept from the stable without support area to the stable with support area while the hanging wall is in the supported transition zone. If fill was available it could be placed in the first region of this stope in order to reduce the hydraulic radius of the stope.

At this stage the creeping cone is now in the region of stable with support zone and the double stub pillars can now help to break the hanging wall span. Broken ore is lashed underneath P4 until all the ore rest on block 11 while mining continues on blocks 9 and 10 as in Figure 11.6. Again P3 and P4 are used to control the flow of ore acting as draw points.

STAGE FIVE
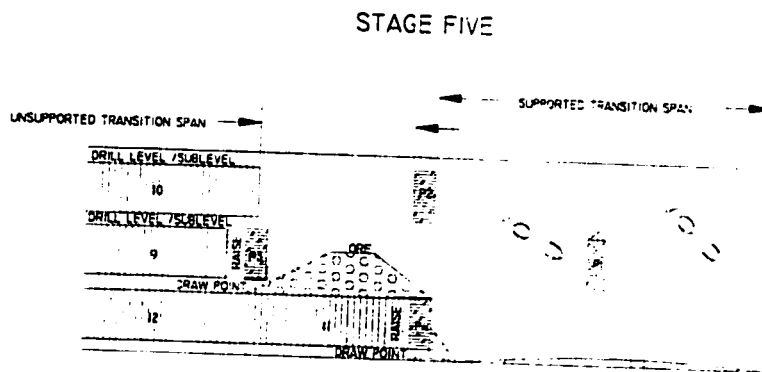
Figure 11.6: The creeping cone entering the second phase of the stope.

At this stage a slot raise between P4 and block 11 can now be blasted as the LHD protection it offered is no longer needed. The broken ore would then flow between P4 and block 11 as shown by Figure 11.7. P4 would now capture any major sloughing of the side wall. And the effect of the double stub pillars would give the stope a fresh start in its second phase.

The broken ore is drawn from the slot raise until the remaining ore rest on block 11 while mining continues on blocks 9 and 10. Controlled blasting is again done on block 11. During the last stage of mining the sequence still offers two extraction points of the broken ore and ore flow is still controlled as shown by Figure 11.8.
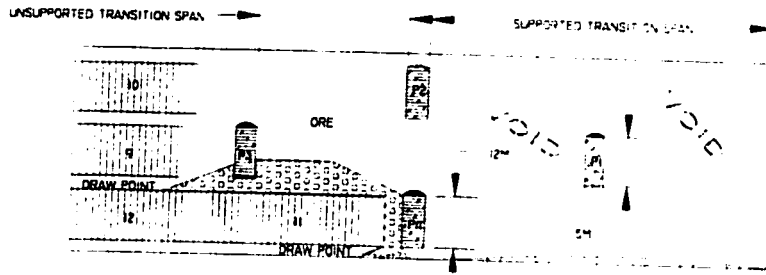
Figure 11.7: Drawing ore from the slot raise
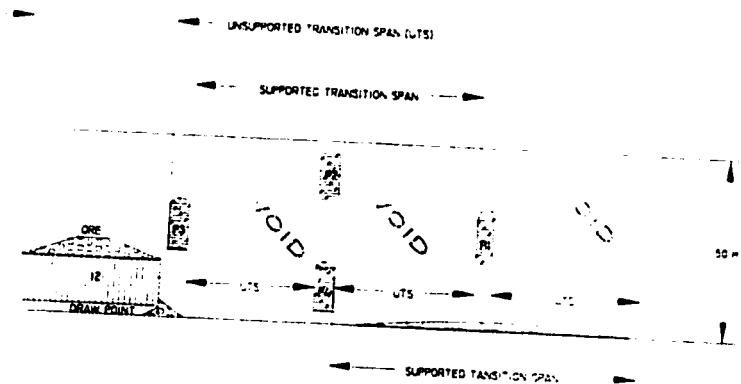
Figure 11.8: Final stage in the mining sequence

The biggest advantage of this proposed modified creeping cone mining method is that it offers double excess to the broken ore at all times throughout the life of the stope. And the stope could be mined as fast as required such that any sloughing doe not cause dilution. At any point in time the minimum broken ore is left in the stope, for instance if blasting cannot continue for some reason but lashing is continued the maximum ore which would be left in the stope undrawn would about 1.4 % of the total tonnage originally contained in the stope.

11.4 DEVELOPMENT

Development is planned to continue as for the Creeping Cone (CC) mining method, however emphasis should be placed on the direction of the drill drives. The hanging wall overbreak has to be controlled as this is the main contributor to hanging wall sloughing. Where possible the drill drive should follow the hanging wall contact and whenever possible the full width of the ore body should be exposed. This will help during production drilling as the drilling crew will know where the contact is and as such will avoid drilling into the barren amphibolite or gneiss on the side walls. The slot raises could be mined as needed, with exception of the one located on the primary extraction level which can only be blasted once the secondary lashing has passed it. Whenever equipment permits, development dimensions should only be confined to the ore thickness, especially in the narrow Detached limb where hanging wall overbreak is inevitable due to large equipment currently used at the mine.

The Atlas Copco drill rig used in development could have its stabilizing jacks extended enough to drill only the specified width while the Secoma rig can be modified to fit in narrow development. According to Chadwick (1995), Kundana mine in Australia use Secoma Quasar NV (Narrow Vein) drill rig, which is a combination unit that can be used for drifting, bolting, cross-cutting and production drilling. The Secoma Quasar NV can drill up holes of 11 to 15 metres and could develop stoping widths of less than a metre. In such narrow developments and stopes, mucking could be by TORO 150 or 151 with a bucket capacity of 1.5 m^3. The small equipment could be dedicated to the narrow

Detached limb and can stockpile the ore for the bigger LHD to transport to the ore pass. Equipment modification to suit this conditions is a well deserved venture and can easily be done in-house without having to incur extra expenses. Equipment has to be adapted to be able to operate in both narrow and wide drill drives especially when the two occur in the same mine as a cost saving measure.

11.5 PRODUCTION

It is assumed here that production lashing is by the TORO 400 LHD with a bucket capacity of 3.8 m³ loading into a 20 tonne dump truck which hauls the ore to the ore pass and into the shaft system as shown by Figure 11.9. Moreover, the success of long hole stoping operations as practised at Selebi North mine is totally dependent upon the drilling and blasting controls. Regardless of the virgin stress ratios, induced mining stresses and their unfavourable orientations, the absolute magnitude of stresses at Selebi North mine is insufficient alone to cause failure of both the hanging wall and foot wall. Failure in the hanging wall is associated with poor drilling, over charging and block sizes, which are formed by intersecting discontinuities, and over dimensioned stopes.
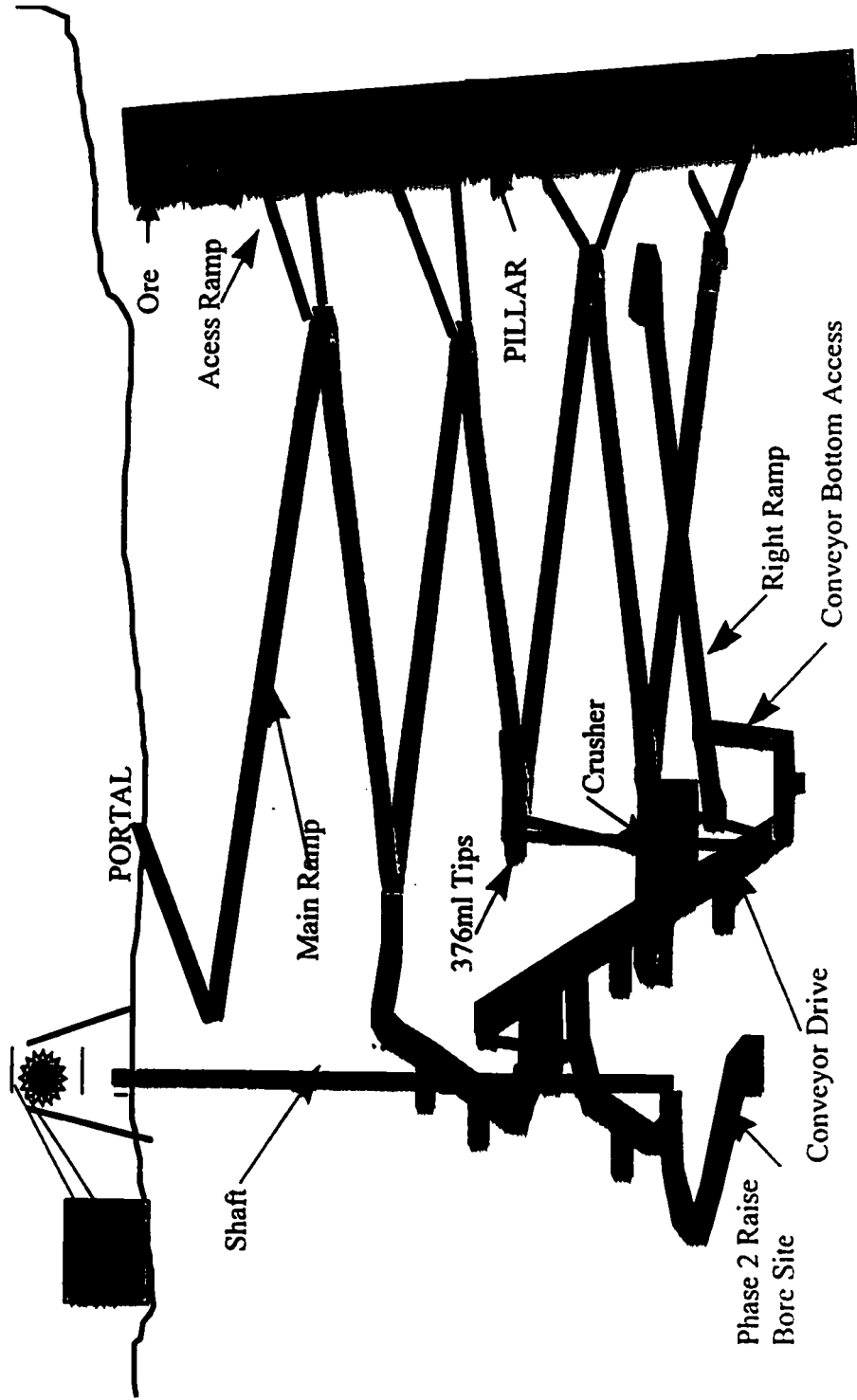
Figure 11.9: Typical Selebi North mine ore flow system

A survey at Selebi North mine has shown that once the Simba long hole rigs were set up along an accurately marked blast hole position and rig line, the resultant hole could be drilled accurately to within 2% of the design layout. However, blast holes need to be collared properly as failure in this regard will inevitably increase the hole burden which results in poor fragmentation.

Table 11.3: Production comparison of the old and proposed creeping cone methods

	Creeping Cone (CC)				Modified Creeping Cone (MCC)			
Place	Height (m)	Span (m)	Tonnes	Tonnes in pillars	Height (m)	Span (m)	Tonnes	Tonnes in Pillars
South	47	185	182595	3150	50	115	120750	5985
North	47	140	138180	3150	50	255	267750	5985
Detached	60	165	138600	2100	50	175	122500	3990
Total tonnage (tonnes)			459375	8400			511000	15960
Extraction ratio (%)				98.2				96.97

Table 11.3 shows that the proposed Modified Creeping Cone (MCC) mining method would achieve 1.23 % less extraction when compared with the existing Creeping Cone (CC) method, this is due to the fact that the proposed method leaves four pillars in a stope while the existing method leaves only two pillars. However, the proposed method is aimed at more support in order to reduce ore dilution at the mine. In addition to the

proposed pillar layout, the stopes are to be cable bolted such that side wall failure could be reduced with a target to eliminate additional dilution and improve the grades in planned dilution due immediate sidewall overbreak.

11.5.1 Dilution Control

The assessment of mined out stopes has shown that sidewall sloughing occurs to about 2 metres into both the hanging wall and footwall. The failure happens along weak planes (joints and shears) parallel to the orebody, well beyond the limits of planned dilution as established by the geological assay hangingwall and footwall, as well as, sidewall overbreak due to blast vibrations and improper drilling. However, the effects of blast on dilution are not well understood, therefore, the impact of sidewall overbreak producing planned dilution is inherent to both the Creeping Cone and Modified Creeping cone. The main difference between the two methods remains the fact that MCC is aimed at eliminating unplanned additional dilution due to sidewall failure along weak planes, a scenario which cannot be addressed by the CC mining method. The MCC eliminates additional dilution by employing the use of cablebolts on the stope hanging wall and back, as well as, utilizing a strategic stub pillar positioning system within a stope dimensioned to its rock mass competency. The stope layout greatly reduces the effective span of the hanging wall, giving the sidewalls the ability to stand up for a period long enough to allow safe extraction of the blasted rock. The method greatly enhances the stand up time of the hanging wall and footwall. In addition, shorter spans introduced by the stub pillars, allows for shortening of the compressive arch formed in the immediate

hanging wall, thereby reducing the depth of sloughing associated with the CC method to about 1m.

Figure 11.10 shows a plan view of a typical 100m long stope mined using MCC with pillars, including the areas of planned dilution and unplanned dilution. If the stope is mined by CC (without pillars and cables) sidewall failure will occur along the weak zone indicated by the dotted line in the Figure 11.10. This will add to the-run-of-mine ore, waste due to planned dilution and waste due to additional dilution equivalent to 34.5% of the stope ore tonnage. However, if the stope is mined using MCC, it is expected that it will be mostly planned dilution of 19.23% that will be added to the run-of-mine ore. The additional dilution will be secured by cable support along the weak zone and hanging wall spans within the stope have been reduced. Given this scenario the MCC method offers a 44 % decrease in dilution when compared with CC method.
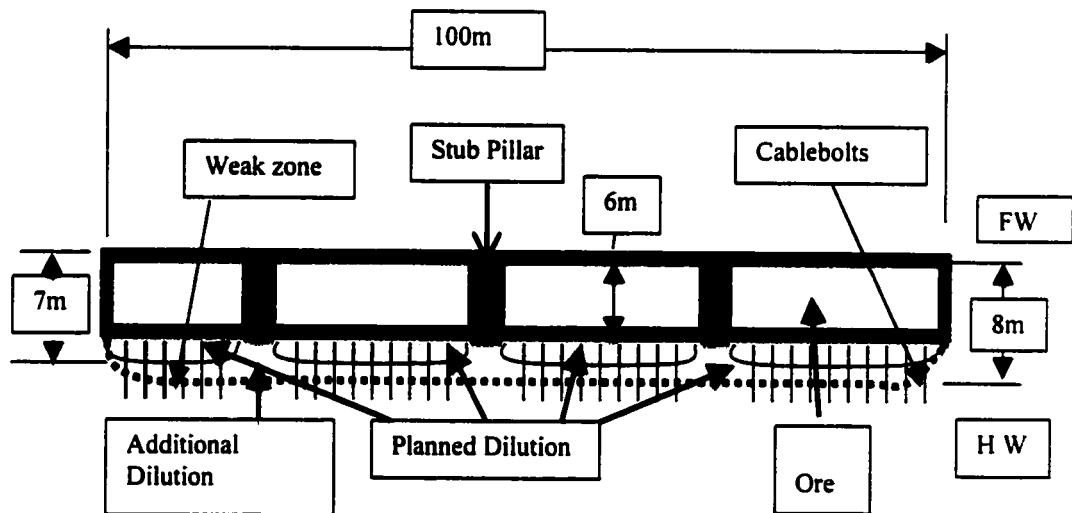
Figure 11.10: Plan view of a stope showing sources of dilution

11.6 MCC ECONOMIC BENEFITS

When the Creeping Cone (CC) mining method was first introduced at Selebi North mine, the increase in metal tonnes as compared to Sublevel mining method was 40% and 46% for nickel and copper respectively. This comparison was done on reconciled metal tonnes over a period of 7 months before the introduction of the creeping cone and 7 months after the method had been operated. The same increase in metal tonnage was envisaged for the Modified Creeping Cone (MCC) mining method over the Creeping Cone (CC) mining method, and it was further assumed that with increased support the MCC could achieve 44% reduction in the current dilution level of CC, the projected results were then tabulated in Table 11.4. The results showed that dilution could be reduced from the current level of 33.2% to 18.6% (Figure 11.11) and the expected increase in revenue over the same period was calculated at 41.44% (Figure 11.12). The metal prices were estimated at P11.36/lb (US$3.29/lb) for nickel and P3.79/lb (C$2.10) using the second half of 1997 exchange rate. The analysis was done using monthly metal tonnages and dilution figures observed from March 1996 to May 1997 on the South and North limbs. The Detached limb was excluded because the fluctuation in the metal tonnage and dilution values was huge, and therefore need to be analysed separately. Data for the Nose area was not available as the stopes are mined combined either with the South or North limb stopes. Figure 11.13 shows the reduction in stoping costs from P8.50/tonne (CC) to P5.00/tonne (MCC) against a budget of P6.60/tonne. These reductions in stoping cost/tonne are marched by an increase in run-of-mine ore grade from 0.71% Ni and 0.62% Cu to 0.79% Ni and 0.69% Cu, respectively, again favouring MCC.

Table 11.4 Comparison of projected MCC revenues and dilution with actual for CC

TIME	Nickel Tonnages		Copper Tonnages		Total Metal Tonnages		Dilution Percentages		Nickel Revenue (P/t)		Copper Revenue (P/t)		Total Revenue (P/t)	
	CC	MCC	CC	MCC	CC	MCC	CC	MCC	CC	MCC	CC	MCC	CC	MCC
Mar-96	226.00	316.4	193	281.78	419.00	474 78	26	14.56	5,650,000.00	7,910,000.00	1608269	2348072.7	7,258,269.00	10,258,072.74
Apr-96	241	337.4	211	308.06	452.00	519 06	27	15.12	6,025,000.00	8,435,000.00	1758263	2567064	7,783,263.00	11,002,063.98
May-96	142	198.8	128	186.88	270.00	314.88	34	19.04	3,550,000.00	4,970,000.00	1066624	1557271	4,616,624.00	6,527,271.04
Jun-96	96	134.4	84	122.64	180.00	206 64	27	15.12	2,400,000.00	3,360,000.00	699972	1021959.1	3,099,972.00	4,381,959.12
Jul-96	152	212.8	123	179 58	275.00	302 58	36	20.16	3,800,000.00	5,320,000.00	1024959	1496440.1	4,824,959.00	6,816,440.14
Aug-96	202	282.8	171	249.66	373.00	420.66	39	21.84	5,050,000.00	7,070,000.00	1424943	2080416.8	6,474,943.00	9,150,416.78
Sep-96	144	201.6	147	214 62	291.00	361 62	30	16.8	3,600,000.00	5,040,000.00	1224951	1788428.5	4,824,951.00	6,828,428.46
Oct-96	145	203	142	207 32	287.00	349 32	48	26.88	3,625,000.00	5,075,000.00	1183286	1727597.6	4,808,286.00	6,802,597.56
Nov-96	106	148.4	103	150.38	209.00	253 38	37	20.72	2,650,000.00	3,710,000.00	858299	1253116.5	3,508,299.00	4,963,116.54
Dec-96	97	135.8	95	138.7	192.00	233.7	45	25.2	2,425,000.00	3,395,000.00	791635	1155787.1	3,216,635.00	4,550,787.10
Jan-97	138	193.2	145	211.7	283.00	356.7	46	25.76	3,450,000.00	4,830,000.00	1208285	1764096.1	4,658,285.00	6,594,096.10
Feb-97	91	127.4	110	160.6	201.00	270.6	30	16.8	2,275,000.00	3,185,000.00	916630	1338279.8	3,191,630.00	4,523,279.80
Mar-97	79	110.6	81	118.26	160.00	199.26	19	10.64	1,975,000.00	2,765,000.00	674973	985460.58	2,649,973.00	3,750,460.58
Apr-97	94	131.6	94	137.24	188.00	231.24	35	19.6	2,350,000.00	3,290,000.00	783302	1143620.9	3,133,302.00	4,433,620.92
May-97	181	253.4	203	296.38	384.00	499.38	19	10.64	4,525,000.00	6,335,000.00	1691599	2469734.5	6,216,599.00	8,804,734.54
AVERAGE	142.2667	199.1733	135.3333	197.5867	277.6	332.92	33.2	18.592	3556666.667	4979333.333	1127733	1646489.7	4684399.333	6625823.027

185
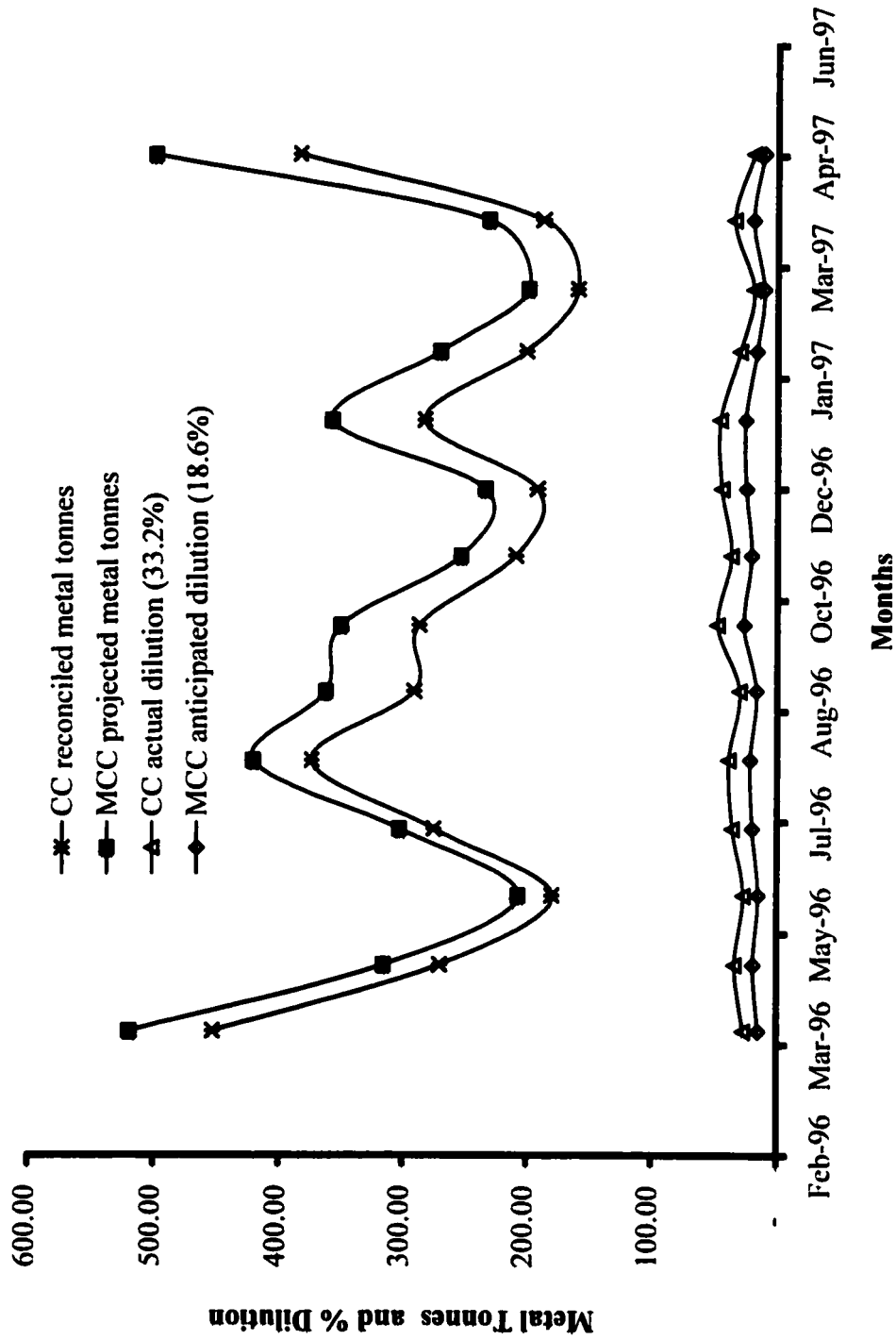
Figure 11.11: Projected Metal Tonnes and % Dilution for MCC compared with CC actual

Legend:
- CC reconciled metal tonnes
- MCC projected metal tonnes
- CC actual dilution (33.2%)
- MCC anticipated dilution (18.6%)

Y-axis: Metal Tonnes and % Dilution

X-axis (Months): Feb-96 Mar-96 May-96 Jul-96 Aug-96 Oct-96 Dec-96 Jan-97 Mar-97 Apr-97 Jun-97
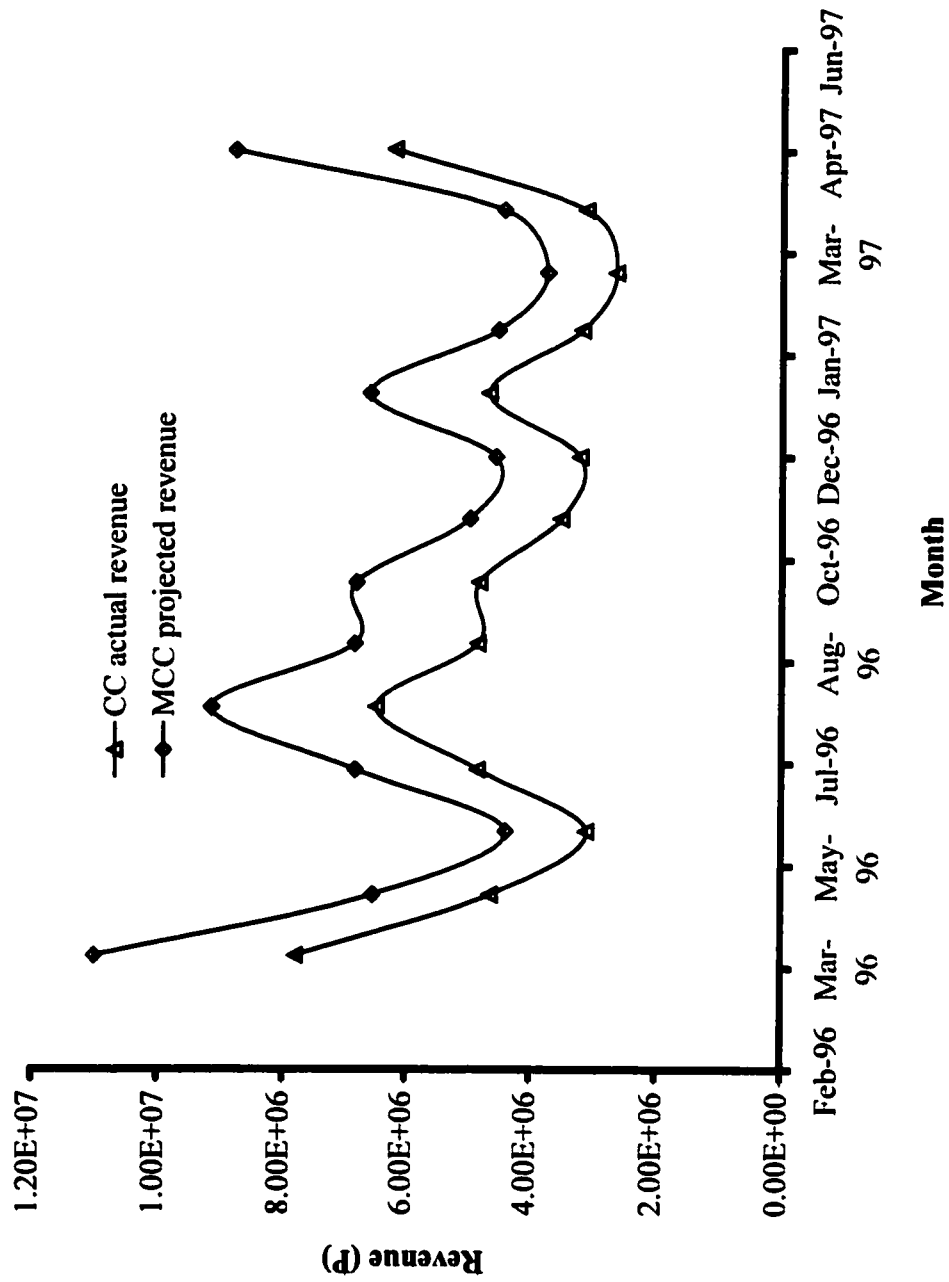
Figure 11.12: Projected Monthly Revenues in Pula for MCC compared with CC actual
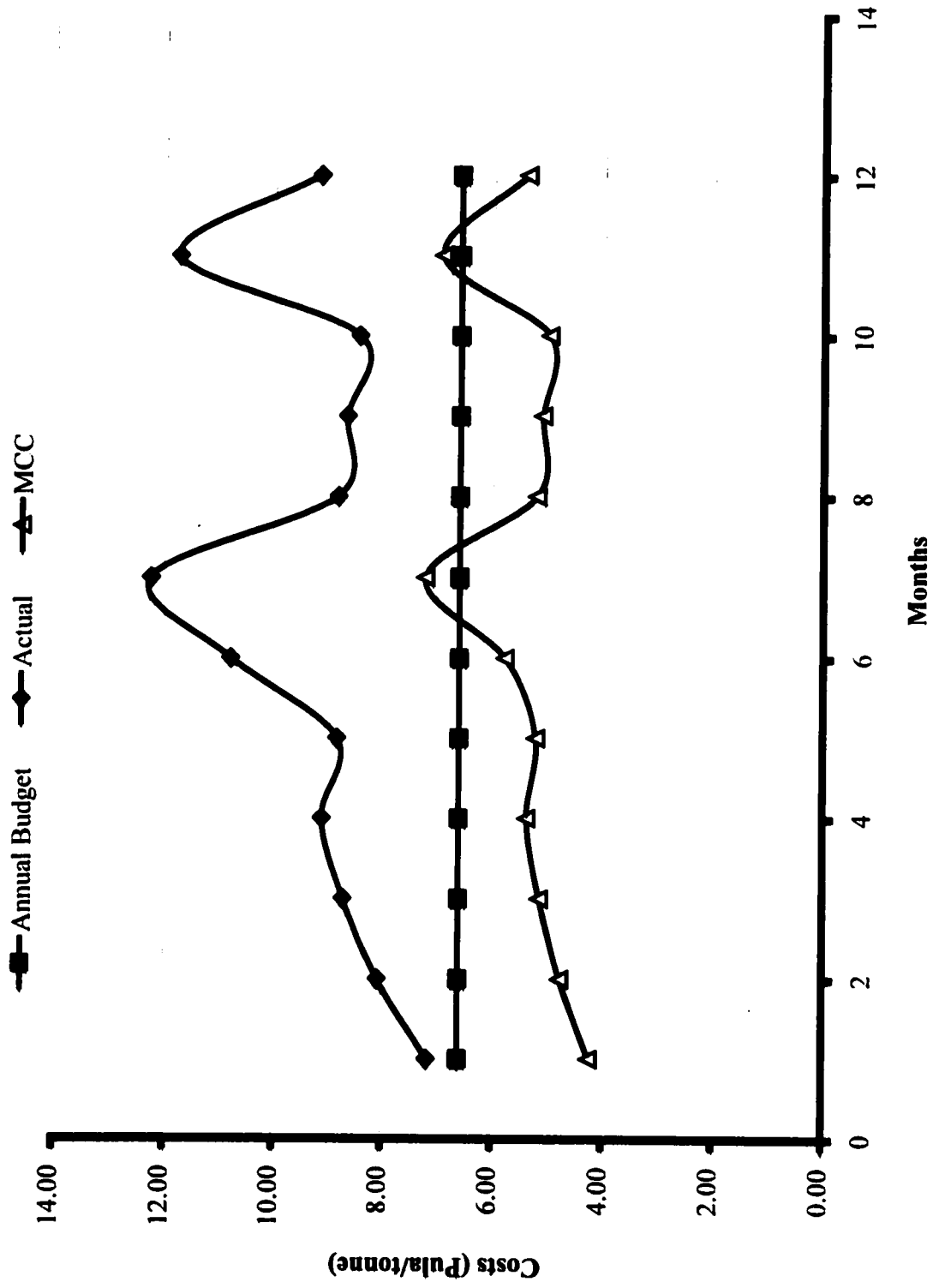
Figure 11.13: Stoping costs comparison between MCC and CC

11.7 CONCLUSION

The Modified Creeping Cone (MCC) mining method has been designed for Selebi North rock mass conditions. Different stope spans have been specified for the North, South and Detached limb as well as for the Nose area. With proper equipment selection the narrow Detached limb could be developed to the ore body width thereby minimizing side wall overbreak which causes additional dilution.

The projected results of the MCC method showed that if dilution is reduced by 44% from 33.2% to 18.6%, the expected revenues could be increased by 41.44%, with an increase of 10.5% in the grade of the run-of-mine ore. Stoping costs/tonne are also reduced from P8.50 to P5.00, well below the budget of P6.60/tonne. These improvements in the economic of the mine can be achieved with proper application of the MCC mining method.

CHAPTER 12

OBSERVATIONS, CONCLUSIONS, AND RECOMMENDATIONS AND FURTHER WORK.

12.1 OBSERVATIONS

The problems pertaining to Selebi North mine and the BCL Ltd mines in general, are not unique to that organization. The problems of ore dilution have been experienced by most mining companies at one stage or another during their life time. The fact of the matter is how individual companies deal with their problems in their particular mining environment. In any case some drastic measures are taken to restructure the organization either by changing its design approach or refining the methods already in place.

Selebi North mine is experiencing a high level of dilution which is rendering the project uneconomic given today's market prices of copper and nickel. The fact that the project is remote and that sandfill is not readily available doesn't mean that other cost saving measures cannot be considered. This research project has been geared to finding alternative means of curbing ore dilution without using traditional artificial methods of sandfill. The research also took into consideration the fact that limited funds are available to the company, hence the method proposed is supposed to pay for its own implementation by the savings achieved in reducing dilution.

Both hangingwall dilution and deformation are caused by a complex response of the rockmass to stress redistribution and arching. If the case of discrete structures that may delineate unstable blocks is ignored (voussoir analysis), both deformation and dilution can be expected to increase with span between the rib pillars. The observations at the mine have shown that in general stopes are being mined in access of their maximum allowable spans before failure can occur. As a result different kinds of failure modes inherent to the mine were identified and studied. The levels of dilution were also studied over a year to ascertain the trend as per individual regions of the mine. The mine was then divided into four regions of similar rock conditions. The competency of the rockmass per region was evaluated and the results were used for the design of the stope spans.

Though various methods have been employed in this study, mathematical methods have been found to be inconclusive, bearing in mind the assumptions made in the determination of the input parameters. For instance, it is not yet clear whether the stress distribution assumed in the voussoir method is triangular or parabolic, while this is still been researched the current consensus is that the distribution is triangular. If it turns out that the distribution is parabolic, obviously different results should be expected.

On the other hand the empirical methods used have shown an acceptable level of confidence. This is mainly due to the fact that the input parameters used were actually observed as the conditions governing the behaviour of the rockmass at Selebi North mine, and the method has also been tested at several other hard rock mines.

12.2 CONCLUSIONS

The Modified Creeping Cone (MCC) mining method has been proposed and designed in this thesis. The maximum allowable spans were determined for the South limb. North limb, Nose area and the Detached limb at Selebi North mine. Based on the rockmass response and stress conditions at the mine, the Modified Creeping Cone (MCC) mining method has been proposed. The proposed mining method introduces stope support in the form of cablebolts and the mining sequence is such that the mining blocks are always located well ahead of the transiting hangingwall. In other words when the hangingwall starts to yield after been destressed, the block being mined is at a relatively safe position where the hangingwall is still competent. Stub pillars have been introduced at strategic places along the orebody to control both the hangingwall sagging and ore flow in the stope.

The proposed MCC mining method stoping layout, was based on the results of the maximum allowable spans for supported stopes. Single stub pillars were placed at the maximum stable span without support, while double stub pillars were placed at the maximum span allowable for stable with support stope. The maximum span of the entire stope is designed at twice the supported transition zone as the double stub pillars divide the stope in two parts, each relatively independent from one another. The dimensions are based on the rockmass response per particular area of the mine.

The Nose area could be mined with supported stopes of 50 metres in length and 22 metres wide, depending on the width of the orebody at that point. The stopes on the South limb were designed at a maximum span of 115 metres with double stub pillars at 55 metres and single stub pillars at 25 metres. Similarly the stopes on the North limb were designed at a maximum span of 255 metres with double stub pillars placed at 125 metres and single stub pillars placed at 60 metres along the strike. The stopes on the Detached limb were designed to 175 metres in length with double and single stub pillars positioned at 85 metres and 40 metres respectively. The stope hanging walls are to be supported with cablebolts in a regular 2 metres by 2 metres pattern. The stub pillars were designed at 5 metres width and their height is determined by the sublevels which are 15 and 12 metres for the secondary and primary sublevels respectively. The height of the stopes is designed at 50 metres. BCL ltd is well experienced in the use of cablebolts as they have been successfully used elsewhere in the organization and as such their introduction to Selebi North mine shouldn't be a problem.

It is expected that the introduction of the proposed MCC mining method could reduce dilution at Selebi North mine from the current level of 33.2% to 18.6%, provided the steps outlined in the design are followed and quality control is exercised. It is also projected that financial gains will be 41%, with the same increase in recovered metals as compared to the Creeping Cone (CC) mining method. The stope yield is expected to be in excess of 96% with only 1.4% of the ore locked in the stope at any one time.

Ore loses are expected to be minimum since the increased side wall stand-up time allows the LHDs the opportunity to go further in the stope while loading, as support offers safety. The method is based on the experiences at the mine and the database built at the mine hence its implementation shouldn't be a problem as experienced personnel are already available.

12.3 RECOMMENDATIONS AND FURTHER WORK

Based on the findings of this research and the confidence in the methods employed, it is recommended that the MCC mining method be tried at Selebi North mine. The method could first be applied to the South limb on trial basis and could later be applied to other parts of the mine. The savings made in reducing dilution should balance the cost of implementing the mining method, including the cost of support. Further work in this research should include the stress modelling using the computer program PHASES which was not available to use during the research period. This should be geared towards finding areas of stress relaxation in the peripheral rocks of the stope and hence predicting the thickness of hangingwall sloughing expected. This could help with the cablebolt design. Mine sequencing of the stopes could also be modeled in order to predict how fast the stopes could be mined in relation to the change in induced stresses. A systematic data collection system should be put in place at Selebi North mine which could continuously be used in the improvement of the mining systems and designs.

Instrumentation of both the hanging wall and mining blocks should also be introduced. Borehole cameras could be used to monitor the deviations of the blastholes and help in the reduction of hanging wall damage. They can also help in monitoring the development and opening of fractures and joints within the rock mass and this can help in decision making regarding support installation. Other instruments could include the use of a remote laser scanning device by the survey crew to measure the profile of every stope. The data recorded could provide valuable information about the source and volume of dilution due to failure of the hangingwall and footwall. This could indicate where ore has sloughed into the stope and where unblasted ore has been left behind. The information derived from a failed stope could be used to design support for other adjacent stopes. The cablebolt spiral strain gauge could provide information to decide whether the cablebolts are being loaded close to their breaking strength, or if they are providing the bond strength used in design or if the cablebolt pattern or length should be changed.

The design of the instrumentation program at a particular site is governed by budget, past experience, relative cost and applicability of the instruments, orebody geometry, underground access and the objective of the monitoring program. Therefore the instrumentation cost should be comparable to the value of the data collected and interpreted. In the case of a new instrumentation program, numerous inexpensive instruments could be used provided they relay the information required and more expensive instruments could be purchased to answer specific questions arising from previous instrumentation.

REFERENCES

Anderson, B. and B. Grebenc (1995), "Controlling dilution at the Golden Giant

Mine", *CIM Mine Operators' Conference*, Timmins, Canada, Paper # 4,

14 p.

Aplin, P. (1997), Reducing dilution by the creeping cone, Mining Magazine,

London, Vol. 176, January, pp 22 - 26.

Barry, H.G.B. (1981), "Determination of Stability of Underground Mine

Structures"; *Design and Operation of Caving and Sublevel Stoping Mines*;

Stewart, Dan (Editor); ©AIMMPE, Inc.; Port City Press; Baltimore. USA.

pp 427 - 458.

Barton, N. et al. (1974), Engineering classification of rock masses for the design

of tunnel support, Rock Mechanics, May, pp 189 - 236.

Bawden, N. et al. (1989), Practical rock engineering in the optimization of stope

dimensions - Application and cost effectiveness, CIM Bulletin. Vol. 82,

(926), pp 63 - 70.

Bawden, W. F. (1993), "The use of rock mechanics principles in Canadian

underground hard rock mine design", *Comprehensive Rock Engineering*:

Principles, Practice and Projects, Hudson (Editor), Oxford, Pergamon

Press, V5, pp 247 - 290.

Bawden, W.F. et al. (1992), "Towards a methodology for performance assessment

in cable bolt design"; *Rock Support in Mining and Underground

Construction*; Kaiser at el., (Editors); ©1992 A.A. Balkema. Rotterdam,

Netherlands. pp 277 - 284.

Baxter, A.R. and G.B. Hooper (1992), Use of 'Three-dimensional solid   modeling'

    system for Baluba Center/South Limb feasibility study at   ZCCM Ltd.;

    Trans. Institn Min. Metall. (Sect. A: Min. Industry), Vol.   101, Jan -

    April. ©The Institution of Mining and Metallurgy 1992;   pp A1 - 74.

BCL Limited, (Unpub.), Rock Parameters for Computer Modeling; Internal

    Document.

Beer. G. and J. I. Meek (1982), Design curves for roofs and hanging-walls in

    bedded rock based on 'voussoir' beam and plate solutions, Trans. Institn

    Min. Metall. (Sect. A: Min. Industry), Vol. 91, ©The Institution of Mining

    and Metallurgy 1982, January, pp A18 - A22.

Belford, J.E. (1981), "Sublevel Stoping at Kidd Creek Mines"; *Design and*

    Operation of Caving and Sublevel Stoping Mines; Stewart, Dan (Editor);

    ©AIMMPE, Inc; Port City Press; Baltimore, USA. pp 577 - 584.

Bieniawski, Z.T. (1976), Rock mass classifications in rock engineering. Proc.

    Symp. On Exploration for Rock Engineering, Johannesburg. November,

    pp 97 - 106.

Bieniawski, Z.T. (1989), Engineering rock mass classifications, New York:

    Wiley.

Bieniawski, Z.T. (1993), "Classification of rock masses for engineering: The

    RMR system and future trends", *Comprehensive Rock Engineering*,

    Hudson (Editor), Oxford, Pergamon, V3, pp 553 - 573.

Brady, B.G.H. and E.T. Brown (1985), Rock Mechanics for Underground Mining,

George Allen and Unwin, London.

Bronkhorst, D. et al. (1993), "Geotechnical principles governing mine design at

the William's Mine"; *Innovative Mine Design for the 21st Century*;

Bawden et al., (Editors); ©1993 A.A. Balkema, Rotterdam, Netherlands;

pp 433 - 442.

Bucky, B. P. (1945), Mining by Block Caving; Hercules Power Company;

Wilmington, Delaware.

Chadwick, J. (1995), Kundana's narrow veins, Mining Magazine, London.

December, pp 316 - 317.

Chatterjee, P. K and G. D. Just (1981), Cost Analysis for the design and   Operation of

Sublevel Open Stoping, Mining Engineering, October, pp 1445 - 1449.

Choquet, P. (1991), Rock Bolting Practical Guide; Canada Communication

Group; Ottawa; ©Minister of Supply and Services Canada 1991.

Coates, D.F. (1965), Rock Mechanics Principles; Mines Branch

Monograph 874;

© Crown copyrights reserved, Ottawa, Canada.

Diederichs, M. S., and E. Hoek (1989), DIPS: Data Interpretation with projected

stereonets. Program for plotting analysis and presentation of structural

data using spherical projection techniques. Rock Engineering Group, 12

Selwood Avenue, Toronto, Ontario, Canada.

Grabinsky, M. W. et al. (1997), Interaction between stress, mine geometry and   rock

mass behaviour at a Canadian shield mine, CIM Bulletin, Sept., pp 45-49.

Gryba, C.M. (1993), "Double post mining (DPM)"; *Innovative Mine Design for*

the 21st Century; Bawden et al.,(Editors); ©1993 A.A. Balkema, Rotterdam, Netherlands; pp 397 - 407.

Hautala, R. L. et al. (1996), Mine systems design and roof control, Mining Engineering, January, pp 36 - 40.

Hoek, E. and E. T. Brown (1994), Underground Excavations in Rock; IMM and E.Hoek and E. T. Brown; London.

Hoek, E. et al. (1995), Support of Underground Excavations in Hard Rock; ©1995 A.A. Balkema, Rotterdam, Netherlands.

Hutchinson, D. J. and M. S. Diedericchs (1996), Cablebolting in Underground Mines, © D. Jean Hutchinson, Mark S. Diederichs and Geomechanics Research Centre, Altona, Manitoba.

Jeremie, M. l. (1984), Influence of Shrinkage and Cut and Fill Mining on Ground Mechanics, South Bay Mine. Northeastern Ontario, Mining Engineering. October, pp 1431 - 1436.

Kaesehagen, F.E. and G.G. Northcote (1993), "Planning the Porgera underground mine"; *Innovative Mine Design for the 21st Century*; Bawden et al.. (Editors); ©1993 A.A. Balkema, Rotterdam, Netherlands; pp 421 - 432.

Laubscher, D. H and H. W. Taylor (1976), "The importance of geomechanics classification of jointed rock masses in mining operations". *Exploration for rock engineering*, Cape Town, Bieniawski (Editor), Vol. 1. © A. A. Balkema, Rotterdam, Netherlands. pp 119 - 128.

Laubscher, D. H. (1977), Geomechanics classification of jointed rock rock masses mining applications. Trans. Institn Min. Metall. (Sect. A: Min.

Industry), Vol. 86, ©The Institution of Mining and Metallurgy 1992. pp A1 - A8.

Laubscher, D. H. (1984), Design aspect and effectiveness of support systems in different mining conditions. Trans. Institn Min. Metall. (Sect. A: Min. Industry), Vol. 93, ©The Institution of Mining and Metallurgy 1992. pp A70 - A82.

Lizotte, Y. C. (1996), Controlled blasting at the CANMET Experimental Mine. Mining Engineering, June, pp 74 - 78.

Lorig, L. (1997), The Role of Numerical Models in Rock Mechanics Problem Solving, ISRM International Symposium, June 29 - July 2, 36th U. S. Rock Mechanics Symposium, Columbia University and the American Rock Mechanics Association.

Mabson, L. R. and F. M. Russell (1981), "Application of Sublevel Open Stoping on the RCM Limited Mines of the Zambian Copperbelt"; *Design and Operation of Caving and Sublevel Stoping Mines*; Stewart, Dan (Editor); ©AIMMPE, Inc; Port City Press; Baltimore, USA. pp 585 - 607.

Mathews et al. (1981), Prediction of stable excavations for mining at depth below 1000 metres in hard rock. CANMET Report DSS Serial No. OSQ80-00081, DSS File No. 17Q.23440-0-9020, Ottawa, Dept. Energy. Mines and Resources, 39 p.

Nickson, (1992), Cable support guidelines for underground hard rock mine operations. M.A.Sc. Thesis, Dept. Mining and Mineral Processing. University of British Columbia, 223 p.

Nilsson, D. S. (1982), Advantages of High Production Level in Underground

Mining, Mining Engineering, August, pp 1252 - 1259.

Pakalnis, R. and S. Vongpaisal (1993), "Mine Design an empirical approach";

Innovative Mine Design for the 21st Century; Bawden et al.,(Editors);

©1993 A.A. Balkema, Rotterdam, Netherlands; pp 455 - 467.

Pakalnis, R. C. et al. (1993), Pillar strength estimation at Westmin Resources' H-

W mine - a case study; Trans. Institn Min. Metall. (Sect. A: Min.

Industry), Vol. 102, September - December 1993. ©The Institution of

Mining and Metallurgy 1993. pp A165-171.

Pakalnis, R. C. et al. (1995), Quantifying the cost of dilution in underground

mines, Mining Engineering, December, pp 1136 - 1141.

Pine, R. J. and I.G.T. Thin (1993), "Probabilistic risk assessment in mine pillar

design"; *Innovative Mine Design for the 21st Century*; Bawden et al.,

(Editors); ©1993 A.A. Balkema, Rotterdam, Netherlands; pp 363 - 373.

Pine, R. J. et al. (1992), Rock engineering design developments at South Crofty

mine; Trans. Institn Min. Metall. (Sect. A: Min. Industry), Vol. 101, Jan. -

April 1992. ©The Institution of Mining and Metallurgy 1992. pp A13 -

A22.

Planeta, S. and J. Szymanski (196); "Ore dilution in underground mines-

Interpretation and evaluation problem"; Mine Planning and Equipment

Selection 1996; Hennes et al. (Editors); © A. A. Balkema, Rotterdam,

Netherlands. pp 71 - 79.

Platford, R. E. et al. (19--), Dilution control at Inco's Thompson Mine Manitoba

Division, Anon.

Potvin, Y. (1988), Empirical open stope design in Canada. Ph.D. Thesis, Dept.

Mining and Mineral Processing, University of British Columbia. 343 p.

Potvin, Y. and D. Milne (1992); "Empirical cable bolt support design"; *Rock*

Support in Mining and Underground Construction; Kaiser at el.. (Editors):

©1992 A.A. Balkema, Rotterdam, Netherlands. pp 269 -275.

Szymanski, J. et al. (1997), The total open stope design approach - part I,

University of Alberta, School of Mining and Petroleum Engineering.

Edmonton, Alberta, Canada. (unpubl.)

Stewart, S. B. V. and W. W. Forsyth (1995), The Mathew's method for open

stope design, CIM Bulletin, July - August, pp 45 - 53.

Takata, H. et al. (1981), "Sublevel Stoping at Tochibora Mine"; *Design and*

Operation of Caving and Sublevel Stoping Mines; Stewart, Dan (Editor):

© AIMMPE, Inc.; Port City Press; Baltimore, USA. pp 635 - 640.

Villaescusa, E. (1995), Sources of External Dilution in Underground Sublevel and

Bench Stoping, EXPLO '95 Conference, Brisbane, 4 - 7 September, pp

217 - 224.

Wakefield, J. (1976), The structural and metamorphic evolution of the Phikwe

nickel/copper sulfide deposit, Selebi-Phikwe, eastern Botswana, Econ.

Geol., Vol. 71, pp 988 - 1005.

Watkeys, M. K. (1983), Brief explanatory notes on the provisional geological

map of the Limpopo Belt and environs. Spec. Publ. Geol. Soc. S. Afr..

Vol. 8, pp 5 - 8.

Wright, J. H. (1984), Method for calculating Tonnage and Grade in a Longhole

Sublevel Stope, Mining Engineering, January, pp 70 - 71.

APPENDIX A

DATABASE

Table A.1: DIPS input datafile for the North Limb

```
SELEBI NORTH MINE  NORTH LIMB FROM 295 TO 349 ML
ENGINEER S. M. Nareetsile  DATE:  June, 1997.
1 traverse
1;LINEAR;120;30; Level 295, Stope 1800, sublevel 295;
DIP/DIPDIRECTION
0 degrees
QUANTITY
[There are] 7 [extra data columns]
```

no;	dip;	dipn;	qua;	traves;	space	type;	surfce	infill	jr;	jn;	ja;
1	70	100	1	1	0.5	joint	3	0	2	9	4
2	85	167	1	1	0.8	joint	3	0	2	9	4
3	65	130	1	1	3.5	joint	3	0	2	9	4
4	85	160	1	1	2.3	joint	3	0	2	9	4
5	55	80	1	1	0.8	joint	3	0	2	9	4
6	70	325	1	1	0.9	joint	3	0	3	6	4
7	70	330	1	1	2.6	joint	3	0	3	6	4
8	65	210	1	1	0.7	joint	5	0	2	9	4
9	45	230	1	1	3.6	joint	4	2	2	9	4
10	85	30	1	1	2.8	joint	3	0	2	9	4
11	55	175	1	1	5.1	joint	3	0	2	9	4
12	70	165	1	1	1.1	joint	3	0	2	9	4
13	70	330	1	1	1.7	joint	3	2	2	9	4
14	65	15	1	1	3.4	joint	3	0	2	9	4
15	65	185	1	1	1.4	joint	1	2	2	9	4
16	80	175	1	1	0.5	joint	2	0	2	9	4
17	55	170	1	1	2.3	joint	2	0	2	9	4
18	75	240	1	1	3.4	joint	3	0	2	9	4
19	80	180	1	1	0.8	joint	3	0	2	9	4
20	65	164	1	1	2.2	joint	3	0	2	9	4
21	60	220	1	1	2.6	joint	2	2	2	9	4
22	45	175	8	1	2.6	joint	2	2	1.5	12	4
23	90	227	1	1	2.6	joint	3	2	1.5	12	4
24	75	85	1	1	0.2	joint	3	2	1.5	12	4
25	60	110	1	1	5	joint	3	2	1.5	12	4
26	75	150	1	1	1.2	joint	3	0	1.5	12	4
27	75	150	1	1	0.4	joint	3	0	1.5	12	4
28	45	30	1	1	2.2	joint	3	0	1.5	12	4
29	50	265	1	1	3.9	joint	3	0	1.5	12	4
30	85	110	1	1	3.2	joint	3	0	1.5	12	4
31	50	98	1	1	1.3	joint	3	0	1.5	12	4
32	40	85	1	1	3.6	joint	3	0	1.5	12	4
33	85	105	1	1	0.8	joint	3	0	1.5	12	4
34	65	170	1	1	0.4	joint	1	1	1.5	12	4
35	80	345	1	1	1	joint	3	1	1.5	12	4
36	55	350	1	1	0.9	joint	3	1	1.5	12	4
37	30	230	1	1	1.8	joint	3	1	1.5	12	4
38	85	205	1	1	2	joint	3	1	1.5	12	4

39	75	195	1	1	1.3	joint	3	1	1.5	12	4
40	65	190	1	1	1.4	joint	3	1	1.5	12	4
41	80	160	1	1	0.8	joint	3	1	1.5	12	4
42	65	160	1	1	0.8	joint	3	1	1.5	12	4
43	80	183	1	1	0.8	joint	3	1	1.5	12	4
44	85	130	1	1	1.2	joint	3	2	1	9	4
45	75	150	1	1	1.1	shear	3	0	1	9	4
46	10	135	1	1	0.6	joint	2	1	1	9	4
47	80	140	1	1	7.4	shear	1	0	1	9	4
48	65	131	1	1	1.8	joint	1	0	1	9	4
49	80	175	1	1	1.9	joint	5	0	1	9	4
50	70	170	1	1	3.2	joint	3	0	1	9	4
51	90	142	1	1	2.4	joint	3	0	1	9	4
52	80	150	1	1	0.9	joint	3	0	1	9	4
53	45	30	1	1	2	joint	4	0	1	9	4
54	65	310	1	1	2.7	joint	4	0	1	9	4
55	67	10	1	1	2.8	joint	4	0	1	9	4
56	50	307	1	1	0.3	joint	4	0	1	9	4
57	55	30	1	1	2.2	joint	4	0	1	9	4
58	85	244	1	1	0.9	joint	4	0	1	9	4
59	80	85	1	1	9.1	joint	4	0	1	9	4
60	70	130	1	1	1.8	shear	4	0	1	9	4
61	45	160	1	1	6.5	shear	4	0	1	9	4
62	45	165	1	1	6	joint	4	0	1	9	4
63	80	155	1	1	1.5	joint	3	0	1	9	4
64	30	180	1	1	1.3	joint	3	0	1	9	4
65	40	160	1	1	2.7	joint	3	0	1	9	4
66	65	170	1	1	3.1	shear	3	0	1	9	4
67	60	170	1	1	3.1	joint	3	0	1	9	4
68	73	112	1	1	1	joint	2	1	1.5	12	4
69	70	203	1	1	2.7	joint	2	1	1.5	12	4
70	70	202	1	1	3.5	joint	2	1	1.5	12	4
71	60	183	1	1	12.6	joint	1	0	1.5	12	4
72	65	140	1	1	1.4	joint	1	0	1.5	12	4
73	80	180	1	1	0.3	joint	1	0	1.5	12	4
74	70	160	1	1	2.8	joint	1	0	1.5	12	4
75	60	150	1	1	8.8	joint	1	0	1.5	12	4
76	45	35	1	1	0.6	joint	1	0	1.5	12	4
77	65	110	1	1	4.3	joint	2	0	1.5	12	4
78	90	185	1	1	15.5	joint	2	0	1.5	12	4
79	50	255	1	1	1.3	joint	1	0	1.5	12	4
80	40	255	1	1	3.2	joint	1	0	1.5	12	4
81	50	245	1	1	3.2	joint	1	0	1.5	12	4
82	65	345	1	1	9.8	joint	2	2	1	4	4
83	80	348	1	1	5.3	joint	2	2	1	4	4
84	75	204	1	1	1.1	shear	1	0	1	4	4

85	35	200	1	1	4.4	joint	1	0	1	4	4
86	70	205	1	1	4.4	joint	1	0	1	4	4
87	40	100	1	1	0.5	joint	1	0	1	4	4
88	55	174	1	1	0.5	joint	1	0	1	4	4
89	40	85	1	1	0.6	joint	1	2	1	4	4
90	60	143	1	1	2.8	joint	1	2	1	4	4
91	70	183	1	1	1.8	joint	1	2	1	4	4
92	70	137	1	1	1.8	joint	1	2	1	4	4
93	70	160	1	1	2.7	joint	1	2	1	4	4
94	45	215	1	1	3.6	joint	2	2	1	4	4
95	67	240	1	1	2.3	joint	2	2	1	4	4
96	70	155	1	1	6.5	joint	3	2	1	4	4
97	70	127	1	1	0.7	joint	3	2	1	4	4
98	75	238	1	1	1.4	joint	3	2	1	4	4
99	65	150	1	1	1.4	joint	3	2	1	4	4
100	60	145	1	1	0.2	joint	3	2	1	4	4
101	80	134	1	1	0.2	joint	1	0	1.5	6	2
102	65	120	1	1	0.3	joint	1	0	1.5	6	2
103	65	110	1	1	0.5	joint	1	0	1.5	6	2
104	85	130	1	1	0.5	joint	1	0	1.5	6	2
105	45	134	1	1	6.5	joint	1	0	1.5	6	2
106	45	75	1	1	1.4	joint	1	1	1.5	6	2
107	80	135	1	1	0.5	joint	1	1	1.5	6	2
108	50	130	1	1	0.8	joint	1	1	1.5	6	2
109	45	127	1	1	1.1	joint	1	1	1.5	6	2
110	20	118	1	1	0.3	joint	1	1	1.5	6	2
111	80	304	1	1	3.3	joint	5	2	3	9	0.8
112	80	305	1	1	5	joint	1	6	4	0.7	4
113	45	272	1	1	3.7	joint	5	0	3	12	0.8
114	65	140	1	1	1.5	joint	3	0	2	9	0.8
115	50	110	1	1	7	joint	1	2	3	12	0.8
116	90	150	1	1	7	joint	1	2	3	12	2
117	60	197	1	1	3	joint	3	2	3	9	4
118	60	200	1	1	2.7	joint	5	0	3	9	4
119	74	215	1	1	6.7	shear	3	0	3	9	4
120	33	125	1	1	4	shear	1	0	3	9	4
121	38	126	1	1	0.3	shear	3	0	3	9	4
122	47	146	1	1	5.6	joint	3	0	3	5	4
123	35	155	1	1	8.3	joint	0	0	3	5	4
124	60	150	1	1	3.7	joint	0	0	3	5	4
125	55	111	1	1	2.5	joint	1	0	3	5	4
126	50	133	1	1	2	joint	3	0	3	5	4
127	50	300	1	1	1.5	shear	3	0	15	12	4
128	55	150	1	1	5	joint	1	2	15	12	4
129	75	300	1	1	5.8	joint	1	2	4	6	4
130	75	195	1	1	3.8	shear	3	2	1.5	1.5	4

```
131  60  335  1     1   9.6 joint   3        0 1.5 1.5   4
132  85  195  1     1   1.3 joint   5        4 1.5 1.5   4
133  80  185  1     1   5.9 joint   5        4 1.5 1.5   4
134  90  215  1     1   7.8 joint   5        4 1.5 1.5   4
135  90  185  1     1   5.8 joint   5        4 1.5 1.5   4
 -1
```

Figure A1: Major planes with their poles for the North limb.

209

Figure 7.3: Rosette showing apparent strike of planes for the North limb.

210
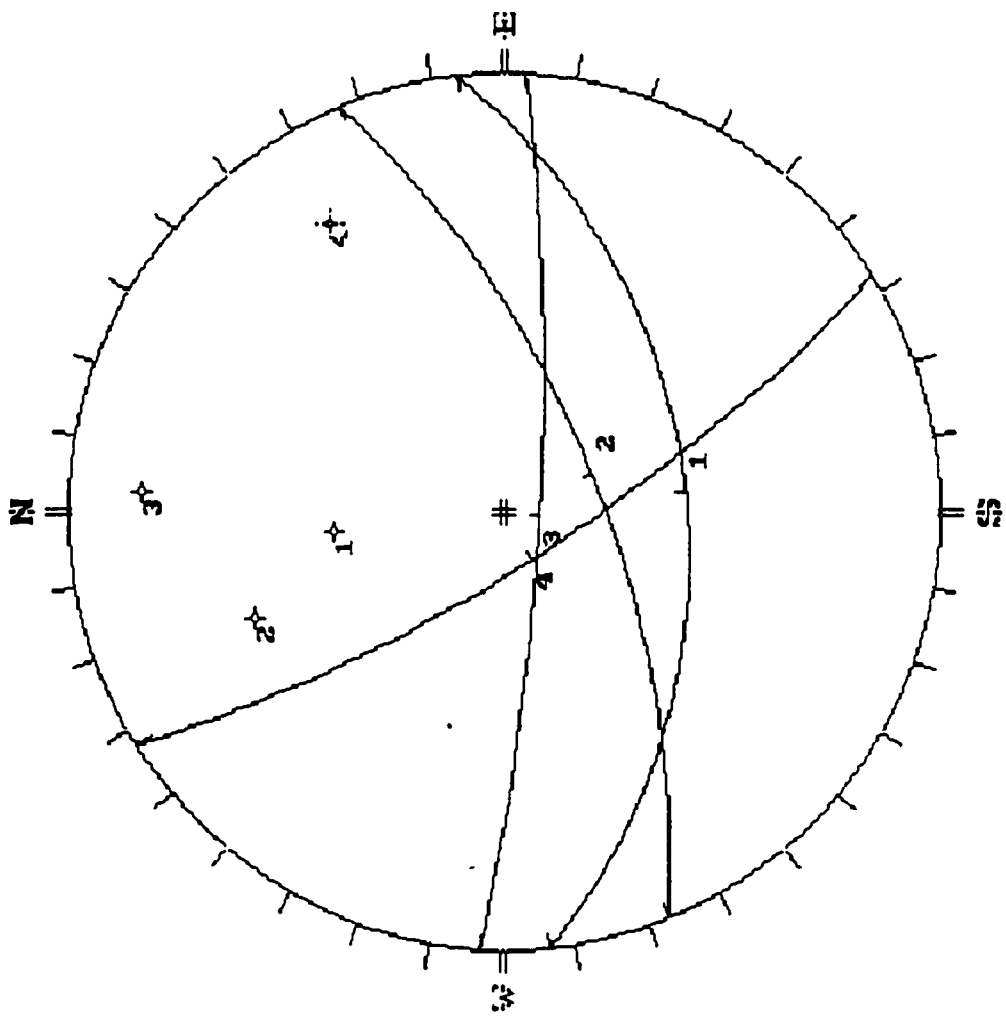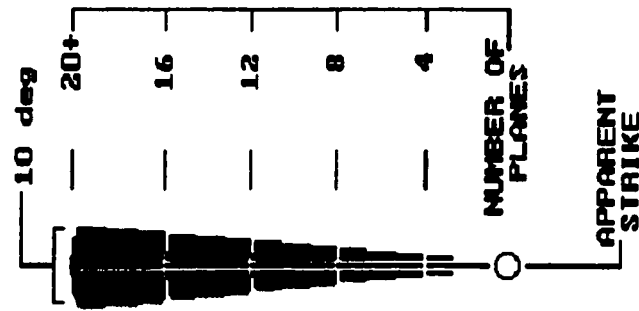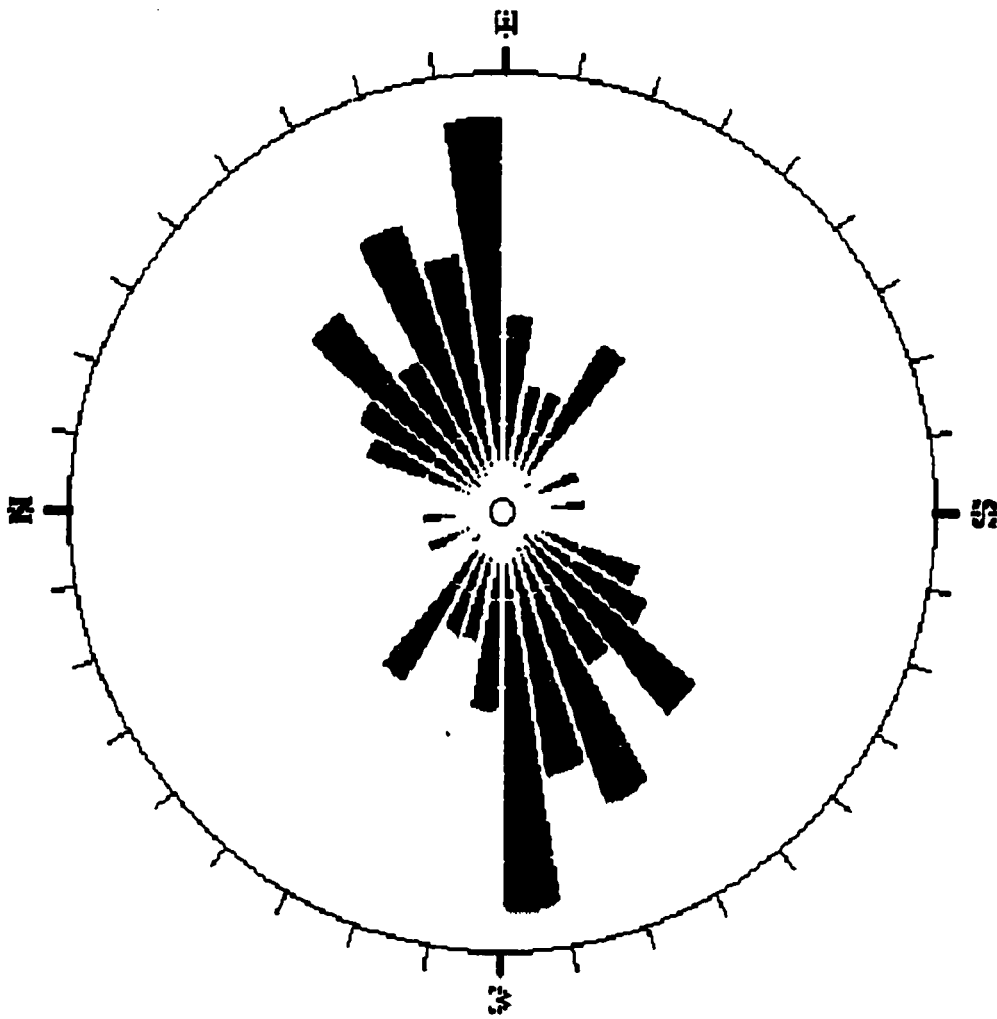
Table A.2: DIPS input datafile for the Nose Area

```
SELEBI NORTH - NOSE AREA FROM 295 ML TO 349 ML DRILL DRIVE
ENGINEER: S. M. Nareetsile              DATE: June 1997.
1 traverse
1;LINEAR;120;30;Level 295, Stope 1900 & 700, sublevel 295;
DIP/DIPDIRECTION
0 degrees
QUANTITY
[There are] 7 [extra columns]
```

no;	dip;	dipn;	qua;	traves;	space	type;	surfce	infill;	jr;	jn;	ja;
1	45	115	1	1	2	joint	3	0	1.5	12	4
2	50	345	1	1	0.5	joint	3	0	1.5	12	4
3	55	345	1	1	4.4	joint	3	0	1.5	12	4
4	65	300	1	1	0.5	shear	3	0	1.5	12	4
5	50	0	1	1	0.8	joint	1	0	1.5	12	4
6	45	270	1	1	1.2	joint	1	0	1.5	12	4
7	40	345	1	1	4.1	joint	1	0	1.5	12	4
8	70	350	1	1	1	joint	1	0	1.5	12	4
9	85	0	1	1	1.1	joint	1	0	1.5	12	4
10	80	210	1	1	1.7	joint	1	2	1.5	12	4
11	65	184	1	1	0.3	joint	1	2	1.5	12	4
12	85	185	1	1	1.7	joint	2	2	1.5	12	4
13	40	110	1	1	1.3	joint	1	0	1.5	12	4
14	75	180	1	1	0.6	joint	1	0	1.5	12	4
15	85	70	1	1	3	joint	1	0	1.5	12	4
16	85	155	1	1	0.6	joint	3	2	3	15	4
17	85	85	1	1	6.7	joint	3	2	3	15	4
18	80	350	1	1	0.7	joint	3	2	3	15	4
19	80	345	1	1	4	joint	3	2	3	15	4
20	85	45	1	1	0.7	joint	3	2	3	15	4
21	50	85	1	1	1.8	joint	3	2	3	15	4
22	85	170	2	1	2.1	joint	3	2	3	15	4
23	90	35	1	1	7.6	joint	3	2	3	15	4
24	90	30	1	1	1	joint	3	2	3	15	4
25	70	120	1	1	0.2	joint	3	2	3	15	4
26	62	50	1	1	1.7	joint	3	2	3	15	4
27	60	105	1	1	1.9	joint	3	2	3	15	4
28	85	100	1	1	2.8	joint	3	2	3	15	4
29	80	55	1	1	0.7	joint	3	2	3	15	4
30	70	50	1	1	0.8	joint	3	2	3	15	4
31	80	130	1	1	0.8	joint	3	0	1.5	12	4
32	75	5	1	1	3.9	joint	3	0	1.5	12	4
33	70	210	1	1	5.5	joint	3	0	1.5	12	4
34	60	210	1	1	1	joint	3	0	1.5	12	4
35	65	200	1	1	0.9	joint	3	0	1.5	12	4
36	75	198	1	1	0.5	joint	3	0	1.5	12	4
37	60	75	1	1	4.1	joint	3	0	1.5	12	4

38	85	165	1	1	1.4	joint	3	0	1.5	12	4
39	75	145	1	1	1.4	joint	3	0	1.5	12	4
40	75	160	1	1	0.7	joint	3	1	1.5	12	4
41	45	75	1	1	2.7	joint	3	2	1.5	12	4
42	90	157	1	1	0.4	joint	3	0	1.5	12	4
43	70	60	1	1	2.2	joint	3	0	1.5	12	4
44	65	55	1	1	1.2	joint	3	0	1.5	12	4
45	85	150	1	1	0.9	joint	3	0	1.5	12	4
46	80	115	1	1	1	shear	3	0	1.5	12	4
47	65	95	1	1	0.2	joint	3	0	1.5	12	4
48	85	110	1	1	1.1	shear	3	0	1.5	12	4
49	80	15	1	1	1.9	joint	5	2	3	12	4
50	45	225	1	1	1.4	joint	5	2	3	12	4
51	65	0	1	1	3.6	joint	5	2	3	12	4
52	45	275	1	1	0.4	joint	6	2	3	12	4
53	70	260	1	1	1.1	joint	6	2	3	12	4
54	30	285	1	1	1.4	joint	3	2	3	12	4
55	45	265	1	1	1.1	joint	2	1	3	12	4
56	60	345	1	1	6.3	joint	1	0	3	12	4
57	90	325	1	1	5.9	shear	1	0	3	12	4
58	60	222	1	1	1.6	joint	1	1	1	12	1
59	55	174	1	1	1.6	shear	2	0	1	12	1
60	50	230	1	1	1	shear	2	0	1	12	1
61	75	165	1	1	1.7	joint	2	0	1	12	1
62	60	240	1	1	0.4	joint	2	0	1	12	1
63	90	157	1	1	1.5	joint	2	0	1	12	1
64	50	90	1	1	5.1	joint	3	0	1	12	1
65	55	280	1	1	2.2	joint	3	0	1	12	1
66	65	140	1	1	1	joint	3	0	1	12	1
67	65	230	1	1	8.6	joint	1	1	1	12	1
68	50	235	1	1	2.2	joint	3	2	1	12	1
69	70	90	1	1	3	joint	1	0	1	12	1
70	75	170	1	1	1.5	joint	1	1	1	12	1
71	40	90	1	1	9.2	joint	2	0	1	12	1
72	30	90	1	1	4.3	joint	2	0	1	12	1
73	85	205	1	1	5.9	joint	2	0	1	12	1
74	45	265	1	1	7.2	joint	4	2	1	15	4
75	50	80		1	3.9	joint	3	4	1	15	4
76	70	50	1	1	6.5	joint	3	2	1	15	4
77	30	40	1	1	1.8	joint	1	0	1	15	4
78	75	20	1	1	2	joint	1	0	1	15	4
79	45	20	1	1	4.6	shear	1	0	1	15	4
80	50	15	1	1	8.1	shear	1	0	1	15	4
81	40	5	1	1	2.9	joint	3	0	2	9	0.8
82	50	340	1	1	4	joint	3	0	2	9	0.8
83	50	30	1	1	1.8	joint	4	2	2	9	0.8
84	35	300	1	1	1.9	joint	5	2	4	15	4
85	60	295	1	1	5.8	joint	5	2	4	15	4

86	80	315	1	1	1.6	joint	5	2	4	15	4
87	62	10	1	1	3	shear	5	2	4	15	4
88	60	25	1	1	1.1	joint	6	2	4	15	4
89	90	80	1	1	3.2	joint	6	2	4	15	4
90	40	80	1	1	2	joint	3	2	4	15	4
91	55	183	1	1	2.2	joint	0	0	3	9	4
92	55	180	1	1	1.5	joint	0	0	3	4	4
93	65	210	1	1	2.3	joint	0	0	3	4	4
94	65	207	1	1	2	joint	0	0	3	4	4
95	70	290	1	1	0.8	joint	0	0	3	4	4
96	75	295	1	1	0.4	joint	0	0	3	4	4
97	73	300	1	1	2	joint	0	0	3	4	4
98	35	245	1	1	1	joint	0	0	3	4	4
99	60	20	1	1	0.7	joint	0	0	2	15	4
100	62	25	1	1	1.4	shear	0	0	2	15	4
101	40	207	1	1	0.3	joint	3	0	1	12	4
102	57	190	1	1	0.6	joint	3	0	1	12	4
103	60	200	1	1	1	joint	3	0	1	12	4
104	50	147	1	1	1	joint	1	0	2	12	4
105	80	232	1	1	4.5	joint	3	0	2	12	4
106	80	140	1	1	0.4	joint	3	1	2	12	4
107	50	135	1	1	0.5	joint	3	1	2	12	4
108	70	200	1	1	2.8	joint	3	2	2	12	4
109	60	192	1	1	0.6	joint	3	2	2	12	4
110	70	195	1	1	0.2	joint	3	2	2	12	4
111	50	80	1	1	1	joint	3	2	2	12	4
112	50	275	1	1	1.1	joint	3	2	2	12	4
113	80	215	1	1	0.5	joint	3	2	2	12	4
114	90	235	1	1	0.7	joint	3	2	2	12	4
115	80	150	1	1	1.2	joint	4	2	2	12	4
116	80	155	1	1	3	joint	4	2	2	12	4
117	90	10	1	1	3	joint	4	2	2	12	4
118	67	185	1	1	0.8	joint	3	0	2	12	4
119	85	330	1	1	6.8	joint	3	1	2	12	4
120	60	320	1	1	1.5	joint	3	1	2	12	4
121	85	210	1	1	1.4	joint	3	1	2	12	4
122	80	190	1	1	0.5	joint	3	1	2	12	4
123	90	215	1	1	1.2	joint	2	1	2	12	4
124	75	310	1	1	0.7	joint	2	1	2	12	4
125	90	50	1	1	1.2	joint	2	1	2	12	4
126	42	345	1	1	1	joint	4	0	1.5	15	4
127	85	123	1	1	4.5	joint	4	0	1.5	15	4
128	85	5	1	1	0.5	joint	3	0	1.5	15	4
129	80	145	1	1	0.9	joint	3	0	1.5	15	4
130	85	303	1	1	0.7	joint	3	0	1.5	15	4
131	60	320	1	1	0.6	joint	3	0	1.5	15	4
132	85	305	1	1	0.5	joint	3	0	1.5	15	4
133	80	320	1	1	0.1	joint	3	0	1.5	15	4

134	80	305	1	1	0.3 joint	3	0	1.5	15	4
135	65	225	1	1	0.4 joint	3	0	1.5	15	4
136	90	330	1	1	0.8 joint	3	0	1.5	15	4
137	75	320	1	1	1.1 joint	3	0	1.5	15	4
138	80	335	1	1	1.3 joint	3	0	1.5	15	4
139	80	305	1	1	1 joint	3	0	1.5	15	4
140	45	245	1	1	0.2 joint	2	0	1.5	15	4
141	45	200	1	1	2.3 joint	2	0	1.5	15	4

-1
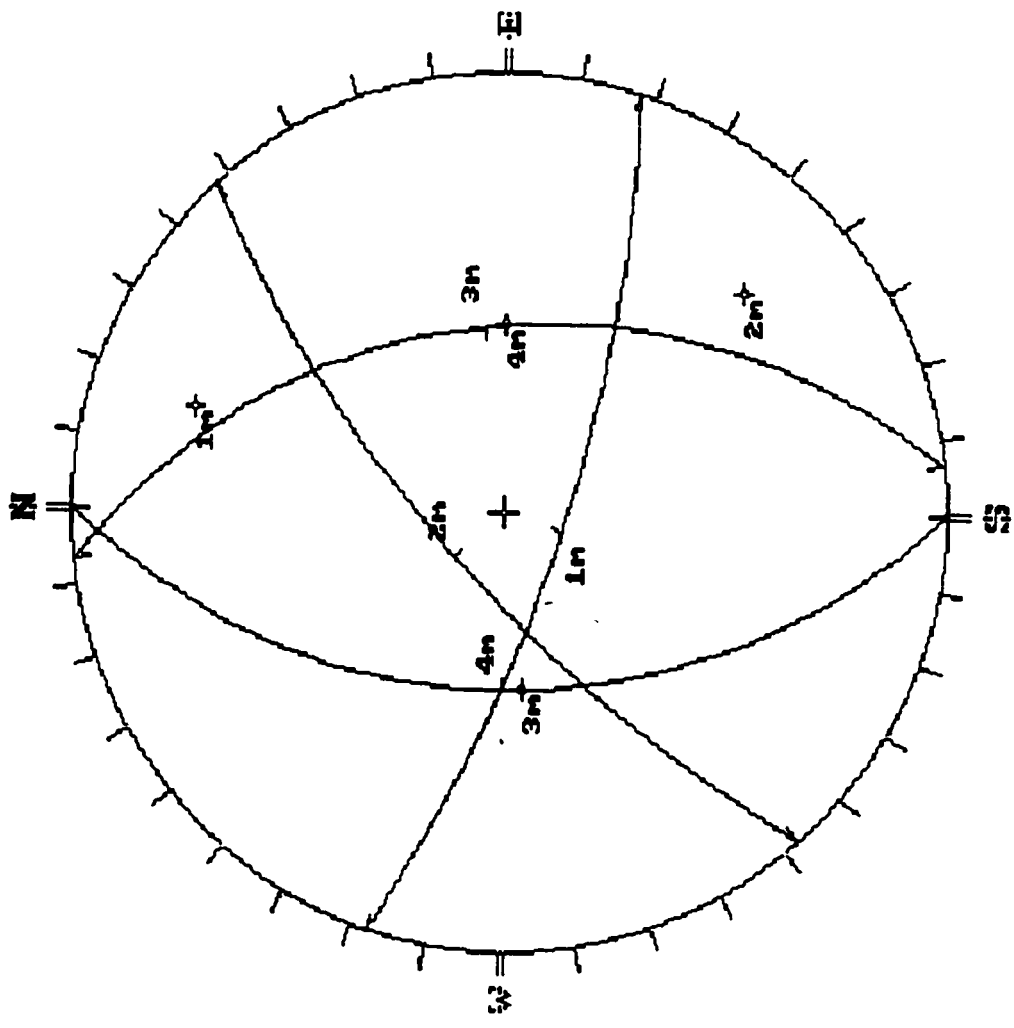
Figure A1: Major planes for the Nose area
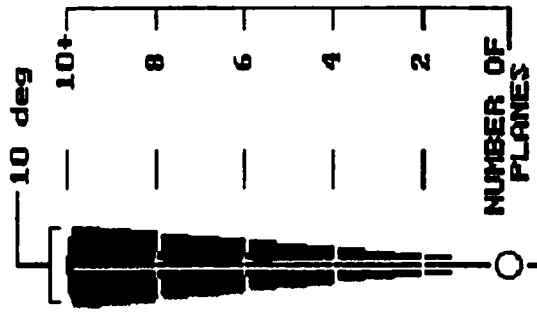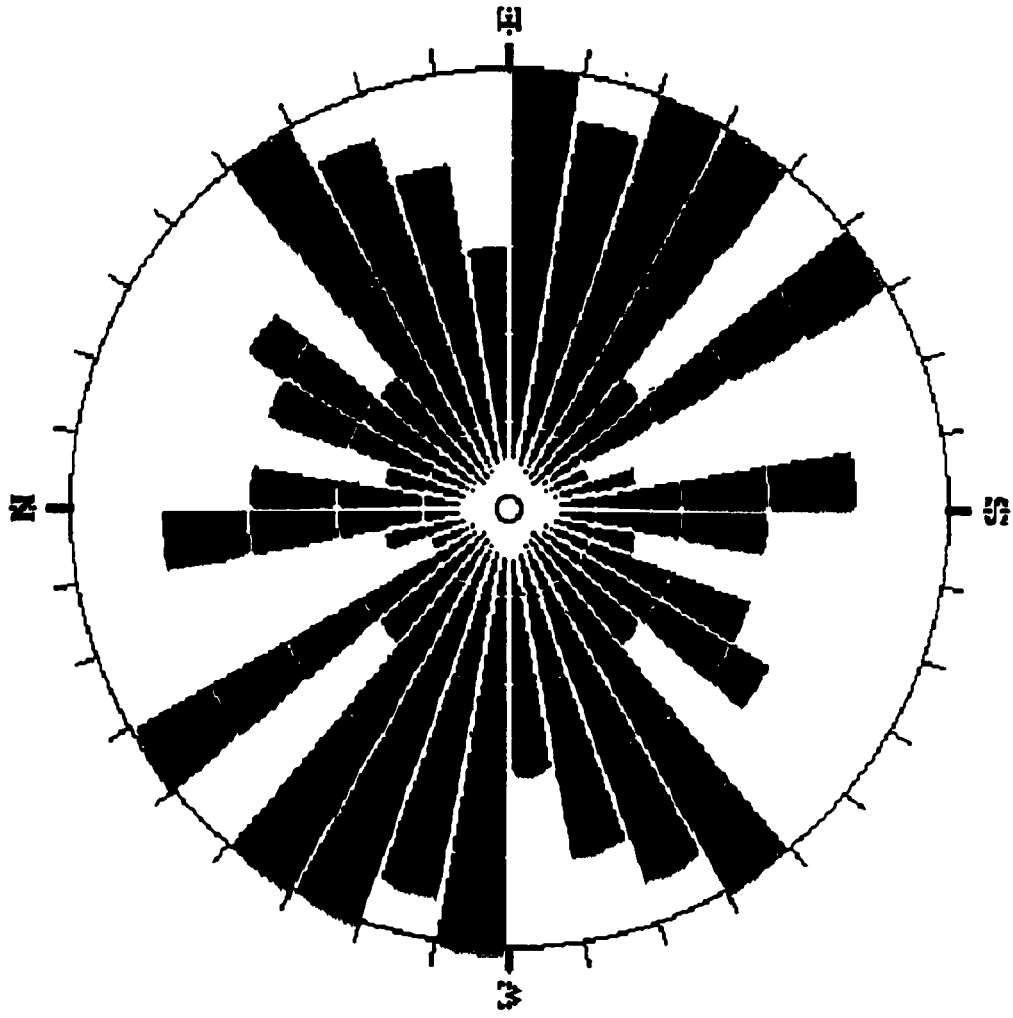
Figure A2: Rosette for the Nose area

Table A.3: DIPS input datafile for the South Limb

```
SELEBI NORTH MINE - SOUTH LIMB FROM 295 ML TO 349 ML
ENGINEER: S. M. Nareetsile                DATE: June 1997
1 traverse
1;LINEAR;120;30;Level 295, Stope 600, sublevel 295;
DIP/DIPDIRECTION
0 degrees
QUANTITY
[There are] 7 [extra data columns]
```

no;	dip;	dipn;	qua;	traves	space;	type;	surfce;	infill;	jr;	jn;	ja;
1	100	5	1	1	2.2	joint	3	0	1.5	15	4
2	50	70	1	1	0.7	shear	3	0	1.5	15	1
3	45	20	1	1	0.9	shear	3	0	1.5	15	4
4	50	120	1	1	1.4	joint	1	0	1.5	15	4
5	75	215	1	1	2.7	joint	1	0	1.5	15	4
6	50	50	1	1	1.3	shear	3	0	1.5	15	4
7	63	25	1	1	0.7	joint	1	0	1.5	15	4
8	87	350	1	1	7.3	joint	3	0	1.5	15	4
9	65	30	1	1	0.7	joint	1	0	1.5	15	4
10	55	185	1	1	1.7	joint	2	0	1.5	15	4
11	55	196	1	1	2.7	joint	2	0	1.5	15	4
12	60	0	1	1	6.2	joint	1	0	1.5	15	4
13	55	15	1	1	1.3	shear	1	0	1.5	15	4
14	70	330	1	1	5.4	shear	5	0	1.5	15	4
15	60	350	1	1	2.3	joint	3	0	1.5	15	4
16	40	60	1	1	0.6	joint	2	0	1.5	15	4
17	60	330	1	1	7.8	shear	3	0	1.5	15	4
18	60	190	1	1	1.8	shear	3	0	1.5	15	4
19	55	20	1	1	3.7	shear	3	0	1.5	15	4
20	50	35	1	1	1.1	joint	1	0	1.5	15	4
21	50	320	1	1	0.7	joint	1	0	1.5	15	4
22	58	335	6	1	1.1	joint	1	0	1.5	15	4
23	85	330	1	1.	3.6	shear	1	0	1.5	15	4
24	60	60	5	1	0.1	joint	1	0	1.5	15	4
25	85	150	1	1	0.1	joint	1	2	1.5	15	4
26	50	220	1	1	5	joint	1	0	1.5	15	4
27	55	185	1	1	2.8	joint	2	0	1.5	15	4
28	55	55	1	1	2.2	joint	2	0	1.5	15	4
29	70	130	1	1	1.2	joint	1	2	1.5	15	4
30	90	150	1	1	1.2	joint	1	2	1.5	15	4
31	60	212	1	1	6.1	joint	1	2	1.5	15	4
32	50	92	1	1	2.2	joint	1	2	1.5	15	4
33	50	250	1	1	4.1	joint	1	2	1.5	15	4
34	65	0	1	1	1.9	shear	2	0	1.5	15	4
35	70	0	1	1	0.2	shear	2	0	1.5	15	4
36	65	125	1	1	0.6	shear	2	0	1.5	15	4
37	20	250	1	1	1.3	joint	2	1	1.5	15	4

38	85	330	1	1	1.1	joint	2	0	1.5	15	4
39	40	270	1	1	1.7	joint	2	2	1.5	15	4
40	55	193	1	1	1.1	joint	2	0	1.5	15	4
41	45	290	1	1	1.2	joint	2	0	1.5	15	4
42	70	20	1	1	1.4	joint	3	0	1.5	15	4
43	45	40	1	1	1.8	joint	3	0	1.5	15	4
44	70	210	1	1	7.3	joint	4	0	1.5	15	4
45	60	220	1	1	1	joint	4	0	1.5	15	4
46	35	223	1	1	1.4	joint	4	0	1.5	15	4
47	70	335	1	1	1.3	joint	3	0	1.5	15	4
48	30	45	1	1	0.4	joint	3	0	1.5	15	4
49	85	320	1	1	2.4	joint	3	0	1.5	15	4
50	75	132	1	1	0.4	joint	3	2	1.5	15	4
51	80	250	1	1	1.3	joint	3	2	1.5	15	4
52	55	80	1	1	1.2	joint	4	0	1.5	15	4
53	40	65	1	1	4.9	joint	4	0	1.5	15	4
54	85	50	1	1	4.1	joint	3	2	1.5	15	4
55	65	50	1	1	0.8	shear	2	0	1.5	15	4
56	55	35	1	1	0.8	shear	2	0	1.5	15	4
57	70	195	1	1	1.8	joint	2	0	1.5	15	4
58	70	190	1	1	1.8	joint	3	1	1.5	15	4
59	70	150	1	1		joint	3	2	1	15	4
60	55	200	1	1	0.4	joint	3	0	1	15	4
61	45	195	1	1	0.3	joint	3	0	1	15	4
62	45	40	1	1	2.4	joint	1	0	1	15	4
63	40	226	1	1	7.7	joint	1	0	1	15	4
64	45	240	1	1	1	shear	1	0	1	15	4
65	65	320	1	1	1.9	joint	1	0	1	15	4
66	60	335	1	1	0.6	shear	3	2	1	15	4
67	50	40	3	1	3	joint	1	0	1	15	4
68	65	25	1	1	1	shear	1	0	1	15	4
69	50	25	1	1	1.3	shear	1	0	1	15	4
70	15	333	1	1	7.1	shear	2	0	1	15	4
71	70	215	1	1	2	shear	2	0	1	15	4
72	30	15	1	1	3.4	shear	0	2	1	15	4
73	40	15	1	1	9	joint	3	0	1	15	4
74	40	5	1	1	2.6	joint	3	0	1	15	4
75	20	95	1	1	2	joint	3	0	1	15	4
76	30	355	1	1	1	joint	3	0	1	15	4
77	30	0	1	1	1	joint	1	0	1	15	4
78	45	265	1	1	7.2	joint	4	2	1	15	4
79	50	80	1	1	3.9	joint	3	4	1	15	4
80	70	50	1	1	6.5	joint	3	2	1	15	4
81	30	40	1	1	1.8	joint	1	0	1	15	4
82	75	20	1	1	2	shear	1	0	1	15	4
83	45	20	1	1	4.6	shear	1	0	1	15	4
84	50	15	1	1	2.9	shear	1	0	1	15	4
85	45	170	1	1	1.9	shear	1	0	1	15	4

86	65	185	1	1	5	shear	1	1	1	15	4
87	40	260	1	1	4.1	joint	1	0	1	15	4
88	55	185	1	1	2	joint	1	0	1	15	4
89	50	140	1	1	1.6	joint	1	0	1	15	4
90	40	40	1	1	1	joint	1	0	1.5	15	4
91	85	70	1	1	0.5	joint	1	2	1.5	15	4
92	90	75	1	1	0.2	shear	1	2	1.5	15	4
93	40	30	1	1	4.6	joint	1	0	1.5	15	4
94	50	0	1	1	2.4	shear	·1	0	1.5	15	4
95	20	50	1	1	8.1	joint	1	0	1.5	15	4
96	80	350	1	1	6.3	joint	2	1	1.5	15	4
97	50	5	1	1	5.5	joint	3	1	1.5	15	4
98	50	35	1	1	5.3	joint	3	1	1.5	15	4
99	60	205	1	1	1	joint	3	0	1	15	4
100	75	193	1	1	1.2	joint	3	0	1	15	4
101	65	25	1	1	0.4	shear	3	0	1	15	4
102	70	190	1	1	1.2	shear	3	0	1	15	4
103	50	20	1	1	1.5	shear	3	0	1	15	4
104	50	0	1	1	7	shear	3	0	1	15	4
105	80	350	1	1	2.6	shear	3	0	1	15	4
106	60	20	1	1		shear	3	0	1	15	4
107	85	345	1	1	5.6	shear	3	0	1	15	4
108	65	180	1	1	4	joint	3	0	1	15	4
109	80	350	1	1	5.8	joint	3	0	1	15	4
110	45	35	1	1	1.3	joint	3	0	1	15	4
111	65	355	1	1	5	shear	3	0	1	15	4
112	60	10	1	1	1	joint	3	0	1	15	4
113	45	20	1	1	3.6	joint	3	0	2	15	2
114	65	10	1	1		joint	3	0	2	15	2
115	55	30	1	1	3.1	joint	3	2	2	15	2
116	50	345	1	1	2.1	joint	3	2	2	15	2
117	50	5	1	1	3.2	joint	3	2	2	15	2
118	50	225	1	1	1	joint	3	0	2	15	2
119	70	50	1	1	9.8	joint	3	0	2	15	2
120	55	335	1	1	0.4	joint	3	0	1.5	15	4
121	70	70	1	1	4	joint	3	0	1.5	15	4
122	55	60	1	1	3.4	joint	3	0	1.5	15	4
123	55	275	1	1	2.8	joint	3	0	1.5	15	4
124	80	195	1	1	2.7	joint	3	0	1.5	15	4
125	55	235	1	1	3.8	joint	3	0	1.5	15	4
126	40	205	1	1	5.1	joint	3	0	1.5	15	4
127	50	235	1	1	5.6	joint	3	0	1.5	15	4
128	50	120	1	1	0.8	joint	3	1	1.5	15	4
129	50	145	1	1	2.4	joint	3	0	1.5	15	4
130	55	135	1	1	2	joint	3	0	1.5	15	4
131	80	165	1	1	0.6	joint	3	0	1.5	15	4
132	35	10	1	1	1	joint	3	0	1.5	15	4
133	60	320	1	1	8	joint	3	0	1.5	15	4

134	78	15	1	1	0.6	joint	3	0	1.5	15	4
135	50	211	1	1	3.6	joint	3	0	1.5	15	4
136	55	30	1	1	4.1	joint	3	0	1.5	15	4
137	60	210	1	1	3.6	joint	3	0	1.5	15	4
138	35	35	1	1	2.6	joint	3	0	1.5	15	4
139	65	120	1	1	5.3	shear	3	0	1.5	15	4
140	20	343	1	1	0.6	joint	3	0	1.5	15	4
141	42	220	1	1	0.8	shear	0	4	1.5	15	6
142	85	215	1	1	2.5	joint	0	2	1.5	15	6
143	30	165	1	1	3.2	shear	1	2	1.5	15	6
144	55	175	1	1	5	joint	1	0	1.5	15	6
145	55	185	1	1	5	joint	0	0	1.5	15	6
146	40	168	1	1	2.2	joint	0	0	1.5	15	11
147	65	155	1	1	1	joint	0	2	1.5	15	11
148	70	168	1	1	2.7	joint	1	2	1.5	15	11
149	49	168	1	1	4.5	joint	3	2	1.5	15	11
150	20	200	1	1	2.9	joint	1	2	1.5	15	11
151	85	190	1	1	5.2	joint	3	0	1.5	15	4
152	55	230	1	1	7.4	joint	2	0	2	15	4
153	42	240	1	1	2	joint	2	0	2	15	4
154	57	250	1	1	7	joint	3	0	2	15	4
155	65	340	1	1	1.5	joint	3	0	2	15	4
156	75	315	1	1	3.6	joint	3	0	2	15	4
157	70	310	1	1	1.3	joint	3	0	2	15	4
158	63	255	1	1	2.5	joint	2	0	2	15	4
159	55	245	1	1	0.2	joint	2	0	1.5	15	4
160	65	233	1	1	1.2	joint	2	0	1.5	15	4
161	75	325	1	1	2	joint	0	2	1.5	15	4
162	45	20	1	1	4.7	joint	0	2	3	15	6
163	55	240	1	1	1.1	joint	2	2	3	15	6
164	60	100	1	1	0.7	shear	0	0	3	15	6
165	55	100	1	1	5.9	joint	0	0	3	15	6
166	55	183	1	1	6.2	shear	0	0	3	15	6
167	55	180	1	1	3.7	shear	0	0	3	15	6
168	65	210	1	1	4	shear	0	0	3	15	6
169	65	207	1	1	0.3	joint	0	0	3	15	6
170	70	290	1	1	2.6	joint	0	0	3	9	4
171	75	295	1	1	2.2	shear	0	0	3	9	4
172	73	300	1	1	1.5	joint	0	0	3	9	4
173	35	245	1	1	2.3	joint	0	0	3	9	4
174	60	20	1	1	2	joint	0	0	3	9	4
175	62	25	1	1	0.8	joint	0	0	3	9	4
176	70	180	1	1	0.4	joint	0	0	3	9	4
177	65	20	1	1	2	joint	0	0	3	9	4
178	55	180	1	1	1	joint	3	0	2	15	4
179	50	170	1	1	0.7	shear	2	0	2	15	4
180	60	180	1	1	1.4	joint	2	0	2	15	4
181	65	175	1	1	5.4	shear	2	0	2	15	4

182	55	193	1	1	1.5	shear	2	0	2	15	4
183	80	110	1	1	2.3	joint	2	0	2	15	4
184	40	80	1	1	4.6	joint	0	0	2	15	4
185	40	100	1	1	8.4	joint	0	0	2	15	4
186	45	95	1	1	3.9	joint	0	0	2	15	4
187	80	125	1	1	0.1	joint	0	0	2	15	4
188	85	25	1	1	1	joint	0	0	2	15	4
189	78	240	1	1	1.5	shear	0	0	2	15	4
190	90	140	1	1	7.8	shear	3	4	2	15	4
191	80	145	1	1	5.3	joint	3	4	2	15	4
192	85	160	1	1	7	joint	3	4	2	15	4
193	75	160	1	1	2.8	joint	3	4	2	15	4
194	74	151	1	1	2.5	joint	3	4	3	3	0.8
195	60	35	1	1	0.2	joint	2	0	3	3	0.8
196	65	40	1	1	0.8	joint	2	0	3	3	0.8
197	50	60	1	1	1.1	joint	2	0	3	3	0.8
198	55	75	1	1	1	joint	2	0	3	3	0.8

-1
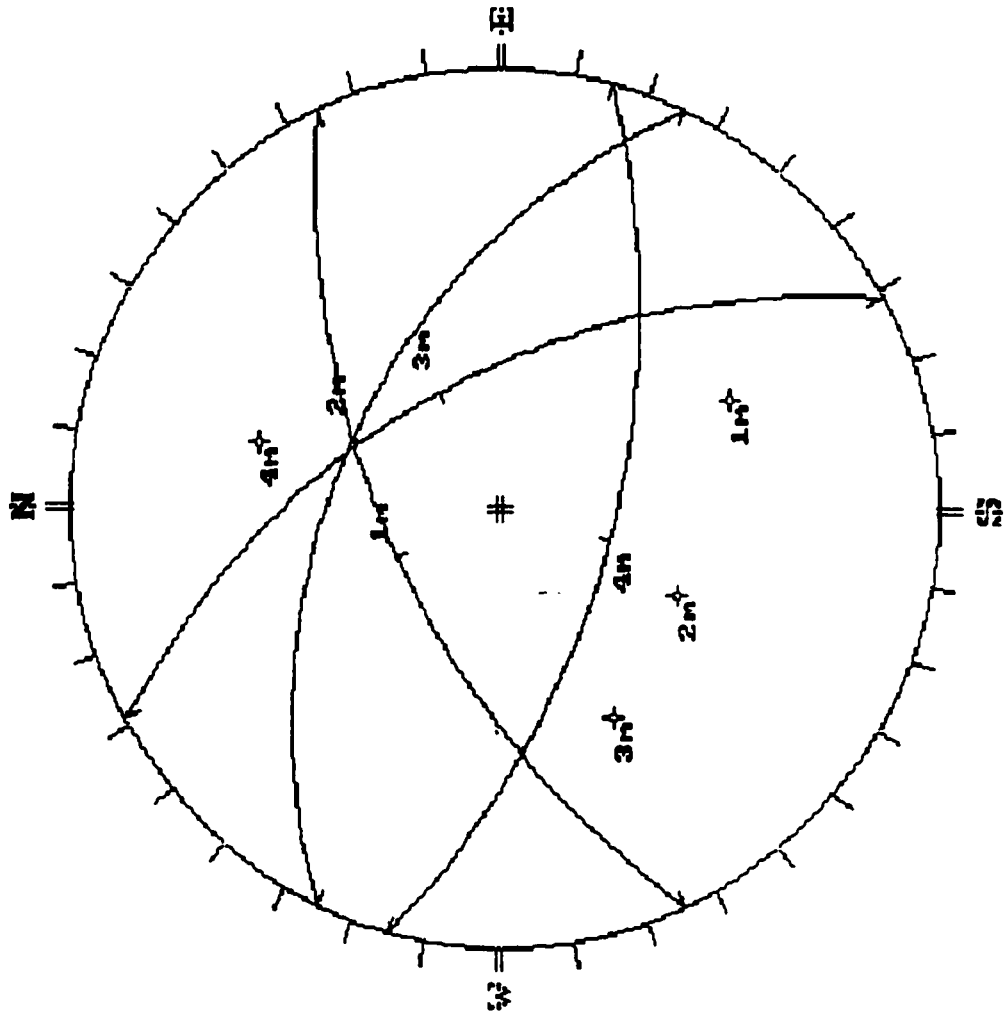
Figure A3: Major planes for the South limb

ORIENTATIONS
DIP/DIR.

1 H 61/335
2 H 49/025
3 H 57/061
4 H 61/195

EQUAL ANGLE
LWR. HEMISPHERE

10 deg

25+
20
15
10
5

NUMBER OF
PLANES
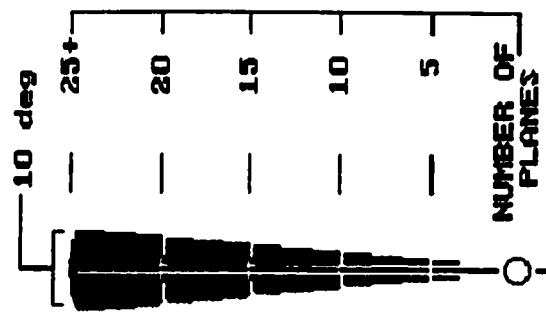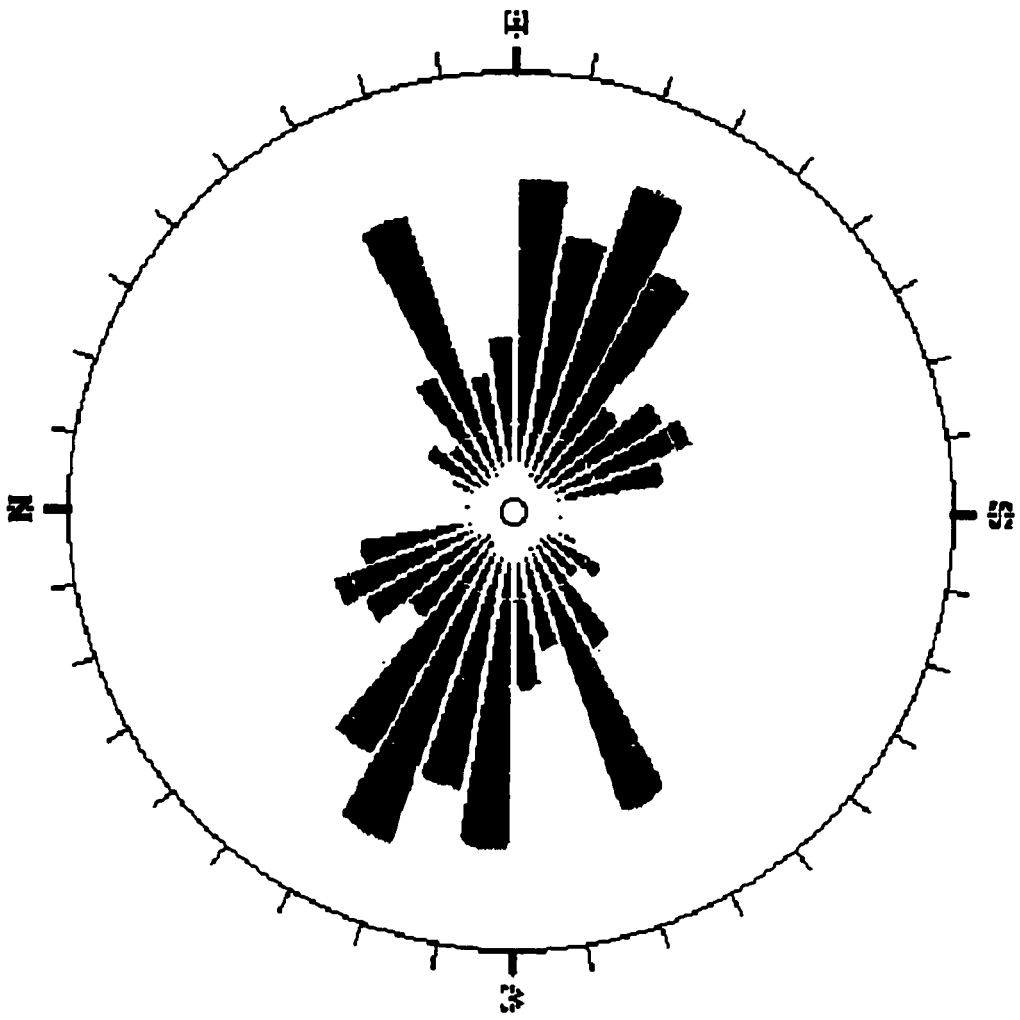
APPARENT
STRIKE
or
Trace of plane
made on face at
000,90

TREND, PLUNGE
OF FACE NORMAL
(pole) directed
away from viewer

177 PLANES
within 45 & 90
degrees of
viewing face

Figure A4: Rosette for the South limb

223

Table A.4: DIPS input datafile for the Detached Limb

```
SELEBI NORTH MINE - DETACHED LIMB FROM 258 TO 289 ML
ENGINEER: S. M. Nareetsile                    DATE: June 1997
1 traverse
1;LINEAR;120;30;Level 258, Stope 1100 - 1400,sublevel 258;
DIP/DIPDIRECTION
0 degrees
QUANTITY
[There are] 7 [extra data columns]
no; dip; dipn; qua; traves; space type; surfce infill; jr; jn; ja;
```

no	dip	dipn	qua	traves	space	type	surfce	infill	jr	jn	ja
1	82	230	1	1	0.6	joint	3	2	3	6	1
2	85	225	1	1	2.6	joint	3	2	3	6	1
3	80	205	1	1	0.6	joint	3	2	3	6	1
4	80	246	1	1	0.5	joint	3	2	3	6	1
5	83	250	1	1	0.9	joint	3	2	3	6	1
6	70	250	1	1	1.7	joint	3	2	3	6	1
7	75	173	1	1	3.9	joint	3	2	3	6	1
8	30	240	1	1	2	joint	3	2	3	6	1
9	25	200	1	1	0.7	joint	3	2	3	6	1
10	45	55	1	1	2.1	joint	3	2	3	6	1
11	30	290	1	1	7	joint	3	2	3	6	1
12	80	210	1	1	2.3	joint	3	2	3	6	1
13	0	155	1	1	2.4	joint	3	2	3	6	1
14	60	235	1	1	3.4	joint	3	2	3	6	1
15	55	230	1	1	1.5	joint	3	2	3	6	1
16	90	10	1	1	3.6	joint	3	2	3	6	1
17	50	227	1	1	3.6	joint	3	2	3	6	1
18	55	55	1	1	2.4	joint	3	2	3	6	1
19	60	250	1	1	1.6	joint	3	2	3	6	1
20	80	160	1	1	6.7	shear	1	2	3	6	1
21	70	230	1	1	4	joint	1	2	3	6	1
22	50	230	1	1	6.6	joint	1	2	3	6	1
23	50	175	1	1	1.9	shear	1	0	3	6	1
24	60	295	1	1	0.1	joint	1	0	3	6	1
25	85	215	1	1	0.1	joint	1	2	3	6	1
26	45	285	1	1	8.8	joint	0	2	1	6	2
27	20	230	1	1	6.5	joint	1	2	1	6	2
28	55	300	1	1	0.3	joint	1	2	1	6	2
29	65	120	1	1	1.7	joint	1	0	1	6	2
30	45	300	1	1	2.1	joint	1	2	1	6	2
31	60	275	1	1	1.1	joint	1	2	1	6	2
32	60	305	1	1	1.3	joint	1	2	1	6	2
33	50	250	1	1	1.6	joint	1	2	1	6	2
34	30	240	1	1	0.5	joint	1	2	1	6	2
35	20	290	1	1	8.4	joint	1	2	1	6	2
36	65	130	1	1	4.5	joint	2	0	1	6	2
37	20	290	1	1	0.5	joint	1	2	1	6	2

38	50	240	1	1	1.6	joint	1	2	1	6	2
39	15	280	1	1	1.3	joint	1	2	1	6	2
40	65	310	1	1	0.8	joint	1	2	1	6	2
41	75	130	1	1	5.2	shear	1	0	1	6	2
42	60	290	1	1	3.2	joint	1	2	1	6	2
43	25	300	1	1	5.5	joint	1	2	1	6	2
44	75	310	1	1	5.5	joint	1	2	1	6	2
47	55	30	1	1	4.3	joint	3	0	1	12	4
48	50	50	1	1	0.5	joint	3	0	1	12	4
49	75	183	1	1	5.3	shear	3	0	1	12	4
50	87	70	1	1	1.4	joint	4	0	1	12	4
51	75	230	1	1	3.7	joint	3	2	1	12	4
52	10	145	1	1	1.5	joint	3	2	1	12	4
53	85	320	1	1	5.8	shear	1	0	1	12	4
54	87	75	1	1	0.1	joint	1	2	1	12	4
55	80	210	1	1	2.1	joint	1	2	1	12	4
56	90	195	1	1	5.6	shear	1	0	1	12	4
57	85	225	1	1	0.2	joint	1	2	1	12	4
58	65	245	1	1	0.1	joint	1	2	1	12	4
59	85	155	1	1	3.5	joint	1	2	1	12	4
60	80	145	1	1	4.2	joint	1	0	1	12	4
61	50	80	1	1	5.5	shear	1	0	1	12	4
62	45	65	1	1	0.2	joint	0	0	1	12	4
63	70	160	1	1	2.9	joint	0	0	1	12	4
64	55	135	1	1	1.5	shear	0	0	1	12	4
65	30	210	1	1	1	shear	0	0	1	12	4
66	80	0	1	1	2.1	joint	1	0	1	12	4
67	75	340	1	1	6.3	joint	1	0	1	12	4
68	70	190	1	1	3.7	joint	4	2	1	12	4
69	60	185	1	1	3.1	joint	4	2	1	12	4
70	55	100	1	1	8.5	joint	4	0	1	12	4
71	80	195	1	1	1.3	joint	4	0	1	12	4
72	85	10	1	1	8.6	joint	3	0	1	12	4
73	30	100	1	1	3	joint	1	0	1	12	1
74	20	200	1	1	2.3	joint	1	2	1	12	1
75	90	160	1	1	1.4	joint	1	0	1	12	1
76	25	195	1	1	3.2	joint	1	2	1	12	1
77	65	175	1	1	0.1	joint	1	2	1	12	1
78	90	305	1	1	6	joint	3	0	1	12	1
79	50	194	1	1	0.4	joint	0	2	1	12	1
80	85	345	1	1	2.6	joint	1	2	1	12	1
81	50	192	1	1	9	joint	1	2	1	12	1
82	65	170	1	1	9	joint	0	2	1	12	1
83	80	350	1	1	2	joint	2	0	1	6	4
84	85	150	1	1	4.6	joint	2	0	1	6	4
85	80	155	1	1	1.1	joint	1	0	1	6	4
86	60	247	1	1	1	joint	3	2	1	6	4
87	80	245	1	1	1.4	joint	3	2	1	6	4

88	75	230	1	1	0.5	joint	3	2	1	6	4
89	80	180	1	1	0.4	joint	3	2	1	6	4
90	80	107	1	1	0.7	joint	3	2	1	6	4
91	10	180	1	1	0.9	joint	1	2	1	6	4
92	5	195	1	1	1.4	joint	1	2	1	6	4
93	65	320	1	1	0.7	shear	1	0	1	6	4
94	75	260	1	1	0.2	joint	1	2	1	6	4
95	75	250	1	1	1.6	joint	1	2	1	6	4
96	80	250	1	1	1.8	joint	1	2	1	6	4
97	85	160	1	1	0.9	shear	1	0	1	6	4
98	50	215	1	1	0.1	joint	1	2	1	6	4
99	75	350	1	1	2.3	joint	2	0	1	6	4
100	65	221	1	1	4	joint	2	2	1	6	4
101	55	200	1	1	3.1	joint	2	2	1	6	4
102	65	150	1	1	2.2	joint	1	0	1	6	4
103	90	175	1	1	6.1	joint	1	2	1	6	4
104	87	60	1	1	0.3	joint	1	2	1	6	4
105	75	240	1	1	5.4	joint	1	2	1	6	4
106	75	225	1	1	0.9	joint	1	2	1	6	4
107	80	150	1	1	0.3	joint	1	0	1	6	4
108	78	145	1	1	0.1	joint	1	0	1	6	4
109	87	145	1	1	0.6	joint	1	0	1	6	4
110	85	150	1	1	1.3	joint	1	0	1	6	4
111	87	220	1	1	2.1	joint	1	0	1	6	4
112	82	150	1	1	2.8	joint	1	1	1	6	4
113	70	350	1	1	2.2	joint	1	0	1	6	4
114	25	55	1	1	7.2	joint	1	2	1	6	4
115	50	5	1	1	0.7	joint	1	2	1	6	4
116	90	157	1	1	0.1	joint	0	2	1	6	4
117	80	161	1	1	4.4	joint	0	2	1	6	4
118	87	340	1	1	1.2	joint	0	0	1	6	4
119	65	170	1	1	0.4	joint	0	0	1	6	4
120	55	235	1	1	1	shear	3	2	1	6	4
121	85	137	1	1	3.4	joint	3	2	1	6	4
122	80	340	1	1	0.8	joint	0	0	1	6	4
123	85	134	1	1	2.3	joint	3	0	1	6	4
124	50	215	1	1	1.8	shear	3	0	1	6	4
125	77	165	1	1	1.1	joint	3	0	1	6	4
126	70	164	1	1	2.4	joint	0	0	1	6	4
127	90	155	1	1	0.9	joint	3	0	1	6	4
128	40	50	1	1	1.7	shear	1	0	1	6	4
129	50	230	1	1	0.1	joint	1	0	1	6	4
130	30	195	1	1	4.5	joint	1	0	1	6	4
131	60	310	1	1	2.9	joint	1	0	1	6	4
132	55	320	1	1	8.8	joint	1	2	1	6	4
133	70	170	1	1	2.4	shear	1	0	1	6	4
134	75	220	1	1	0.5	joint	1	2	1	15	4
135	85	205	1	1	4.7	joint	1	2	1	15	4

136	55	130	1	1	0.3	joint	3	0	1	15	4
137	50	230	1	1	2.8	joint	1	0	1	15	4
138	70	135	1	1	2.4	joint	1	0	1	15	4
139	25	275	1	1	3.8	joint	3	2	1	15	4
140	60	145	1	1	3.1	shear	3	0	1	15	4
141	60	320	1	1	1.7	joint	3	0	1	15	4
142	70	135	1	1	1.9	joint	3	0	1	15	4
143	60	290	1	1	3.7	joint	0	0	1	15	4
144	85	160	1	1	0.5	joint	3	0	1	12	4
145	60	180	1	1	1.2	joint	2	0	1	12	4
146	70	165	1	1	2.9	shear	2	0	1	12	4
147	70	35	1	1	0.5	shear	3	0	1	12	4
148	80	295	1	1	1.7	shear	2	0	1	12	4
149	85	155	1	1	0.2	joint	2	0	1	12	4
150	75	240	1	1	0.4	joint	3	1	1	12	4
151	50	40	1	1	0.5	joint	1	0	1	12	4
152	55	220	1	1	1.7	joint	1	0	1	12	4
153	85	165	1	1	0.5	joint	1	0	1	12	4
154	90	165	1	1	1	shear	1	0	1	12	4
155	70	345	1	1	1.7	shear	0	0	1	12	4
156	70	160	1	1	3.1	joint	3	0	1	12	4
157	80	162	1	1	2.9	shear	3	0	1	12	4
158	65	210	1	1	0.9	joint	0	0	1	12	4
159	75	188	4	1	5.9	joint	0	0	1	12	4
160	60	10	1	1	0.2	joint	0	0	1	12	4
161	40	40	1	1	0.7	joint	0	0	1	12	4
162	15	70	1	1	0.5	joint	0	1	1	12	4
163	30	50	1	1	2.8	joint	0	1	1	12	4
164	55	230	1	1		joint	3	0	1	12	4
165	85	340	1	1	0.5	joint	2	0	1	12	4
166	45	25	1	1	0.7	joint	2	0	1	12	4
167	90	340	1	1	0.5	joint	1	0	1	12	4
168	85	340	1	1	0.4	shear	1	0	1	12	4
169	65	150	1	1	0.5	joint	1	0	1	12	4
170	70	127	1	1	1.9	joint	1	0	1	12	4
171	65	145	1	1	0.3	joint	1	1	1	12	4
172	70	160	1	1	0.2	joint	1	1	1	12	4
173	45	180	1	1	1.4	joint	1	1	1	12	4
174	75	85	1	1	1.9	joint	0	0	1	12	4
175	65	125	1	1	1.2	joint	0	0	1	12	4
176	70	120	1	1	2.5	joint	0	0	1	12	4
177	60	115	1	1	2	joint	0	0	1	12	4
178	85	144	1	1	5.4	joint	0	0	1	12	4
179	70	55	1	1	0.6	joint	0	0	1	12	4
180	80	69	1	1	1.2	joint	0	0	1	12	4
181	75	240	1	1	2.6	joint	3	1	2	12	4
182	80	150	1	1	0.2	joint	3	1	2	12	4
183	80	147	1	1	0.2	joint	3	1	2	12	4

184	75	155	1	1	0.2	joint	3	0	2	12	4
185	75	156	1	1	0.3	joint	3	0	2	12	4
186	75	149	1	1	0.4	joint	0	0	2	12	4
187	70	150	1	1	0.8	joint	0	0	2	12	4
188	80	135	1	1	0.2	joint	1	0	2	12	4
189	80	10	1	1	0.3	joint	3	0	2	12	4
190	55	160	1	1	0.7	joint	3	0	2	12	4
191	50	175	1	1	0.2	joint	3	0	2	12	4
192	85	190	1	1	5	joint	3	0	2	12	4
193	70	195	1	1	3.1	joint	0	0	2	12	4
194	90	175	1	1	0.8	joint	0	0	2	12	4
195	65	345	1	1	1.4	joint	0	0	2	12	4
196	60	160	1	1	4.7	joint	0	0	2	12	4
197	55	180	1	1	0.4	joint	0	0	2	12	4
198	55	190	1	1	1.4	joint	0	0	2	12	4
199	75	355	1	1	2.6	joint	0	0	2	12	4
200	55	220	1	1	2.7	joint	0	1	2	12	4
201	65	185	1	1	4.7	joint	0	1	2	12	4
202	15	220	1	1	3	joint	3	1	2	12	4
203	30	310	1	1	3	joint	0	0	2	12	4
204	30	195	1	1	3.4	joint	1	1	2	12	4
205	50	180	1	1	1.9	joint	1	1	2	12	4
206	60	200	1	1	2.1	joint	3	1	2	12	4
207	25	190	1	1	0.2	joint	3	1	2	12	4
208	65	170	1	1	1.2	joint	4	0	2	12	4
209	85	164	1	1	0.5	joint	3	1	2	12	4
210	70	170	1	1	3.7	joint	3	0	2	12	4
211	60	85	1	1	3	joint	3	2	2	12	4
212	35	145	1	1	5.6	joint	1	1	1	6	1
213	70	222	1	1	1	joint	1	1	1	6	1
214	35	200	1	1	2.6	joint	1	1	1	6	1
215	75	100	1	1	2.4	joint	1	1	1	6	1
216	80	135	1	1	6.6	joint	1	0	1	6	1
217	75	140	1	1	2.1	joint	1	1	1	6	1
218	90	150	1	1	1	joint	1	1	1	6	1
219	60	20	1	1	0.9	joint	1	0	1	6	1
220	50	30	1	1	1.8	joint	3	1	1	6	4
221	85	155	1	1	3	joint	3	1	1	6	4
222	85	167	1	1	3.8	joint	1	1	1	6	4
223	75	175	1	1	3.5	joint	1	1	1	6	4
224	85	166	1	1	1.9	joint	1	1	1	6	4
225	83	345	1	1	5.5	shear	1	0	1	6	4
226	90	240	1	1	4	joint	1	1	1	6	4
227	80	170	1	1	2.1	joint	1	1	1	6	4
228	87	160	1	1	1.2	joint	1	1	1	6	4
229	85	180	1	1	0.5	joint	1	0	1	6	4
230	70	237	1	1	2.7	joint	1	1	1	6	4
231	70	223	1	1	0.8	joint	1	1	1	6	4

232	80	247	1	1	0.7	joint	1	1	1	6	4
233	82	162	1	1	2.3	joint	1	1	1	6	4
234	80	160	1	1	3.3	joint	1	1	1	6	4
235	87	248	1	1	1.5	joint	1	1	1	6	4
236	75	255	1	1	0.9	joint	1	1	1	6	4
237	50	225	1	1	0.6	joint	1	1	1	6	4
238	60	222	1	1	0.3	joint	1	1	1	6	4
239	85	150	1	1	1.7	joint	1	1	1	6	4
240	80	155	1	1	1.7	joint	1	0	1	6	4
241	85	342	1	1	3	shear	1	0	1	6	4
242	60	45	1	1	2	joint	1	1	1	6	4
243	87	155	1	1	2	joint	1	1	1	6	4
244	85	165	1	1	1	joint	0	0	1	6	4
245	60	90	1	1	2.1	joint	1	1	1	6	4
246	85	260	1	1	2.2	joint	1	1	1	6	4
247	78	225	1	1	1.2	joint	1	1	1	6	4
248	50	230	1	1	1.6	joint	1	1	1	6	4
249	80	163	1	1	1.6	joint	1	1	1	6	4
250	75	180	1	1	1.3	joint	3	1	2	12	4
251	85	169	1	1	2.2	joint	1	0	2	12	4
252	80	160	1	1	0.9	joint	1	0	2	12	4
253	90	235	1	1	1.8	joint	1	1	2	12	4
254	30	145	1	1	4.8	joint	1	1	2	12	4
255	35	60	1	1	1	joint	3	1	2	12	4
256	85	55	1	1	0.7	joint	3	1	2	12	4
257	90	50	1	1	0.6	joint	3	1	2	12	4
258	90	55	1	1	0.3	joint	3	1	2	12	4
259	65	195	1	1	0.4	joint	1	1	2	12	4
260	85	100	1	1	1.1	joint	1	1	2	12	4
261	85	300	1	1	1.6	joint	1	1	2	12	4
262	75	345	1	1	2	joint	1	1	2	12	4
263	85	157	1	1	1.2	joint	3	0	2	12	4
264	90	165	1	1	0.7	shear	3	0	2	12	4
265	60	140	1	1	1.2	shear	3	0	2	12	4
266	60	125	1	1	4.2	shear	3	0	2	12	4
267	85	20	1	1	0.5	joint	3	0	1	15	4
268	65	150	1	1	3.5	shear	3	0	1	15	4
269	85	160	1	1	1.9	shear	3	0	1	15	4
270	30	90	1	1	0.4	joint	0	0	1	15	4
271	75	335	1	1	1.3	joint	0	0	1	15	4
272	15	130	1	1	1.6	joint	1	1	1	15	4
273	90	174	3	1	4.9	joint	1	1	1	15	4

-1
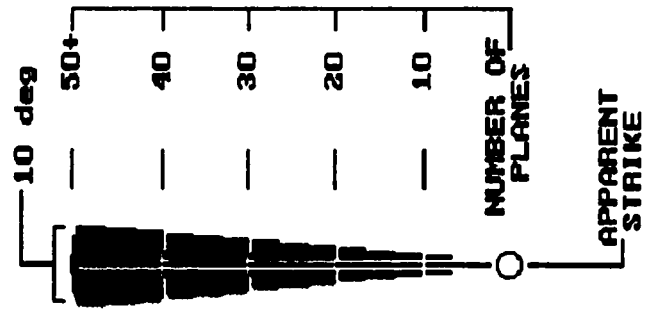
Figure A6: Rosette for the Detached limb

10 deg

50+
40
30
20
10

NUMBER OF PLANES

or

APPARENT STRIKE

Trace of plane made on face at 000,90

TREND, PLUNGE OF FACE NORMAL

(pole) directed away from viewer
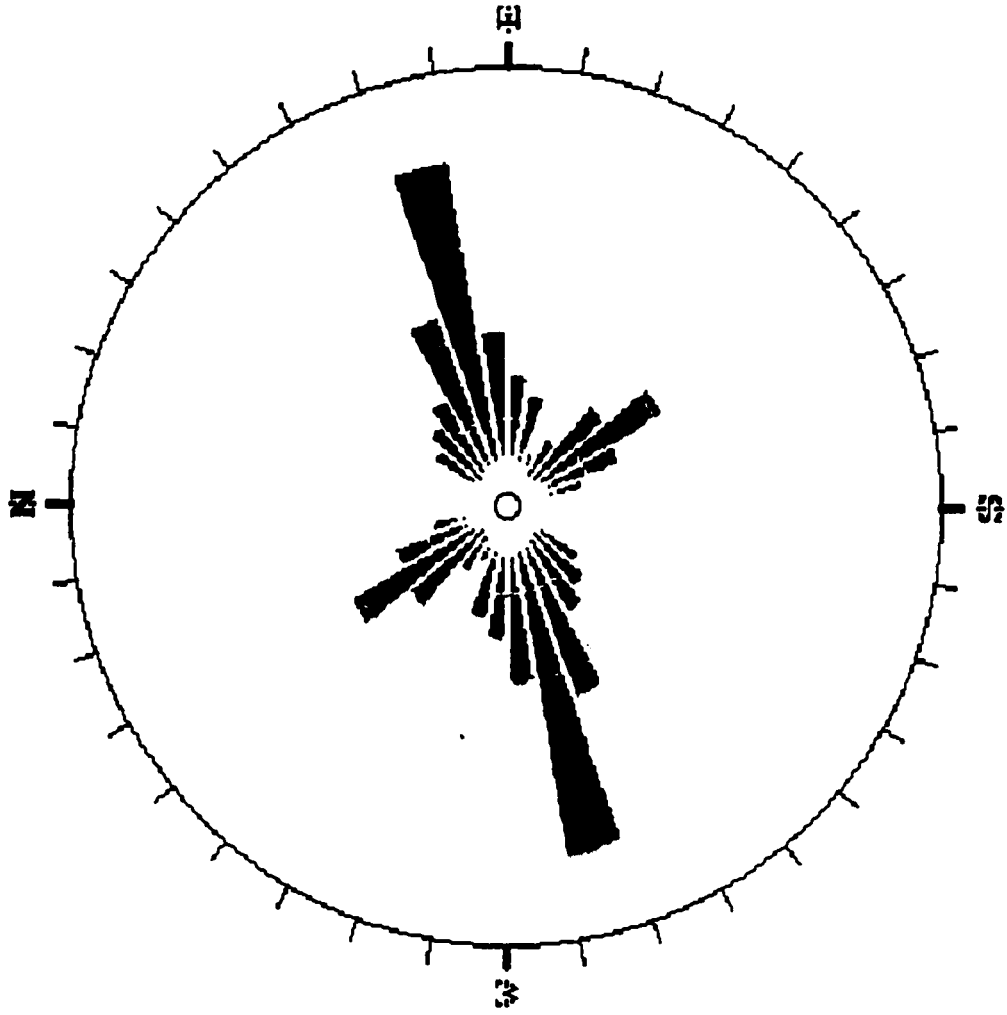
239 PLANES within 45 & 90 degrees of viewing face
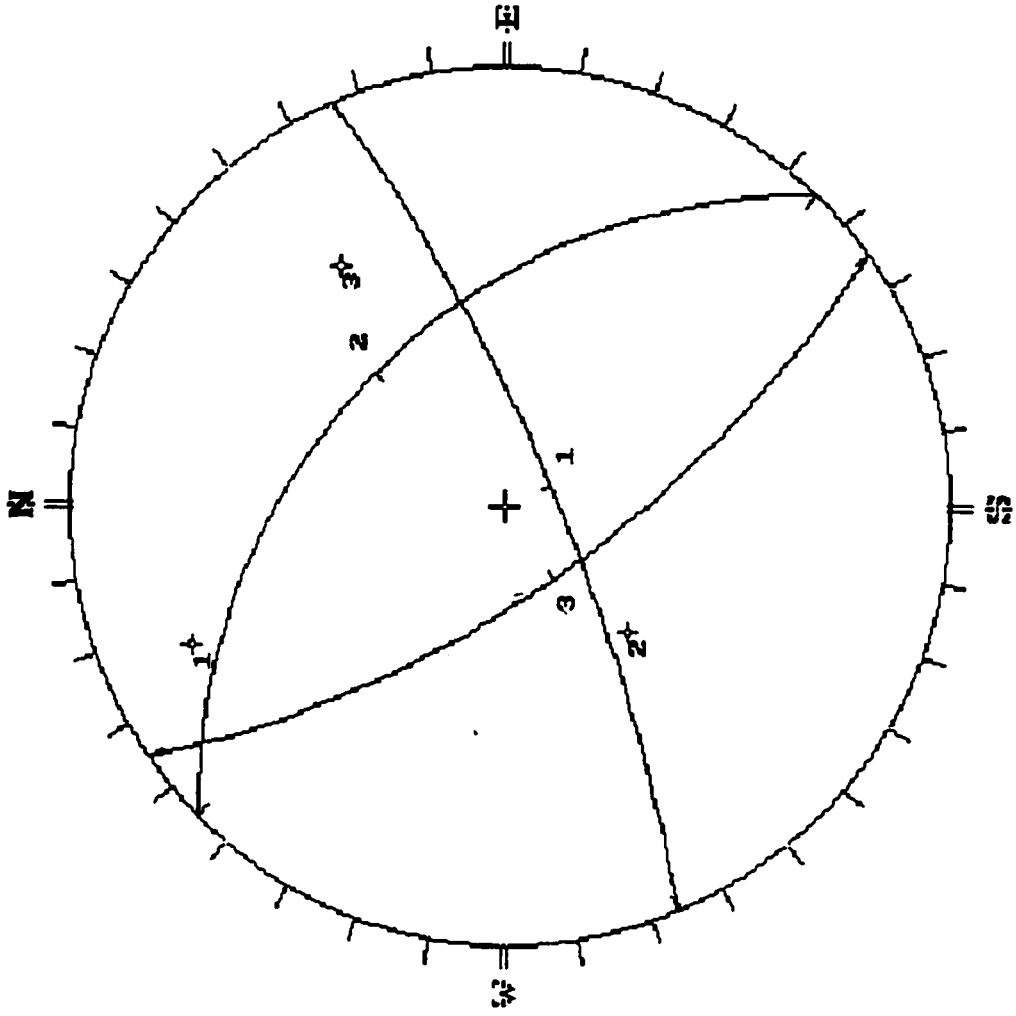
N

E

S

W

Figure A5: Major planes for the Detached limb

231

APPENDIX B

STRESS MEASUREMENTS

.

APPENDIX B

STRESS MEASUREMENTS

All deformation modulus and Poisson's ratio values calculated from the biaxial tests are given in Table B1 together with some relevant comments while Table B2 give the strain relief values used for the calculation of the stresses. The values used to determine the stresses are given in Table B3.2, B4.2 and B5.2. The stress strain curves from the biaxial tests are presented in Figure B1 to B8.

The principal stresses and directions are given in Table B3.3, B4.3 and B5.3 for each of the three boreholes tested. Values derived from the various statistical tests are presented in Tables B3.1, B4.1 and B5.1.

The stress strain curves produced by the biaxial tests are shown in Figures B1 to B8. The results of RM1 display an isotropic response though the results of RM2 are better. The first test at 13.0 m in borehole RM3 at Selebi Shaft shows a good isotropic response while the second test indicates a poor isotropic response. The last test, at 14 m, does not give reliable results at all with the possible exception of gauges 9-12. Modulus values used to calculate the stresses from the last test RM3 at 14 m, was taken as the average of all modulus values from RM3.

On the basis of the statistical tests reported in Table B3.1 and B4.1, the following two tests were considered dubious, test 2 at 14 m depth in borehole RM1 and also test 2 at 13 m depth in borehole RM2. The remaining test results in each of the boreholes are fairly in good agreement.

One test result, test 4 from RM3 has been discarded. The remaining two, however. are not in good agreement, and would only serve to give an indication of stresses. It must be noted that borehole RM3 is diagonally opposite a large gully, while the presence of the gully does not explain the scatter of results, the results are not necessarily a reflection of the virgin stresses.

Table B1: Deformation parameters calculated from the biaxial test

Test 810-RM1	Axial Gauge	Slope	Lateral Gauge	Slope	Extern. Dia. (mm)	Inter. Dia. (mm)	K correct.	Modulus	μ
13.5	1	30.398	2	145.992	73.00	38.10	2.749	83.56	0.21
	5	26.388	6	151.063				72.53	0.17
	9	32.754	10	169.231				90.03	0.19
14.0	1	25.931	2	121.900	73.00	37.80	2.733	70.86	0.21
	5	31.285	6	133.725				85.49	0.23
	9	34.809	10	141.488				95.12	0.25
14.5	1	28.649	2	168.930	73.00	37.90	2.738	78.44	0.17
	5	31.664	6	145.278				86.70	0.22
	9	33.561	10	119.219				91.89	0.28
750-RM2 12.5	1	33.758	2	179.983	72.20	38.00	2.766	93.38	0.19
	5	33.993	6	152.176				94.03	0.22
	9	37.038	10	191.613				102.46	0.19
13.5	1	32.056	2	139.433	72.70	37.90	2.746	88.04	0.23
	5	34.900	6	126.492				95.85	0.28
	9	35.418	10	189.530				97.27	0.19
14.0	1	31.660	2	137.257	72.60	37.80	2.744	86.87	0.23
	5	31.111	6	137.853				85.36	0.23
	9	35.523	10	140.264				97.47	0.25
Sel.-RM3 13.0	1	32.500	2	143.328	72.70	37.70	2.736	88.91	0.23
	5	34.728	6	145.149				95.00	0.24
	9	34.855	10	143.843				95.35	0.24
13.5	1	23.806	2	210.303	72.90	38.00	2.746	65.38	0.11
	5	28.982	6	173.596				79.59	0.17
	9	18.037	10	192.160				49.53	0.09
14.0	1		2		73.00	38.00	2.743		
	5	11.884	6					32.60	
	9	21.151	10	75.592				58.02	0.28

Note: 750-RM2-13.5 m - Hole water logged and RM3 12.5 m and 14 m core damaged during overcoring.

235

Table B2: Strain relief values used for stress calculation

Location	Borehole	Level(m)	Depth (m)	1	2	3	4	5	6	7	8	9	10	11	12	Note	Test No.
Selebi-Phikwe 3#	RM1	810	12.5													1	
		810	13													1	
		810	13.5	770	29	319	471	689	100	693	89	378	68	102	338		1
		810	14	1412	122	1038	634	651	124	310	440	662	120	417	335		2
		810	14.5	1102	119	773	383	431	77	137	373	555	44	312	303		3
Selebi-Phikwe 3#	RM2	750	12.5	390	162	12	571	340	159	397	101	200	167	157	25		1
		750	13													2	
		750	13.5	1075	785	711	1128	987	796	965	808	1011	371	150	824		2
		750	14	411	171	5	644	351	151	407	87	173	54	162	22		3
Selebi Shaft	RM3	650	12.5													3	
		650	13	186	47	57	-264	344	280	4	240	348	-403	-291	381		1
		650	13.5	1596	47	1152	501	-48	27	96	-121	645	55	223	591		2
		650	14	-15	-166	91	-1416	313	1149	384	1015	1168	116	855	765		3

Notes: 1. Core damaged during overcoring; 2. Hole water logged; 3. Core broke along a joint for gauges 1 - 4

236

TABLE B3: Results of borehole RM1, 810 ml, Selibe-Phikwe, 3#

Table B3.1: Statistical tests

Test No.	R1	R2	R3	RAV	D1	D2
1	0.2	0.16	0.14	0.17	1.56	3.33
2	2.58	0.5	0.6	1.56	0.96	5.49
3	1.26	0.01	0.27	0.74	1.19	2.52

(Standard Deviation of Residues = 52 91316)

Table B3.2: Calculated stress components in common coordinate system

Test No.	Elastic	Constants	Normal Stresses(MPa)			Shear Stresses(MPa)		
	E(Gpa)	μ	X	Y	Z	XY	YZ	ZX
1	72.53	0.19	12.48	26.7	21.2	-1.88	4.32	-6.7
*			0.94	0.58	0.58	0.47	0.33	0.46
2	70.86	0.23	26.59	44.44	25.07	6.1	-0.48	1.7
*			0.93	0.58	0.58	0.44	0.33	0.44
3	78.44	0.22	20.3	36.23	20.72	7.17	-1.85	2.14
			1.03	0.64	0.63	0.5	0.37	0.49

* Standard Deviation (MPa)

Table B3.3: Principal Stresses and directions in cpommon coordinate system

Test No.	SIGMA 1			SIGMA 2			SIGMA 3		
	Stress (MPa)	Bear. (Deg.)	Dip (Deg.)	Stress (MPa)	Bear. (Deg.)	Dip (Deg.)	Stress (MPa)	Bear. (Deg.)	Dip (Deg.)
1	30.56	153	51	-20.98	150	-39	8.84	241	-1
2	46.32	270	73	26.66	221	-12	23.11	133	13
3	39.03	99	-69	22.19	209	-8	16.03	122	19

Bearing: Clockwise from north considered positive
Dip   : Down from horizontal considered positive

237

TABLE B4: Results of borehole RM2, 750 ml, Selibe-Phikwe, 3#

Table B4.1: Statistical tests

Test No	R1	R2	R3	RAV	D1	D2
1	0.69	0.46	0.88	0.7	0.41	0.77
2	0.31	0.39	2.49	1.47	4.39	5.52
3	0.95	0.41	0.15	0.6	1.21	1.06

(Standard Deviation of Residues = 52 91316)

Table B4.2: Calculated stress components in common coordinate system

Test No.	Elastic	Constants	Normal Stresses(MPa)			Shear Stresses(MPa)		
	E(Gpa)	μ	X	Y	Z	XY	YZ	ZX
1	93.38	0.2	18.74	20.3	13.12	-10.17	2.44	-1.3
*			3.18	1.96	1.95	1.56	1.13	1.55
2	88.04	0.23	78.48	56.56	48.11	-4.03	4.62	-6.64
*			3.03	1.87	1.86	1.43	1.08	1.43
3	85.36	0.24	16.7	20.51	12.18	-9.93	2.7	-1.28
			2.95	1.82	1.82	1.38	1.05	1.37

* Standard Deviation (MPa)

Table B4.3: Principal Stresses and directions in cpommon coordinate system

Test No.	SIGMA 1			SIGMA 2			SIGMA 3		
	Stress (MPa)	Bear. (Deg.)	Dip (Deg.)	Stress (MPa)	Bear. (Deg.)	Dip (Deg.)	Stress (MPa)	Bear. (Deg.)	Dip (Deg.)
1	30.14	103	47	12.84	194	1	9.18	105	-49
2	80.87	103	12	56.86	222	67	45.41	189	-19
3	29.21	105	50	11.84	195	0	8.34	106	-40

Bearing: Clockwise from north considered positive
Dip   : Down from horizontal considered positive

238

TABLE B5: Results of borehole RM2, 750 ml, Selibe-Phikwe, 3#

Table B5.1: Statistical tests

Test No	R1	R2	R3	RAV	D1	D2
1	1.91	1.31	0.73	1.4	1.05	1.29
2	0.16	0.21	0.24	0.21	0.26	1.58
3	4.5	0.44	1.1	2.68	7.06	3.06

(Standard Deviation of Residues = 52 91316)

Table B5.2: Calculated stress components in common coordinate system

Test No.	Elastic	Constants	Normal Stresses(MPa)			Shear Stresses(MPa)		
	E(Gpa)	μ	X	Y	Z	XY	YZ	ZX
1	88.91	0.24	7.35	3.81	15.28	4.11	7.68	-0.73
*			4.43	3.55	4.43	2.39	2.39	3.18
2	49.53	0.22	6.47	29.49	14.46	-1.14	8.52	-2.02
*			2.45	1.96	2.45	1.34	1.34	1.79

* Standard Deviation (MPa)

Table B5.3: Principal Stresses and directions in cpommon coordinate system

Test No.	SIGMA 1			SIGMA 2			SIGMA 3		
	Stress (MPa)	Bear. (Deg.)	Dip (Deg.)	Stress (MPa)	Bear. (Deg.)	Dip (Deg.)	Stress (MPa)	Bear. (Deg.)	Dip (Deg.)
1	19.26	187	28	8.98	107	-18	-1.8	226	-56
2	33.47	171	65	11.01	162	-25	5.94	254	-3

Bearing: Clockwise from north considered positive
Dip : Down from horizontal considered positive

239

$$\mathcal{T}_{yx} = \mathcal{T}_{xy}$$
$$\mathcal{T}_{zy} = \mathcal{T}_{yz}$$
$$\mathcal{T}_{xz} = \mathcal{T}_{zx}$$
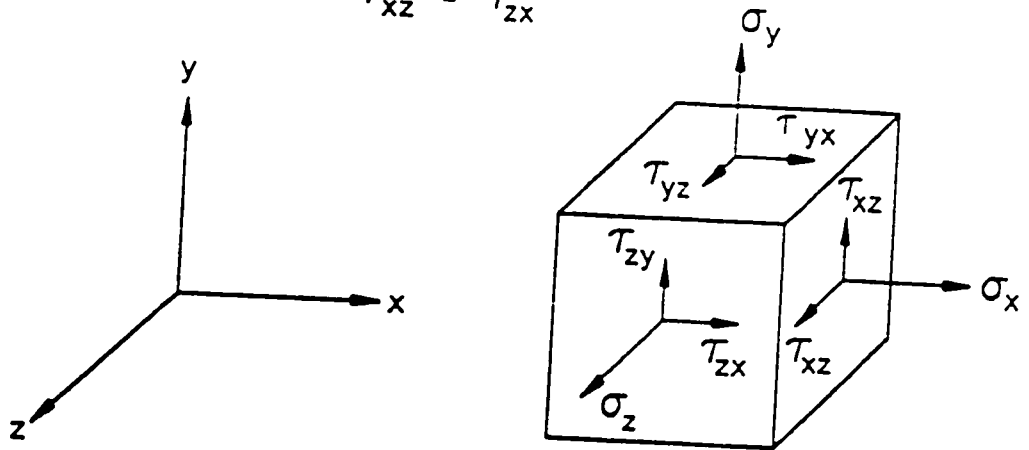
Figure B1: Orientation of Stresses
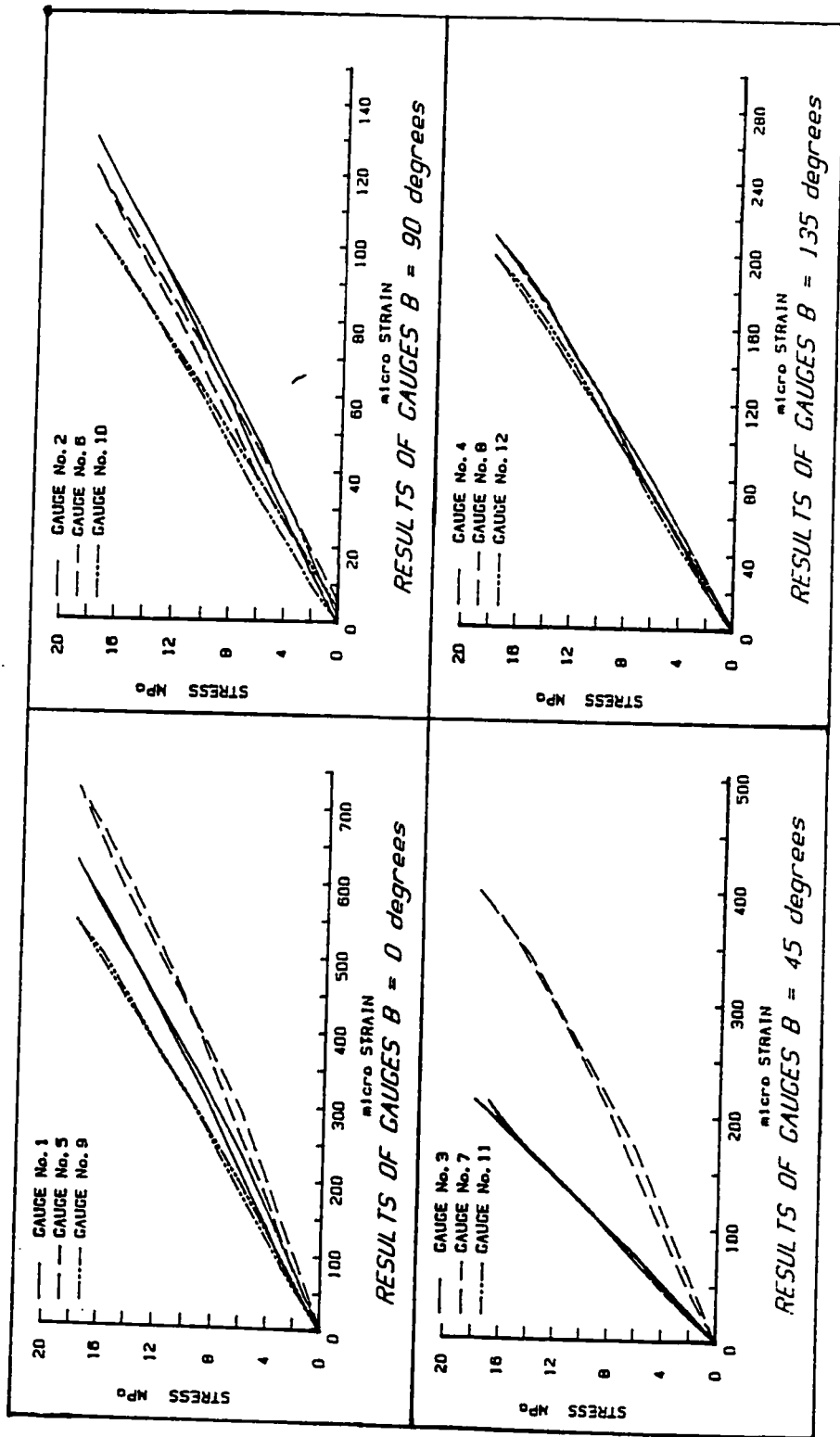
Figure B2: Biaxial test results from stress measurement at 810 ml, 1,13.5 m.
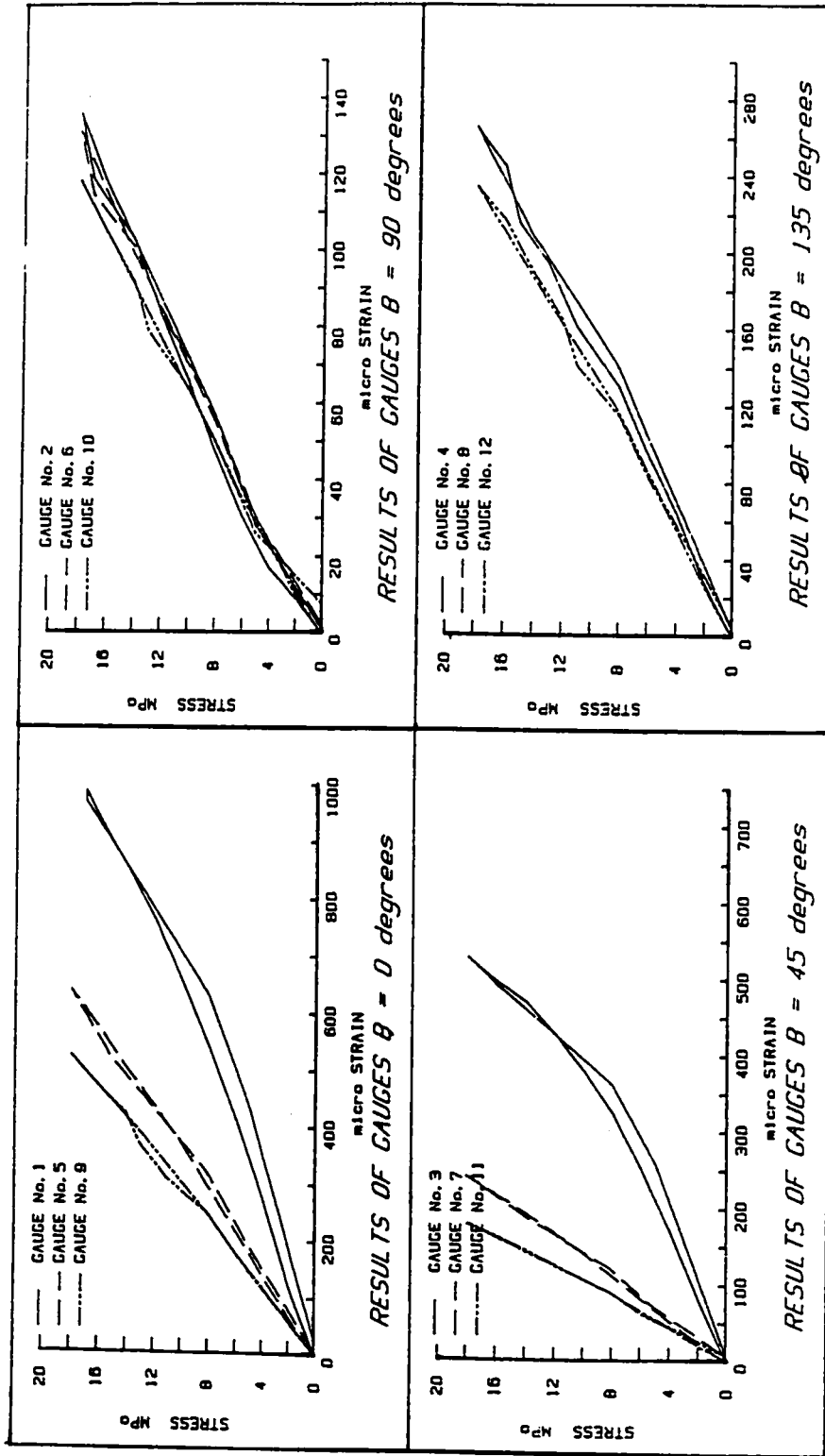
Figure B3: Biaxial test results from stress measurements at 810 ml, gauge 2, at 14 m
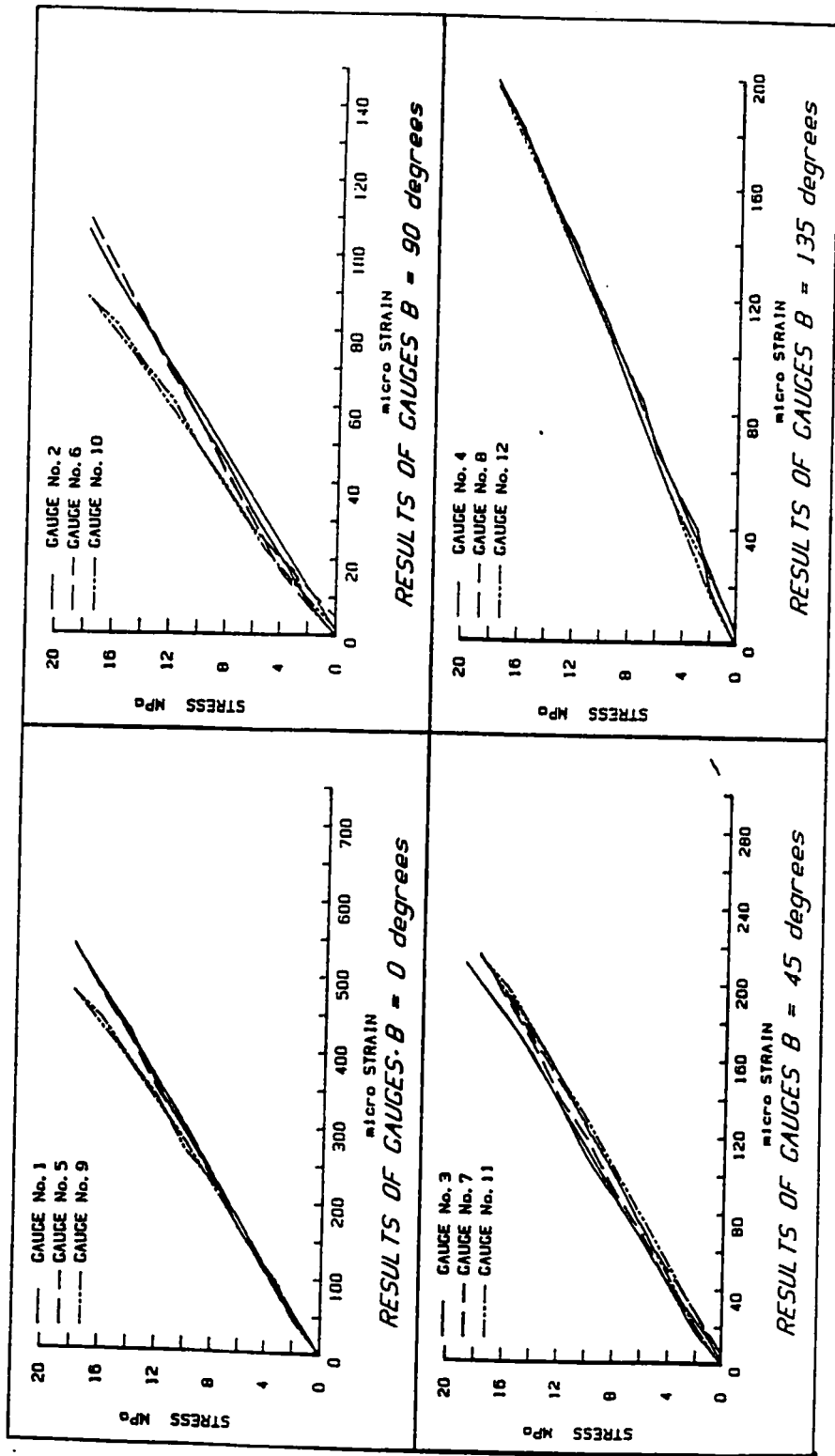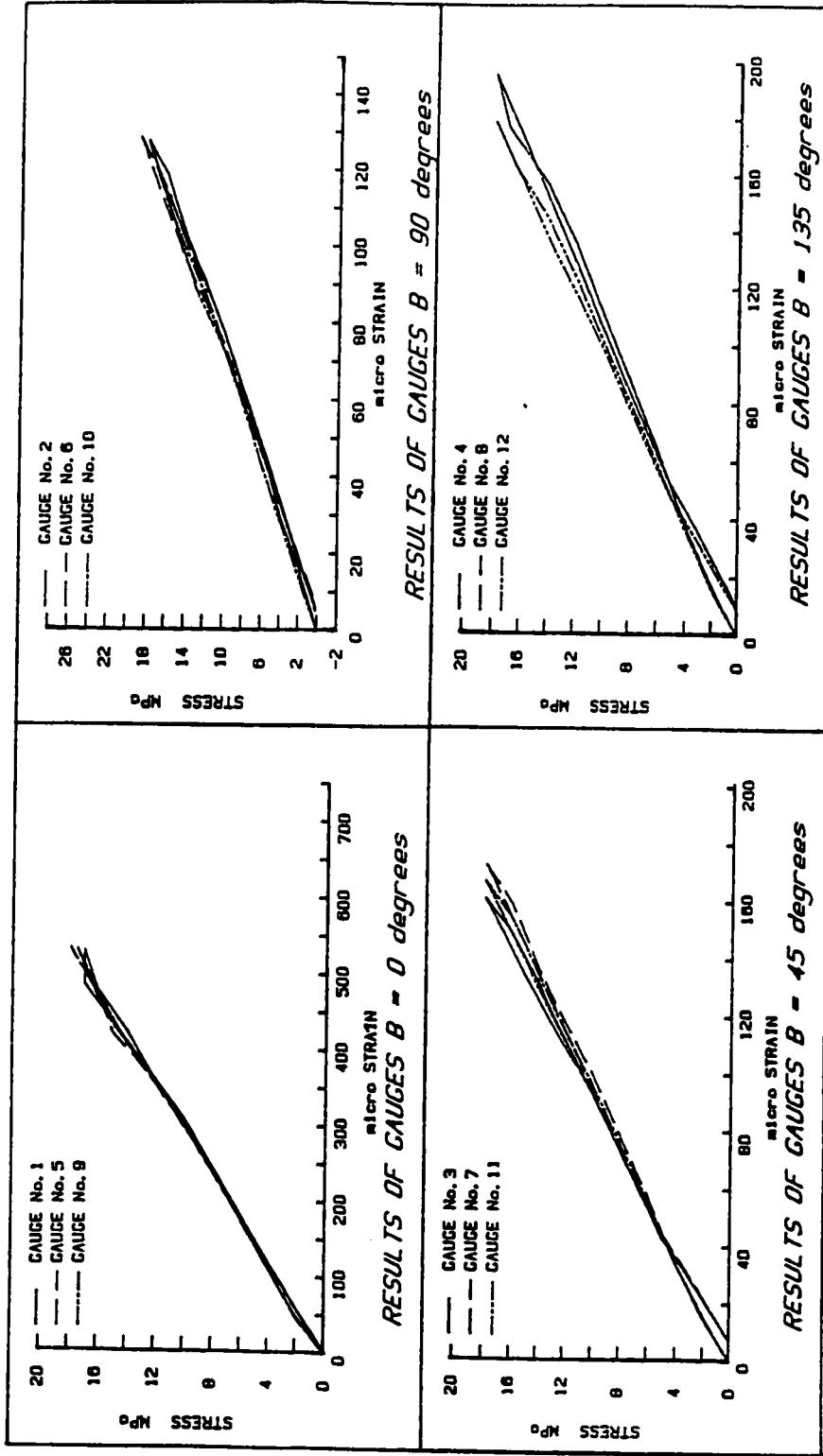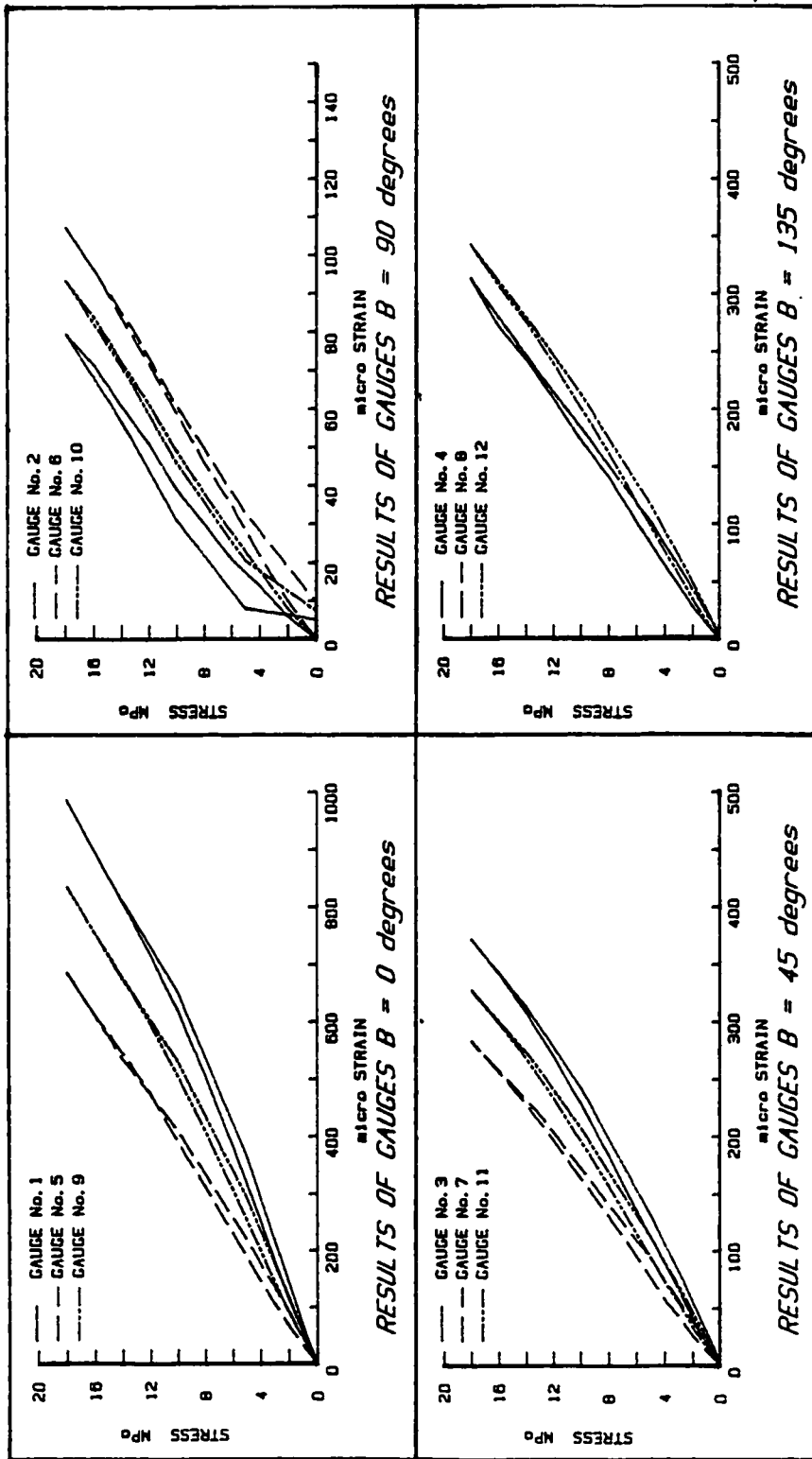
242
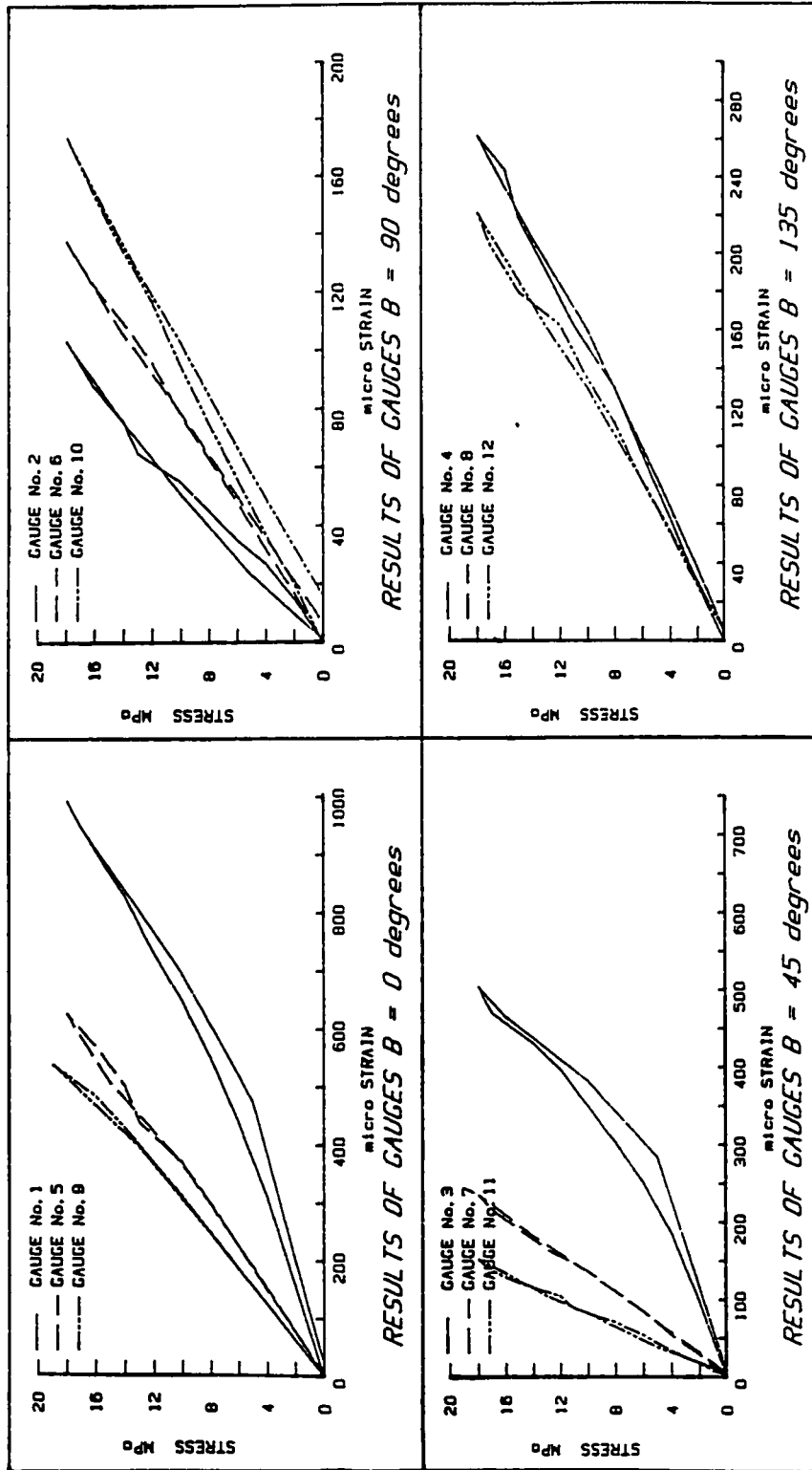
Figure B4: Biaxial test results from stress measurement at 810 ml, 3, 14.5 m

243
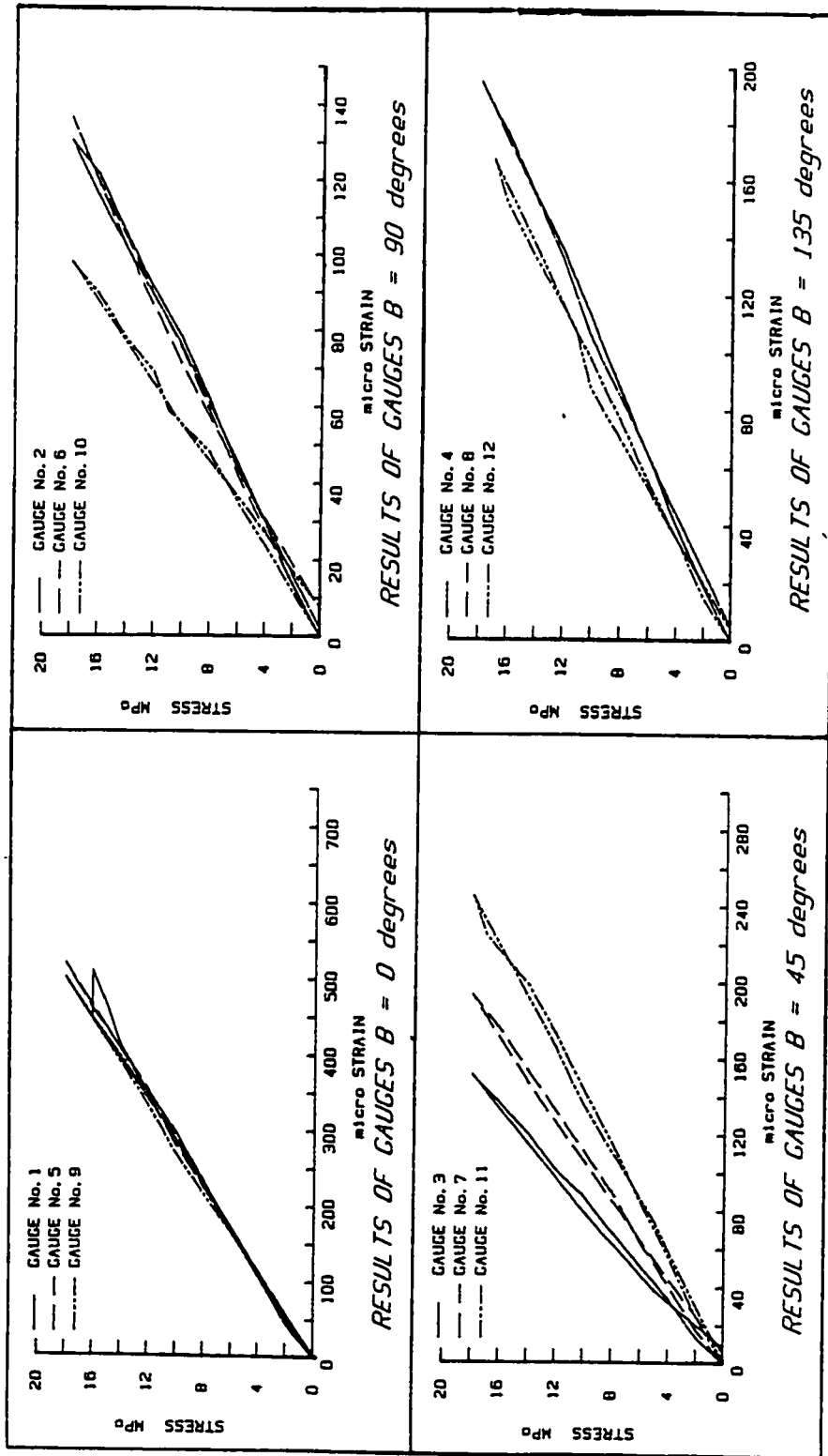
Figure B5: Biaxial test results from stress measurement at 750 ml, 1, 12.5 m
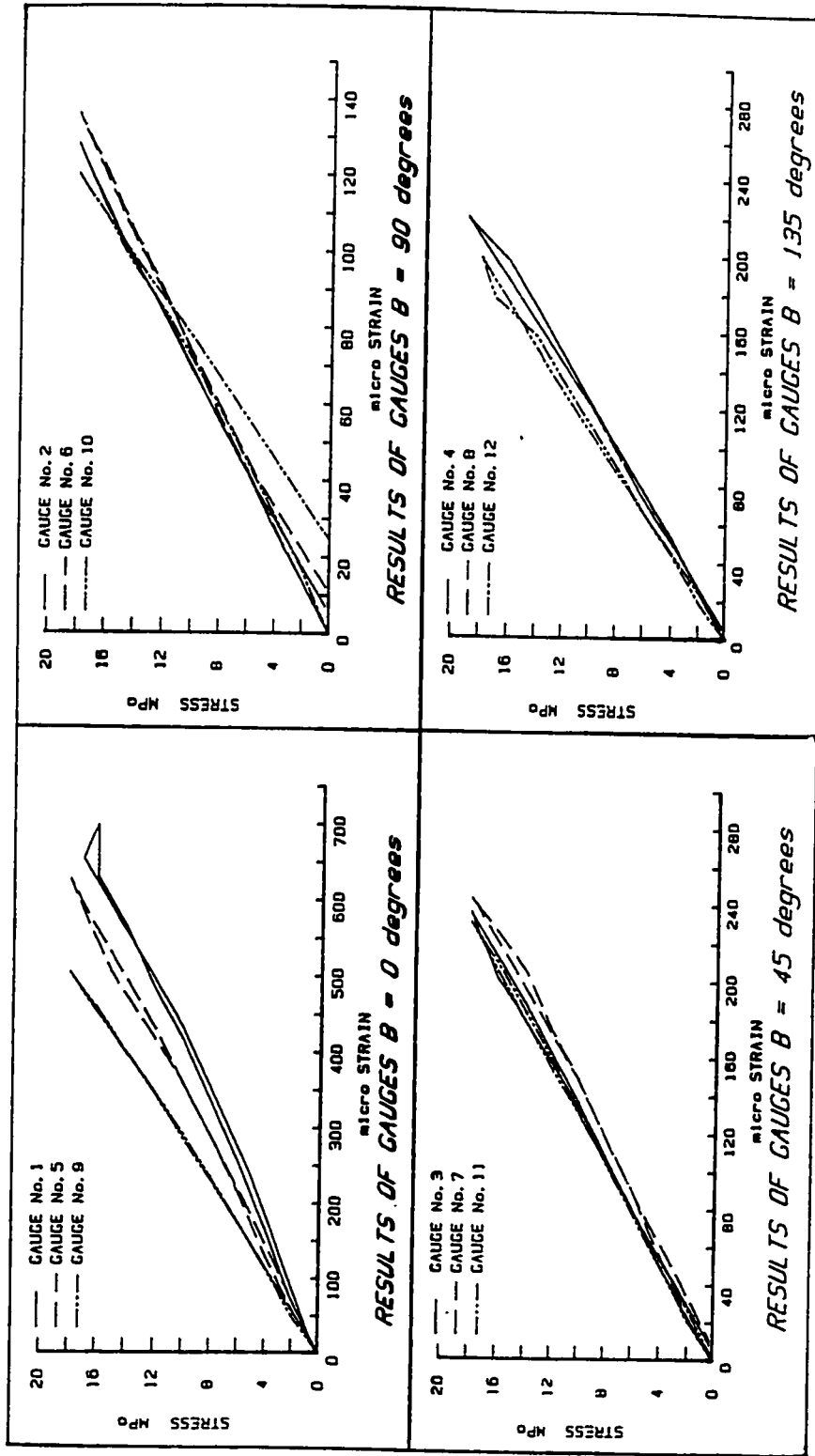
Figure B6: Biaxial test results from stress measurements at 750 ml, gauge 2, at 13.5 m.

Figure B7: Biaxial test results from stress measurements at 750 ml, gauge 3, at 14 m.

Figure B8: Biaxial test results from stress measurements at Selebi Shaft at 650 ml, gauge 1, at 13 m.

Figure B9: Biaxial test results from stress measurement at Selebi, 650 ml, 2, 13.5 m

248
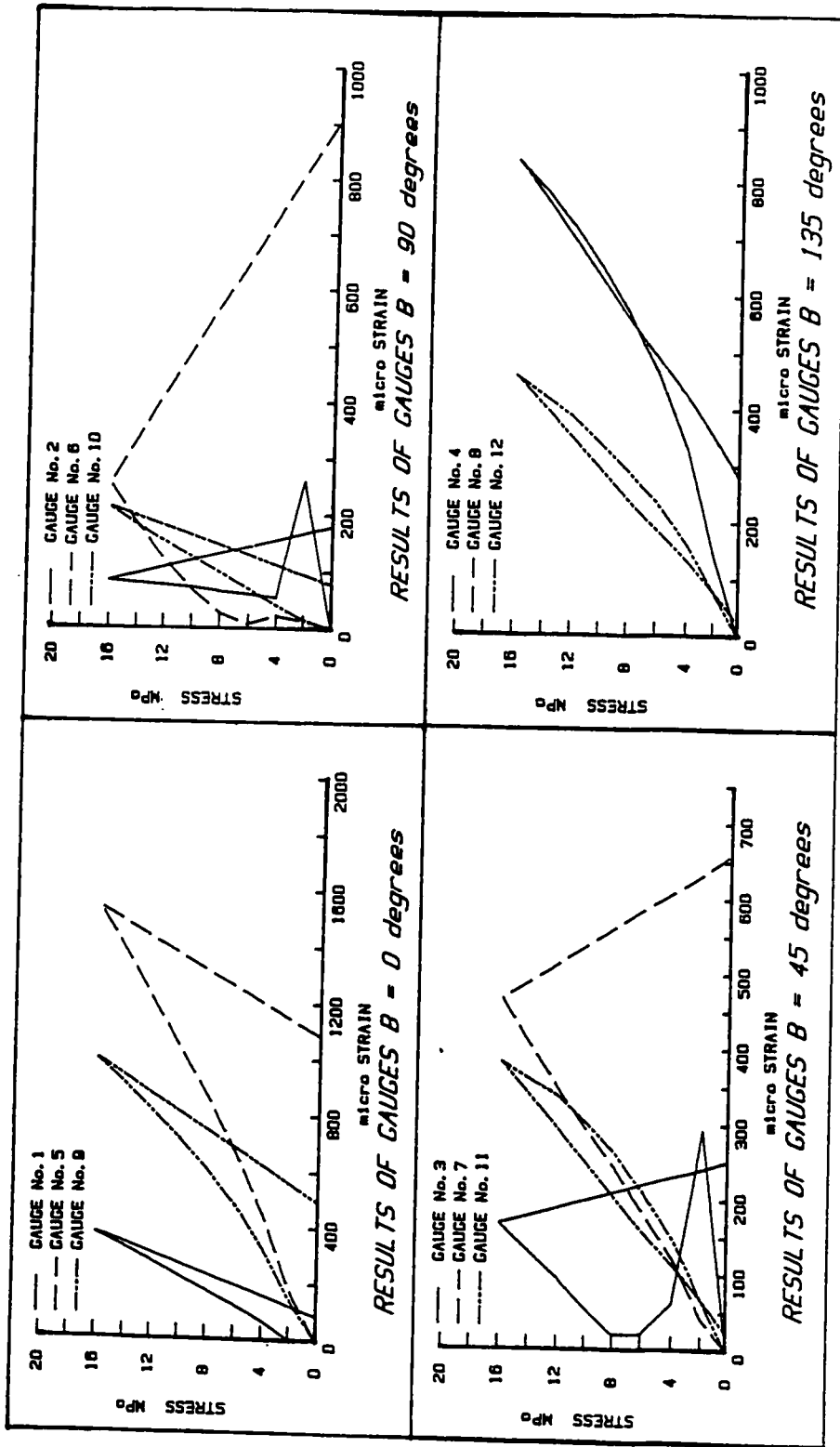
Figure B10: Biaxial test results from stress measurement at Selebi, 650 ml, 3, 14 m

APPENDIX C

MATHEMATICAL CALCULATIONS

APPENDIX C

MATHEMATICAL CALCULATIONS

C.1 Voussoir Arch Method

The arch thickness T, is calculated using the width of the orebody, H and the buckling factor k as follows,

$$T = \frac{H}{k-1} \tag{C.1}$$

$$= \frac{6}{1.33-1}$$
$$18 \text{ m}$$

Using the Brady and Brown approximate solution of N = 0.75, the moment arm of the couple force, Z is calculated as:

$$Z = T\left\{1 - \frac{2}{3}N\right\} = 0.5T \tag{C.2}$$

The maximum stress at the ends or at the center of the beam, Fm is calculated as:

$$Fm = \frac{1}{4}\frac{\gamma s^2}{Nz} = \frac{2.88S^2}{0.5TN}, \text{ for the hangingwall gneiss} \tag{C.3}$$

$$Fm = \frac{1}{4}\frac{\gamma s^2}{Nz} = \frac{3.5S^2}{0.5TN}, \text{ for the orebody sulphides}$$

If failure occurs by crushing at the abutments, the uniaxial compressive stress (σc) would be the same as the maximum shear stress (Fm) at the abutments and the resulting span would be as follows.

$$S = \sqrt{\frac{4\sigma_c NZ}{\gamma}} = \left\{ -\frac{4 \times 122 \times 10^6 \times 0.75 \times 0.5 \times 18}{2.88 \times 9800} - \right\}^{\frac{1}{2}} = 342 \text{ m} \quad \text{allowable span for}$$

hanging wall gneiss

$$S = \sqrt{\frac{4\sigma_c NZ}{\gamma}} = \left\{ -\frac{4 \times 95 \times 10^6 \times 0.75 \times 0.5 \times 18}{3.5 \times 9800} - \right\}^{\frac{1}{2}} = 275 \text{ m} \quad \text{allowable span for the}$$

crown pillar.

The analysis indicate that the hangingwall is capable of reaching 342 m and the crown pillar 275m before failure can occur due to crushing at the abutments.

However, it is necessary to assess whether buckling of either the hangingwall or the crown pillar would occur by calculating the revised arch length, Z1, using ΔL as the incremental length. For buckling to occur $Z1 \le 0$ and the following conditions should apply.

$$\Delta L \ge \frac{8Zo^2}{3S} \ge \frac{8 \times 9^2}{3 \times 342} \ge 0.632 \text{ m for the hanging wall gneiss} \tag{C.4}$$

$$\Delta L \ge \frac{8Zo^2}{3S} \ge \frac{8 \times 9^2}{3 \times 275} \ge 0.785 \text{ m for the crown pillar rock.}$$

The average stresses, Fav, at the center of the crown pillar or at hangingwall abutments are calculated below.

$$Fav = \frac{Fm}{2}\left\{\frac{2}{3} + \frac{N}{2}\right\} = \frac{1}{2}.122 \times 10^6\left\{\frac{2}{3} + \frac{0.75}{2}\right\} = 63.54 \times 10^6 \, MPa \quad \text{for the hangingwall}$$

gneiss.

$$Fav = \frac{Fm}{2}\left\{\frac{2}{3}+\frac{n}{2}\right\} = \frac{1}{2}.95 \times 10^6 \left\{\frac{2}{3}+\frac{0.75}{2}\right\} = 49.48 \times 10^6 \ MPa \ \text{ for the crown pillar rock}$$

Therefore, the incremental lengths are as follows:

$$\Delta L = \frac{63.54 \times 10^6 \times 342}{78 \times 10^{12}} + \frac{5 \times 122 \times 10^6 \times 0.75 \times 18}{78 \times 10^{12}} = 0.0003 + 0.0001 = 0.0004 \ \text{m} \ \text{ for the}$$

hangingwall gneiss

$$\Delta L = \frac{49.48 \times 10^6 \times 275}{80 \times 10^{12}} + \frac{5 \times 95 \times 10^6 \times 0.75 \times 18}{80 \times 10^{12}} = 0.0002 + 0.00008 = 0.00028 \ \text{m} \quad \text{for}$$

the crown pillar

Since the incremental lengths calculated above are less than the conditions stated in equation (C.4), buckling would occur first. However, to solve for the critical buckling length an iterative procedure would have to be setup because $Fm = \sigma c$ can no longer be assumed. However, it is still necessary to check if the voussoir arch would fail by shearing at the abutments as shown below.

The lateral thrust, P, at the abutment is calculated as follows,

$$P = \frac{1}{2}.Fm. NT = \frac{1}{2}.122 \times 10^{6.0}.0.75.18 = 823.5 \times 10^6 \ N \ \text{ for the hangingwall gneiss}$$

$$P = \frac{1}{2}.Fm. N. T = \frac{1}{2}.95 \times 10^{6.0}.0.75.18 = 641.25 \times 10^6 \ N \ \text{ for the crown pillar}$$

In order to be able to calculate the shear force, V, the angle of friction is assumed to be 40 and 50 degrees, respectively, for the hangingwall gneiss and the sulphides forming the crown pillar. The forces resisting failure in the hangingwall gneiss and in the sulphides

crown pillar are respectively calculated below.

$P \tan \phi = 823.5 \times 10^6 . \tan 40 = 691 \times 10^6 \, N$ for the hangingwall gneiss

$P \tan \phi = 641.25 \times 10^6 . \tan 50 = 764.21 \times 10^6 \, N$ for the sulphide crown pillar

The corresponding shear forces are as follows:

$$V = \frac{1}{2} . \gamma . S . T = \frac{1}{2} .2.88 \times 9800.342.18 = 86.87 \times 10^6 \quad \text{for the hangingwall gneiss}$$

$$V = \frac{1}{2} . \gamma . S . T = \frac{1}{2} .3.5 \times 9800.275.18 = 84.89 \times 10^6 \quad \text{for the sulphide crown pillar}$$

The safety factor, F_s, for both the hanging wall gneiss and the sulphide crown pillar is calculated as follows:

$$F_s = \frac{691 \times 10^6}{86.87 \times 10^6} = 7.95 \quad \text{for the hanging wall gneiss.}$$

$$F_s = \frac{764.21 \times 10^6}{84.8910^6} = 9.00 \quad \text{for the sulphide crown pillar}$$

For this project the limiting safety factor has been set at 4, therefore, the implication of the above results is such that shear failure would not occur at the abutment for both the hanging wall gneiss and the crown pillar sulphides. It is worthy to note that if a solution other than that proposed by Brady and Brown (1985) was used different results would have been obtained as the ration of arch thickness to beam thickness, N range from 0.01 to 1.0.

C.2 Beam Theory

Therefore, for a safety factor of 4, the hangingwall span, L, is calculated as follows:

$$4 = \frac{Erh}{\sigma_m} = \frac{86.87 \times 10^6}{\frac{1}{12} \times 28253 \times L^2} \qquad (C.5)$$

$$L = \sqrt{\frac{86.87 \times 10^6 \times 12}{4 \times 28253}} = 96 \text{ metres}$$

This is the maximum span allowable for the hangingwall before failing by rapture. The hangingwall rock is further investigated for the allowable span before failure could occur by shearing at the abutments. The shear stress, τ, is given as:

$$\tau = V\left(\frac{\bar{y} \times A_r}{I \times b}\right) = 86.87 \times 10^6 \times \left(\frac{4.5 \times 9 \times 1}{\frac{1}{2} \times 1 \times 18^3 \times 1}\right) = 1206523 \text{ N/m} \qquad (C.6)$$

For a safety factor of 4,

$$\tau = \frac{1206523}{4} = 301631 \text{ N/m}$$

and the shear force is,

$$V = \frac{301631}{0.083} = 3634105 \text{ N}$$

Therefore, the span allowable before shear failure is given by equation (A.7).

$$L = \frac{2 \times V}{\gamma} = \frac{2 \times 3634105}{28253} = 257 \text{ metres} \qquad (C.7)$$

From the beam theory, for failure to occur by shearing at the hangingwall abutments the span of the hangingwall between the rib pillars have to exceed 257 meters. Therefore

failure would not occur through shearing of the abutment but would occur by rapture once the hangingwall span exceed 96 meters for a safety factor of 4.

C.3 STUB PILLAR DESIGN

The tributary area theory gives the average pillar stress for a rectangular pillar as in equation C.8
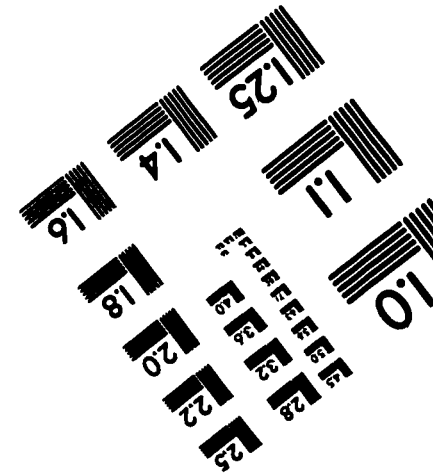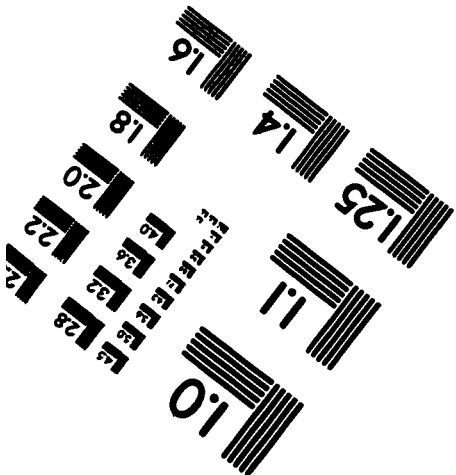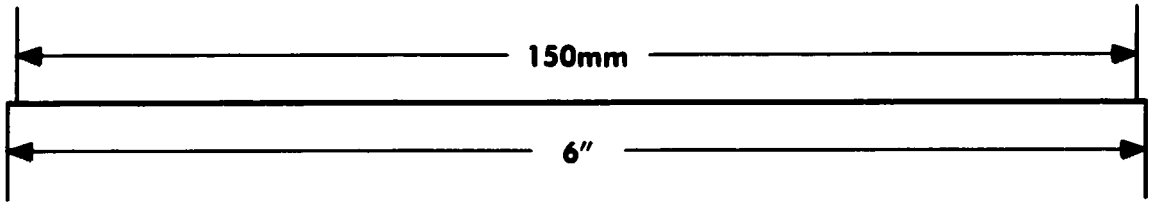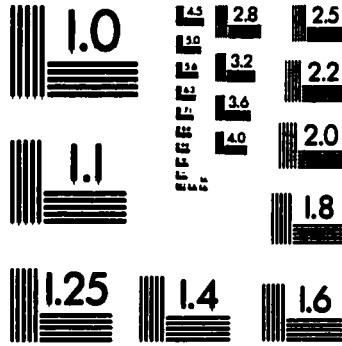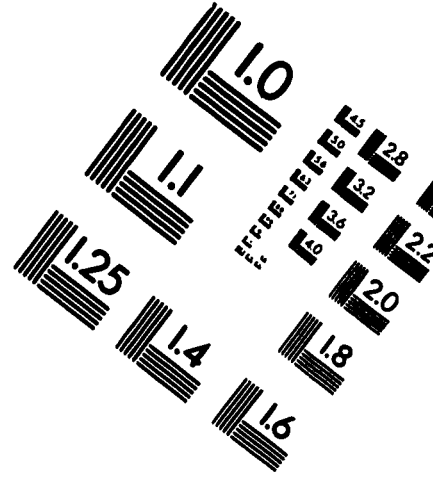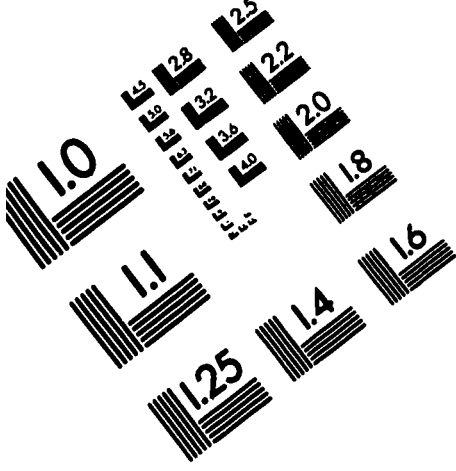
$$\sigma_p = \gamma z \left(1 + \frac{w_o}{w_p}\right)\left(1 + \frac{l_o}{l_o}\right) \tag{C.8}$$

For an orebody inclined at an angle α, the pillar stress is given by equation C.9.

$$\sigma_p = \gamma z \left(1 + \frac{w_o}{w_p}\right)\left(1 + \frac{l_o}{l_o}\right) * \tan(180 - (90 + \alpha)) \tag{C.9}$$

For the case of Selebi North mine, where the orebody is inclined at 75° and the stub pillars are 5 metres wide and 6 metres high at a depth of 300 metres. and the unit weight of the orebody sulphide is 0.035 MN/m³ with the uniaxial compressive strength of 95 MPa. The sulphides also satisfy the Hoek and Brown constants of m=4 and s=0.016, giving the ratio of the average pillar strength to uniaxial compressive stress as 0.7 and the pillar stress as 66.5 MPa. Therefore using equation C.9, the stub pillar strength is calculated as 42.7 MPa at a safety factor of 1.56.

TEST TARGET (QA-3)

1.0
1.1
1.25
1.4
1.6
1.8
2.0
2.2
2.5
2.8
3.2
3.6
4.0

150mm

6"